




*Identifying the Mechanism of Action of
Valproic Acid on Phosphoinositide
Signalling*

Elizabeth Fionnaua Kelly

Research thesis submitted for the degree of Doctor of Philosophy at
Royal Holloway, University of London in August 2018.

Declaration of Authorship

I, Elizabeth Kelly, declare that all work within this thesis is my own, unless otherwise stated. I have not fabricated or falsified the results presented in this thesis and I have acknowledged all published work.

Signed: 

Date: 7/08/18

Abstract

A third of epilepsy patients are resistant to currently available medication, highlighting a need to identify new antiepileptic drugs. To identify new drugs, researchers often explore new chemical structures with a common mechanism of action, but surprisingly the direct cellular target for many drugs remains unclear. One such drug is valproic acid (VPA), commonly used in the treatment of both epilepsy and bipolar disorder (BD). Previous research using the single celled amoeba *Dictyostelium discoideum* identified phosphoinositide recycling as a potential therapeutic mechanism for VPA and this has been validated in animal seizure models, however, the molecular target for this mechanism is unclear. To identify this target, research in this thesis initially focuses on assessing the role of several key enzymes involved in phosphoinositide signalling as potential VPA targets. Loss of these proteins did not confer resistance to VPA in this model, suggesting that VPA may function through targeting proteins in the phosphatidylinositol (PI) salvage pathway. In this pathway three key enzymes, cytidine-diphosphate-diacylglycerol synthase (CDS), cytidine-diphosphate-diacylglycerol-inositol-3-phosphatidyltransferase (CDIPT) and diacylglycerol kinase (DGK) were investigated, with phylogenetic analysis establishing evolutionary conservation. Attempts to ablate the single *D. discoideum* *Cds* (*CdsA*) and *Cdipt* encoding genes were unsuccessful, suggesting a vital role for these proteins. In contrast, overexpressing both proteins showed that cells with elevated expression of CDIPT, but not CDSA, were resistant to therapeutic VPA concentrations. Furthermore, deletion of the single *D. discoideum* DGK (*DGKA*) gene was successful, with the mutant resistant to VPA during both acute and chronic treatment, that was restored on reintroduction of *DGKA*. To investigate whether loss of *DGKA* is related to epilepsy and BD, a range of related compounds were investigated for an effect on cell development. These experiments suggest that in *D. discoideum*, *DGKA* may provide a common target for both epilepsy and BD treatments, supporting data provided from preclinical and clinical studies in both disorders. Together this

work suggests that DGK may provide a new therapeutic target for the treatment of both epilepsy and BD.

Table of Contents

Chapter 1 Introduction	18
1.1 VPA	19
1.1.1 VPA as a Therapeutic Treatment	19
1.1.2 Problems Associated with VPA Treatment	25
1.1.3 Studies Investigating the Mechanism of Action of VPA	26
1.2 Phosphatidylinositol Salvage Pathway	27
1.2.1 Phosphoinositides	27
1.2.2 Phosphatidylinositol Salvage Pathway	28
1.3 Proteins of Interest	31
1.3.1 Interacting Signalling Pathways	31
1.3.1.1 PI3K Signalling	32
1.3.1.2 DAG Signalling	32
1.3.1.3 PA Signalling	32
1.3.1.4 CDP-DAG Signalling	33
1.3.2 Potential Novel Targets of VPA	33
1.3.2.1 CDS	33
1.3.2.2 CDIPT	33
1.3.2.3 DGK	34
1.4 <i>D. discoideum</i> as an Alternative Model	34
1.4.1 Developmental Cycle	35
1.4.2 Methodology	38
1.4.3 Identifying the Target of VPA	44
1.5 Aims and Specific Objectives	45
Chapter 2 Materials and Methods	47
2.1 Materials	48
2.1.1 General Reagents	48
2.2 Methods	51
2.2.1 Bioinformatic Analysis	51
2.2.2 <i>D. discoideum</i> Protocols	52
2.2.3 Molecular Biology Protocols	55
2.2.4 Proteomic Protocols	62
2.3 Statistics	63
2.4 Software	64
2.5 Websites	64
2.5.1 Information of <i>D. discoideum</i> Gene and Protein	64
2.5.2 Basic Local Alignment Tool (BLAST)	64
2.5.3 Alignment of Protein Sequences	64
2.5.4 Gene and Protein Information of Organisms	65

Chapter 3 Analysis of PI3K1-5/ PTEN, PLC and LPIN2 as a Target of VPA	66
3.1 <i>pi3k1-5⁻/pten⁻ Cells.....</i>	70
3.1.1 Analysis of pi3k1-5 ⁻ /pten ⁻ Acute Cell Behaviour in the Presence of VPA .71	
3.1.2 Analysis of pi3k1-5 ⁻ /pten ⁻ Cell Development in the Presence of VPA	75
3.1.3 Analysis of pi3k1-5 ⁻ /pten ⁻ Cell Development in the Presence of Anti-Seizure Compounds and LiCl	77
3.2 <i>plc⁻ Cells</i>	79
3.2.1 Analysis of plc ⁻ Acute Cell Behaviour in the Presence of VPA.....	79
3.2.2 Analysis of plc ⁻ Cell Development in the Presence of VPA	82
3.2.3 Analysis of plc ⁻ Cell Development in the Presence of Anti-Seizure Compounds and LiCl.....	83
3.3 <i>lpin2⁻ Cells.....</i>	86
3.3.1 Analysis of lpin2 ⁻ Acute Cell Behaviour in the Presence of VPA	86
3.3.2 Analysis of lpin2 ⁻ Cell Development in the Presence of VPA	90
3.3.3 Analysis of lpin2 ⁻ Cell Development in the Presence of Anti-Seizure Compounds and LiCl.....	92
3.4 <i>Discussion</i>	94
3.5 <i>Summary</i>	99
Chapter 4 Bioinformatic Analysis of CDSA, CDIPT and DGKA	101
4.1 <i>CDSA</i>	105
4.1.1 CDSA BLAST Analysis	105
4.1.2 CDSA Phylogenetic Analysis	106
4.1.3 CDSA Sequence Alignment.....	108
4.1.4 CDSA Domain Structure and Analysis	111
4.2 <i>CDIPT</i>	112
4.2.1 CDIPT BLAST Analysis	112
4.2.2 CDIPT Phylogenetic Analysis	113
4.2.3 CDIPT Sequence Alignment.....	115
4.2.4 CDIPT Domain Structure and Analysis	116
4.3 <i>DGKA</i>	117
4.2.1 DGKA BLAST Analysis	117
4.2.2 DGKA Phylogenetic Analysis.....	119
4.2.3 DGKA Sequence Alignment	121
4.2.4 DGKA Domain Structure and Analysis.....	123
4.4 <i>Discussion</i>	126
4.5 <i>Summary</i>	131
Chapter 5 Analysis of CDSA as a Target of VPA	132
5.1 <i>Construction of CdsA Knockout Vector.....</i>	134
5.2 <i>Screening of Potential cdsA⁻ D. discoideum Cells</i>	136
5.3 <i>Preparing a CdsA Overexpression Construct</i>	137

5.4 Phenotypic Characterization of WT::RFP-cdsA Cells	139
5.4.1 Analysis of WT::RFP-cdsA Cell Growth in the Presence of VPA	139
5.4.2 Analysis of WT::RFP-cdsA Cell Development in the Presence of VPA	142
5.4.3 Analysis of WT::RFP-cdsA Cell Development in the Presence of Anti-Seizure Compounds and LiCl	144
5.5 Discussion	146
5.6 Summary	149
Chapter 6 Analysis of CDIPT as a Target of VPA	151
6.1 Construction of Cdipt Knockout Vector Part 1	153
6.2 Screening Potential cdipt ⁻ D. discoideum Cells Part 1	155
6.3 Construction of cdipt ⁻ Knockout Vector Part 2	156
6.4 Screening and Confirmation of Potential cdipt ⁻ D. discoideum Cells Part 2...	159
6.5 Preparing a Cdipt Overexpression Construct	162
6.6 Phenotypic Characterization of WT::RFP-cdipt Cells.....	164
6.6.1 Analysis of WT::RFP-cdipt Cell Growth in the Presence of VPA.....	165
6.6.2 Analysis of WT::RFP-cdipt Cell Development in the Presence of VPA....	167
6.6.3 Analysis of WT::RFP-cdipt Cell Development in the Presence of Anti-Seizure Compounds and LiCl	169
6.7 Discussion	171
6.8 Summary	175
Chapter 7 Analysis of DGKA as a Target of VPA.....	176
7.1 Confirmation of DgkA Knockout Vector	178
7.2 Screening Potential dgkA ⁻ D. discoideum Cells.....	181
7.3 Confirming the DgkA Insert Within the Overexpression Construct.....	184
7.4 Phenotypic Characterization of dgkA ⁻ and dgkA ^{-/+} Cells	186
7.4.1 Localization of Myosin II Heavy Chain in dgkA ⁻ Cells During the Vegetative Phase	187
7.4.3 Analysis of Myosin II Heavy Chain Movement in Response to cAMP.....	188
7.4.4 4 Analysis of DGKA on Cell Growth in the Presence of VPA	191
7.4.5 Analysis of DGKA on Acute Cell Behaviour in the Presence of VPA.....	193
7.4.6 Analysis of DGKA Cell Development in the Presence of VPA.....	199
7.4.7 Analysis of DGKA Cell Development in the Presence of Anti-Seizure Compounds and LiCl.....	201
7.4.8 Analysis of DAG Levels in dgkA ⁻ and dgkA ^{-/+} Cell Lines in Response to Other Compounds	203
7.5 Discussion	206
7.6 Summary	212
Chapter 8 Conclusions.....	214

8.1	<i>Background</i>	215
8.2	<i>Proteins Dismissed as VPA Targets</i>	216
8.3	<i>Proteins Identified as Novel VPA Targets.....</i>	218
8.4	<i>Predicted Mechanism of Action of VPA.....</i>	220
8.5	<i>Implications of These Findings</i>	226
8.6	<i>Summary</i>	227
References		229
Supplementary Material		260

List of Figures and Tables

Figure 1.1.	Chemical structure of VPA.	19
Figure 1.2.	Chemical structure of valproic acid identifying the regions responsible for the teratogenic effects.	26
Figure 1.3.	Schematic of the generalized chemical structure of phosphoinositides.	28
Figure 1.4.	Schematic of the phosphatidylinositol salvage pathway and interlinking pathways.	30
Figure 1.5.	Schematic tree of life showing the relationship of different biological kingdoms.	35
Figure 1.6.	Schematic of the <i>D. discoideum</i> developmental cycle.	38
Figure 1.7.	Schematic of the gene ablation protocol resulting in the characterization of mutant cells.	41
Figure 1.8.	Schematic of the gene overexpression protocol resulting in the characterization of mutant cells.	43
Figure 1.9.	Schematic of measurable acute cell behaviour criteria.	45
Figure 2.1.	Schematic illustrating the locations of the PCR screening primers.	60
Figure 3.1.	The role of PI3K, PTEN and LPIN2 in phosphoinositide regulation.	68
Figure 3.2.	The catalytic activity of phosphatidylinositol-3-kinase and phosphatase and tensin homolog phosphatidylinositol-3,4,5-triphosphate-3-phosphatase.	68
Figure 3.3.	The catalytic activity of phospholipase C.	69
Figure 3.4.	The catalytic activity of lpin2.	70
Table 3.1.	WT and <i>pi3k1-5⁻/pten⁻</i> changes in acute cell behaviour in both the absence and presence of VPA.	73
Figure 3.5.	WT and <i>pi3k1-5⁻/pten⁻</i> acute cell behaviour in both the absence and presence of VPA.	74

Figure 3.6.	WT and <i>pi3k1-5⁻/pten⁻</i> development in both the absence and presence of VPA.	76
Figure 3.7.	WT and <i>pi3k1-5⁻/pten⁻</i> development in both the absence and presence of a range of other compounds.	78
Table 3.2.	WT and <i>lpin2⁻</i> changes in acute cell behaviour in both the absence and presence of VPA.	80
Figure 3.8.	WT and <i>plc⁻</i> acute cell behaviour both in both the absence and presence of VPA.	81
Figure 3.8.	WT and <i>plc⁻</i> development in both the absence and presence of VPA.	83
Figure 3.10.	WT and <i>plc⁻</i> development in both the absence and presence of a range of other compounds.	85
Figure 3.11.	WT and <i>lpin2⁻</i> acute cell behaviour in both the absence and presence of VPA.	89
Figure 3.12.	WT and <i>lpin2⁻</i> development in both the absence and presence of VPA.	91
Figure 3.13.	WT and <i>lpin2⁻</i> development in both the absence and presence of a range of other compounds.	93
Figure 4.1.	Simplified phosphatidylinositol salvage pathway.	103
Table 4.1.	<i>D. discoideum</i> CDSA protein homology search results identifying related proteins in other organisms.	106
Figure 4.2.	Phylogenetic analysis of CDS proteins within a range of kingdoms.	108
Figure 4.3.	Conservation of the CDS predicted catalytic site.	110
Figure 4.4.	Domain structure analysis of <i>D. discoideum</i> CDSA and <i>H. sapiens</i> CDS1 and CDS2.	111
Table 4.2.	<i>D. discoideum</i> CDIPT protein homology search results identifying related proteins in other organisms.	113
Figure 4.5.	Phylogenetic analysis of CDIPT proteins within a range of kingdoms.	114
Figure 4.6.	Conservation of the CDIPT predicted catalytic site.	116

Figure 4.7.	Domain structure analysis of <i>D. discoideum</i> and <i>H. sapiens</i> CDIPT.	117
Table 4.3.	<i>D. discoideum</i> DGKA protein homology search results identifying related proteins in other organisms.	118
Figure 4.8.	Phylogenetic analysis of DGK proteins within a range of kingdoms.	120
Figure 4.9.	Conservation of the DGK catalytic site.	121
Figure 4.10.	Conservation of the DGK catalytic site between <i>D. discoideum</i> and the 10 <i>H. sapiens</i> isoforms.	123
Figure 4.11.	Domain structure analysis of <i>D. discoideum</i> DGKA and the 10 <i>H. sapiens</i> DGK isoforms.	125
Figure 5.1.	The catalytic activity of cytidine diphosphate diacylglycerol synthase.	133
Figure 5.2.	Confirmation of the <i>CdsA</i> knockout construct.	135
Figure 5.3.	PCR screening of potential <i>cdsA</i> ⁻ transformant cells.	137
Figure 5.4.	Confirmation of the RFP- <i>CdsA</i> overexpression construct.	138
Figure 5.5.	CDSA expression and localization.	139
Figure 5.6.	WT::RFP and WT::RFP- <i>cdsA</i> growth in both the absence and presence of VPA.	141
Figure 5.7.	WT::RFP and WT::RFP- <i>cdsA</i> development in both the absence and presence of VPA.	143
Figure 5.8.	WT::RFP and WT::RFP- <i>cdsA</i> development in both the absence and presence of a range of other compounds.	145
Figure 6.1.	The catalytic activity of cytidine diphosphate diacylglycerol inositol 3 phosphatidyltransferase.	152
Figure 6.2.	Confirmation of the <i>Cdipt</i> knockout construct 1.	154
Figure 6.3.	PCR screening of potential <i>cdipt</i> ⁻ transformant cells using knockout cassette 1.	156
Figure 6.4.	Confirmation of the <i>Cdipt</i> knockout construct 2.	158
Figure 6.5.	PCR screening of potential <i>cdipt</i> ⁻ transformant cells using knockout cassette 2.	161

Figure 6.6.	Confirmation of the RFP- <i>Cdipt</i> overexpression construct.	163
Figure 6.7.	CDIPT expression and localization.	164
Figure 6.8.	WT::RFP and WT::RFP- <i>cdipt</i> growth in both the absence and presence of VPA.	166
Figure 6.9.	WT::RFP and WT::RFP- <i>cdipt</i> development in both the absence and presence of VPA.	168
Figure 6.10.	WT::RFP and WT::RFP- <i>cdipt</i> development in both the absence and presence of a range of other compounds.	170
Figure 7.1.	The catalytic activity of diacylglycerol kinase.	177
Figure 7.2.	Confirmation of the <i>DgkA</i> knockout construct.	180
Figure 7.3.	PCR screening of <i>dgkA</i> ⁻ isogenic transformant cell lines.	183
Figure 7.4.	Confirming the <i>DgkA</i> insert within the GFP- <i>dgkA</i> overexpression construct.	185
Figure 7.5.	GFP-DGKA expression and localization.	186
Figure 7.6.	Comparison of myosin II heavy chain localization in WT and <i>dgkA</i> ⁻ cells.	188
Figure 7.7.	F-actin- GFP and myosin II heavy chain- GFP localization in response to cAMP stimulation.	190
Figure 7.8.	WT and <i>dgkA</i> ⁻ growth in both the absence and presence of VPA.	192
Table 7.1.	WT, <i>dgkA</i> ⁻ and <i>dgkA</i> ^{-/+} changes in acute cell behaviour in both the absence and presence of VPA.	195
Figure 7.9.	WT, <i>dgkA</i> ⁻ and <i>dgkA</i> ^{-/+} acute cell behaviour in both the absence and presence of VPA primary plots.	197
Figure 7.10.	WT, <i>dgkA</i> ⁻ and <i>dgkA</i> ^{-/+} acute cell behaviour in the presence of VPA secondary plots.	198
Figure 7.11.	WT, <i>dgkA</i> ⁻ and <i>dgkA</i> ^{-/+} development in both the absence and presence of VPA.	200
Figure 7.12.	WT, <i>dgkA</i> ⁻ and <i>dgkA</i> ^{-/+} development in both the absence and presence of a range of other compounds.	202

Figure 7.13.	WT, <i>dgkA</i> ⁻ and <i>dgkA</i> ^{-/+} analysis of DAG levels in response to anti-seizure compounds and a bipolar disorder treatment.	205
Table 8.1.	Summary of results obtained within this thesis.	217
Figure 8.1.	Schematic comparing changes in cellular components during seizures and VPA treatment.	222
Figure 8.2.	Schematic of proposed mechanism of action of VPA.	224
Table S1.	List of primer oligonucleotide sequences used for PCR amplification of DNA fragments for cloning and PCR screening protocols.	261- 263
Table S2.	<i>D. discoideum</i> and <i>H. sapiens</i> PI3K and PTEN protein homology search results identifying related proteins.	264- 266
Table S3.	<i>D. discoideum</i> and <i>H. sapiens</i> PLC protein homology search results identifying related proteins.	267
Table S4.	<i>D. discoideum</i> and <i>H. sapiens</i> LPIN2 protein homology search results identifying related proteins.	268
Figure S1.	CDS full sequence alignment.	269- 272
Figure S2.	CDIPT full sequence alignment.	273- 274

Abbreviations

-OH	Hydroxyl group
=O	Double bonded oxygen
2-MHA	2-methylhexanoic acid
4-EOA	4-ethyloctanoic acid
5'P	5-phosphatase (type 1)
AED	Antiepileptic drug
ALC	Anterior- like cells
ANK	Ankyrin repeat
APS	Ammonium persulfate
BD	Bipolar disorder
BLAST	Basic local alignment tool
bp	Base pairs
BSA	Bovine serum albumin
<i>Bsr</i>	Blasticidin resistance gene
cAMP	Cyclic-adenosine-3,5-cyclic monophosphate
CDIPT	Cytidine-diphosphate- diacylglycerol-inositol-3-phosphatidyltransferase
cDNA	coding DNA
CDP-DAG	Cytidine diphosphate-diacylglycerol
CDS	Cytidine diphosphate-diacylglycerol synthase
CTP	Cytidine triphosphate
DA	Decanoic acid
DAG	Diacylglycerol
DGK	Diacylglycerol kinase
DMSO	Dimethyl sulfoxide
dNTPs	deoxynucleotides
E-value	Expectation-value
EDTA	Ethylenediaminetetraacetic acid

ELISA	Enzyme linked immunosorbent assay
G	Genomic control
GFP	Green fluorescent protein
I	<i>myo</i> -inositol
IMPase	Inositol monophosphatase
IP	Inositol-4-phosphate
IP ₂	Inositol-1,4-bisphosphate
IP ₃	Inositol-1,4,5-triphosphate
IPPase	Inositol polyphosphatase
K	Knockout diagnostic
Kb	Kilobase
LB	Luria broth
LiCl	Lithium chloride
LPIN2	Phosphatidate phosphatase LPIN2
MB	Megabase
MCT	medium chain triglyceride
MEGA	Molecular Evolutionary Genetic Analysis
MgCl ₂	Magnesium chloride
mTOR	Mammalian target of rapamycin
MHC	Myosin II heavy chain
NCBI	National Centre for Biotechnology Information
NMDA	<i>N</i> -methyl-D-aspartate
nr	Non-redundant
OA	Octanoic acid
PA	Phosphatidic acid
PC	Phosphatidylcholine
PCR	Polymerase chain reaction
PDVF	Polyvinylidene fluoride (PDVF) Transfer membrane
PE	Phosphatidylethanolamine
PenStrep	Penicillin-streptomycin
pERK	Phosphorylated extracellular signal-regulated kinase

PG	Phosphatidylglycerol
PI	Phosphatidylinositol
PI3K	Phosphatidylinositol-3-kinase
PIA	Propylisopropylacetic acid
PIK	Phosphatidylinositol kinase
PIP	Phosphatidylinositol-4-phosphate
PIP ₂	Phosphatidylinositol-4,5-bisphosphate
PIP ₃	Phosphatidylinositol-3,4,5-trisphosphate
PIPK	Phosphatidylinositol-4-phosphate kinase
PITP	Phosphatidylinositol-transfer protein
PKC	Protein kinase C
PLC	Phospholipase C
PLD	Phospholipase D
PS	Phosphatidylserine
PSI	Position- specific iterative
PTEN	Phosphatase and tensin homolog
PTZ	Pentylentetrazol
RFP	Red fluorescent protein
RT-PCR	Reverse transcriptase- polymerase chain reaction
SDS	Sodium dodecyl sulphate polyacrylamide
SUDE	Sudden unexpected death in epilepsy
TBE	Tris-borate-EDTA
TBS-T	Tris buffered saline with tween
TEMED	N'N'N'N'- tetramethylethylenediamine
TSAP	Thermosensitive alkaline phosphatase
V	Vector control
VPA	Valproic acid
VPD	Valpromide
WT	Wild type

Acknowledgements

I would like to thank my PhD supervisor Professor Robin Williams and my advisor Doctor Christopher Wilkinson for their advice and guidance throughout this PhD project.

I would also like to thank the National Centre for the Replacement, Refinement and Reduction of Animals in Research (NC3Rs) for their funding which made this PhD project possible.

Finally, I would also like to thank all my family, friends and colleagues for all their help and encouragement throughout this project. Especially, my parents Maureen and Lawrence, my brother Luke and partner Ben who have always believed in me and Bella who has been a constant rock. I would also like to thank Ruth for always being there to talk to. I would especially like to thank my late uncle George who always kept up-to-date with my research and took the time to fully understand the results I showed him with a smile on his face.

Chapter 1

Introduction

1. Introduction

1.1 VPA

1.1.1 VPA as a Therapeutic Treatment

Valproic acid (2-propylpentanoic acid, VPA) is an 8-carbon molecule with a carboxylic acid side chain (**Figure 1.1**). The role of VPA as an anti-epileptic was discovered accidentally in 1963, where the drug protected rodents against pentylenetetrazol (PTZ)- induced convulsions (Meunier, et al., 1963). VPA was then studied in animal models as a therapeutic treatment for epilepsy (a disease characterized by recurrent seizures) and was first licensed as an anti-epileptic drug (AED) in France, 1967 (Carraz, et al., 1964; Mutani, et al., 1968; Tulloch, et al., 1982). Following the license of VPA as an AED, a small patient study (22 patients) conducted in 1980 found a 75 % improvement when treated with VPA for 1 year, where the drug protected patients experiencing a range of seizure types, from states of unconsciousness (absences) to muscles stiffening and jerking (tonic-clonic) (Bruni, et al., 1980). VPA today is marketed under the brand names Depakote, Depakene, Divalproex and Epilim.

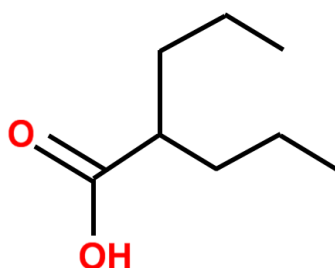


Figure 1.1. Chemical structure of valproic acid. Valproic acid (VPA) is a branched chain fatty acid with a 5-carbon backbone and a 3-carbon side chain branched at the second carbon.

In addition to treating epileptic seizures, VPA is also a therapeutic option for bipolar disorder (BD) (characterized by manic and depressive states) (Pope, et al., 1991)

and migraine (characterized by a severe headache) (Hering and Kuritzky, 1992; Yurekli, et al., 2008) and is currently being studied as a treatment option for cancer (Göttlicher, et al., 2001; Tang, et al., 2004; Witt, et al., 2013). VPA could be used to treat a range of cancer types, including leukaemia (Göttlicher, et al., 2001; Tang, et al., 2004) and prostate cancer (Witt, et al., 2013), due to its role as a histone deacetylase inhibitor (Phiel, et al., 2001). VPA has been listed by the World Health Organisation as an essential medicine, which is defined as a drug which improves health for the majority of patients within a population (World Health Organisation, 2017).

1.1.1.1 *Epilepsy*

Epilepsy is a neurological disease characterized by recurrent seizures. To date, approximately 50 million people worldwide have epilepsy, with around 130,000 children in Europe diagnosed with the disease each year (Forsgren, et al., 2005; World Health Organisation, 2018). Epilepsy, therefore, accounts as a worldwide disease burden of approximately 0.7 % (Wilmschurst, et al., 2014). As 10% of the general population will encounter a one-off seizure before the age of 85, epilepsy is diagnosed after a patient has experienced 2 or more unprovoked seizures (Wilden and Cohen-Gadol, 2012). Epilepsy affects both children and adults, with the risk of developing the disease lessening with increasing age (Lee, et al., 2014). For example, the incidence of epilepsy diagnosis before the age of 1 is 90-212 per 100,000 people, which drops considerably for those patients identified in adolescence (20-70 per 100,000 people) (Wilmschurst, et al., 2014). However, the risk of developing epilepsy increases in the elderly and is higher in children with intellectual (learning) difficulties (Illingworth, Watson and Ring, 2014; Wilmschurst, et al., 2014).

There are 3 classifications of epilepsy- symptomatic or provoked, cryptogenic and idiopathic (Shorvon, 2011). Symptomatic or provoked epilepsy occurs as a result of neurological damage from disease or trauma (e.g. meningitis, stroke or head trauma), a genetic cause or birth defects (such as cerebral palsy, autism, significant developmental delay and cognitive impairment). Cryptogenic epilepsy occurs when

symptoms, such as learning difficulties, suggests brain damage has occurred. Idiopathic epilepsy is when no known cause is found. Independent of the disease classification, all patients will experience recurrent seizures. Epileptic seizures arise through calcium- dependent pathways where inositol-1,4,5-trisphosphate (IP₃) initiates calcium release (Alswied and Parekh, 2015). One theory suggests seizures are maintained through attenuating *N*-methyl-D-aspartate (NMDA) receptor activation (Slater, Stelzer and Galvan, 1985; Holmes, et al., 1990). At the onset of a seizure, there is a rapid increase in diacylglycerol (DAG) levels, followed by the accumulation of almost 2-fold free fatty acids (Bazán, 1970; Bazán and Rakowski, 1970; Bazán, Morelli de Liberti and Rodriguez de Turco, 1982; Rodriguez de Turco, Morelli de Liberti and Bazán, 1983). This is accompanied with a decrease in phosphatidylinositol (PI) levels with free fatty acids being converted into triglycerides (Yoshida, et al., 1987). During seizures, there is no change in phosphatidylethanolamine (PE) (Marku, et al., 1987), however phosphatidylcholine (PC) levels decrease 6 minutes after seizure induction (Corazzi, et al., 1986). Following 6 minutes of seizure induction, the levels of the water-soluble precursors cytidine-diphosphate (CDP)- ethanolamine, phosphoethanolamine (Marku, et al., 1987), CDP-choline and phosphocholine double (Corazzi, et al., 1986). It is the excitation of NMDA receptors which causes the characteristic neuronal damage of repeated seizures (Zeise, Kasparow and Zieglgänsberger, 1991).

There are two main categories of seizures, focal and generalized (Berg, et al., 2010). Focal seizures occur in one hemisphere of the brain within a single or few neuronal networks and have a repeated site of onset within subcortical structures (e.g. thalamus, brainstem and cerebellum). In comparison, generalised seizures spread rapidly and bilaterally throughout the brain, affecting cortical (e.g. frontal or temporal lobes) and subcortical structures and originate in different locations depending on seizure type (Berg, et al., 2010). Generalized seizures range from absences to tonic- clonic. Seizures can be triggered by a number of factors, including sleep deprivation, stress, time of day and menstrual status (Illingworth, Watson and Ring, 2014).

All epilepsy treatments aim at reducing seizures. These include the medium chain triglyceride diet (MCT, also known as the ketogenic diet), a high fat- low carbohydrate diet administered to children, which causes an accumulation of decanoic acid (DA) and octanoic acid (OA) (Haidukewych, Forsythe and Sills, 1982; Augustin, et al., 2018). This diet was originally thought to work through ketone production, however, recent studies suggest that neuroprotection arises through a direct role of fatty acids (Chang, et al., 2016). Surgery is offered to patients with medical refractory epilepsy as it can reduce or completely prevent seizure recurrence (Kelly and Chung, 2011). Surgery is only offered when the seizure focus is known at a confident level and when removal of the area will not result in neurological problems. The primary treatment for epilepsy is AED, including VPA, gabapentin, lacosamide, lamotrigine and vigabatrin (Becerra, et al., 2011; Brodie and Sills, 2011; Ramgopal, et al., 2014). AEDs are administered either as a single drug (monotherapy), or as is the case for approximately 40 % of patients, as a combination of two or more treatments (polytherapy) (Tan, et al., 2012). Polytherapy is given when monotherapy fails at preventing seizures. However, despite treatment, if a seizure has a duration of over 5 minutes, rescue medications such as benzodiazepines, need to be administered (Arzimanoglou, et al., 2014). Even when a patient becomes seizure free there is a risk of relapse e.g. when taking medications, during periods of stress, tiredness, changes in daily routines and medication compliance. This is because AEDs need to be taken long-term and can have undesirable side effects (Ferrari, de Sousa and Castro, 2013). After a patient has been seizure free for 2 years, medication is gradually withdrawn, where the risk of a breakout seizure is between 20-40 % in children (Bouma, et al., 1987; Olmez, et al., 2008). An uncommon consequence of epilepsy, affecting 9 % of patients, is sudden unexpected death in epilepsy, which is confirmed after a patient has undergone a 30 minute seizure and has died within an hour (Sillanpää and Shinnar, 2010). The total cost of epilepsy in Europe in 2010 was estimated at € 13.8 million (Gustavsson, et al., 2011).

1.1.1.2 *Bipolar Disorder*

BD is a chronic disabling condition characterised by recurrent episodes of depression, mania and hypomania. Mania and hypomania are similar in that they both involve abnormally elevated irritability or mood. Mania and hypomania differ by severe psychotic symptoms or functional impairment with a duration of over 7 days in mania, compared with hypomania where function is either increased or decreased and lasts for a minimum of 4 days (Morriss, 2015). Worldwide, 2.4 % of the population have BD (Merikangas, et al., 2011), of which there are two types- BD-I and -II, which differ in the degree of mania symptoms. BD-I involves excessive mania and depression, whereas BD-II is less severe with hypomania and depression (Pini, et al., 2005). The disease prevalence for BD-I in adults is approximately 1 % and for BD-II 0.4 % (Morriss, 2015). BD is difficult to diagnose as the symptoms of combined disorders such as attention deficit hyperactivity disorder, substance misuse, personality disorders and anxiety prevent initial identification of the disorder. BD commonly develops during adolescence (15-19 year olds) and early adulthood and very rarely in children under the age of 12. Diagnosis of BD is confirmed once a patient has undergone at least one mixed or manic episode (Pini, et al., 2005). The hereditary risk of offspring developing BD is approximately 85 % (McGuffin, et al., 2003). Studies have linked BD to a range of pathways including hormonal regulation and the signalling of calcium, phospholipase C (PLC) and glutamate (Nurnberger, et al., 2014).

BD is treated with drugs which aim to rapidly stabilize and maintain a constant state within the patient, i.e. especially aimed at treating mania (e.g. lithium and VPA) or depression (Geddes and Miklowitz, 2013). Problems with treatment occur as the aim of each medication is to reduce either the manic or depressive state and can result in a rise in the second state. In addition, a third of BD patients are resistant to currently available medication (Perlis, et al., 2006). VPA was first investigated as a therapeutic treatment option for acute mania in a small pilot study of 5 patients, which had a success rate of 80 % (Emrich, et al., 1980). This pilot study was followed with 7 further patients who were unresponsive to lithium treatment alone (Emrich, et al., 1980). All 7 patients were administered a combined treatment of

VPA and low-dose lithium and showed improvement with no relapse after 1.5-3 years of observation (Emrich, et al., 1980). VPA was then further investigated in 3 studies for use as an alternative treatment for BD in the 1990s (Calabrese and Delucchi, 1990; Pope, et al., 1991; Freeman, et al., 1992). The results from all of these studies confirmed VPA treatment improved manic symptoms when treated with VPA alone or as a combination with lithium. In 1986, the VPA amide derivative valpromide (VPD, Depamide), was also investigated as a treatment option for acute psychotic states for BD and schizophrenic patients (Altamura, et al., 1986). In this study, it was found that VPD reduced patient agitation.

BD affects patients' health status and quality of life. The disease is associated with irresponsible behaviour, sleep loss and extreme talking due to excess energy. Half of BD patients will attempt suicide at least once in their lifetime, with 15-19 % of patients going through with it (Nabuco de Abreu, et al., 2009). In addition, the disease is associated with high medical costs, both directly and indirectly. In the United States, the estimated direct cost of BD in 2009 was \$ 30.7 billion and the indirect cost was \$ 120.3 billion (Dilsaver, 2010).

1.1.1.3 *Migraine*

Migraine is characterised by a severe headache positioned in a unilateral location at the front of the head, with pain occurring in a pulsating manor for 4-72 hours (Headache Classification Committee of the International Headache Society, 2013). Migraine is associated with photophobia, phonophobia, vomiting, nausea and aura. In 2000, the World Health Organisation estimated migraine to reduce life expectancy by 1.4 % years in both men and women of all ages. For women aged 15-44 years, life expectancy was estimated to be reduced by 2.1 % years and was ranked 14th in the leading cause of disease for women in this age range (World Health Organization, 2001). Women (18.2 %) are more susceptible to developing migraine compared with men (6.5 %) (Lipton, et al., 2001).

The primary treatment of migraine is to write a headache diary to identify initiation triggers (Pryse-Phillips, et al., 1997). If migraines continue, prophylactic (drug)

treatment is given. Prophylactic treatment is thought successful if migraine attacks are reduced by 50 %, and include β - blockers (Propranolol hydrochloride), calcium channel blockers (Verapamil), serotonin receptor agonists (Pizotifen) and AEDs/ tricyclic antidepressants (VPA) (BNF, 2018). Migraines arise from an increase in calcium signalling, where familial hemiplegic migraine is caused by missense mutations in sodium/ potassium pump (Maurizio De Fusco, et al., 2003), calcium (Ophoff, et al., 1996) or sodium voltage gated channels (Dichgans, et al., 2005).

VPA was shown to be an effective treatment for migraine in 1992, where the drug either prevented or reduced the frequency, duration and severity of migraines in 86.2 % of patients (Hering and Kuritzky, 1992). The estimated total cost of migraine in Europe in 2010 was € 43.5 million (Gustavsson, et al., 2011).

1.1.2 Problems Associated with VPA Treatment

Epilepsy, BD and migraine are all associated with calcium signalling and can be treated with VPA. Interestingly, both VPA and lithium treatment cause a rise in cytidine diphosphate- diacylglycerol (CDP-DAG) (Watson, Shipman and Godfrey, 1990; Stubbs Jr., et al., 1992; Stubbs Jr. and Agranoff, 1993; Ju and Greenberg, 2003), DAG (Drummond and Raeburn, 1984; Bami, Leli and Hauser, 1993) and the phosphorylated extracellular signal-regulated kinase (pERK) (Ludtmann, Boeckeler and Williams, 2011) levels. pERK is activated by DAG activated protein kinase C (PKC) and is responsible for protein phosphorylation. VPA and lithium alter PI levels (Allison, et al., 1976) and inhibit PKC (Wang and Friedman, 1989; Bitran, et al., 1990; Chen, et al., 1994). As with all medications, VPA has side effects. The most common of these include heartburn, nausea and vomiting. Under 10 % of patients taking VPA can develop rashes, alopecia, drowsiness, ataxia, irritability or dose-related tremors (Davis, Peters and McTavish, 1994; Zarate, et al., 1999). The most severe and rare side effects of VPA are hepatotoxicity (liver damage) and teratogenicity (defects of a developing embryo) (Hauck and Nau, 1989), which are believed to be caused by β - oxidation (Coudé, et al., 1983; Kesterson, Granneman and Machinist, 1984; Granneman, et al., 1984) and histone deacetylase inhibition (Phiel, et al., 2001) respectively. Teratogenicity is also a side effect for the VPA

amide analogue, VPD, which has been used as an epilepsy and BD treatment (Favel, et al., 1973; Pacifici, et al., 1985).

Hepatotoxicity from VPA results in increased activation of reactive oxygen species, which causes tissue and organ damage (Tong, et al., 2005). Teratogenicity caused by VPA arises through the activation of the peroxisome proliferator- activated receptor δ (Lampen, et al., 1999; Werling, et al., 2001). Teratogenic compounds contain a free carboxyl group, an α - hydrogen atom (present on the carbon atom also containing the carboxyl group) and has branching on carbon 2 (**Figure 1.2**) (Nau, Hauck and Ehlers, 1991).

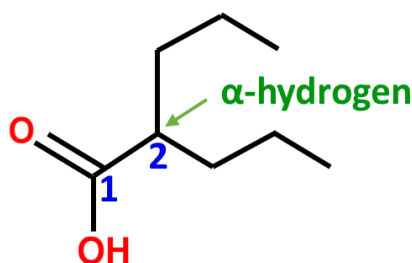


Figure 1.2. Chemical structure of valproic acid identifying the regions responsible for the teratogenic effects. The chemical structure of valproic acid. Carbon atoms 1 and 2 are labelled in blue with the location of the α - hydrogen shown in green. Teratogenic compounds contain an α - hydrogen atom, branching on carbon 2 and a free carboxyl group.

1.1.3 Studies Investigating the Mechanism of Action of VPA

Despite the side effects, VPA is one of the most highly prescribed AEDs (37.8 %) (Haroon, et al., 2012). For this reason, many studies have been conducted to determine the mechanism of action of VPA. These studies have shown VPA to work through enhancing brain γ -amino butyrate levels (Godin, et al., 1969); NMDA excitation (Slater, Stelzer and Galvan, 1985; Holmes, et al., 1990; Zeise, Kasparow and Zieglgänsberger, 1991); inhibiting voltage gated potassium, sodium and calcium channels (VanDongen, VanErp and Voskuyl, 1986; Kelly, Gross and Macdonald, 1990); histone deacetylase (Göttlicher, et al., 2001); and reducing inositol

phosphate and phosphoinositide levels (Williams, et al., 2002; Eickholt, et al., 2005; Chang, et al., 2012; Chang, Walker and Williams, 2014). VPA reduces phosphoinositide levels in both a time and dose-dependent manner, independent of PI-3-kinase (PI3K) activity, inositol recycling, *de novo* inositol production and *de novo* inositol biosynthesis (Chang, et al., 2012; Frej, et al., 2016). This leaves the PI salvage pathway as potentially containing the molecular target of VPA.

1.2 Phosphatidylinositol Salvage Pathway

1.2.1 Phosphoinositides

Phosphoinositides are minor lipid molecules belonging to the acidic phospholipid family of proteins, with cellular membranes comprising of 2-12 % PI (Flint, et al., 1986; Falkenburger, et al., 2010). Phosphoinositides consists of 2 fatty acid tails attached to a glycerol backbone through ester linkages. To the glycerol backbone, an inositol head in the *myo*- conformation is attached via a phosphate group which extends into the cytoplasm (**Figure 1.3**). The inositol used in the synthesis of phosphoinositides comes from either the diet, the *de novo* pathway or from the PI salvage pathway (Saul, et al., 2004). Phosphorylation events occur by cytoplasmic lipid kinases which utilize the free oxygen atoms on the *myo*-inositol group (Falkenburger, et al., 2010).

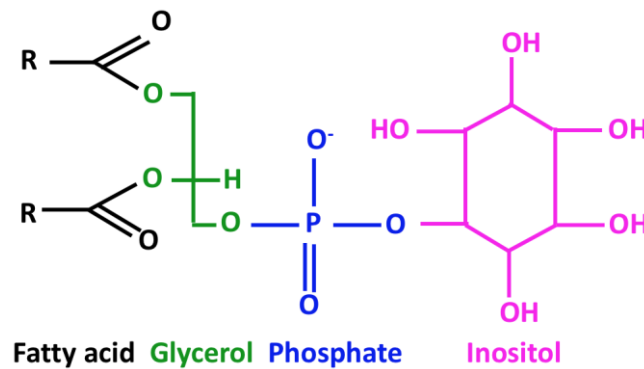


Figure 1.3. Schematic of the generalized chemical structure of phosphoinositides.

Schematic of the generalized chemical structure of phosphoinositides showing the fatty acid groups (black) with the “R” groups indicating the locations of the fatty acid chains, the glycerol group (green), the phosphate groups (blue) and the inositol ring (pink).

Both the *de novo* PI pathway and the PI salvage pathway cross over in the utilization of phosphatidic acid (PA), which is synthesized within the plasma membrane (Nuwayhid, et al., 2006). The *de novo* pathway utilizes glucose to produce PA via the production of the intermediates dihydroxyacetone phosphate and glycerol phosphate (Paulus and Kennedy, 1960; Katz and Wood, 1960; Prottey and Hawthorne, 1967). The PI salvage pathway regulates the long-term supply of the signalling molecule PI-4,5-bisphosphate (PIP₂) through its synthesis and hydrolysis (Paulus and Kennedy, 1960; Prottey and Hawthorne, 1967; Whatmore, et al., 1999).

1.2.2 Phosphatidylinositol Salvage Pathway

The PI salvage pathway involves the hydrolysis of PIP₂ into IP₃ and DAG by PLC within the plasma membrane (**Figure 1.4**). This creates a branch point in the salvage pathway, whereby IP₃ is dephosphorylated into inositol-1,4-bisphosphate (IP₂), inositol-4-phosphate (IP) and then *myo*-inositol (I) by the enzymes 5-phosphatase (type 1) (5’P), inositol polyphosphatase (IPPase) and inositol monophosphatase (IMPase), respectively. Meanwhile, DAG is phosphorylated into PA by DAG kinase (DGK). PA then moves across the cytosol from the plasma membrane to the endoplasmic reticulum where it is involved in a condensation reaction with cytidine

triphosphate (CTP) to form CDP-DAG, catalysed by the enzyme CDP-DAG synthase (CDS). CDP-DAG and *myo*-inositol are converted into PI by CDP-DAG-inositol 3-phosphatidyltransferase (CDIPT). PI is then transferred to the plasma membrane by a PI-transfer protein (PIPT) where it is phosphorylated into PI-4-phosphate (PIP) and PIP₂ by PI kinase and PIP kinase respectively, thereby restarting the cycle (Paulus and Kennedy, 1960; Prottey and Hawthorne, 1967; Whatmore, et al., 1999). A rate-limiting step in this pathway is the conversion of PA into CDP-DAG as the PA pool is larger than that of the intermediate CDP-DAG (Raetz and Kennedy, 1973).

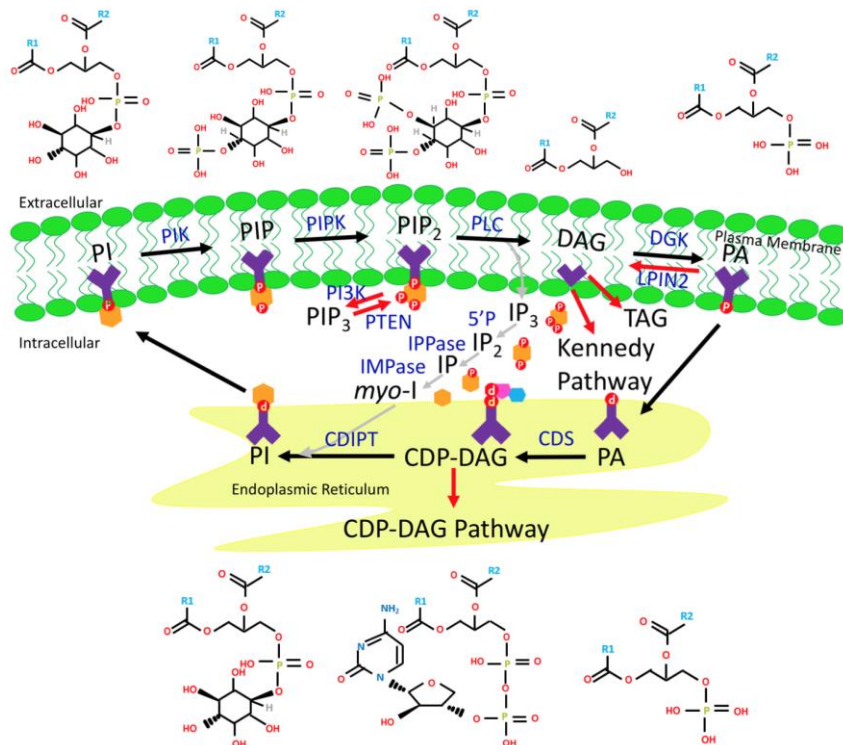


Figure 1.4. Schematic of the phosphatidylinositol salvage pathway and interlinking pathways.

Schematic of the phosphatidylinositol (PI) salvage pathway (black arrows), inositol recycling (grey arrows) and interlinking pathways. The locations of each reaction step within the plasma membrane (green) and endoplasmic reticulum (yellow) with the names of the reaction product (black) and enzymes (yellow) given. The chemical structures of each component of the pathway are shown above or below the product name with the “R” groups indicating the fatty acid chains. Phosphatidylinositol-4,5-bisphosphate (PIP₂) is dephosphorylated by phospholipase C (PLC) into diacylglycerol (DAG) and inositol-1,4,5-trisphosphate (IP₃). IP₃ is then dephosphorylated into inositol-1,4-bisphosphate (IP₂) by 5-phosphatase (type 1) (5’P), inositol-4-phosphate by inositol polyphosphatase (IPPase) and *myo*-inositol by inositol monophosphatase (IMPase). Meanwhile, DAG is phosphorylated into phosphatidic acid (PA) by DAG kinase (DGK). PA is then converted into cytidine diphosphate-DAG (CDP-DAG) by

CDP-DAG synthase in a rate-limiting step before being converted into phosphatidylinositol (PI) by CDP-diacylglycerol-inositol 3 phosphatidyltransferase (CDIPT). PI is then phosphorylated into phosphatidylinositol-4-phosphate (PIP) by phosphatidylinositol kinase (PIK) and into PIP₂ by phosphatidylinositol-4-phosphate kinase (PIPK). Interlinking with the salvage pathway is a redox reaction between the phosphorylation of PIP₂ into PIP₃ by PI-3-kinase (PI3K) and the dephosphorylation of PIP₃ into PIP₂ by phosphatase and tensin homolog (PTEN). Phosphatidate phosphatase LPIN2 (LPIN2) dephosphorylates PA into DAG, which is a substrate for triacylglycerol (TAG) synthesis and the Kennedy pathway. CDP-DAG is utilized during the PI salvage pathway and the CDP-DAG pathway.

1.3 Proteins of Interest

1.3.1 Interacting Signalling Pathways

A number of pathways interact with the PI salvage pathway, including PI3K signalling, the Kennedy pathway and the CDP-DAG pathway. From these pathways, PKC activity is regulated through components of the PI salvage pathway (DAG) and CDP-DAG pathway (cardiolipin). Of the PI salvage pathway and interacting pathways, there are 7 key enzymes involved in regulating phosphoinositide levels. These are PI3K, phosphatase and tensin homolog (PTEN), PLC, phosphatidate phosphatase LPIN2 (LPIN2), CDS, CDIPT and DGK. All of these proteins have been associated with epilepsy and AED research. Seizure generation and development has been linked to both the PI3K/PI-3,4,5-trisphosphate(PIP_3)/Akt (Akt is also known as serine -threonine protein kinase and the protein kinase B) (Backman, et al., 2001; Shinoda, et al., 2004) and mammalian target of rapamycin (mTOR) pathways (Takei, et al., 2004; Ehninger, et al., 2008; Zeng, et al., 2008; van Vliet, et al., 2012), which are regulated through PI3K/ PTEN and LPIN2 signalling respectively (Jaworski, et al., 2005; Kumar, et al., 2005; Meikle, et al., 2008).

PI salvage pathway proteins have also been linked with epilepsy, BD and VPA treatment of these two disorders. Mutations within PLC (Kurian, et al., 2010) and a number of DGK isoforms (DGK- β , - δ and - ϵ) have been linked with epilepsy (Rodriguez de Turco, et al., 2001; Leach, et al., 2007; Tokuoka, Saiardi and Nurrish, 2008; Ishisaka, et al., 2013), with DGK- β and - η also being associated with BD (Baum, et al., 2008; Squassina, et al., 2009; Kakefuda, et al., 2010). Additionally, during VPA treatment, the levels of CDP-DAG and phosphatidylglycerol (PG) are significantly increased, suggesting a role of the enzyme CDS in the mechanism of action of the drug (Ju and Greenberg, 2003). These proteins are important due to the range of signalling pathways the reaction products regulate.

1.3.1.1 PI3K Signalling

Levels of the signalling molecule PIP₂ can be maintained through the PI salvage pathway via the phosphorylation of PIP₂ and by the dephosphorylation of PIP₃. PIP₂ is phosphorylated into PIP₃ by PI3K to activate a number of pathways including actin reorganisation (Arcaro and Wymann, 1993), chemotaxis (Wennstroem, et al., 1994), glucose uptake (Hara, et al., 1994), mitosis and cell growth and survival through Akt (Fantl, et al., 1992; Burgering and Coffey, 1995; Franke, et al., 1995). PIP₃ signalling is reduced by dephosphorylation into PIP₂ by PTEN.

1.3.1.2 DAG Signalling

DAG regulates a number of signalling pathways including PKC (van Baal, et al., 2005), synaptic plasticity (Lee, Kim and Tanaka-Yamamoto, 2016) and the synthesis of triglycerides, PC and PE (Kennedy and Weiss, 1956; Gibellini and Smith, 2010). PC and PE are synthesised through the Kennedy pathway (Kennedy and Weiss, 1956; Gibellini and Smith, 2010). The Kennedy pathway begins as a branch point of the PI salvage pathway, bypassing the formation of PA from DAG catalysed by DGK. In this pathway, PA is dephosphorylated into DAG by the enzyme LPIN2. DAG is then converted directly into PC by the enzyme choline phosphotransferase or indirectly into PE via ethanolamine phosphotransferase and then into PC. Phospholipase D (PLD) then catalyses the formation of PA from PC (Kennedy and Weiss, 1956; Henneberry and McMaster, 1999). The Kennedy pathway is essential for neuronal function and mammalian development (Ahmed, et al., 2017).

1.3.1.3 PA Signalling

PA is an important signalling molecule involved in cell proliferation (Banfić, et al., 1993; Cerbón, et al., 2005), lipid metabolism (Milne, et al., 2008) and calcium signalling (Carpio and Dziak, 1998). In addition, PA is a precursor of DAG via PLD and therefore a regulator of PKC. The involvement of PA in cell proliferation is via the platelet derived growth factor and epidermal growth factor (Fukami and Takenawa, 1992; Kaszkin, Richards and Kinzel, 1992). A rise in PA is correlated with accumulation of calcium which activates PLC and PLD (Kawase and Suzuki, 1990; Bourgoin, Harbour and Poubelle, 1996). PA accumulation has also been associated

with high levels of glucose (Farese, et al., 1986) and insulin secretion (Ma, Park and Han, 2010) via PLD.

1.3.1.4 CDP-DAG Signalling

CDP-DAG is an intermediate molecule used to synthesise PI within the PI salvage pathway and PG and phosphatidylserine (PS) within the CDP-DAG pathway (Paulus and Kennedy, 1960; Kiyasu, et al., 1963; Kanfer and Kenendy, 1964). PG is used to synthesise cardiolipin (Lecocq and Ballou, 1964), which has a role in mitochondria morphology (Xu, et al., 2006), thereby effecting the electron transport chain (Fry and Green, 1981) and the respiratory burst (Paradies, et al., 2004); and calcium (Kamer, Grabarek and Mootha, 2017) and PKC (Nobori, et al., 1987) signalling.

1.3.2 Potential Novel Targets of VPA

Proteins which have not previously been investigated as potential targets of VPA are the PI salvage pathway components CDS, CDIPT and DGK.

1.3.2.1 CDS

CDS is an integral membrane protein whose activity occurs at the cytoplasmic side of the endoplasmic reticulum for the synthesis of PI and at the inner mitochondrial matrix for PG and cardiolipin (Thompson and MacDonald, 1975; Kuchler, Daum and Paltauf, 1986; Shen, et al., 1996; Henry, Kohlwein and Carman, 2012; Lilley, et al., 2014). CDS is activated by potassium ions, with enzyme activity dependent on magnesium (Nigou and Besra, 2002). Higher organisms contain multiple isoforms of CDS which differ in their substrates, i.e. CDS1 has no isomeric preference for its lipid target, whereas CDS2 targets lipids with acyl groups at positions *sn1* and *sn2* of the glycerol molecule (D'Souza, et al., 2014).

1.3.2.2 CDIPT

CDIPT is the protein responsible for the synthesis of PI within the endoplasmic reticulum plasma membrane and whose activity depends on magnesium ions (Agranoff, Bradley and Brady, 1958; Paulus and Kennedy, 1960). CDIPT was first discovered in the late 1950s and has since been found to be highly conserved

among many organisms (Agranoff, Bradley and Brady, 1958; Paulus and Kennedy, 1960; Lykidis, et al., 1997; Lilley, et al., 2014).

1.3.2.3 DGK

DGKs are a family of enzymes which resides in the cytosol until activation is required at the plasma membrane. There are 5 types of DGK isoenzymes, divided according to the presence of specific protein domains. All DGKs contain 2 or 3 phorbol-ester/ DAG type 1 binding domains which is followed with the catalytic site. Type 1 DGKs (DGK- α , - β and - γ) have a recoverin homology domain and EF hand motifs, whereas type 2 (DGK- δ , - η , - κ) have pleckstrin homology domains. Type 3 DGKs (DGK- ϵ) contain arachidonate- DAG domains, whereas type 4 (DGK- ζ and - ι) have PDZ and ankyrin repeat (ANK) domains and type 5 (DGK- θ) contain 3 phorbol-ester/ DAG type 1 binding domains and Ras associating domains. The DGK isoenzymes are tissue specific, with DGK- α , - β , - γ , - ϵ , - ζ , - η , - θ and - ι being predominantly found within the central nervous system (Tu-Sekine and Raben, 2011).

1.4 *D. discoideum* as an Alternative Model

Dictyostelium discoideum is a well-established non-animal model, listed by the National Institute of Health (Drayer, et al., 1994; Abu-Elneel, Karchi and Ravid, 1996; Keizer-Gunnink, Kortholt and van Haastert, 2007; Couto, et al., 2011; Cunliffe, et al., 2014; Rakhimova, et al., 2017; National Institute of Health, 2017). *D. discoideum*, like the model organism zebrafish, can be used to screen potential therapeutic treatments and identify the mechanism of action of drugs, including AEDs (Terbach, et al., 2011; Chang, et al., 2012; Mahmood, et al., 2013).

D. discoideum belongs to the Dictyostelia class of Mycetozoa phylum. *D. discoideum* is an excellent model for biomedical research as isogenic (from a single cell) cell lines can be cultured with ease and the effects of drugs can be visualised by changes in cell behaviour, e.g. in studying cell motility, signalling and differentiation and the mechanism of action of epilepsy and BD treatments (Williams, et al., 2002;

Eickholt, et al., 2005; Williams, 2005; Elphick, et al., 2012; Chang, et al., 2012). The haploid eukaryote *D. discoideum* consists of a single cell with a genome of approximately 11,000 genes, of which, 33 % are found in humans (Williams, 2005). *D. discoideum* contains six chromosomes which accounts for a genome size of 34 Mb and a mitochondria genome of 54 Kb (Cole and Williams, 1994; Kuspa and Loomis, 1996). There are a high number of adenine and thymine base pairs (average of 60-70 % adenine and thymine in protein coding and 80-95 % in non-coding regions) (Escalante and Vicente, 2000). *D. discoideum* is a monophyletic organism whose genes are further away from plants and fungi and closer to vertebrates (**Figure 1.5**).

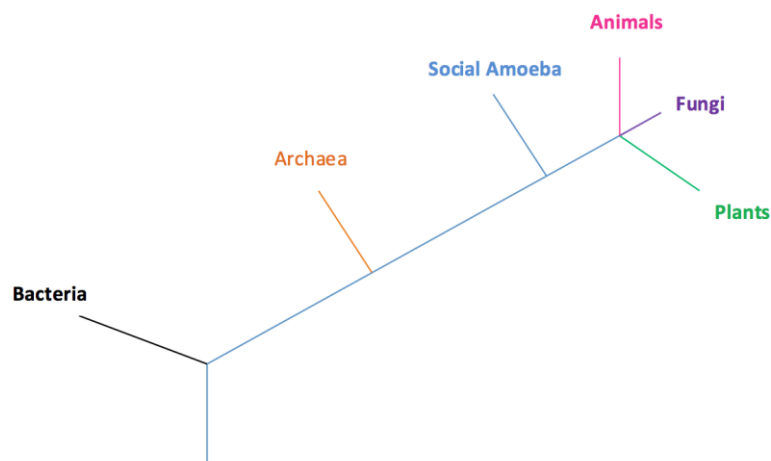


Figure 1.5. Schematic tree of life showing the relationship of different biological kingdoms. Schematic tree of life showing the evolution from bacteria, archaea, social amoeba, animals, fungi and plants.

1.4.1 Developmental Cycle

D. discoideum was discovered in 1935 and is naturally found within soil where it survives on micro-organisms by phagocytosis, or, as in the laboratory, on liquid media by micropinocytosis (Raper, 1935; Williams, et al., 2006). *D. discoideum* replicates every 8-10 hours by binary fission, which stops during times of starvation and switches to the start of the multicellular developmental cycle (**Figure 1.6**). The development cycle can be divided into two stages- the aggregation phase and the post-aggregation phase. The developmental cycle involves programmed gene

expression and morphogenesis and is initiated when cyclic-adenosine-3,5-cyclic monophosphate (cAMP) is released in pulses from the amoeba 4 hours after the onset of starvation (Parent and Devreotes, 1996; Williams, 2005). cAMP is produced at 6 minute intervals and is degraded between pulses by extracellular phosphodiesterase. Individual *D. discoideum* cells migrate towards the site of cAMP by chemotaxis where they group together to form a mound of approximately 10^5 cells at a single point, 10 hours after starvation. Chemotaxis occurs as cAMP binds to G- protein coupled receptors (primarily cAR1) which initiates F-actin polymerization (increased by 80 % within 2 seconds of cAMP exposure) and pseudopodium extension towards the highest cAMP concentration at the front of the cell (Wessels, et al., 1989). At the back end of the cell, myosin filaments are formed. These cellular changes occur through the release of the second messages cAMP, cyclic guanosine monophosphate, phospholipid methylation and calcium (Mato, et al., 1977; Mato and Marin-Cao, 1979). Within the mound, cell-to-cell interactions are initiated by cell adhesion molecules (Xu, et al., 2014). This signal is relayed to the more distant cells, initiating their movement towards the mound. As the mound forms, the cells become more compact until multicellular differentiation occurs by cAMP induced transcription factor activation. At this stage, the cells differentiate into either a pre-stalk and pre-spore cell, before forming either a stalk or spore cell, which together form the multicellular fruiting body. Differentiation into one of the two cellular subtypes depends on what stage of the cell cycle individual cells were at on the onset of starvation and through the action of ammonia, adenosine and the differentiation-inducing growth factor. Once a tight mound has formed, the different cell types reorganise so that the spore cells are at the tip of the structure, causing elongation into a finger-like shape. The top 20 % of the finger-structure contains pre-stalk cells and consists of a subpopulation of pre-stalk A at the anterior end, extracellular matrix protein B in the middle and pre-stalk O at the posterior end (Escalante and Vicente, 2000). Throughout the finger-like structure anterior-like cells (ALC) are present. ALCs either express no markers, or one or both extracellular matrix protein A and extracellular matrix protein B expression. ALCs move both up and down the finger-like structure to form the upper cup or lower cup that surrounds the sporus/ spore head respectively, and the

basal disc. Pre-spores are located at the posterior end of the finger. Once in the finger structure, cells either form a slug or differentiate further into a fruiting body.

Under unfavourable conditions (absence of heat or light), partially differentiated stalk (15 %), spore (75 %) and ALCs (10 %) located in the pre-spore region undergo an extra step in the developmental cycle where they form a multicellular migratory organism called a slug (Smith and Williams, 1981; Wilkins and Williams, 1995). The slug has a dense epithelium-like layer, at a thickness of a few cells, which is able to migrate through the continuous synthesis of an extracellular protein and cellulose matrix, termed a slime sheath. During movement to a more advantageous spot for spore formation and dispersal, this slime sheath is lost (Newell, Telser and Sussman, 1969). Once migration stops, these partially differentiated cells fully develop into stalk or spore cells and then form a fruiting body. If a slug is not formed, the finger-like structure continues culmination and forms a Mexican hat and mid culminant structures before forming a fruiting body.

The formation of a 1 mm high fruiting body marks the end of the developmental cycle and arises after cell differentiation and morphogenetic cell movement. The fruiting body consists of a cellulose covered basal disc, a stem of 20,000 vacuolated dead stalk cells on which 80,000 spore cells are supported. Once conditions become favourable again, the spores can germinate and survive as unicellular cells.

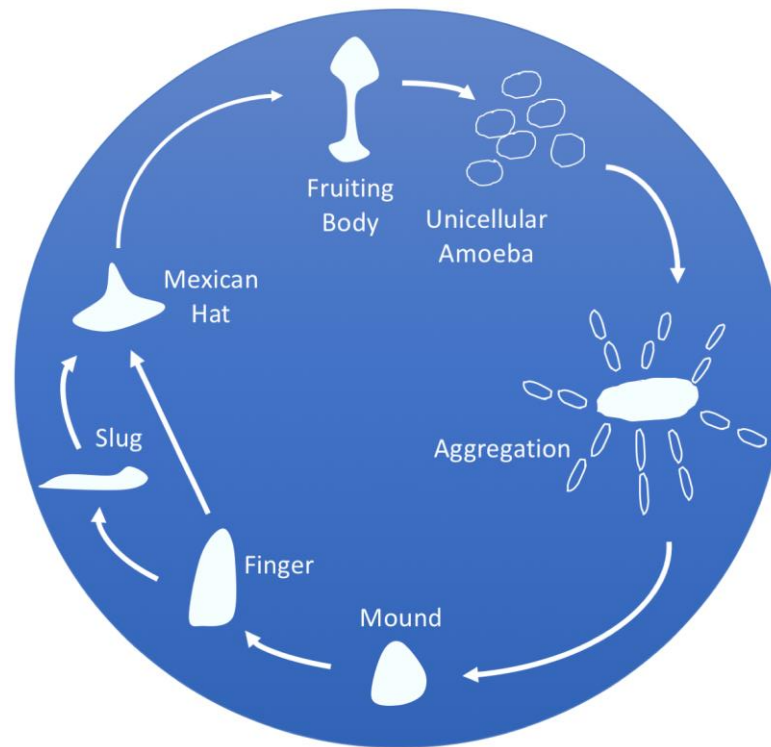


Figure 1.6. Schematic of the *D. discoideum* developmental cycle. Schematic of the *D. discoideum* developmental cycle whereby unicellular vegetative cells migrate together to form a multicellular fruiting body over 24 hours. The intermediate structures formed are shown and labelled in the figure.

It is the ability of *D. discoideum* to exist as a single cell and form a multicellular fruiting body which makes the amoeba a suitable non-mammalian model for biomedical research. At the unicellular stage the amoeba can be transformed, whereby specific genes of interest can be manipulated and grown rapidly. The formation of the homologous cell fruiting body requires a number of signalling events which are common to those found in vertebrates (Williams, 2005). For this reason, the effect of drugs on individual pathways can be investigated using *D. discoideum* as a model organism.

1.4.2 Methodology

Previous studies using *D. discoideum* as a model to determine the molecular action of therapeutic drugs has involved the ablation and overexpression of specific genes

of interest (Terbach, et al., 2011; Chang, et al., 2012; Frej, et al., 2016). These mutant cell lines are then phenotypically characterized in both the absence and presence of a drug of interest during cell growth, acute cell behaviour (random cell movement) and development. If the null cell line shows resistance to the drug, i.e. the calculated value of 50 % inhibition (IC_{50}) is approximately double that of wild type (WT) cells, the gene ablated is then reintroduced, creating rescue cells. Phenotypic characterization is then repeated to ensure drug resistance is due to the ablated gene by drug-sensitivity being restored in the rescue cell line.

1.4.2.1 *Gene manipulation*

To identify a target of VPA, genes of interest within the PI salvage pathway were first identified (**Figure 1.7A** and **Figure 1.8A**). These genes were then ablated or overexpressed by creating recombinant plasmids (**Figure 1.7B** and **Figure 1.8B**). To ablate a gene, two open reading frame regions of the gene of interest are polymerase chain reaction (PCR) amplified from genomic DNA and cloned into a vector on either side of an antibiotic resistance gene, creating a knockout cassette. This knockout cassette contains the two PCR gene fragments and the antibiotic resistance gene. The plasmid is then sequenced to ensure that there are no errors in the two gene fragments. This knockout cassette is then digested out from the recombinant plasmid using restriction enzymes and electroporated into WT *D. discoideum* cells. Transformant cells are then selected by growth in the presence of an antibiotic determined by the resistance gene. PCR screening is then conducted on surviving cell colonies to determine homologous recombinant cells which contain a correctly inserted knockout cassette, as this results in a truncated protein, interrupted by the presence of the antibiotic resistance gene and loss of part of the coding sequence. PCR screening is then conducted and involves 3 sets of primers for the 5'- and 3'- terminus of the gene of interest (**Figure 1.7C**). The first primer set are genomic control (G) primers which confirm the presence of the 2 PCR gene fragments and is present in both WT and transformant cells. The second primer set are vector control (V) primers which confirm the gene fragment is adjacent to the antibiotic resistance gene and so is only present in transformant cells. The third primer set is the knockout diagnostic (K) which confirms the gene of interest is

interrupted by the antibiotic resistance gene at the 5' and 3' gene terminus and has a portion of the amino acid sequence removed. A PCR band for the knockout diagnostic is only present in homologous recombinant cells. When a knockout diagnostic band is identified at both the 5' and 3' gene terminus, isogenic homologous recombinant cell lines are then produced and confirmed as a knockout cell line by PCR amplifying a region of the deleted gene by reverse transcriptase (RT)-PCR. Isogenic knockout cells are then used for phenotypic characterization in both the absence and presence of VPA (**Figure 1.7D**).

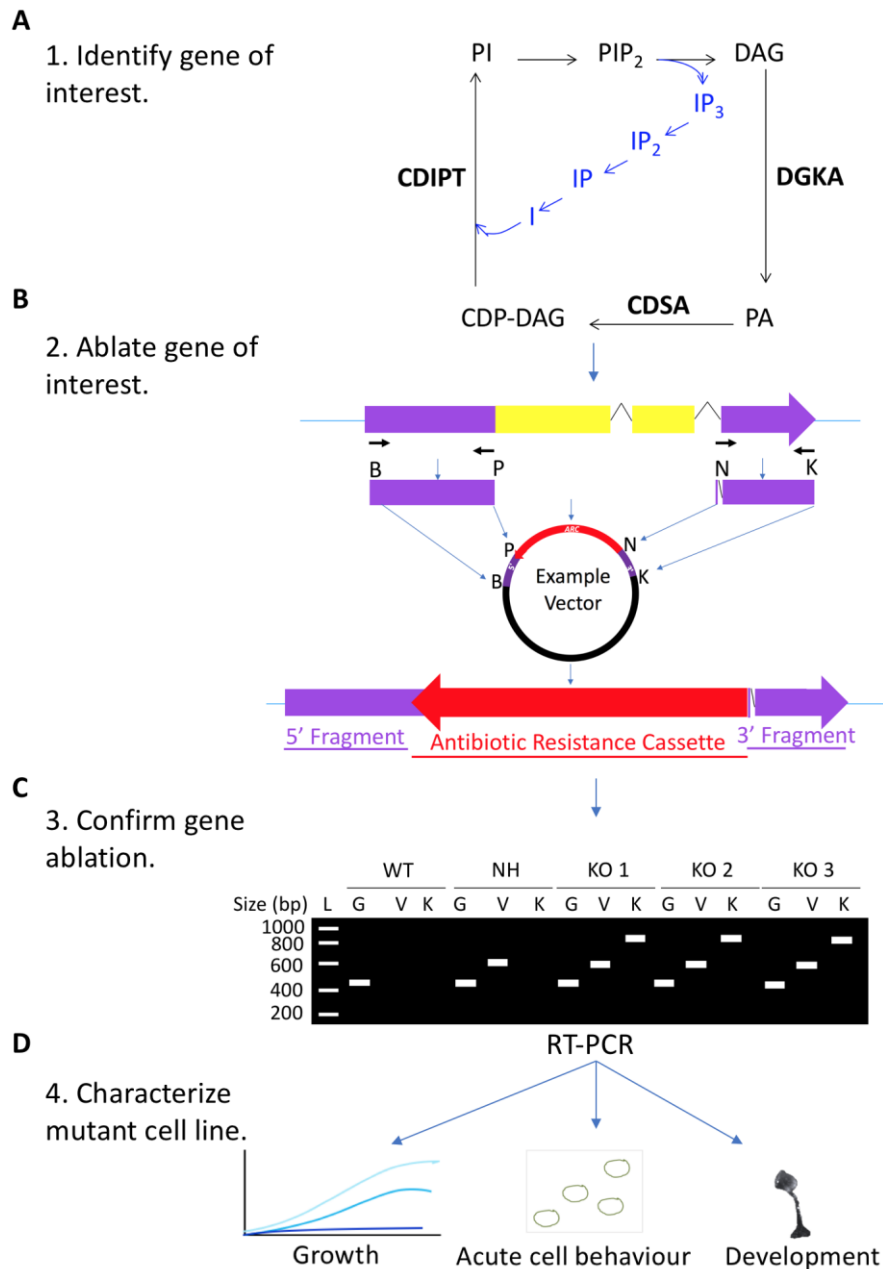


Figure 1.7. Schematic of the gene ablation protocol resulting in the characterization of mutant cells. Schematic of gene ablation procedure where (A) genes of interest are identified within the phosphoinositide salvage pathway. Genes are then cloned into (B) knockout vector and electroporated into WT cells. Resulting isogenic transformant cell lines are confirmed by (C) RT-PCR screening using primers for genomic (G) and vector (V) control and knockout diagnostic (K). Confirmed transformant cells are then (D) phenotypically characterized in both the absence and presence of VPA during cell growth, acute cell behaviour and development. Each step is shown to the far left of the figure.

To overexpress or reintroduce an identified gene of interest in *D. discoideum*, the entire gene sequence is PCR amplified from coding DNA (cDNA) (**Figure 1.8A**). The cDNA PCR product is then cloned into a plasmid adjacent to a fluorescent tag, e.g. green or red fluorescent protein (GFP or RFP respectively) (**Figure 1.8B**). The overexpression plasmid is then sequenced to ensure there are no errors in the PCR gene fragment. The overexpression plasmid is then electroporated into WT or null cells and selected by growth in the presence of an antibiotic determined by the resistance gene present on the plasmid. Expression of the fluorescently-tagged protein of interest is then confirmed by Western blot and fluorescence microscopy (**Figure 1.8C**). Once confirmed, the overexpressing cells are used for phenotypic characterization in both the absence and presence of VPA (**Figure 1.8D**).

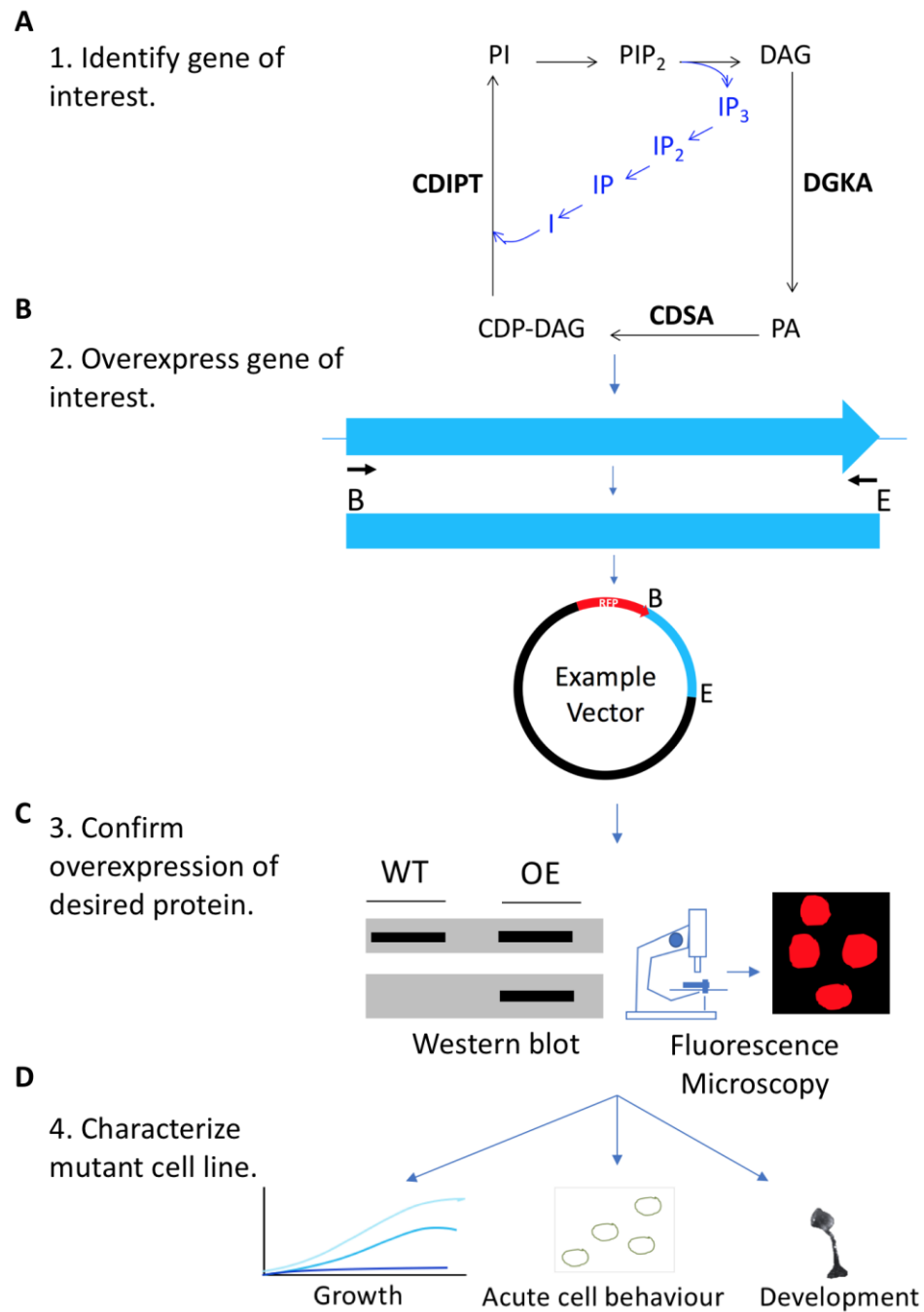


Figure 1.8. Schematic of the gene overexpression protocol resulting in the characterization of mutant cells. Schematic of the gene overexpression procedure where (A) genes of interest are identified within the phosphoinositide salvage pathway. Genes are then cloned into an (B) overexpression vector containing a fluorescent tag and electroporated into WT cells. Resulting transformant cells are then confirmed by (C) Western blot and fluorescence microscopy. Confirmed cells are then (D) phenotypically characterized in both the absence and presence of VPA during cell growth, acute cell behaviour and development. Each step is shown to the far left of the figure.

1.4.3 Identifying the Target of VPA

Potential molecular targets of VPA can be identified by the phenotypic characterization of mutant cells in both the absence and presence of VPA. Characterization involves comparing the effects of VPA on cell growth (Terbach, et al., 2011), acute cell behaviour (Xu, et al., 2007) and development (Williams, et al., 2002), as VPA has previously been shown to inhibit these processes. If mutant cells are resistant to VPA during cell growth, cells will proliferate at a similar rate to that of control conditions when exposed to the drug. However, if cells proliferate at a slower rate when exposed to VPA compared with control conditions, when cells are not exposed to the drug, then the cells are drug- sensitive. VPA resistance and sensitivity will be illustrated in a secondary plot which compares the rate of cell growth between WT and mutant cells in the presence of increasing VPA concentrations. The secondary plot is used to calculate an IC_{50} value for each cell line.

During acute cell behaviour, cell displacement, circularity, membrane protrusions and motility are measured (**Figure 1.9**). Cell displacement is the shortest distance a cell travels from point A to point B (**Figure 1.9A**). Circularity is a measure of cell shape (**Figure 1.9B**). Membrane protrusions are extensions of the cell membrane which enables a cell to elongate and move forward (**Figure 1.9C**). Motility is the speed at which a cell has travelled (**Figure 1.9D**). If mutant cells are resistant to VPA, the overall calculated distance travelled by each individual cell and the average value for circularity, number of membrane protrusions and motility will be similar to control conditions when no drug was added. However, if cells are drug-sensitive, cell displacement will be lower than control conditions and there will be a decrease in the average number of membrane protrusions and speed, correlated with an increased value for circularity, which is a measure of cell rounding. VPA sensitivity or resistance will be shown in the secondary plots, which will compare either total displacement or average circularity, membrane protrusions and motility within the final 300 seconds of the assay with increasing VPA concentrations. An IC_{50} value will be calculated for each cell line for displacement, average membrane protrusions and motility.

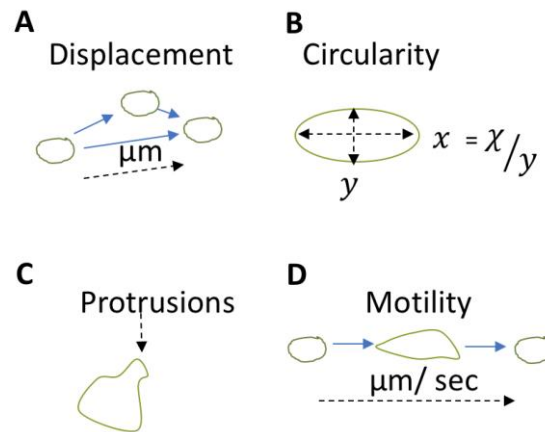


Figure 1.9. Schematic of measurable acute cell behaviour criteria. Schematic of the measurable acute cell behaviour criteria displacement (shortest distance a cell travels between two points), circularity (a measure of cell shape, with round cells given a value of “1”), membrane protrusions (number of cell membrane extensions) and motility (speed).

VPA treatment has previously been shown to inhibit *D. discoideum* development at the mound stage (Williams, et al., 2002). Therefore, if a mutant cell line is resistant to VPA, multicellular fruiting bodies resembling control conditions will develop when exposed to the drug. If cells are VPA-sensitive, cell development will mimic that of WT cells and not develop into mature fruiting bodies containing a basal disc, stalk and spore head.

1.5 Aims and Specific Objectives

The aim of this PhD thesis, therefore, is to investigate whether the PI salvage pathway contains the molecular target(s) of VPA using *D. discoideum* as a model organism. If successful, new AEDs can be developed around this target which have a similar potency to VPA but without the side effects of teratogenicity and hepatotoxicity, by altering the drugs chemical structure. Identifying molecular targets of VPA will be achieved by investigating the interlinking pathways and individual components of the PI salvage pathway.

Previous studies investigating PLC and all 5 *D. discoideum* PI3K and PTEN (*pi3k1-5*/*pten*⁻) in response to VPA did not characterize the effect of the drug on acute cell behaviour and development (Chang, et al., 2012). For this reason, *D.*

discoideum *pi3k1-5⁻/pten⁻* of the PI3K pathway and *plc⁻* and *lpin2⁻* of the PI salvage pathway were initially investigated as potential targets of VPA, along with other anti-seizure compounds and the bipolar disorder treatment lithium chloride (LiCl). Conservation of CDS, CDIPT and DGK proteins from *D. discoideum* and a range of other organisms was then investigated. *D. discoideum* PI salvage pathway proteins CDSA, CDIPT and DGKA were then either ablated or overexpressed. The resulting mutant cells were phenotypically characterized in both the absence and presence of VPA and the other anti-seizure compounds and the BD treatment LiCl.

Chapter 2

Materials and Methods

2. Materials and Methods

2.1 Materials

2.1.1 General Reagents

2.1.1.1 Reagents from Sigma-Aldrich (Gillingham, Dorset, U.K.)

1,2-Dioleoyl-sn-glycero-3-phospho-rac-(1-glycerol) sodium salt, 2-mercaptoethanol, 4-ethyloctanoic acid (4-EOA), acetic acid, ammonium persulfate (APS), bacteriological agar, bovine serum albumin (BSA), cyclic adenosine monophosphate (cAMP), ethylenediaminetetraacetic acid (EDTA), HEPES, horse serum, L- α -PI from Glycine max (soybean), LiCl (8 mM), Immobilon-FL polyvinylidene fluoride (PDVF) transfer membrane, Lurina broth (LB) tablets, magnesium chloride, magnesium sulphate, N'N'N'N'- tetramethylethylenediamine (TEMED), phosphatase inhibitors, potassium acetate, potassium chloride, sodium acetate, sodium chloride, sodium dihydrogen phosphate, sodium dodecyl sulphate polyacrylamide (SDS), sodium hydroxide, Tris base, Tris buffered saline with tween (TBS-T), Tween-20, VPA and water came from Sigma-Aldrich (Gillingham, Dorset).

2.1.1.2 Reagents from Other Suppliers

2-methylhexanoic acid (2-MHA), DA and OA (Alfa Aesar, Heysham, U.K.).
2-(propan-2-yl)pentanoic acid (propylisopropylacetic acid, PIA) and VPD (Meir Bialer, The Hebrew University of Jerusalem, Israel).
Ethidium bromide and 2X Laemeli sample buffer (Bio-Rad, Hemel Hempstead, U.K.).
5x loading dye, agarose, ammonia buffer, deoxynucleotides (dNTPs) and magnesium chloride (MgCl₂) (Bioline, London, U.K.).
Axenic media, LoFlo medium and SM medium (Formedium, Norfolk, U.K.).
SM agar (Gibco, Paisley, U.K.).
Protogel 30 % solution (National Diagnostics, Nottingham, U.K.).
Tris-borate-EDTA (TBE) buffer (Severn Biotech Ltd, Kidderminster, U.K.).
Fluoromount-G, glycine, TBS-T, Tris pH 6.8 and Tris pH 8.0 (Thermo Fisher Scientific, Hemel Hempstead, U.K.).

Acetic acid, bromophenol blue, ethanol, dimethyl sulfoxide (DMSO), glucose, glycerol, hydrochloric acid, methanol, paraformaldehyde and propan-2-ol (VWR, Lutterworth, U.K.).

2.1.1.3 Antibiotics

Penicillin- streptomycin (PenStrip) (Gibco, Paisley, U.K.).

Blasticidin (PAA Laboratories Ltd, Somerset, U.K.).

Ampicillin (Sigma Aldrich, Gillingham, Dorset, U.K.).

Geneticin and hygromycin (Thermo Fisher Scientific, Hemel Hempstead, U.K.).

2.1.1.4 Molecular Weight Standards

Hyperladder 1 kb (Bioline, London, U.K.).

PageRuler Plus Pre-stained Protein Ladder (Thermo Fisher Scientific, Hemel Hempstead, U.K.).

2.1.1.5 Enzymes and Corresponding Buffers

BioTAQ Polymerase (Bioline, London, U.K.).

*Hind*III and thermosensitive alkaline phosphatase (TSAP) (Promega, Southampton, U.K.).

Q5 DNA polymerase (New England Biolabs, Hitchin, U.K.).

*Bam*HI, DNase, *Eco*RI, *Kpn*I, *Nco*I, Proteinase K, *Pst*I and T4 DNA ligase (Thermo Fisher Scientific, Hemel Hempstead, U.K.).

RNase A (Sigma- Aldrich, Gillingham, U.K.).

2.1.1.6 Antibodies

3H9-GFP and 6G6-RFP (ChromoTek, Planegg, Germany).

Calreticulin and myosin II heavy chain (MHC) primary antibody (Developmental Studies Hybridoma Bank, Iowa, U.S.).

IRDye 800 Goat Anti-Mouse and IRDye 800 Goat Anti-Rat (LI-COR Bioscience, Nebraska, U.S.).

Streptavidin (MccA/ MCCR1) (Thermo Fisher Scientific, Hemel Hempstead, U.K.).

2.1.1.7 Kits

General Diacyl Glycerol, DAG/ DG enzyme linked immunosorbent assay (ELISA) Kit (Amsbio, Abingdon, U.K.).

DNeasy Blood and Tissue kit, HiSpeed Plasmid Purification kit, QIAquick Gel Extraction kit, QIAquick PCR Purification kit and RNeasy Mini kit (Qiagen, West Sussex, U.K.).

DNase Treatment Removal kit and First Strand cDNA Synthesis kit (Thermo Fisher Scientific, Hemel Hempstead, U.K.).

2.1.1.8 *Escherichia coli* Strain

Chemically competent *Escherichia coli* (*E. coli*) JM107 cells (Invitrogen, Gröningen, Netherlands).

2.1.1.9 Primers

All primers were custom made and purchased from Sigma-Aldrich (Gillingham, Dorset, U.K.) (**Supplementary Table S1**).

2.1.1.10 Equipment

Bio-Rad gel casting system, Bio-Rad gel doc 2000, Bio-Rad GenePulser Xcell electroporator, Bio-Rad Power Pack 300, Bio-Rad wide mini-sub cell electrophoresis system and BioRad Mini-PROTEIN Tetra Cell (Bio-Rad, Hemel Hempstead, U.K.).

Airstream ESCO class II biological safety cabinet (ESCO, Barnsley, U.K.).

Lab-Tek Chambered Coverglass 8 well (Lab-Tek, Thermo Fisher Scientific, Hemel Hempstead, U.K.).

Odyssey CLx (LI-COR Biosciences, Nebraska, U.S.).

MCE MF-Millipore hydrophobic plain edge 0.45 µm pore size 47 mm membrane filter and MCE MF-Millipore plain black 0.45 µm pore size 47 mm diameter membrane filter (Millipore, Oxfordshire, U.K.).

Plate reader spectra Mac 190 (Molecular Devices, Wokingham, U.K.).

Neubauer Improved haemocytometer (Neubauer Improved, Hawksley, Sussex, U.K.).

Excella E25 incubator shaker series (New Brunswick Scientific, St Albans, U.K.).

Light Microscope (Nikon, Kingston Upon Thames, U.K.).

Olympus IX71 (microscope), Olympus TH4-200 (halogen lamp power supply unit) and Olympus U-RFL-T (fluorescent lamp) (Olympus, Southend-On-Sea, U.K.).

0.2 mm electroporation cuvettes (PEQLAB Ltd, Portsmouth, U.K.)

2X Gradient PCR machine (Pegstar, Southampton, U.K.).

QImaging RetigaExi Fast 1394 digital camera (QImaging, British Columbia, Canada).

Spectra Mac 190 Plate Reader (Molecular devices, Wokingham, U.K.).

Sartorius certomat RM rotatory platform (Sartorius, Epsom, U.K.).

Magnetic Heat Stir CB/62 (Stuart, Stone, Staffordshire).

GeneFlash gel system (Syngene, Cambridge, U.K.).

Dri-block DB-2D (Techne, Stone, U.K.)

Heraeus Fresco 21 centrifuge and nanodrop (Thermo Fisher Scientific, Hemel Hempstead, U.K.).

Galaxy Mini Star and MEGA STAR 1.6 centrifuge (VWR, Leighton Buzzard, U.K.).

2.1.1.11 Plasmids and *D. discoideum* Cell Lines

N-terminal RFP tagged mRFPmars in pDEXH (338-19) (Annette Müller-Taubenberger, Ludwig-Maximilians-University, Munich, Germany).

LB150B (F-actin GFP) and pBIGGFPmyo (GFP-myosin II heavy chain (MHC)) (Arjan Kortholt, University of Groningen, Groningen, Netherlands).

D. discoideum Ax2, Ax3, *plc*⁻ Ax3 and *pikA*⁻/*pikB*⁻/*pikC*⁻/*pikF*⁻/*pikG*⁻/*pten*⁻ Ax2 (*pi3k1-5/pten*⁻) cells (Dicty Stock Centre, Chicago, U.S.).

pLPBLP plasmid (Dictybase, www.dictybase.org).

D. discoideum *lpin2*⁻ Ax2 cells and Ax2 parental cells used to make this mutant (Markus Maniak, University of Kassel, Hesse, Germany).

pTX-DGK1 (Tomas Egelhoff, Case Western Reserve University, Cleveland, U.S.).

2.2 Methods

2.2.1 Bioinformatic Analysis

2.2.1.1 BLAST

Homologs of *D. discoideum* proteins in other organisms were identified using the position-specific iterative (PSI)-basic local alignment tool (BLAST) database provided by the National Centre for Biotechnology Information (NCBI). This search

was conducted using the non-redundant protein sequence (nr) database. The protein-protein- BLAST database provided by NCBI was used to compare *D. discoideum* protein sequences with specific *H. sapiens* protein isoforms.

2.2.1.2 Phylogenetic Tree

Evolutionary conservation of proteins across a range of organisms was determined by phylogenetic analysis. This involved using the Molecular Evolutionary Genetic Analysis (MEGA) 7 software to input protein sequences from the website UniProt.org. Protein sequences were aligned in order to produce a phylogenetic tree using the neighbour- joining method with bootstrap replicates (500), corrected using the Poisson correction method.

2.2.1.3 Protein Sequence Alignment

Protein sequences were obtained from the website UniProt.org and aligned using the Clustal Omega webpage. Once aligned, amino acids conserved in *D. discoideum* and other organisms were highlighted in blue using the website bioinformatics.org.

2.2.1.4 Domain Analysis

Key protein domains were determined using the UniProt.org website. These domains were then plotted in a schematic to illustrate homology of key sites between *D. discoideum* and *H. sapiens* proteins. Where the catalytic site was not stated on the UniProt.org website, this domain was predicted from areas of high homology from the protein sequence alignment.

2.2.2 *D. discoideum* Protocols

2.2.2.1 Cell Culture

D. discoideum stocks were stored at -80 °C in freezing medium (7 % DMSO and horse serum). Every 4 weeks, cells from frozen stocks were scraped onto SM agar plates streaked with 350 µl *Raoutella planticola*. Plates were incubated at 22 °C for 4-5 days to enable colonies to form. Cells within a single colony growth zone were inoculated into liquid axenic media containing PenStrep (100 µg/ml) to obtain isogenic cell lines. Cells were maintained in the log phase ($1-4 \times 10^6$ cells/ml) and cell number was determined using a haemocytometer.

2.2.2.2 Live Cell Imaging

For live cell imaging, *D. discoideum* cells containing fluorescent tags were grown to the log phase prior to washing and being placed into low fluorescing media. Cells were then grown for 16 hours at 22 °C. Cells were then transferred to the top of a large round glass coverslip and allowed to adhere for 10 minutes. This was followed by placing a square of 1 % agar diluted in phosphate buffer (16.2 mM potassium phosphate monobasic and 4 mM potassium phosphate dibasic in double distilled water) above the cells and allowing cells to adhere for a further 5 minutes. Protein localization was determined using fluorescence microscopy at x 60 objective.

2.2.2.3 Fixed Cell Imaging

D. discoideum cells (1×10^7) were transferred to a 6-well plate to which glass cover slips were added and allowed to adhere for 16 hours at 22 °C. Cells were fixed to the glass cover slips using paraformaldehyde. This was followed by immunofluorescent staining whereby fixed cells were incubated in the presence of a calreticulin (diluted 1:4) (control) or MHC (diluted 1:3) primary antibody for 1 hour. Both antibodies were diluted in 2 % BSA in TBS-T. Cells were then washed in 2 % BSA in TBS-T before being incubated for a further hour in a relevant secondary antibody diluted 1:1000 in 2 % BSA in TBS-T. Cells were again washed in 2 % BSA in TBS-T, followed by attaching the cell fixed cover slips to a glass slide using Fluoromount-G. The slides were then incubated in the dark for 16 hours as fluorescent antibodies are light sensitive. Fluorescing cells were visualised at x 60 objective using a fluorescence microscope.

2.2.2.4 Live Cell Imaging of MHC Localization

Shaking *D. discoideum* cells containing a plasmid driving the expression of a GFP fluorescently tagged F-actin (LB15-B) or MHC (pBIGGFPmyo) (1×10^7) were washed and resuspended in 6 ml phosphate buffer. Cells were shaken (120 rpm) and pulsed every 6 minutes with cAMP (30 nM) for 5 hours. This was followed by washing and resuspending cells in 4 ml phosphate buffer. Cells were then diluted 1:10 times in phosphate buffer before 250 µl of cells were transferred to a Nunc Lab-Tek 8-well glass chamber. Cells were allowed to adhere to the chamber for 15 minutes at 22 °C. This was followed by fluorescence microscopy using the x 40 objective where

images of cells were taken at 0, 10, 20, 30, 60 and 120 seconds following stimulation by cAMP (100 μ M).

2.2.2.4 Growth Curve Assay

A 24-well plate was used to grow 2×10^4 *D. discoideum* cells per experimental sample. Cells were diluted in axenic media (giving a final volume of 495 μ l per well) prior to being added to the 24-well plate and allowed to adhere for 15 minutes at 22 °C. This was followed by the addition of 100 X VPA dissolved in double distilled water to give final concentrations ranging between 0.01 mM-2 mM. Cells were incubated for 168 hours at 22 °C with cell density calculated every 24 hours between 72-168 hours. Growth within the exponential phase was used to calculate the concentration of VPA which inhibited growth by 50 % (IC_{50}) using a haemocytometer and light microscope.

2.2.2.5 Acute Cell Behaviour Assays

D. discoideum cells (1×10^7) were harvested from shaking culture mid-log phase and washed in phosphate buffer. Cells were resuspended in 6 ml phosphate buffer and pulsed with cAMP (30 nM) every 6 minutes for 5 hours shaking at 120 rpm. Cells were then washed and resuspended in 4 ml phosphate buffer prior to being diluted 1:10 times in phosphate buffer. Cells (250 μ l) were then transferred to a Nunc Lab-Tek 8-well glass chamber and incubated at 22 °C for 15 minutes to allow cells to adhere. Cell movement was then recorded by time-lapse microscopy for 900 seconds at x 40 objective using the Image-Pro 6.3 software. During the recording, there was a control period of 225 seconds which was followed by the addition of 250 μ l 2 X VPA to give a final concentration ranging between 0.01 mM-0.7 mM for the remaining 675 seconds. Cell behaviour in both the absence and presence of VPA was monitored using 30 cells per condition in a minimum of 3 independent replicates.

From the time-lapse recordings, acute cell behaviour was analysed using the software ImageJ 1.48 g software package where individual cells were segmented. This was followed by MATLAB R2011b analysis of the accompanying scripts,

enabling the quantification of individual cell displacement, circularity, membrane protrusions and motility between all video frames.

2.2.2.6 Development Assay

D. discoideum cells (1×10^7) were harvested from a shaking culture, washed and resuspended in 10 ml and 1 ml phosphate buffer respectively. Cells were evenly distributed across a Millipore membrane filter which was added on top of a Millipore hydrophobic membrane filter soaked in either phosphate buffer (control) or relevant compound. Cells were incubated for 24 hours at 22 °C before being analysed under a light microscope at x 1.25 objective for an overhead view or x 6.3 for a single fruiting body.

2.2.2.7 DAG ELISA Assay

D. discoideum cells (5×10^6) were harvested from a shaking culture, washed and resuspended in 6 ml phosphate buffer. Cells were then shaken with pulsatile cAMP for 5 hours prior to being washed with phosphate buffer. Cells were then treated with VPA (0.3 mM-0.5 mM), LiCl (8 mM), VPD (6.5 mM), PIA (1.4 mM), DA (1.65 mM), OA (0.22 mM) or 4-EOA (0.5 mM) for 10 minutes in shaking suspension. Following treatment, cells were then washed and the cell wall fraction was obtained following 6 rounds of freeze-thaw (3 minutes each) and centrifuged (10,000 g, 10 minutes, 4 °C). The cell pellet was then resuspended in 100 µl Sample Diluent provided in the Amsbio General Diacyl glycerol DAG/DG ELISA kit. Samples were stored at -20 °C prior to the ELISA assay. The ELISA assay was conducted following the instructions provided from the supplier.

2.2.3 Molecular Biology Protocols

2.2.3.1 Polymerase Chain Reaction

Genomic DNA was amplified using PCR under the conditions: 2 µl DNA, 0.8 µl 50 mM MgCl₂, 2 µl 10 % BIOTAQ ammonia buffer, 2 µl 2 mM dNTPS, 0.1 µl BIOTAQ DNA polymerase ($5 \text{ U} \mu\text{l}^{-1}$), 1 µl 10 pmol 5' primer, 1 µl 10 pmol 3' primer and 11.1 µl double distilled water to make a total volume of 20 µl.

The PCR reaction was carried out under the following conditions: denaturation at 95 °C for 1 minute followed with 32 cycles of denaturation at 95 °C for 15 seconds, annealing at 50 °C for 30 seconds (temperature dependent on primer annealing points) and extension at 72 °C where length was dependent on the product length being amplified (1 minute per 1000 bp). This cycle was followed with a final extension of 5 minutes at 72 °C prior to samples being stored at 8 °C.

2.2.3.2 Agarose Gel Electrophoresis

DNA was separated and visualised on 1 % agarose gels spiked with ethidium bromide in 1 X TBE buffer. 5 X DNA loading dye was added to DNA. DNA fragment sizes were determined using a 1 kb hyperladder. Gels were run for 30-40 minutes at 100 V in a gel electrophoresis tank and visualised by UV light on a GeneFlash gel system (Syngene Bio Imaging).

2.2.3.3 Restriction Digest

Qiagen AAMP Gel Extraction kit and the Qiagen QIAquick PCR Purification kit were used according to the manufacturer's instructions to purify the pLPBLP plasmid and genomic PCR fragments respectively.

Restriction digests were carried out in the following conditions: 10 µl DNA, 0.2-0.5 µl each of the relevant restriction enzyme (100 U/µL⁻¹) (volume dependent on the restriction enzymes being used and their effectiveness in the buffer), 2 µl appropriate buffer (according to the manufacturer's instructions) made up to a total volume of 20 µl with double distilled water. Samples were incubated for 2-4 hours at 37 °C, depending on the purpose of the reaction (2 hours for creating a recombinant plasmid, 4 hours for obtaining the knockout cassette).

For creating knockout plasmids, TSAP was added after 1 hour to the pLPBLP sample only to remove any 5' phosphate groups to prevent re-ligation or recircularization of the plasmid. After a further hour incubation, TSAP was inactivated by incubating the sample at 74 °C (15 minutes).

Enzyme efficiency for all digests was determined by 1 % agarose gel electrophoresis (30-40 minutes, 100 V).

2.2.3.4 Knockout Vector Construction

Knockout constructs were created using the pLPBLP plasmid. Two fragments of the open reading frame of the gene of interests were PCR amplified from Ax2 cell genomic DNA. Primers used for PCR amplification contained restriction sites to enable cloning into the pLPBLP vector. PCR products were purified using the Qiagen QIAquick PCR Purification kit. This was followed by digesting the pLPBLP vector and gene fragments with the appropriate restriction enzymes. A sample (5 µl) of the digested PCR fragments were analysed by gel electrophoresis with the remaining sample being purified using the Qiagen QIAquick PCR Purification kit. The whole pLPBLP digested sample was analysed by gel electrophoresis and the digested band at the correct size was excised from the gel and purified using the Qiagen QIAquick Gel Extraction kit. The PCR gene fragments were then ligated into the purified pLPBLP vector at a ratio of 2:1 using 1 µl T4 DNA ligase (1 U/µl⁻¹), the corresponding T4 DNA ligase buffer (2 µl) provided with the enzyme with the total volume of the ligation reaction being made up to 20 µl with double distilled water. Ligation reactions were incubated at 16 °C for 16 hours. This was followed by denaturing T4 ligase at 65 °C for 20 minutes. The ligation reaction was transformed into chemically competent *E. coli* cells (30 µl) by incubating the sample on ice for 2 minutes, followed by heat- shock treatment for 1 minute at 42 °C and then returning the sample to ice for a further 2 minutes. LB media (100 µl) was then added to the samples which were then incubated for 1 hour at 37 °C, 200 rpm. Cells were streaked onto a spiked LB plate with 1 µl/ml ampicillin and incubated at 37 °C overnight. Transformant colonies selected by ampicillin were added to LB liquid broth spiked with 2 µl/ml ampicillin and incubated at 37 °C for 16 hours.

Plasmid cultures were then purified. Plasmid cultures to be used for sequencing or electroporating into *D. discoideum* cells were purified using the Qiagen HiSpeed Plasmid Purification kit according to the manufacturer's instructions. Plasmid preparations which were not purified with the commercial kit and used for further cloning, were extracted from *E. coli* using verified a using an in- house protocol. This involved centrifuging 2 ml *E. coli* culture, aspirating the supernatant and resuspending the cell pellet in 200 µl P1 buffer (1 M glucose, 0.5 M EDTA, 2 M Tris

pH 8 and water). Cell lysis occurred by the addition of 200 µl P2 buffer (5 M sodium hydroxide in 10 % SDS and water) and was followed with neutralization of the lysis mixture by the addition of 200 µl P3 buffer (3 M potassium acetate and 2 M glacial acetic acid in water). Samples were centrifuged at 17,000 g for 15 minutes, after which the supernatant was added to 420 µl 100 % propan-2-ol and further centrifuged (17,000 g, 15 minutes). DNA precipitation occurred by the addition of 500 µl 80 % ethanol, after which samples were centrifuged at 13,000 rpm for 5 minutes. The DNA pellet was then air dried for 10 minutes to remove any residual ethanol. DNA was resuspended in 30 µl double distilled water.

The concentration of the purified plasmid was then determined using a nanodrop. This was followed by single and double restriction digests to confirm the insertion of the fragment of interest. The whole cloning process was then repeated for the insertion of the second gene fragment. Once both fragments were inserted into the pLPBLP vector, the purified plasmid was sequenced by MWG-Biotech to ensure no mutations were present.

2.2.3.7 *D. discoideum* Knockout Transformation by Electroporation

For each knockout construct, the knockout cassette (2 PCR gene fragments flanking either side of a blasticidin resistance cassette) was excised from the pLPBLP plasmid via a 4-hour restriction digest. This was achieved by digesting the knockout construct (20 µg) at 37 °C in the relevant enzyme buffer using the two restriction enzymes whose cut sites were present at either end of the knockout cassette. Gel electrophoresis was then used to confirm efficiency of the digest. DNA was then precipitated by the addition of 10 µl 3 M sodium acetate and 330 µl 100 % ethanol. Samples were centrifuged at 17,000 g for 15 minutes and the resulting DNA pellet was washed in 80 % ethanol (750 µl) and spun under the same conditions. The DNA pellet was then air dried for 10 minutes before being resuspended in 20 µl double distilled water.

The knockout cassette was then electroporated into *D. discoideum* cells. *D. discoideum* cells (1×10^7) were incubated on ice for 10 minutes and then centrifuged

at 1500 g for 3 minutes. Cells were washed twice in phosphate buffer and sterile filtered electroporation buffer (20 mM HEPES, 50 mM potassium chloride, 10 mM sodium chloride, 1 mM magnesium sulphate, 5 mM sodium bicarbonate and 1 mM monosodium phosphate). The cell pellet was resuspended in 20 μ l of the 20 μ g digested knockout construct and transferred into a 0.2 cm electroporation cuvette and incubated on ice for 10 minutes. *D. discoideum* cells were then electroporated with a Bio-Rad GenePulser Xcell electroporator using 2 pulses with 15 seconds rest in between, 25 μ F and 850 V. Cells were then allowed to recover by incubating on ice for a further 10 minutes before being transferred to 10 ml axenic media spiked with 0.1 % PenStrep. Cells were then transferred to a 96-well plate with 100 μ l added to each well. After 24 hours incubation at 22 °C, 100 μ l of axenic media containing 0.1 % PenStrep and 20 μ g/ml blasticidin was added to each well, giving a final blasticidin concentration of 10 μ g/ml. Where stated, cells were also grown in the presence of 100 μ M PI and/or 100 μ M PG liposomes, produced from sonication. Cells were then incubated at 22 °C for 2 weeks for wells to become confluent.

2.2.3.8 DNA Extraction of Transformed Cells

Once transformant cells became confluent after selection in blasticidin, 200 μ l of cells were spun in a microfuge and the cell pellet was washed in 100 μ l phosphate buffer. The cell pellet was lysed in 2 μ l Proteinase K (20 mg/mL) and 48 μ l lysis buffer (50 mM potassium chloride, 10 mM Tris pH 8.3, 2.5 mM MgCl₂, 0.45 % NP-40 detergent, 0.45 % Tween-20 and water) following a 5 minute incubation at room temperature. Proteinase K was inhibited by an incubation at 95 °C for 1 minute. The extracted DNA was then used for PCR screening reactions to identify colonies where homologous recombination of the knockout cassette had occurred at the correct location.

2.2.3.9 PCR Screening of Transformed *D. discoideum* Cells

Screening primers were designed for determining correctly transformed *D. discoideum* cells. Homologous recombinant cells would have the blasticidin resistance cassette located within the gene of interest at a site where part of the coding sequence had been deleted, thereby preventing the synthesis of a functional

protein. Three primer pairs were used to screen for homologous integration of the knockout cassette: genomic control, vector control and knockout conformation (**Figure 2.1**). PCR analysis was conducted on freshly extracted genomic DNA based upon these 3 sets of primers designed for both the 5' and 3' fragments of each gene of interest. The genomic control confirmed the non-deleted region of the gene; the vector control confirmed the presence of the blasticidin resistance gene adjacent to the genomic DNA fragment and the knockout diagnostic confirmed homologous integration of the knockout cassette at the correct location.



Figure 2.1. Schematic illustrating the locations of the PCR screening primers. Schematic representation of a gene knockout construct containing the 5' and 3' PCR gene fragments (purple) and the blasticidin resistance gene (*Bsr*, red). The locations of the screening primers (arrows) and the corresponding PCR product (dotted line) used for determining homologous integration are shown for the genomic control (pink), vector control (blue) and knockout diagnostic (yellow) primers.

2.2.3.10 Creation of Isogenic Transformant *D. discoideum* Cells

Once PCR confirmed the correct insertion of the resistance gene within transformant cells, colonies were plated on sterile SM agar plates with 200 μ l *R. planticola*. Plates were incubated for 3-4 days at 22 °C, after which individual cell colonies appeared. Cells were obtained from these colonies and grown and selected in axenic media containing 0.1 % PenStrep and 10 μ g/ml blasticidin.

2.2.3.11 Confirmation of Gene Disruption By Reverse Transcription-PCR

Isogenic homologous intergrants determined by PCR screening were confirmed as knockout cell lines by RT-PCR. This involved harvesting and washing *D. discoideum* cells (1×10^7) in phosphate buffer. RNA was extracted using the RNeasy Mini kit following the manufacturer's protocol. RNA extraction was followed by the removal

of DNA using a DNase Treatment Removal Kit following the manufacturer's instructions. cDNA was then created from 1 µg of treated RNA using the First Strand cDNA Synthesis kit according to the manufacturer's protocol. This was then followed by RT-PCR using 2 µl of cDNA with Q5 DNA polymerase following the manufacturer's instructions and the description of PCR given in section 2.2.3.1.

2.2.3.12 Fluorescently Tagged Overexpression Vector Construction

D. discoideum overexpressing cells were created using the N-terminal RFP tagged mRFPmars in pDEXH (338-19) kindly provided by Annette Müller-Taubenberger. For each overexpressing construct, RNA was extracted from WT cells, treated with DNase and used to synthesise cDNA as described in section 2.2.3.12. RT-PCR was then conducted using primers targeting the start and end of the coding sequence of the gene of interest. To these primers, restriction sites were added which corresponded to sites present in the N-terminal RFP tagged mRFPmars in pDEXH vector, to enable cloning. These primers were used to amplify the gene of interest using 2 µl of cDNA and the Q5 DNA polymerase following the manufacturer's protocol and as described in section 2.2.3.1. Gel electrophoresis was conducted on a portion of the sample to confirm PCR efficiency. PCR products were then purified using the Qiagen QIAquick PCR Purification kit. The overexpressing vector and gene fragments were then digested in the presence of the two relevant restriction enzymes whose cut sites were present in the cDNA PCR product. Gel electrophoresis was conducted on a portion of the sample to confirm efficiency of the digest. This was followed by ligating the PCR fragment into the overexpressing vector and transforming the ligated recombinant plasmid into chemically competent *E. coli* cells as described in section 2.2.3.4. The recombinant plasmid was then purified from *E. coli* cells using the Qiagen HiSpeed Plasmid Purification kit according the manufacturer's instructions. The concentration of the purified plasmid was determined using a nanodrop. The purified plasmid was then sequenced by MWG-Biotech to ensure no errors were present in the gene sequence.

2.2.3.13 *D. discoideum* Overexpression Vector Transformation by Electroporation

The overexpressing construct was then electroporated into Ax2 WT cells to create overexpressing cells or into *dgkA*⁻ cells to produce a rescue cell line. *D. discoideum* cells (1×10^7) were incubated for 10 minutes on ice prior to being centrifuged (1500 g for 3 minutes). Cells were then washed twice in phosphate buffer followed by washing in sterile filtered electroporation buffer (20 mM HEPES, 50 mM potassium chloride, 10 mM sodium chloride, 1 mM magnesium sulphate, 5 mM sodium bicarbonate and 1 mM monosodium phosphate). The resulting cell pellet was resuspended in 20 µg overexpressing plasmid prior to being transferred to a 0.2 cm electroporation cuvette and incubated on ice for 10 minutes. *D. discoideum* cells were then electroporated using a Bio-Rad GenePulser Xcell electroporator using 2 pulses with 15 seconds rest in between, 25 µF and 850 V. This was followed by a further incubation in ice (10 minutes) before the cells were transferred to 10 ml axenic media spiked with 0.1 % PenStrep. Cells were then incubated at 22 °C for 24 hours. This was followed by the addition of 10 µg/ml G418 (geneticin) or hygromycin to select for transformant cells and incubated at 22 °C for 2 weeks. Transformant cell lines were analysed using fluorescence microscopy.

2.2.4 Proteomic Protocols

2.2.4.1 Sodium Dodecyl Sulphate Polyacrylamide Gel Electrophoresis

Each SDS gel was produced using the following: resolving gel (12.5 %) containing: 2 ml Protogel 30 % solution, 1.25 ml 1.5 M Tris pH 8.8, 50 µl 10 % SDS, 50 µl 10 % APS and 2 µl TEMED made up to 5 ml with double distilled water; and stacking gel containing: 167.5 µl Protogel 30 % solution, 250 µl 0.5 M Tris pH 6.8, 10 µl 10 % SDS, 10 µl 10 % APS, 1 µl TEMED and 925 µl double distilled water. Sample loading dye (5 X) contained 0.001 g bromophenol blue, 30 ml 2 X Laemeli sample buffer, 3 ml 2-mercaptoethanol, 6 ml 100 % glycerol, 7.5 ml Tris-HCl pH 7.5 and 12 ml 10 % SDS made up to 30 ml with double distilled water.

Protein samples to be run on the SDS gel were prepared by pelleting 1.5×10^6 cells per sample by centrifugation (1500 g, 3 minutes). The cell pellet was resuspended in protein loading dye (20 µl per sample) and boiled at 98 °C for 6.5 minutes. The

protein ladder PageRuler Plus Pre-stained Protein Ladder and protein samples were loaded into the stacking gel and run in the presence of 1 X running buffer diluted in double distilled water (stock 10 X running buffer contained 144 g glycine, 30 g Tris base, 100 ml SDS made up to a total volume of 1000 ml with double distilled water) at 69 V for 30 minutes, followed by 100 V for 1 hour.

2.2.4.2 Western Blotting

Once the proteins were separated, the SDS gel was blotted onto a methanol activated PDVF membrane. Both PDVF membrane, blotting paper (3 mm) and sponges were incubated in transfer buffer. The transfer buffer comprised of 10 % methanol and 10 X ETB buffer (10 X ETB buffer contained: 360 g glycine, 75 g Tris base and 10 % SDS) and 800 ml double distilled water. Protein transfer occurred by placing the transfer blot into a tank containing a magnetic stirring bar and ice-cold transfer buffer and running the transfer on a magnetic stirrer at 15 V for 16 hours.

Proteins were visualised by immunostaining the membrane for 16 hours at 4 °C with appropriate antibodies (Streptavidin (MccA), 6G6-RFP and 3H9-GFP) at a 1:1000 dilution. The membrane was then washed with TBS-T prior to an hour shaking incubation in the dark in the relevant secondary antibody (anti-rat or anti-mouse) diluted 1:10000. The secondary antibody was then washed away with TBS-T. Proteins on the membrane were visualized using the Odyssey CLx (LI-COR Biosciences).

2.3 Statistics

Growth assays and acute cell behaviour assays were analysed using the Kruskal-Wallis test and Dunn's post hoc test which compared the differences between WT and mutant cell lines at each VPA concentration. This test was used as all sample sets compared are independent of each other and the data was not normally distributed.

DAG ELISA assay was analysed using the Mann-Whitney test which compared differences between cell lines in the presence of each drug. This test was used as

the samples compared are independent of each other and the data is not normally distributed.

2.4 Software

Development assay results were analysed using QCapture Pro 6.0 (QImaging).

ELISA plates were analysed using SoftMax Pro 5.4.1 (Molecular Devices).

Graphical images and statistical analysis was conducted using Prism 7 (GraphPad).

Phylogenetic trees were created using Molecular Evolutionary Genetic Analysis (MEGA) 7 (Mega Software).

Acute cell behaviour assays were recorded using Image-Pro 6.3 (Media Cybernetics) and analysed using ImageJ 1.48 g (National Institute of Health) using the QiumP 11 b software (University of Warwick) and MATLAB R2011 b (Mathworks).

Western blot membranes images were obtained using Image Studio Version 5.2 (LI-COR Biosciences).

2.5 Websites

2.5.1 Information of *D. discoideum* Gene and Protein

www.dictybase.org

www.uniprot.org

<https://dictyexpress.research.bcm.edu>

2.5.2 Basic Local Alignment Tool (BLAST)

<http://blast.ncbi.nlm.nih.gov/Blast.cgi>

www.dictybase.org/tools/blast

2.5.3 Alignment of Protein Sequences

www.ebi.ac.uk/Tools/msa/clustalo/

https://bioinformatics.org/sms/multi_align.html

2.5.4 Gene and Protein Information of Organisms

www.uniprot.org

Chapter 3

Analysis of PI3K1-5/ PTEN, PLC and
LPIN2 as a Target of VPA

3. Analysis of PI3K1-5/PTEN, PLC and LPIN2 as a Target of VPA

Studies have shown VPA lowers phosphoinositide levels (Chang, et al., 2012; Chang, Walker and Williams, 2014). This mechanism of action is of interest as seizure generation has been linked with PTEN and the PI3K/PIP₃/Akt pathway (Backman, et al., 2001; Shinoda, 2004). To investigate this further, 4 potential VPA targets (PI3K, PTEN, PLC and LPIN2) were examined using knockout mutants to test for reduced VPA sensitivity, with all 4 proteins having roles in phosphoinositide regulation (**Figures 1.4 and 3.1**). Within this chapter, *D. discoideum* knockout mutants of all 5 PI3K and PTEN (PIKA, PIKB, PIKC, PIKF, PIKG, PTEN, *pi31-5⁻/pten⁻*), PLC (*plc⁻*) and LPIN2 (*lpin2⁻*) have been investigated as potential targets of VPA. This begun with investigating *pi3k1-5⁻/pten⁻* cells. PIP₂ can be phosphorylated into PIP₃ by PI3K, with the reverse reaction catalysed by PTEN (**Figures 3.1 and 3.2**). Both the forward and reverse reactions of the conversion of PIP₂ and PIP₃ are essential due to the range of pathways regulated. PIP₃ activates a range of cellular responses including mitosis (Fantl, et al., 1992), chemotaxis (Wennstroem, et al., 1994), actin reorganisation (Arcaro and Wymann, 1993), oxidative stress, glucose uptake (Hara, et al., 1994; Okada, et al., 1994) and cell growth and survival through Akt (Burgering and Coffey, 1995; Franke, et al., 1995).

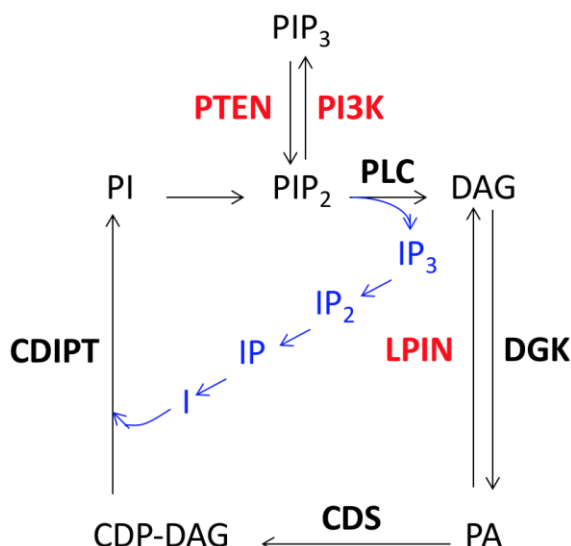


Figure 3.1. The role of PI3K, PTEN and LPIN2 in phosphoinositide regulation. Schematic of the phosphatidylinositol (PI) salvage pathway (black arrows) and interlinking enzymes (red). Within the PI salvage pathway, diacylglycerol (DAG) phosphorylated into phosphatidic acid (PA) by DAG kinase (DGK). Cytidine diphosphate- diacylglycerol (CDP-DAG) is produced from PA using the enzyme CDP-DAG synthase (CDS). PI is then synthesized from CDP-DAG and *myo*-inositol. PI then undergoes a 2-step phosphorylation reaction to produce phosphatidylinositol-4,5-bisphosphate (PIP₂). From this pathway, PI-3-kinase (PI3K) phosphorylates PIP₂ to produce PI-3,4,5-triphosphate (PIP₃). PIP₃ is dephosphorylated into PIP₂ by phosphatase and tensin homolog (PTEN). PA can be dephosphorylated into DAG by phosphatidate phosphatase LPIN2 (LPIN2).

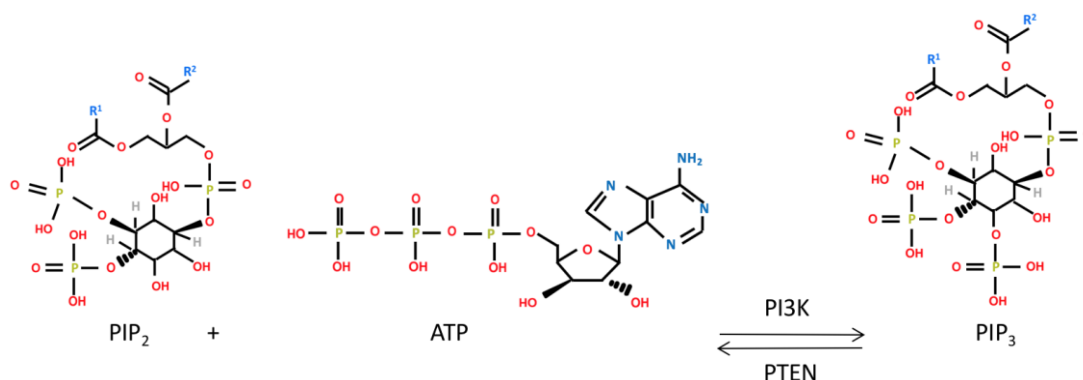


Figure 3.2. The catalytic activity of phosphatidylinositol-4,5-bisphosphate-3-kinase and phosphatase and tensin homolog. Phosphorylation of phosphatidylinositol-4,5-bisphosphate (PIP₂) by phosphatidylinositol-4,5-bisphosphate-3-kinase (PI3K) results in the generation of phosphatidylinositol-3,4,5-triphosphate (PIP₃). This reaction is reversed by the phosphatase and tensin homolog (PTEN).

PLC is a protein of interest as VPA has been shown to reduce PIP₂ levels (Chang, et al., 2012). PLC has the role of diminishing PIP₂ signalling by hydrolysis into IP₃ and DAG (**Figures 3.1 and 3.3**). Both reaction products, IP₃ and DAG, are important signalling molecules involved in a range of biological pathways. IP₃ stimulates a rise in intracellular calcium concentration, which has been linked with epileptogenesis (Berridge, 1983; Streb, et al., 1983; Alswied and Parekh, 2015). DAG is involved in the signalling of PKC (van Baal, et al., 2005), synaptic plasticity (Lee, Kim and Tanaka-Yamamoto, 2016) and triglyceride synthesis (Dahlqvist, et al., 2000). Both IP₃ and DAG have been implicated in epilepsy (Yoshida, et al., 1987; Carmant, et al., 1995; Tokuoka, Saiardi and Nurrish, 2008) and BD (Drummond and Raeburn, 1984; Bami, Leli and Hauser, 1993; Sade, et al., 2016). A loss-of-function point mutation in PLC has been identified in an epilepsy patient (Kurian, et al., 2010). Therefore, PLC was investigated as a potential target of VPA.

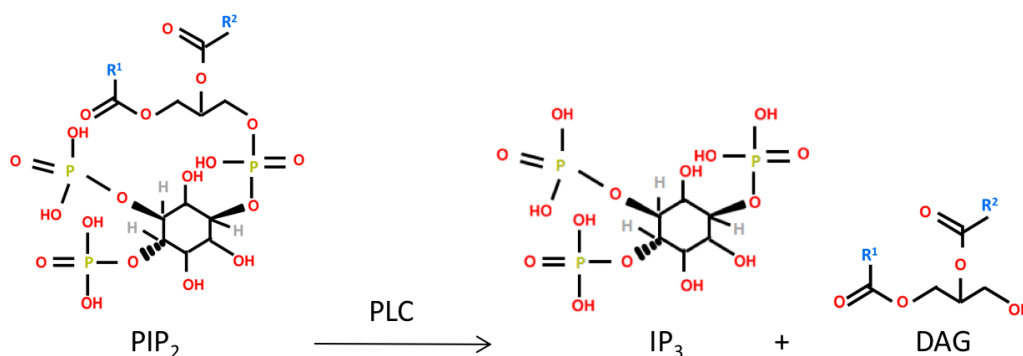


Figure 3.3. The catalytic activity of phospholipase C. Phospholipase C (PLC) is responsible for the hydrolysis of phosphatidylinositol-4,5-bisphosphate (PIP₂) into inositol-1,4,5-triphosphate (IP₃) and diacylglycerol (DAG).

LPIN2 is a protein of interest due to its role in catalysing the formation of DAG from the dephosphorylation of PA (**Figure 3.1 and 3.4**), thereby being a key regulator in lipid homeostasis. PA is an important signalling molecule with a range of roles including cell growth and signalling (Banfić, et al., 1993; Cerbón, et al., 2005), glucose metabolism and lipid regulation (Milne, et al., 2008). The role of PA in regulating lipids and therefore potentially PIP₂, means LPIN2 may be a target of VPA.

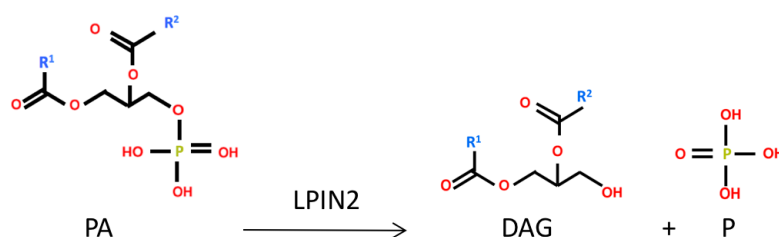


Figure 3.4. The catalytic activity of Lpin2. Lpin2 (also referred to as phosphatidate phosphatase lpin2, lipin-2) is responsible for the dephosphorylation of phosphatidic acid (PA) into diacylglycerol (DAG).

This chapter, therefore, describes the phenotypic characterization of *pi3k1-5/pten*⁻, *plc*⁻ and *lpin2*⁻ cells in both the absence and presence of VPA during acute cell behaviour and development. In addition, other anti-seizure compounds and the BD treatment LiCl have been investigated during development to determine whether the mechanism of action of these drugs is similar to that of VPA.

3.1 *pi3k1-5/pten*⁻ Cells

D. discoideum has 5 PI3K gene isoforms, *PikA* (DDB_G0278727), *PikB* (DDB_G0283081), *PikC* (DDB_G0275011), *PikF* (DDB_G0268548) and *PikG* (DDB_G0282625) and one *Pten* gene. Both PI3K and PTEN in *D. discoideum* are expressed during the developmental phase (Hoeller and Kay, 2007; Parikh, et al., 2010; Stajdohar, et al., 2015). The 5 *D. discoideum* PI3K enzymes have similar identity to the *H. sapiens* proteins (**Supplementary Table S2**). PI3K are divided into 3 classes, where class-I synthesise PI-3-phosphate and are either catalytic or regulatory proteins, class-II produce PI-3,4-bisphosphate and class-III catalyse PIP₃ production (Jean and Kiger, 2014). *PikA* has highest identity to *H. sapiens* class-II *Pik3c2b* (40 %, E-value 5e⁻¹³⁵), *PikB* to class-I catalytic *Pik3cg* (43 %, E-value 5e⁻¹³⁸), *PikC* to class-I catalytic *Pik3cb* (37 %, E-value 1e⁻¹²⁹), *PikF* to class-II *Pik3c2b* (40 %, E-value 1e⁻¹³⁶) and *PikG* to class-III *Pik3c2g* (48 %, E-value 2e⁻⁸⁸). There was also similar identity (55 %) between the *D. discoideum* and *H. sapiens* PTEN proteins (E-value 9e⁻⁸¹), suggesting a similar catalytic role for both of these enzymes in the two organisms.

In 2007 Hoeller and Kay deleted all 5 PI3K and PTEN from Ax2 *D. discoideum* parental cells, thereby blocking the reversible reaction of PIP₂ to PIP₃. This resulted in *pi3k1-5/pten*⁻ cells. The *pi3k1-5/pten*⁻ cells have been phenotypically characterized through a series of experiments and compared with WT cells in both the absence and presence of VPA during acute cell behaviour and to a range of anti-seizure compounds and a BD drug during development.

3.1.1 Analysis of *pi3k1-5/pten*⁻ Acute Cell Behaviour in the Presence of VPA

Since the genes encoding PI3K and PTEN are expressed during early development, acute cell behaviour was investigated. VPA is known to inhibit *D. discoideum* acute cell behaviour (Xu, et al., 2007) and therefore, the effects of VPA on *pi3k1-5/pten*⁻ cells was investigated. For this assay, cells were pulsed with cAMP for 5 hours to enable them to enter early development. Time-lapse microscopy was then conducted where computer-generated cell outlines detected variations in displacement (the shortest distance a cell travel between 2 points), circularity (cell shape, with an arbitrary value of “1” given to round cells), membrane protrusions and motility (speed) (**Figure 3.5A**). Initial differences in cell behaviour was determined by a control period of 225 seconds prior to VPA treatment (ranging from 0.01 mM-0.7 mM) for 525 seconds (**Table 3.1 and Figures 3.5B- 3.5E**). Under control conditions with no VPA added, no significant differences were identified between WT and *pi3k1-5/pten*⁻ cells, which behaved in a similar manner for displacement at 750 seconds and average circularity, membrane protrusions and motility within the final 300 seconds of the assay. In the presence of VPA, both cell lines had a dose-dependent reduction in acute cell behaviour. However, significant differences were detected between WT and *pi3k1-5/pten*⁻ cells when exposed to 0.3 mM (P value 0.0059) and 0.5 mM (P value <0.0001) VPA for displacement and when exposed to 0.5 mM VPA only for circularity (P value 0.001) and membrane protrusions (P value 0.0016).

<u>Cell Line</u>	<u>[VPA] (mM)</u>						<u>VPA IC₅₀ Value (mM)</u>
	<u>Control</u>	<u>0.01</u>	<u>0.1</u>	<u>0.3</u>	<u>0.5</u>	<u>0.7</u>	
<i>Displacement (μm)</i>							
WT	67.2 ± 4.2	70.9 ± 3.2	58.7 ± 4.3	47.3 ± 3.3	40.0 ± 3.5	46.5 ± 2.9	0.4 ± 0.08
<i>pi3k1-5⁻/pten⁻</i>	85.1 ± 4.7	84.3 ± 3.7	60.8 ± 2.9	59.9 ± 2.3	62.3 ± 3.8	54.1 ± 3.1	0.8 ± 0.18
<i>Circularity</i>							
WT	0.71 ± 0.004	0.67 ± 0.004	0.73 ± 0.004	0.85 ± 0.004	0.90 ± 0.001	0.88 ± 0.004	-
<i>pi3k1-5⁻/pten⁻</i>	0.58 ± 0.004	0.55 ± 0.004	0.66 ± 0.003	0.86 ± 0.002	0.83 ± 0.003	0.89 ± 0.002	-
<i>Protrusions</i>							
WT	8.7 ± 0.13	9.0 ± 0.07	5.8 ± 0.17	3.6 ± 0.05	1.5 ± 0.06	1.7 ± 0.07	0.2 ± 0.05
<i>pi3k1-5⁻/pten⁻</i>	7.7 ± 0.07	10.0 ± 0.04	7.4 ± 0.08	5.1 ± 0.06	5.1 ± 0.03	3.6 ± 0.07	0.4 ± 0.06
<i>Motility (μm/sec)</i>							
WT	0.013 ± 0.0009	0.016 ± 0.0009	0.010 ± 0.0005	0.004 ± 0.0006	0.003 ± 0.0002	0.002 ± 0.0003	0.1 ± 0.01
<i>pi3k1-5⁻/pten⁻</i>	0.018 ± 0.0007	0.022 ± 0.0006	0.012 ± 0.0006	0.004 ± 0.0007	0.004 ± 0.0006	0.003 ± 0.0005	0.1 ± 0.06

Table 3.1. WT and *pi3k1-5⁻/pten⁻* changes in acute cell behaviour in both the absence and presence of VPA. Comparison of WT (Ax2) and *pi3k1-5⁻/pten⁻* acute cell behaviour values of total displacement during the assay and average circularity, protrusions and motility within the final 300 seconds. The calculated IC₅₀ values are shown to the right of the table for each cell line for displacement, number of protrusions and motility. Data presented as mean (+/- SEM). *n* = 30.

The response of WT and *pi3k1-5⁻/pten⁻* cells to increasing VPA concentrations is also shown in the secondary plots for displacement (**Figure 3.5F**), circularity (**Figure 3.5G**), membrane protrusions (**Figure 3.5H**) and motility (**Figure 3.5I**). Both cell lines had a reduction in displacement, membrane protrusions and motility with increasing VPA concentration, which was correlated with an increase in circularity, although the extent of VPA sensitivity on *pi3k1-5⁻/pten⁻* cells was not as potent as

WT. As the *pi3k1-5⁻/pten⁻* cells are more resistant to VPA during displacement and protrusion formation compared with WT cells, these results suggest a role for PI3K and PTEN in the mechanism of action of VPA during acute cell behaviour.

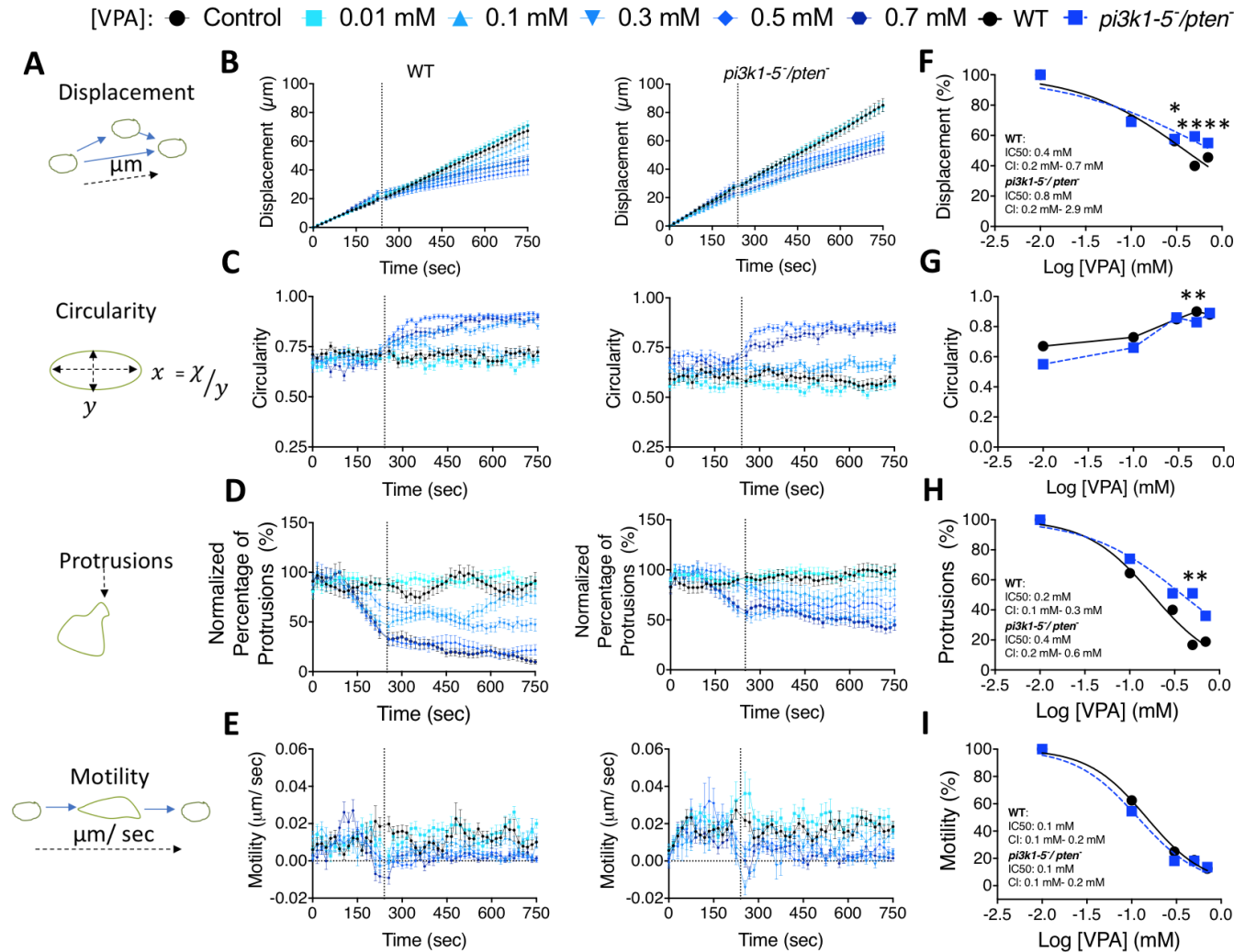


Figure 3.5. WT and *pi3k1-5/pten*⁻ acute cell behaviour in both the absence and presence of VPA. (A) Schematic of the quantitative measurements taken during the assay where the black dashed arrows represent the measurement being taken for the primary data (B) displacement, (C) circularity, (D) normalized percentage of membrane protrusions and (E) motility for WT (Ax2) (left) and *pi3k1-5/pten*⁻ (middle) cells. Secondary plot data for (F) displacement, (G) circularity, (H) membrane protrusions and (I) motility with WT shown in black circles and *pi3k1-5/pten*⁻ shown in blue squares (right). *P* value: * *P* value = ≤ 0.05, ** *P* value = ≤ 0.01 and **** *P* value = ≤ 0.0001. Data presented as mean (+/- SEM) *n* = 30 cells

3.1.2 Analysis of *pi3k1-5/pten*⁻ Cell Development in the Presence of VPA

VPA is known to inhibit the *D. discoideum* developmental cycle, a process whereby starved cells migrate together to form multicellular fruiting bodies over 24 hours (Williams, et al., 2002). To examine if VPA functions through a PI3K/PTEN dependent mechanism, cell development was investigated using WT and *pi3k1-5/pten*⁻ cells in the absence (control) and presence of VPA (0.3 mM-1 mM) (**Figure 3.6**). Under control conditions, both WT and *pi3k1-5/pten*⁻ cells were able to develop into multicellular fruiting bodies containing a basal disc, stalk and spore head of similar sizes. In the presence of 0.3 mM and 0.5 mM VPA, both cell lines developed into finger structures. When exposed to 1 mM VPA, both cell lines developed into mounds. These results suggest that neither of the 5 *D. discoideum* PI3K nor PTEN are targets of VPA during development.

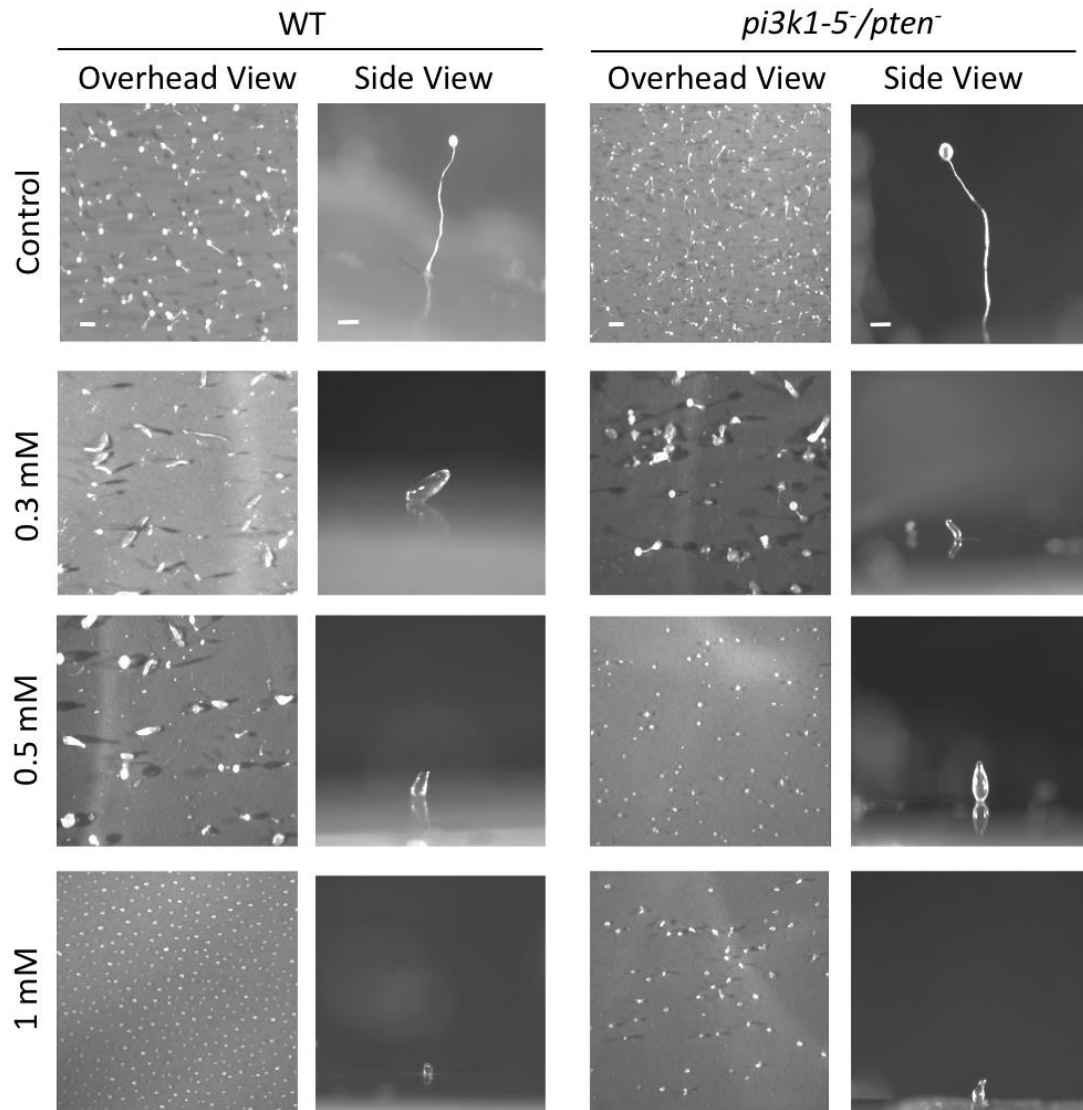


Figure 3.6. WT and *pi3k1-5/pten⁻* development in both the absence and presence of VPA.

WT (Ax2) (left) and *pi3k1-5/pten⁻* (right) cells were developed on nitrocellulose membranes for 24 hours in both the absence (top row) and presence (descending rows) of 0.3 mM, 0.5 mM and 1 mM VPA. Images were taken of an overhead view (left) of the whole membrane and of a single fruiting body (right). Fruiting bodies developed in both cell lines in the absence of VPA and developed into fingers in the presence of 0.3 mM and 0.5 mM and into mounds in the presence of 1 mM VPA. $n = 3$. Scale bar of the overhead view represents 0.5 mm and of the side view 0.1 mm.

3.1.3 Analysis of *pi3k1-5⁻/pten⁻* Cell Development in the Presence of Anti-Seizure Compounds and LiCl

The *pi3k1-5⁻/pten⁻* cells were then investigated as a potential target of other anti-seizure compounds and the BD treatment LiCl. The compounds tested have previously been shown to effect *D. discoideum* and *in vivo* epilepsy model growth, development and phosphoinositide and inositol phosphate signalling (Williams, et al., 1999; Williams, et al., 2002; Ludtmann, Boeckeler and Williams, 2011; Chang, et al., 2012; Chang, et al., 2013; Chang, Walker and Williams, 2014; Chang, et al., 2015; Chang, et al., 2016). In these experiments, cells were starved for 24 hours on nitrocellulose filters to induce development in the absence (control) and presence of a range of compounds at concentrations which blocked fruiting body development in WT cells (**Figure 3.7**). VPA structurally related epilepsy compounds VPD (6.5 mM) and PIA (1.4 mM) (Eickholt, et al., 2005; Ludtmann, Boeckeler and Williams 2011; Elphick, et al., 2012) were tested, as well as key components of the MCT diet DA (1.65 mM) and OA (0.22 mM) (Chang, et al., 2012; Chang, et al., 2013; Chang, et al., 2016). A branched chain compound, 4-EOA (0.5 mM), with known seizure control and neuroprotective effects was also tested (Chang, et al., 2013; Chang, et al., 2015). As a negative control, a compound which does not control seizures, 2-MHA (0.5 mM), was tested (Chang, et al., 2012). Under control conditions with no drug added, both WT and *pi3k1-5⁻/pten⁻* were able to develop into mature fruiting bodies after 24 hours of starvation. In the presence of all compounds tested, including LiCl, both WT and *pi3k1-5⁻/pten⁻* cells developed into fingers, slug or mounds. These results suggest that the mechanism of action of these compounds in *D. discoideum* does not involve the 5 PI3K or PTEN.

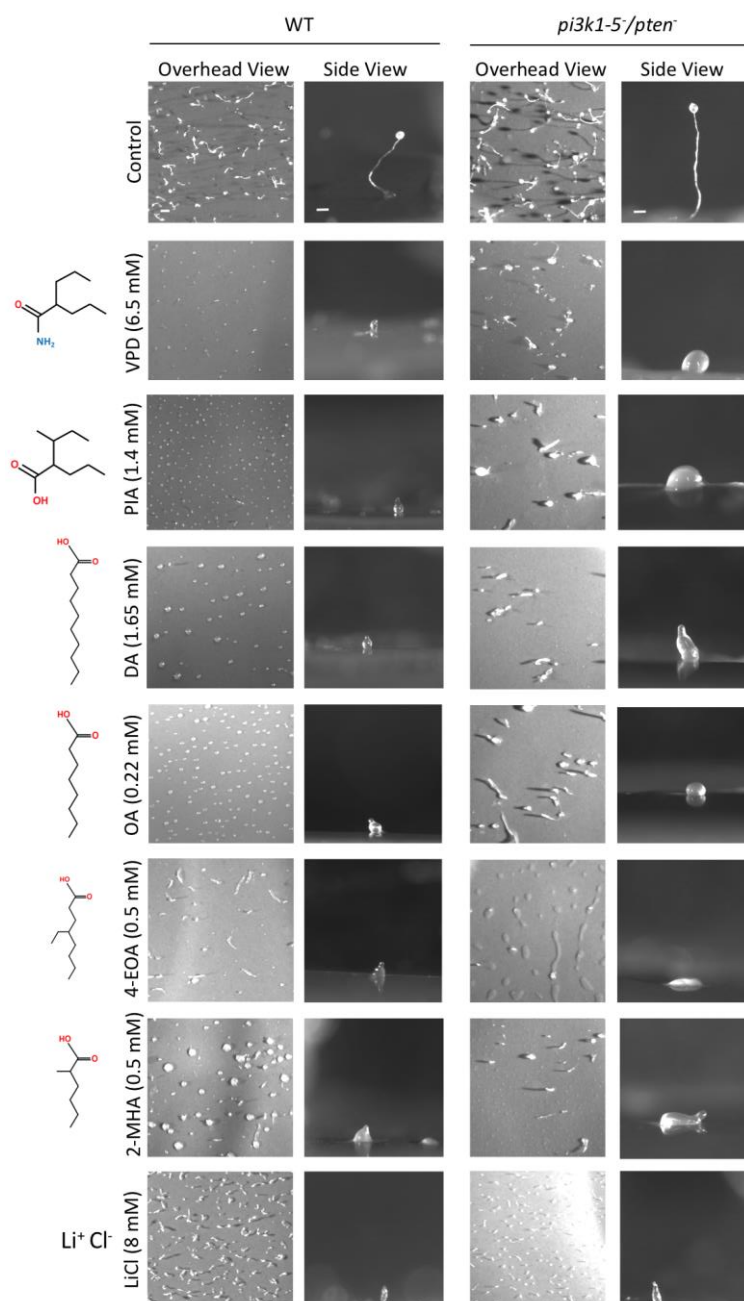


Figure 3.7. WT and *pi3k1-5/pten* development in both the absence and presence of a range of other compounds. WT (Ax2) (left) and *pi3k1-5/pten* (right) cells were developed on nitrocellulose membranes for 24 hours in both the absence (top row) and presence (descending rows) of VPD, PIA, DA, OA, 4-EOA, 2-MHA and LiCl at the stated concentrations to the left of the development images. Images were taken of an overhead view of the whole membrane (left) and of a single fruiting body (right). Both cell lines developed into fruiting bodies in the absence of any compound. In the presence of VPD, PIA, DA, OA, 4-EOA, 4-MOA and LiCl both WT and *pi3k1-5/pten* cells developed to the mound stage. $n = 3$. Scale bar of the overhead view represents 0.5 mm and of the side view 0.1 mm.

3.2 *plc*⁻ Cells

D. discoideum has one *Plc* isoform (DDB_G0292736), with peak expression during the developmental cycle (Drayer, et al., 1994; Parikh, et al., 2010; Stajdohar, et al., 2015). Of the 11 *H. sapiens* PLC isoforms, *D. discoideum* PLC has highest identity to PLC ϵ 1 (45 %, E-value $4e^{-43}$) (**Supplementary Table S3**), suggesting both the *D. discoideum* and *H. sapiens* PLC enzymes have a similar catalytic role. In 1994 Drayer et al deleted PLC from Ax3 parental cells, thereby blocking the hydrolysis of PIP₂ into IP₃ and DAG, resulting in *plc*⁻ cells. Through a series of experiments, *plc*⁻ cells have been phenotypically characterized and compared with WT in both the absence and presence of VPA during acute cell behaviour and to a range of anti-seizure compounds and the BD drug LiCl during *D. discoideum* development.

3.2.1 Analysis of *plc*⁻ Acute Cell Behaviour in the Presence of VPA

As peak PLC expression is during the developmental cycle, acute cell behaviour of starved *plc*⁻ cells in both the absence and presence of VPA was investigated. This is because VPA is known to inhibit *D. discoideum* cell movement (Xu, et al., 2007). In this assay, cells were pulsed for 5 hours with cAMP to stimulate cells to enter early development. Time lapse microscopy was then employed in which computer-generated cell outlines detected changes in cell displacement (the shortest distance a cell travels between 2 points), circularity (cell shape, with an arbitrary value of “1” given to round cells), membrane protrusions and motility (speed) (**Figure 3.8A**). A control period of 225 seconds prior to VPA treatment (ranging from 0.01 mM-0.7 mM) for 525 seconds was used to determine any initial differences in cell behaviour (**Table 3.2** and **Figures 3.8B- 3.8E**). No significant differences (P values over 0.05) were identified between WT and *plc*⁻ cells in the absence of VPA for displacement, circularity, membrane protrusions and motility. In the presence of VPA, both cell lines had a dose-dependent reduction in acute cell behaviour (displacement, circularity, membrane protrusions and motility) with no significant differences being identified.

<u>Cell Line</u>	<u>[VPA] (mM)</u>						<u>VPA IC₅₀ Value (mM)</u>
	<u>Control</u>	<u>0.01</u>	<u>0.1</u>	<u>0.3</u>	<u>0.5</u>	<u>0.7</u>	
<i>Displacement (μm)</i>							
WT	115.4 ± 5.7	116.3 ± 7.1	70.8 ± 4.1	62.9 ± 3.1	65.1 ± 3.0	62.1 ± 3.6	0.4 ± 0.12
<i>plc⁻</i>	112.2 ± 8.8	114.3 ± 8.3	84.0 ± 5.2	74.7 ± 3.6	68.9 ± 4.0	62.1 ± 3.2	0.4 ± 0.07
<i>Circularity</i>							
WT	0.76 ± 0.005	0.70 ± 0.003	0.74 ± 0.005	0.89 ± 0.005	0.89 ± 0.002	0.86 ± 0.005	-
<i>plc⁻</i>	0.65 ± 0.005	0.64 ± 0.006	0.78 ± 0.006	0.88 ± 0.003	0.87 ± 0.004	0.86 ± 0.005	-
<i>Protrusions</i>							
WT	7.5 ± 0.07	8.8 ± 0.07	8.4 ± 0.03	5.0 ± 0.08	3.9 ± 0.05	2.6 ± 0.06	0.4 ± 0.03
<i>plc⁻</i>	7.2 ± 0.09	7.8 ± 0.10	8.4 ± 0.08	5.0 ± 0.09	3.1 ± 0.13	2.6 ± 0.06	0.4 ± 0.04
<i>Motility (μm/sec)</i>							
WT	0.021 ± 0.0016	0.021 ± 0.0013	0.012 ± 0.0008	0.007 ± 0.0007	0.006 ± 0.0006	0.003 ± 0.0005	0.2 ± 0.06
<i>plc⁻</i>	0.030 ± 0.0015	0.030 ± 0.0018	0.019 ± 0.0016	0.008 ± 0.0008	0.004 ± 0.0006	0.003 ± 0.0005	0.1 ± 0.01

Table 3.2. WT and *plc⁻* changes in acute cell behaviour in both the absence and presence of VPA. Comparison of WT (Ax3) and *plc⁻* acute cell behaviour values of total displacement during the assay and average circularity, protrusions and motility within the final 300 seconds. The calculated IC₅₀ values are shown to the right of the table for each cell line for displacement, number of protrusions and motility. Data presented as mean (+/- SEM). *n* = 30.

The similarity in response to VPA of WT and *plc⁻* cells to displacement (**Figure 3.8F**), circularity (**Figure 3.8G**), membrane protrusions (**Figure 3.8H**) and motility (**Figure 3.8I**) is shown in the secondary plots, where the curves for the two cell lines overlap. The similarity in response to VPA for the two cell lines is also shown by the calculated IC₅₀ values for WT and *plc⁻* cells (**Table 3.2**).

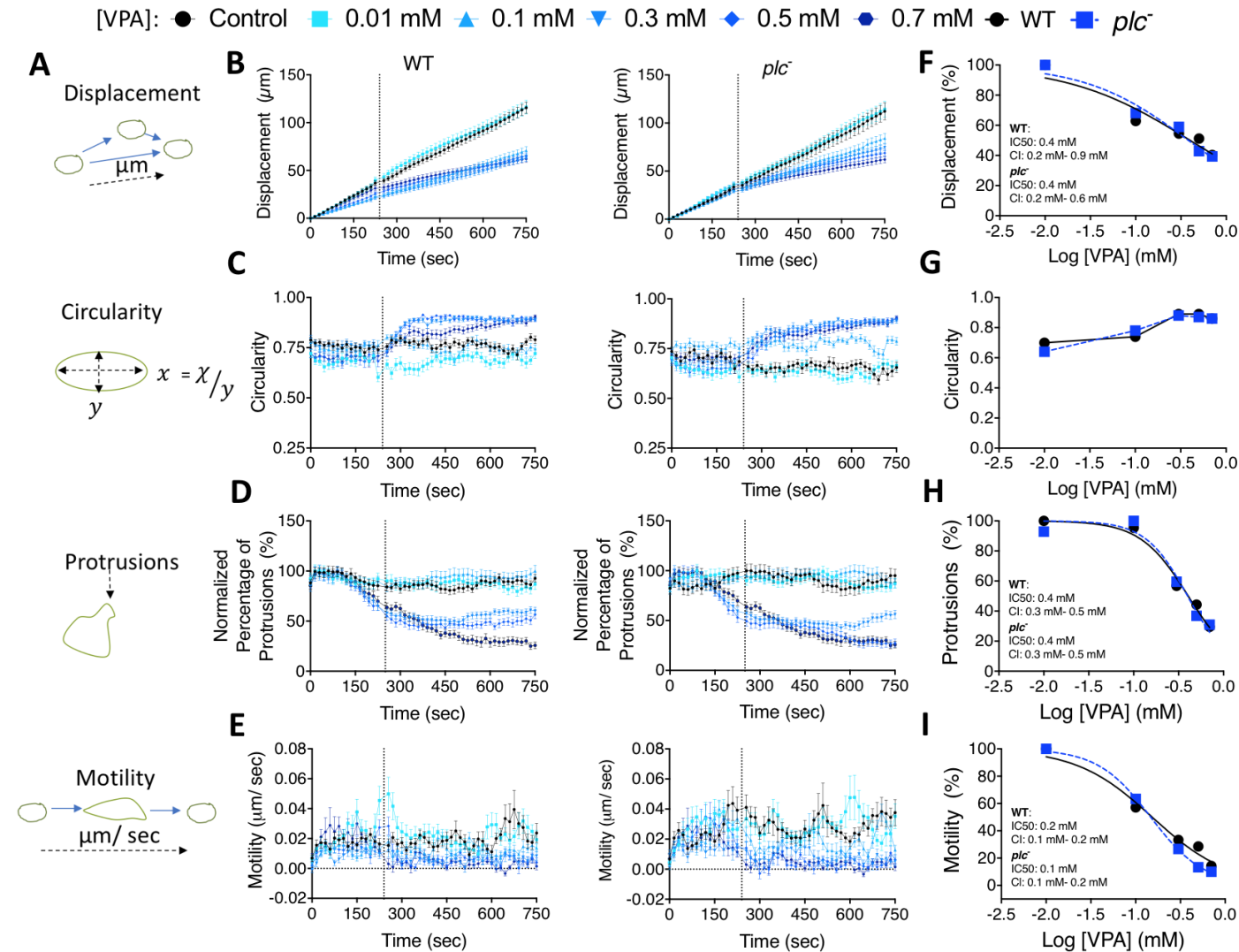


Figure 3.8. WT and *plc*⁻ acute cell behaviour in both the absence and presence of VPA. (A) Schematic of the quantitative measurements taken during the assay where the black dashed arrows represent the measurement being taken for the primary data (B) displacement, (C) circularity, (D) membrane protrusions and (E) motility for WT (Ax3) (left) and *plc*⁻ (middle) cells. Secondary plot data for (F) displacement, (G) circularity, (H) membrane protrusions and (I) motility with WT shown in black circles and *plc*⁻ shown in blue squares (right). Data presented as mean (+/- SEM) *n* = 30 cells.

3.2.2 Analysis of *plc*⁻ Cell Development in the Presence of VPA

As VPA is known to inhibit the development of multicellular fruiting bodies within 24 hours (Williams, et al., 2002), *D. discoideum* development was investigated using WT and *plc*⁻ cells in the absence (control) and presence of VPA (0.3 mM-1 mM) (**Figure 3.9**). In the absence of VPA, both WT and *plc*⁻ cells were able to develop into similar sized multicellular fruiting bodies containing a basal disc, stalk and spore head. In the presence of 0.3 mM and 0.5 mM VPA, WT cells developed into finger structures, whereas *plc*⁻ cells developed into mounds. In the presence of 1 mM VPA, both cell lines developed into mounds, suggesting *plc*⁻ cells are more sensitive to VPA compared with WT cells during development.

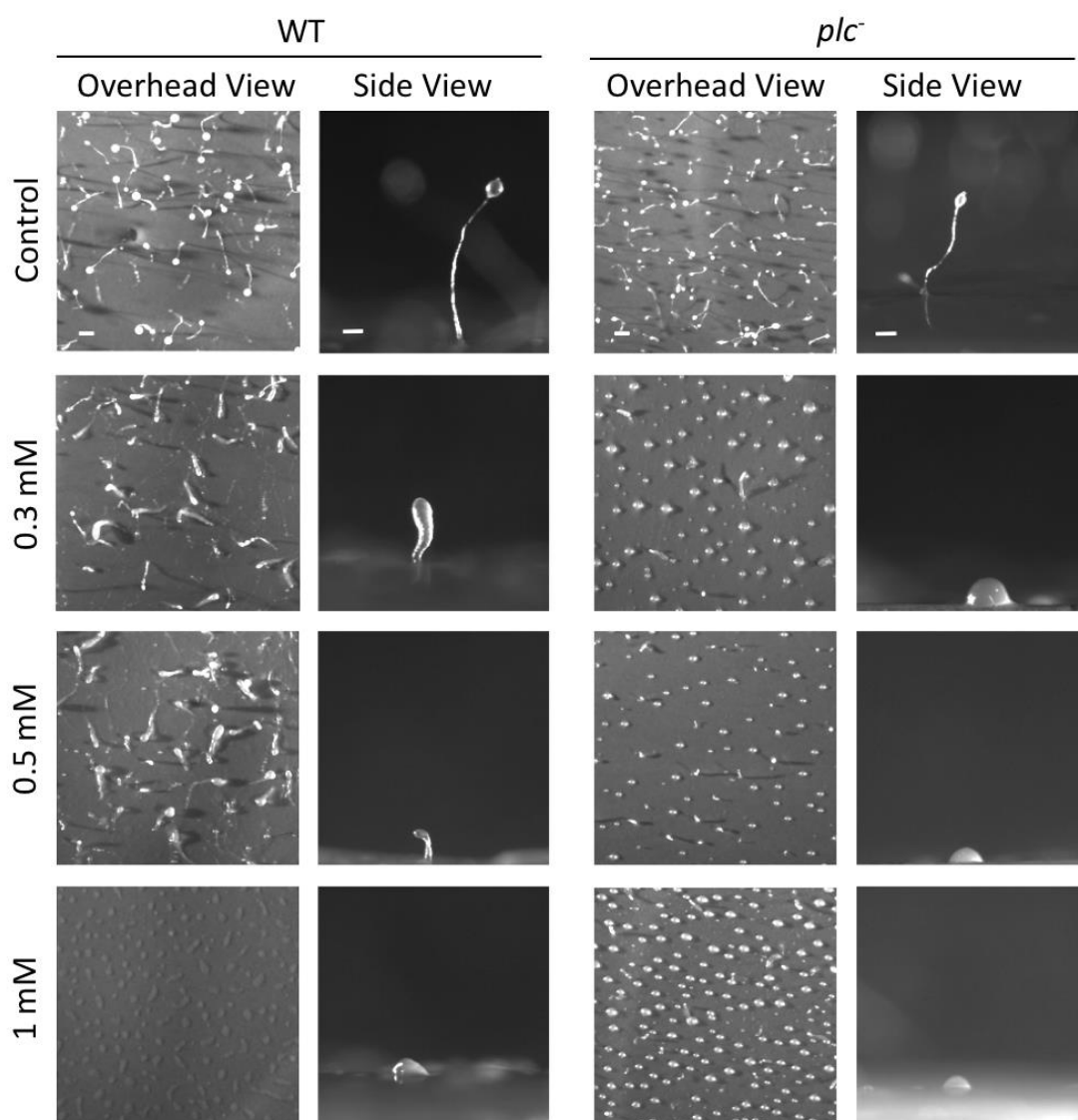


Figure 3.9. WT and *plc*⁻ development in both the absence and presence of VPA. WT (Ax3 (left)) and *plc*⁻ (right) cells were developed on nitrocellulose membranes for 24 hours in both the absence (top row) and presence (descending rows) of 0.3 mM, 0.5 mM and 1 mM VPA. Images were taken of an overhead view (left) of the whole membrane and of a single fruiting body (right). Fruiting bodies developed in both cell lines in the absence of VPA and developed into either fingers or mounds in the presence of 0.3 mM, 0.5 mM and 1 mM VPA. *n* = 3. Scale bar of the overhead view represents 0.5 mm and of the side view 0.1 mm.

3.2.3 Analysis of *plc*⁻ Cell Development in the Presence of Anti-Seizure Compounds and LiCl

PLC was then investigated as a potential target of other anti-seizure compounds and the BD treatment LiCl. These compounds were investigated during

development, which was induced by starving cells for 24 hours on nitrocellulose filters in both the absence (control) and presence of a range of treatments at concentrations which blocked fruiting body development in WT cells (**Figure 3.10**). The anti-seizure compounds tested were VPD (6.5 mM), PIA (1.4 mM), DA (1.65 mM), OA (0.22 mM), 4-EOA (0.5 mM) and 2-MHA (0.5 mM) (Eickholt, et al., 2005; Ludtmann, Boeckeler and Williams 2011; Elphick, et al., 2012; Chang, et al., 2012; Chang, et al., 2013; Chang, et al., 2015; Chang, et al., 2016). Both WT and *plc*⁻ cells developed into mature fruiting bodies after 24 hours of starvation under control conditions. In the presence of all compounds tested, both WT and *plc*⁻ cells developed into finger or mound structures respectively, suggesting that the mechanism of action of these compounds does not involve PLC in *D. discoideum*. These results suggest that *plc*⁻ cells are more sensitive to the anti-seizure compounds tested here and LiCl, compared with WT.

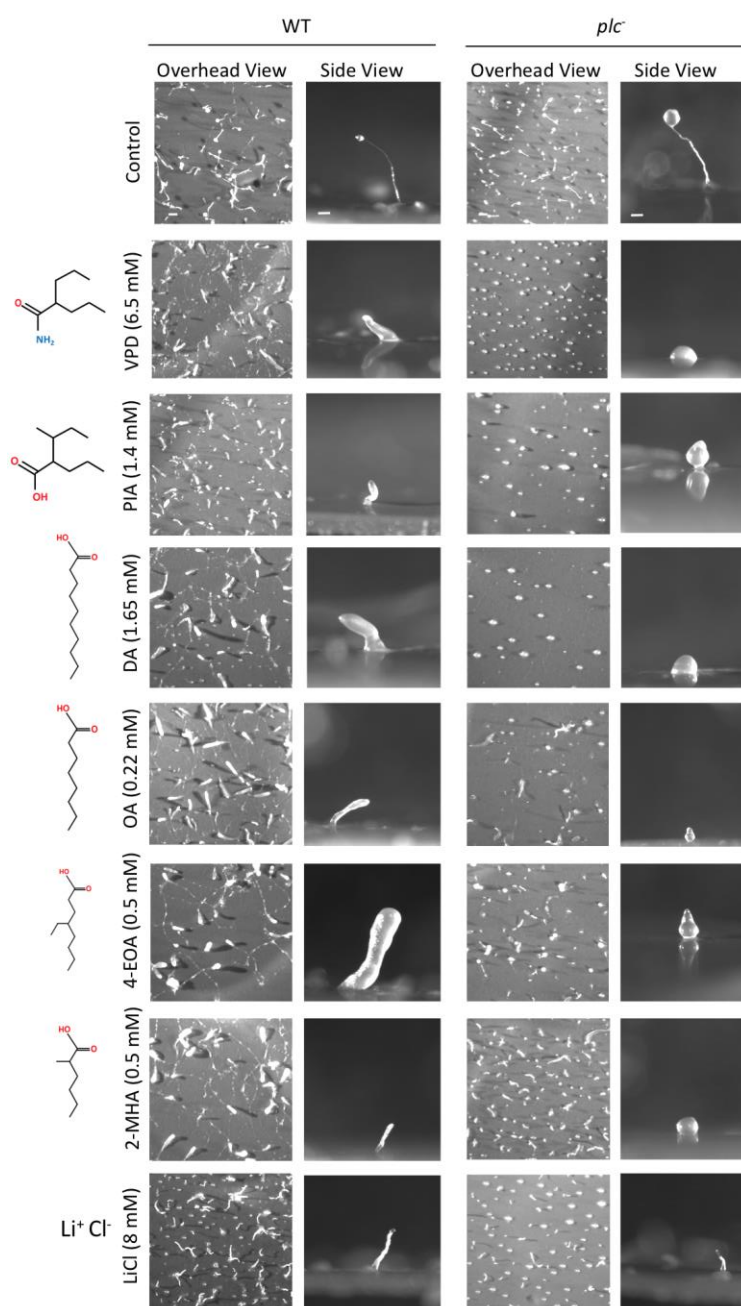


Figure 3.10. WT and *plc⁻* development in both the absence and presence of a range of other compounds. WT (Ax3) (left) and *plc⁻* (right) cells were developed for 24 hours on nitrocellulose membranes both in the absence (top row) and presence (descending rows) of VPD, PIA, DA, OA, 4-EOA, 2-MHA and LiCl at the stated concentrations to the left of the development images. Images were taken of an overhead view of the whole membrane (left) and of a single fruiting body (right). Both cell lines developed into fruiting bodies in the absence of any compound. In the presence of VPD, PIA, DA, OA, 4-EOA, 4-MOA and LiCl both WT and *plc⁻* cells developed to the finger or mound stage. $n = 3$. Scale bar of the overhead view represents 0.5 mm and of the side view 0.1 mm.

3.3 *lpin2*⁻ Cells

There is one *Lipin* isoform in *D. discoideum*, *Lpin2* (DDB_G0271730), which has peak expression during the vegetative phase and at the latter stages of the developmental cycle (Parikh, et al., 2010; Stajdohar, et al., 2015). *D. discoideum* LPIN2 has 33 % identity (E-value 4e⁻⁸⁶) to the LPIN2 *H. sapiens* isoform (**Supplementary Table S4**), suggesting a similar catalytic role for this enzyme in both organisms. LPIN2 was ablated in Ax2 cells by Markus Maniak, thereby blocking the dephosphorylation of PA into DAG, resulting in *lpin2*⁻ cells. The *lpin2*⁻ cells have been phenotypically characterized and compared with WT in both the absence and presence of VPA during acute cell behaviour and to a range of anti-seizure compounds and a BD drug during *D. discoideum* development.

3.3.1 Analysis of *lpin2*⁻ Acute Cell Behaviour in the Presence of VPA

Acute cell behaviour of *lpin2*⁻ cells was investigated due to high protein expression during the developmental cycle. This is because VPA is known to inhibit *D. discoideum* cell movement (Xu, et al., 2007). In this assay, cells were pulsed for 5 hours with cAMP to stimulate cells to enter early development, which was followed by time-lapse microscopy. Changes in cell displacement (the shortest distance a cell travels from point A to B), circularity (cell shape, with an arbitrary value of “1” given to round cells), membrane protrusions and motility (speed) were then determined in both the absence and presence of VPA (**Figure 3.11A**). A control period of 225 seconds prior to VPA treatment (ranging from 0.01 mM-0.7 mM) for 525 seconds was used to determine any initial differences in cell behaviour (**Table 3.3** and **Figures 3.11B- 3.11E**). No significant differences (P value above 0.05) were identified between WT and *lpin2*⁻ cells under control conditions with no VPA treatment, for displacement, circularity and membrane protrusions. However, there was a significant difference in motility (P value 0.01) between the two cell lines in the absence of VPA. This result suggests that LPIN2 has a role in cell motility. In the presence of VPA, both cell lines had a dose-dependent reduction in acute cell behaviour (displacement, circularity, membrane protrusions and motility), with a significant difference identified for displacement in the presence of

0.1 mM VPA (P value 0.027). These results suggest that LPIN2 is not a target of VPA during acute cell behaviour.

<u>Cell Line</u>	<u>[VPA] (mM)</u>						<u>VPA IC₅₀ Value (mM)</u>
	<u>Control</u>	<u>0.01</u>	<u>0.1</u>	<u>0.3</u>	<u>0.5</u>	<u>0.7</u>	
<i>Displacement (μm)</i>							
WT	75.6 ± 5.2	71.2 ± 4.0	60.7 ± 3.2	55.6 ± 3.0	42.5 ± 2.1	38.5 ± 1.8	0.6 ± 0.03
<i>lpin2⁻</i>	68.0 ± 3.2	73.8 ± 5.2	49.0 ± 3.6	52.1 ± 1.8	50.8 ± 3.7	48.2 ± 2.2	1.3 ± 0.3
<i>Circularity</i>							
WT	0.67 ± 0.004	0.71 ± 0.003	0.81 ± 0.004	0.86 ± 0.003	0.91 ± 0.002	0.92 ± 0.002	-
<i>lpin2⁻</i>	0.70 ± 0.003	0.62 ± 0.003	0.73 ± 0.003	0.79 ± 0.003	0.84 ± 0.003	0.89 ± 0.001	-
<i>Protrusions</i>							
WT	7.6 ± 0.04	6.9 ± 0.09	4.4 ± 0.07	4.3 ± 0.06	2.4 ± 0.03	1.4 ± 0.06	0.3 ± 0.11
<i>lpin2⁻</i>	8.4 ± 0.10	9.0 ± 0.08	6.6 ± 0.05	5.7 ± 0.06	4.5 ± 0.05	3.9 ± 0.12	0.5 ± 0.06
<i>Motility (μm/sec)</i>							
WT	0.019 ± 0.0004	0.016 ± 0.0007	0.007 ± 0.0007	0.005 ± 0.0006	0.003 ± 0.0003	0.002 ± 0.0003	0.1 ± 0.09
<i>lpin2⁻</i>	0.009 ± 0.0006	0.016 ± 0.0009	0.008 ± 0.0006	0.008 ± 0.0004	0.006 ± 0.0007	0.004 ± 0.0005	0.2 ± 0.15

Table 3.3. WT and *lpin2⁻* changes in acute cell behaviour in both the absence and presence of VPA. Comparison of WT (Ax2) and *lpin2⁻* acute cell behaviour values of total displacement during the assay and average circularity, protrusions and motility within the final 300 seconds. The calculated IC₅₀ values are shown to the right of the table for each cell line for displacement, number of protrusions and motility. Data presented as mean (+/- SEM). *n* = 30.

The similarity in response to VPA between WT and *lpin2⁻* cells to displacement (**Figure 3.11F**), circularity (**Figure 3.11G**), membrane protrusions (**Figure 3.11H**) and motility (**Figure 3.11I**) is shown in the secondary plots. The extent of VPA inhibition

on *lpin2*⁻ cells displacement, membrane protrusions and motility was not as potent as that on WT cells as shown in the calculated IC₅₀ values for the two cell lines (**Table 3.3**). These results suggest that the potency of VPA on *D. discoideum* acute cell behaviour is independent of LPIN2 activity.

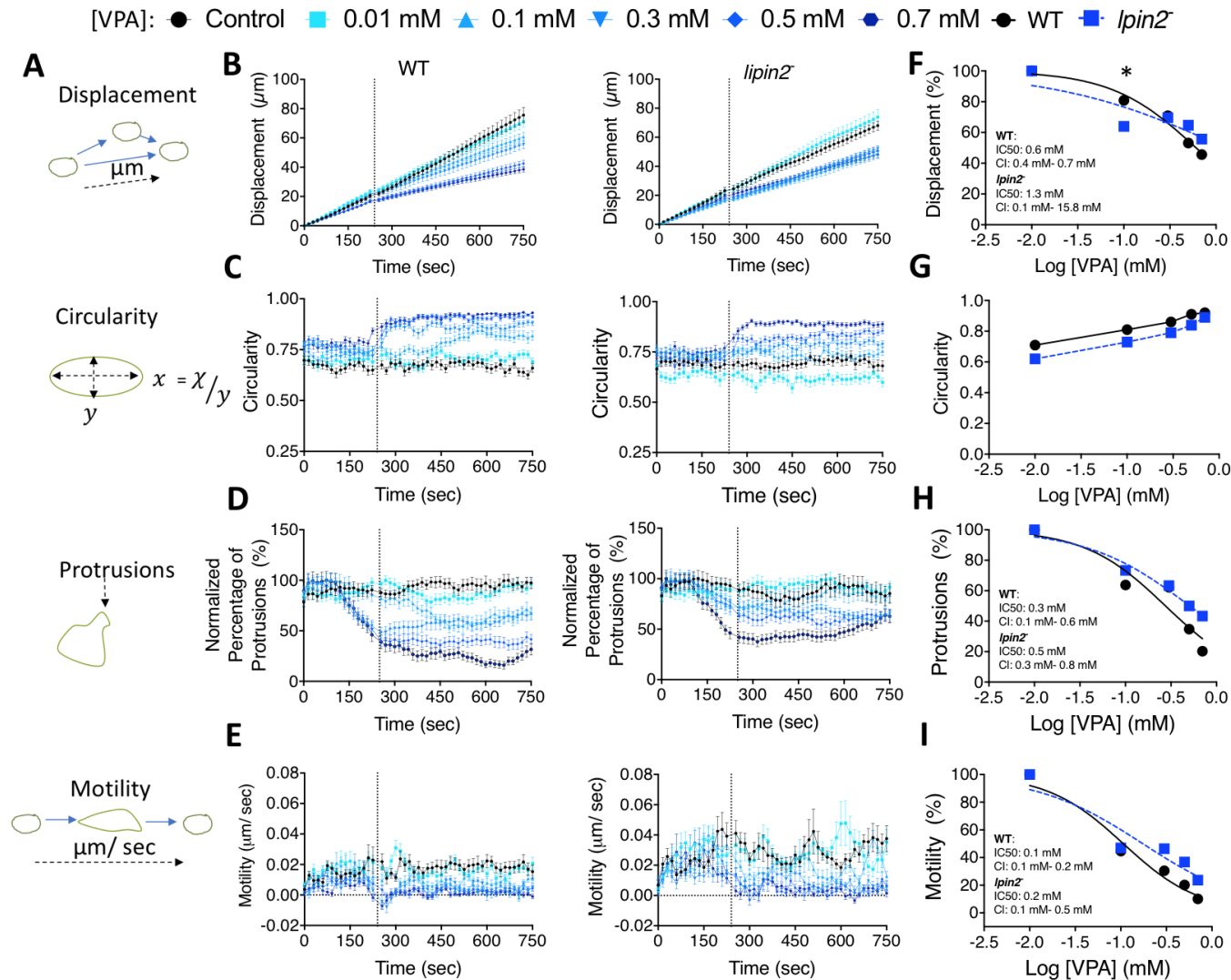


Figure 3.11. WT and *lpin2*⁻ acute cell behaviour in both the absence and presence of VPA. (A) Schematic of the quantitative measurements taken during the assay where the black dashed arrows represent the measurement being taken for the primary data (B) displacement, (C) circularity, (D) membrane protrusions and (E) motility for WT (Ax2) (left) and *lpin2*⁻ (middle) cells. Secondary plot data for (F) displacement, (G) circularity, (H) membrane protrusions and (I) motility with WT shown in black circles and *lpin2*⁻ shown in blue squares (right). *P* value: * *P* value = ≤ 0.05. Data presented as mean (+/- SEM) *n* = 30 cells.

3.3.2 Analysis of *lpin2*⁻ Cell Development in the Presence of VPA

Due to the expression of LPIN2 during *D. discoideum* development and as previous studies have shown VPA to inhibit development of *D. discoideum* within 24 hours (Williams, et al., 2002), cell development was investigated. In this assay, WT and *lpin2*⁻ cell development was compared in both the absence (control) and presence of VPA (0.3 mM-1 mM) (**Figure 3.12**). Under control conditions, both WT and *lpin2*⁻ cells developed into multicellular fruiting bodies containing a basal disc, stalk and spore head of a similar size. In the presence of 0.3 mM and 0.5 mM VPA, both WT and *lpin2*⁻ cells developed into finger structures. In the presence of 1 mM VPA, both cell lines developed into mounds, suggesting LPIN2 is not the target of, or regulated by, VPA during development.

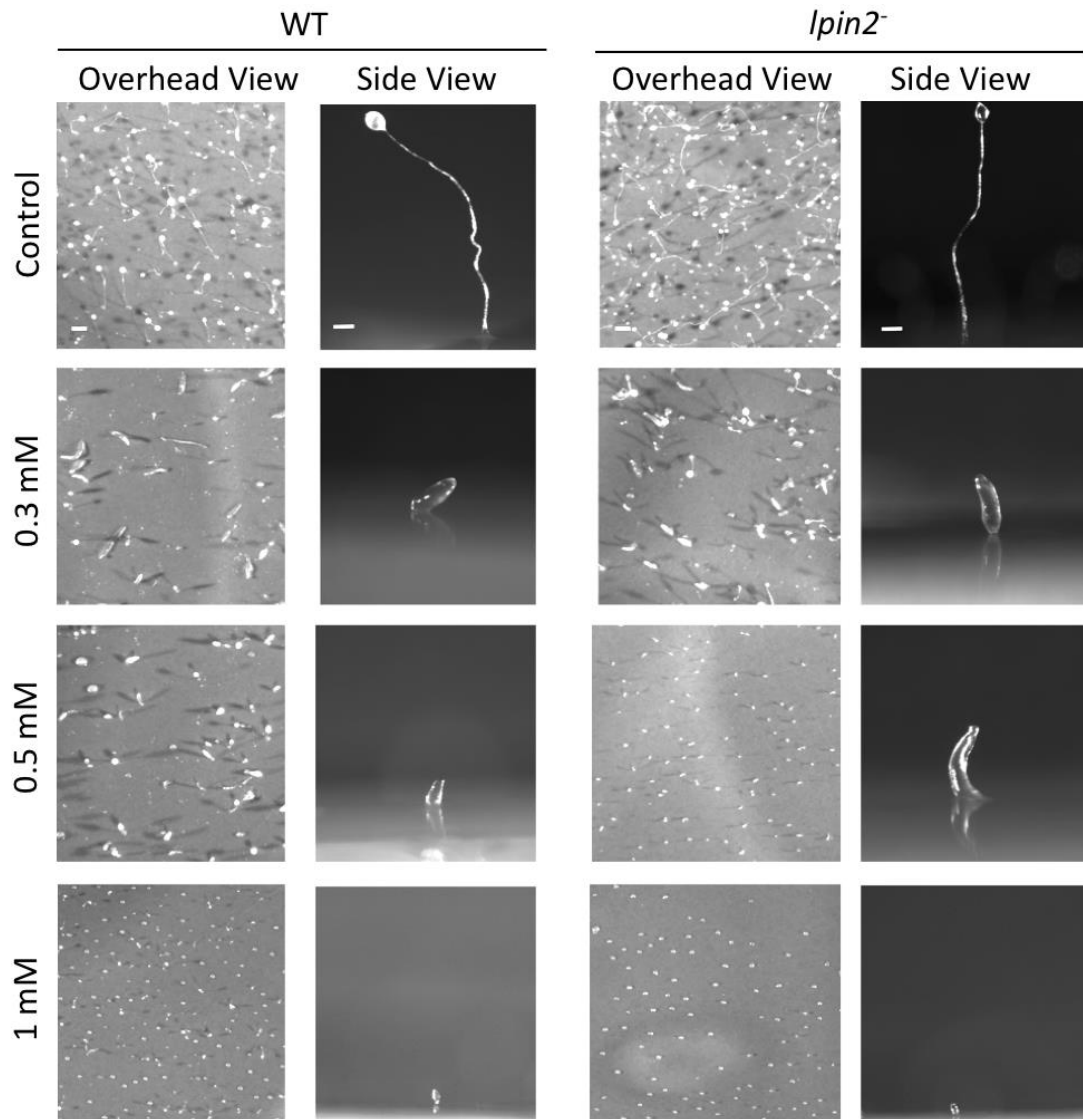


Figure 3.12. WT and *lpin2⁻* development in both the absence and presence of VPA. WT (Ax2) (left) and *lpin2⁻* (right) cells were developed for 24 hours on nitrocellulose membranes in both the absence (top row) and presence (descending rows) of 0.3 mM, 0.5 mM and 1 mM VPA. Images were taken of an overhead view (left) of the whole membrane and of a single fruiting body (right). Fruiting bodies developed in both cell lines in the absence of VPA and developed into fingers in the presence of 0.3 mM and 0.5 mM and into mounds in the presence of 1 mM VPA. $n = 3$. Scale bar of the overhead view represents 0.5 mm and of the side view 0.1 mm.

3.3.3 Analysis of *lpin2*⁻ Cell Development in the Presence of Anti-Seizure Compounds and LiCl

LPIN2 was also investigated as a possible target of other potential anti-seizure compounds and the BD treatment LiCl. *D. discoideum* cells were starved for 24 hours on nitrocellulose filters in both the absence (control) and presence of a range of compounds at concentrations which blocked fruiting body development in WT cells (**Figure 3.13**). The compounds tested were structural derivatives of VPA, VPD (6.5 mM) and PIA (1.4 mM) (Eickholt, et al., 2005; Ludtmann, Boeckeler and Williams 2011; Elphick, et al., 2012), the main components of the MCT diet DA (1.65 mM) and OA (0.22 mM) and two branched chain compounds, 4-EOA (0.5 mM), which has known neuroprotection effects and 2-MHA (0.5 mM), which does not control seizures and was used as a negative control (Chang, et al., 2012; Chang, et al., 2013; Chang, et al., 2015; Chang, et al., 2016). Both WT and *lpin2*⁻ cells developed into mature fruiting bodies after 24 hours of starvation under control conditions. In the presence of all compounds tested, both WT and *lpin2*⁻ cells developed into fingers or mounds, suggesting that the mechanism of action of these compounds does not involve LPIN2 in *D. discoideum*.

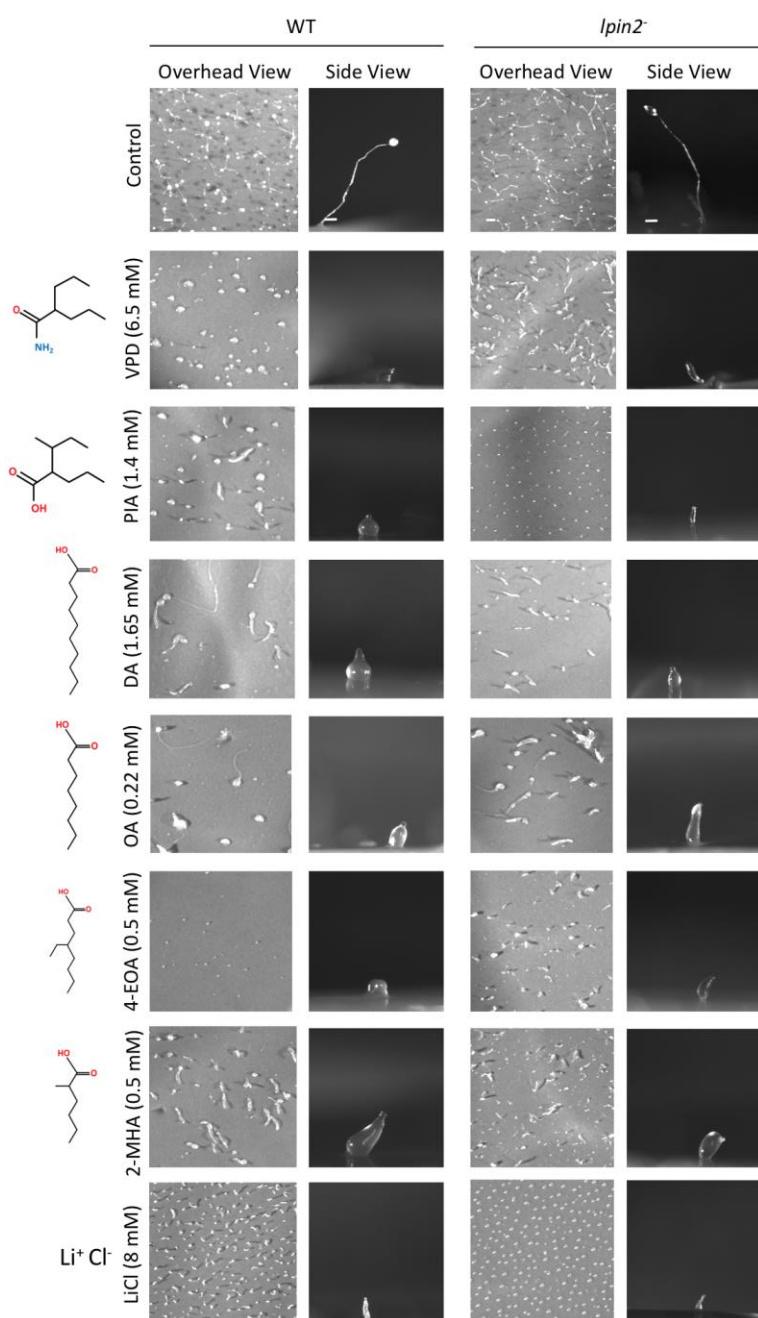


Figure 3.13. WT and *lpin2⁻* development in both the absence and presence of a range of other compounds. WT (Ax2) (left) and *lpin2⁻* (right) cells were developed for 24 hours on nitrocellulose membranes both in the absence (top row) and presence (descending rows) of VPD, PIA, DA, OA, 4-EOA, 2-MHA and LiCl at the stated concentrations to the left of the development images. Images were taken of an overhead view of the whole membrane (left) and of a single fruiting body (right). Both cell lines developed into fruiting bodies in the absence of any compound. In the presence of VPD, PIA, DA, OA, 4-EOA, 4-MOA and LiCl both WT and *lpin2⁻* cells developed to the finger or mound stage. $n = 3$. Scale bar of the overhead view represents 0.5 mm and of the side view 0.1 mm.

3.4 Discussion

Previous research determining the mechanism of action of VPA has shown the AED reduces phosphoinositide levels in a time and dose-dependent manner (Chang, et al., 2012). This chapter, therefore, reports the phenotypic characterization of *D. discoideum* knockout mutants of all 5 PI3K (PIKA, PIKB, PIKC, PIKF, PIKG) and PTEN (termed *pi3k-/pten-*), PLC and LPIN2 during acute cell behaviour and development in response to a range of anti-seizure compounds and the BD treatment LiCl. PI3K and PTEN were phenotypically characterized in response to VPA during acute cell behaviour and development as this has not been conducted previously.

A key component of the PI salvage pathway is the signalling molecule PIP₂, which can be phosphorylated by PI3K into PIP₃ to regulate a number of signalling pathways. This reaction is reversible, whereby PTEN dephosphorylates PIP₃ back into PIP₂. Due to the importance of both the forward and reverse reactions, *pi3k1-5-/pten-* cells lacking all 5 *D. discoideum* PI3K and PTEN was created by Hoeller and Kay (2007). The phenotype of these cells was investigated to determine VPA sensitivity or resistance during acute and chronic drug exposure. During acute cell behaviour, *pi3k1-5-/pten-* cells were sensitive to VPA, although the extent of 0.5 mM VPA inhibition on cell displacement, circularity and membrane protrusions was not as severe compared with WT cells. This could be due to *D. discoideum* PIP₃ chemotactic gradients arising at the plasma membrane. This allows the cell to orientate itself to external cAMP gradients, thereby enabling the cell to move forward. However, starvation of *pi3k1-5-/pten-* cells with pulsate cAMP enables the cells to become chemotactically competent (Hoeller and Kay, 2007). Consistent with previous studies, *pi3k1-5-/pten-* cells were able to chemoattract like WT cells (Hoeller and Kay, 2007), suggesting cell displacement and membrane protrusions would also be similar to WT, as it is the protrusions which enables the cell to move towards a cAMP gradient. In contrast, it has previously been reported that *pi3k1-5-/pten-* cells had a 36 % reduction in motility compared with WT cells (Hoeller and Kay, 2007), which was not demonstrated in this experiment. The reason for these differences could be genetic variation within the same and different *D. discoideum*

WT strains between different laboratories. This arises as gene duplications are common and can result from the number of times a cell has divided (copy number) (Bloomfield, et al., 2008). To continue investigating these two proteins, independent cell lines lacking all 5 *D. discoideum* PI3K and PTEN should be characterized in both the absence and presence of VPA to ensure there are no single mutational effects nor that the phenotype of one mutant is concealed by the other.

Chronic VPA treatment of *pi3k1-5/pten*⁻ was investigated as all of the genes ablated in the mutant are expressed during the *D. discoideum* developmental cycle. This involved comparing fruiting body development of *pi3k1-5/pten*⁻ cells with WT, in both the absence and presence of VPA. Unlike previous work (Hoeller and Kay, 2007), under control conditions both WT and *pi3k1-5/pten*⁻ cells developed into mature fruiting bodies of similar size. In the presence of VPA, the drug blocked development of mature fruiting bodies, whereby both cell lines developed into fingers and mounds. These results are consistent with the molecular phenotype shown previously where there was a reduction in PIP and PIP₂ levels by 28 % and 44 % in *pi3k1-5/pten*⁻ cells compared with WT, which was significantly reduced in the presence of 0.5 mM VPA (Chang, et al., 2012). In addition, VPA has been shown to enhance the effects of a PI3K inhibitor in WT cells (Chang, et al., 2012). This result suggests that VPA acts like a PI3K inhibitor in *D. discoideum* and together with the VPA-sensitive phenotype shown here during *D. discoideum* development, it appears that neither PI3K nor PTEN are targets, or are regulated by, VPA in *D. discoideum*.

In addition to investigating VPA, a range of structurally related compounds, key components of the MCT diet or branched compounds, as well as the BD treatment LiCl, were also tested on *pi3k1-5/pten*⁻ cell development. In the presence of all of the compounds tested (VPD, PIA, DA, OA, 4-EOA, 2-MHA and LiCl) both WT and *pi3k1-5/pten*⁻ cells developed into fingers, slugs or mounds, and thereby demonstrated drug-sensitivity. This result suggests that the mechanism of action of all of these compounds does not involve the 5 PI3K or PTEN in *D. discoideum*. This

result was of interest as previous studies have linked the PI3K/PIP₃/Akt pathway, apoptosis and PTEN with seizure generation (Backman, et al., 2001; Shinoda, 2004) and the compounds tested here do not appear to target PI3K nor PTEN. Apoptosis can be caused by the catabolite farnesol, a component of the cholesterol/isoprenoid biosynthetic pathway, whose mechanism of action is suppressed by the PI salvage pathway component DAG (Taylor, et al., 2005). This therefore, suggests a role of the PI salvage pathway in seizure prevention independent of PI3K and PTEN.

As the *pi3k1-5⁻/pten⁻* cells were sensitive to all compounds tested, the PI salvage pathway component PLC was investigated. PLC is the enzyme responsible for the hydrolysis of PIP₂ into IP₃ and DAG, thereby diminishing PIP₂ levels. *plc⁻* cells were created by Drayer et al (1994) and these were used for phenotypic characterization during acute and chronic VPA exposure. Under control conditions and acute treatment of VPA, *plc⁻* cells responded almost identically to WT, with a dose-dependent reduction in displacement, membrane protrusions and motility, correlated with an increase in circularity when exposed to higher VPA concentrations. This suggests that PLC is not a target of VPA in *D. discoideum*. The similarity of the *plc⁻* cell behaviour to WT is consistent with a previous report (Drayer, et al., 1994). A point mutation resulting in loss-of-function of PLC was identified in a drug-resistant epilepsy patient (Kurian, et al., 2010). This mutation in PLC resulted in neurological regression and death (Kurian, et al., 2010). Additionally, a PLC knockout mouse (PLCβ1^{-/-}) displayed an epileptic phenotype and PLCβ4^{-/-} mutant mice demonstrated signs of ataxia (affected coordination, speech and balance) (Kim, et al., 1997), suggesting a role of PLC in mammalian development. However, VPA does not appear to target or regulate PLC in response to acute VPA treatment during the early stages of *D. discoideum* development. This difference between *D. discoideum* and the mammalian phenotype could be a result of other cellular effects. This is because mammals contain multiple PLC isoforms, whereas *D. discoideum* has only one. Therefore, ablation of one PLC isoform in mammalian models may result in the upregulation of other PLC isoforms, which in turn results in the upregulation of other inositol phosphate and DAG species which are responsible for the epileptic phenotype demonstrated in PLC knockout mice.

Next, the *D. discoideum* developmental cycle was investigated by comparing *plc*⁻ cells with WT in both the absence and presence of VPA. Both cell lines developed into mature fruiting bodies over 24 hours under control conditions, consistent with previous work (Drayer, et al., 1994). In the presence of VPA, both WT and *plc*⁻ cells developed into fingers or mounds over 24 hours, suggesting that during chronic exposure to VPA, PLC is not a target of the drug in *D. discoideum*. However, the PI salvage pathway has been linked with seizures where kainic acid, a seizure inducing compound, resulted in mild seizures in rats with severe hippocampal damage and sustained release of IP₃ within the initial 10 minutes of seizure induction (Bodjarian, et al., 1993). In *C. elegans*, VPA has been shown to reduce inositol-1-phosphate and DAG levels (Tokuoka, Saiardi and Nurrish, 2008), highlighting the potential target of VPA to be a component of the PI salvage pathway.

In addition to VPA, a range of structurally related analogues, key components of the MCT diet and branched chain anti-seizure compounds, as well as the BD treatment LiCl, were investigated on *plc*⁻ cell development. In the presence of VPD, PIA, DA, OA, 4-EOA, 2-MHA and LiCl, both WT and *plc*⁻ cells developed into fingers or mounds within 24 hours, suggesting PLC is not the target of these compounds nor the BD treatment in *D. discoideum*. In addition to epilepsy, both reaction products of PLC, IP₃ and DAG, have been implicated with BD. PLC was a protein of interest as a range of studies have associated lithium treatment with a decrease in inositol and an increase in DAG levels in GH3 pituitary tumour cells (Drummond and Raeburn, 1984), neuroblastoma x glioma hybrid cells (NG108-15) (Brami, Leli and Hauser, 1991; Brami, Leli and Hauser, 1993) and in rat (Sherman, et al., 1981) and mouse (Sade, et al., 2016) models. However, PLC does not appear to be a target, or is regulated by, the anti-seizure or BD compounds tested in this study in *D. discoideum*.

Next, *Lpin2*, the enzyme responsible for the dephosphorylation of PA into DAG, was investigated. LPIN2 was an enzyme of interest as it controls lipid homeostasis by regulating cell growth and signalling (Banfić, et al., 1993; Cerbón, et al., 2005), glucose metabolism and lipid regulation (Milne, et al., 2008). Phenotypic

characterization of *lpin2*⁻ cells begun with acute cell behaviour where both WT and *lpin2*⁻ cells behaved in a similar manner for displacement and membrane protrusions. The *lpin2*⁻ cells had a lower circularity value compared with WT and moved significantly faster compared with parental WT. In the presence of VPA, both cell lines had a dose-dependent reduction in displacement, membrane protrusions and motility, correlating with an increase in circularity. However, this dose-dependent effect in the presence of VPA was typically delayed in *lpin2*⁻ cells compared with WT, with statistically significant differences between WT and *lpin2*⁻ cell displacement in the presence of 0.1 mM VPA. However, this VPA concentration is lower than the therapeutic concentration (0.3 mM-0.6 mM) (Kanner, 2003; Vázquez-Calvo et al., 2013). These results suggest that LPIN2 is not the target of VPA in *D. discoideum* during acute cell behaviour. The *lpin2*⁻ cells increased motility observed during control conditions is similar to that of LPIN2 deficient mice which displayed abnormal uncontrollable movement (ataxic gait) with rapid tail flicking compared with WT mice (Dwyer, et al., 2012).

The *D. discoideum* developmental cycle was then investigated to determine the effects of chronic VPA treatment on *lpin2*⁻ cells. Under control conditions, both WT and *lpin2*⁻ cells were able to develop into similar sized mature fruiting bodies. In the presence of VPA, both cell lines developed into finger or mound structures, suggesting LPIN2 is not a target of VPA during *D. discoideum* development. LPIN2 was a protein of interest as epilepsy patients can develop a condition called rhabdomyolysis, which is associated with seizures and results in damaged skeletal muscle breakdown (Walker, Duddy and Sagar, 1993). A study carried out in 1976 concluded that the onset of rhabdomyolysis in an epilepsy patient was associated with administration of the AED phenytoin, however, this has rarely been reported (Michael and Mitch, 1976; Kim, et al., 2016). Rhabdomyolysis arises from deficiency within LPIN1, resulting from a homozygous frameshift mutation and from both chromatids on chromosome 2 being maternally inherited (Michot, et al., 2010; Michot, et al., 2012; Meijer, et al., 2015). Therefore, it was a possibility that VPA targets or regulates LPIN2.

Other anti-seizure treatments, including VPA structurally related compounds (VPD and PIA), key components of the MCT diet (DA and OA) and branched compounds (4-EOA and 2-MHA) as well as the BD treatment LiCl were tested on *lpin2⁻* cell development. In the presence of all of these compounds, both WT and *lpin2⁻* cells developed into finger or mounds over 24 hours, with drug sensitivity suggesting LPIN2 is not the target, or is regulated by these compounds in *D. discoideum*. LPIN proteins are of interest in epilepsy and BD research as the reaction product DAG has increased levels during seizures (Yoshida, et al., 1987). Also, LPIN phosphorylation activates the mTOR pathway (Huffman, Mothe-Satney and Lawrence, 2002) which is important in epilepsy research as it regulates synaptic plasticity (Tang, et al., 2002), neuronal development, dendrite growth and morphology (Takei, et al., 2004; Jaworski, et al., 2005; Kumar, et al., 2005). Inhibitors of the mTOR pathway have been shown in animal models to reduce seizures and delay their development as well as prevent epileptogenesis (Zeng, et al., 2008; Ehninger, et al., 2008; Meikle, et al., 2008; van Vliet, et al., 2012). However, LPIN2 does not appear to be a target, or is regulated, by VPA in this study.

3.5 Summary

In *D. discoideum* the 5 PI3K, PTEN, PLC and LPIN2 are not essential for survival. Cell lines in which these genes had been ablated were used for phenotypic characterization in both the absence and presence of a range of anti-seizure compounds and the BD drug LiCl. Characterization begun using *pi3k1-5⁻/pten⁻* cells which had all *D. discoideum* PI3K and PTEN removed, therefore, preventing the forward and reverse reaction of PIP₂ to PIP₃. The *pi3k1-5⁻/pten⁻* cells were sensitive to VPA during acute and chronic drug exposure, suggesting these proteins are not a target, or are regulated by VPA in *D. discoideum*. The *pi3k1-5⁻/pten⁻* cells were also sensitive to the other anti-seizure compounds (VPD, PIA, DA, OA, 4-EOA and 2-MHA) and LiCl, highlighting these proteins are not targets or regulated by the compounds tested in this study in *D. discoideum*. The *plc⁻* cells were then characterized, where the hydrolysis reaction of PIP₂ into IP₃ and DAG was blocked.

During acute expose to VPA, *plc*⁻ cells had a dose-dependent reduction in cell movement mirroring that of WT cells. This was also demonstrated during chronic VPA treatment, suggesting VPA sensitivity in *D. discoideum* is not due to PLC. The *plc*⁻ cells were also sensitive to VPD, PIA, DA, OA, 4-EOA, 2-MHA and LiCl during development, suggesting PLC is not targeted or regulated by these drugs in *D. discoideum*. Finally, *lpin2*⁻ cells were characterized in the presence of a range of anti-seizure compounds and a BD treatment (VPA, VPD, PIA, DA, OA, 4-EOA, 2-MHA and LiCl) and showed sensitivity to all of these compounds. These results suggest that the mechanisms of action of these compounds is not through LPIN2 in *D. discoideum*. In this study, neither PI3K, PTEN, PLC nor LPIN2 are targets, or are regulated by VPA or the anti-seizure compounds tested here nor the BD treatment LiCl in *D. discoideum*.

Chapter 4

Bioinformatic Analysis of CDSA, CDIPT and DGKA

4. Bioinformatic Analysis of CDSA, CDIPT and DGKA

Research conducted in *D. discoideum* to investigate the molecular effects and target(s) of VPA has proposed a role for the drug regulating phosphoinositide and phospholipid signalling in both a time and dose-dependent manner (Chang, et al., 2012; Elphick, et al., 2012). To investigate the mechanism of this effect, a range of enzymes involved in regulating phosphoinositide signalling have been investigated as potential targets for VPA by gene ablation or overexpression. This approach suggested that PI3K signalling, inositol recycling and *de novo* inositol biosynthesis and production are unlikely to be responsible for the effects of VPA (Chang, et al., 2012; Frej, et al., 2016). The previous chapter described the analysis of VPA-sensitivity in cells lacking all 5 *D. discoideum* PI3K and PTEN, PLC and LPIN2, with all 3 cell lines showing sensitivity during both acute and chronic VPA treatment. These results suggested there are other targets of VPA responsible for this mechanism. One unexplored target for this effect is through the inhibition of the PI salvage pathway (**Figure 4.1**).

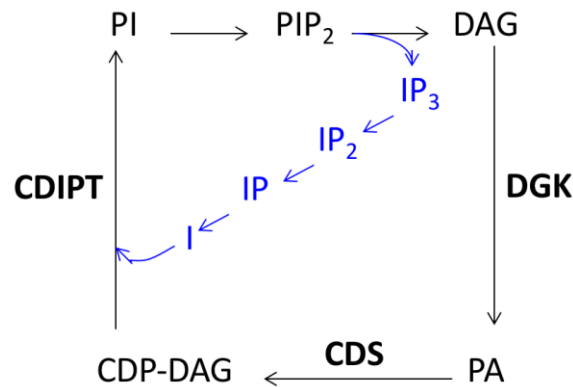


Figure 4.1. Simplified phosphatidylinositol salvage pathway. Regulation of inositol signalling involves both the phosphatidylinositol (PI) salvage pathway (black) and the inositol phosphate signalling pathway (blue) where phosphatidylinositol- 4,5-bisphosphate (PIP₂) is hydrolysed to produce inositol-1,4,5-triphosphate (IP₃) and diacylglycerol. IP₃ is dephosphorylated into inositol-1,4-bisphosphate (IP₂), inositol-1-phosphate (IP) and inositol (I). Meanwhile, DAG is phosphorylated to form phosphatidic acid (PA) by diacylglycerol kinase (DGK) and converted into cytidine diphosphate diacylglycerol (CDP-DAG) by a condensation reaction requiring CTP catalysed by cytidine diphosphate-diacylglycerol synthase (CDS). CDP-DAG is then converted into PI by cytidine diphosphate-diacylglycerol-inositol 3-phosphatidyltransferase (CDIPT). PI then undergoes two phosphorylation reactions to produce phosphatidylinositol-4, 5-bisphosphate. The interconnected and cyclic nature of this pathway suggests that inhibition of any enzyme may impact the other components.

D. discoideum is a useful model to study the PI salvage pathway since the model contains one isoform of each of the 3 key proteins- CDSA, CDIPT and DGKA. CDSA (UniProt ID: Q54N49) is a key enzyme involved in the PI salvage pathway as it catalyses the condensation reaction of PA and CTP into CDP-DAG. This reaction is a rate-limiting step due to the small size of the CDP-DAG pool (Raetz and Kennedy, 1973; Wu, et al., 1995; Lykidis, et al., 1997). CDP-DAG is a precursor to PI, PG, PE, PS and cardiolipin (Thompson and MacDonald, 1975; Shen, et al., 1996; Henry, Kohlwein and Carman, 2012; Lilley, et al., 2014). CDIPT (UniProt ID: Q54P27) is an important enzyme within the PI salvage pathway as it catalyses the formation of PI from CDP-DAG. PI is an essential product as it comprises 2-12 % of the total phospholipids within eukaryotic cells (Flint, et al., 1986). PI is phosphorylated into

various PI- species which regulate a number of signalling pathways, including tyrosine kinases, G-protein coupled receptors, membrane anchoring and transduction pathways of calcium and PKC (Lykidis, et al., 1997; Bankaitis and Grabon, 2011). DGKA (UniProt ID: P34125) is a fundamental enzyme as it regulates two signalling molecules, DAG and PA. DAG is required for triacylglycerol synthesis (Dahlqvist, et al., 2000), synaptic plasticity (Lee, Kim and Tanaka-Yamamoto, 2016), PKC (van Baal, et al., 2005) and the Kennedy pathway components PC and PE (Kennedy and Weiss, 1956; Tokuoka, Saiardi and Nurrish, 2008; Gibellini and Smith, 2010). PA regulates cell growth and signalling (Banfić, et al., 1993; Cerbón, et al., 2005), lipid regulation and glucose metabolism (Milne, et al., 2008). Therefore, CDSA, CDIPT and DGKA are key PI salvage pathway proteins and could potentially be the molecular target of VPA in *D. discoideum*.

This chapter, therefore, describes the bioinformatic analysis of the *D. discoideum* PI salvage pathway proteins CDSA, CDIPT and DGKA. In order to gain a detailed understanding of the structural characteristics and evolutionary conservation of these 3 proteins throughout different kingdoms, the *D. discoideum* protein sequences and domain structures were compared to that of a range of other species, including *Homo sapiens* (humans). This was achieved by comparing the *D. discoideum* protein sequence of each specific gene of interest to a database of amino acid sequences, to identify related sequences by a homology search (protein basic local alignment search tool (BLAST) analysis) (Altschul, et al., 1990). The evolutionary similarities and differences between each protein in a range of organisms was then determined by construction of a phylogenetic tree. Protein sequences were aligned with conserved amino acids in both *D. discoideum* and *H. sapiens* to a range of other organisms. The presence and location of protein structural domains was then compared in *D. discoideum* and *H. sapiens* proteins in order to determine functional similarity.

4.1 CDSA

4.1.1 CDSA BLAST Analysis

To determine the similarity of the *D. discoideum* CDSA protein to that of other CDS isoforms across various kingdoms, BLAST analysis was conducted. This involved comparing the *D. discoideum* CDSA protein sequence (DDB_G0269742) to all sequenced genomes from other species. This analysis revealed a number of related CDSA proteins across a range of species of similar lengths, with homologous proteins being defined as having an expectation (E)-value below 10^{-40} as previously suggested (**Table 4.1**) (Eichinger, et al., 2005). Homologous CDSA proteins were found in a range of kingdoms including Animalia, Plantae and Fungi, which all had a similar percentage of identity (ranging from 33- 42 %). The large number of CDSA homologs suggests a high degree of evolutionary conservation, highlighting the importance of CDP-DAG signalling.

Organism	Protein Name	Accession Number	Protein Length (aa)	Identity (%)	E-value
<i>Dictyostelium discoideum</i> (social amoeba)	CDSA	XP_646241.1	479	100	0
<i>Homo sapiens</i> (human)	CDS1	NP_001254.2	461	35	2e ⁻⁹²
	CDS2	NP_003809.1	479	34	2e ⁻⁸²
<i>Rattus norvegicus</i> (rat)	CDS1	NP_112521.2	461	36	8e ⁻⁹²
	CDS2	NP_446095.1	443	34	4e ⁻⁸⁰
<i>Mus musculus</i> (mouse)	CDS1	NP_775546.2	461	36	2e ⁻⁹¹
	CDS2	NP_619592.1	444	34	3e ⁻⁸³
<i>Danio rerio</i> (zebrafish)	CDS1	XP_001341899.2	431	35	1e ⁻⁹¹
	CDS2	NP_957480.1	444	34	2e ⁻⁸⁵
<i>Drosophila melanogaster</i> (fruit fly)	CDSA	NP_524661.1	447	34	2e ⁻⁸⁰
<i>Xenopus tropicalis</i> (frog)	CDS1	XP_002937924.1	441	35	3e ⁻⁹⁰
	CDS2	NP_001119975.1	465	33	4e ⁻⁹²
<i>Caenorhabditis elegans</i> (worm)	CDS	NP_501298.1	465	35	2e ⁻⁸⁹
<i>Arabidopsis thaliana</i> (plant)	CDS1	OAP19122.1	421	39	2e ⁻⁹⁸
	CDS2	OAP01102.1	423	38	6e ⁻⁹⁸
	CDS3	NP_194407.5	471	35	4e ⁻⁹⁵
<i>Saccharomyces cerevisiae</i> (budding yeast)	CDS1	AJP87380.1	457	39	8e ⁻⁸⁵
<i>Rhizophagus irregularis</i> (fungus)	CDS	PKC68884.1	437	42	3e ⁻¹¹⁰

Table 4.1. *D. discoideum* CDSA protein homology search results identifying related

proteins in other organisms. The accession numbers of related proteins are given and the name of the organism to which they relate. Protein length in number of amino acids are stated in addition to the percentage of identity relating to the *D. discoideum* protein. Statistical significance of a given pairwise alignment relating to the scoring system and size of the database used for comparison is shown by the E-value, with lower E-values indicating greater significance in homology. Results obtained using the NCBI PSI-BLAST database.

4.1.2 CDSA Phylogenetic Analysis

In order to determine the evolutionary conservation of the different CDS protein isoforms, a phylogenetic tree was constructed. This involved using the software Molecular Evolutionary Genetic Analysis (MEGA) 7 and the method neighbour-joining. Reliability of the tree nodes were assessed using the bootstrap test (500 replicates) and evolutionary distances were computed using the Poisson correction method (Kumar, Stecher and Tamura, 2016). Comparison of the entire CDS protein

sequences in a range of organisms showed conservation of the two CDS isoforms in higher organisms of the Animalia kingdom and a cluster towards the bottom of the tree for genus with one isoform, followed by the Plantae kingdom (**Figure 4.2**). The first node had a bootstrap value of 49 and separated the vertebrate and invertebrate CDS proteins. The bootstrap value of the second node was 39, which separated *D. discoideum* CDSA from the 3 *Arabidopsis thaliana* (plants) CDS isoforms, consistent with the higher percentage of identity between these two proteins compared with higher organisms such as *H. sapiens* and *Drosophila melanogaster* (fruit flies). From this phylogenetic analysis, there are 3 clear groups of CDS clustering, of CDS1, CDS2 and organisms with only one isoform. This suggests conservation of each protein isoform.

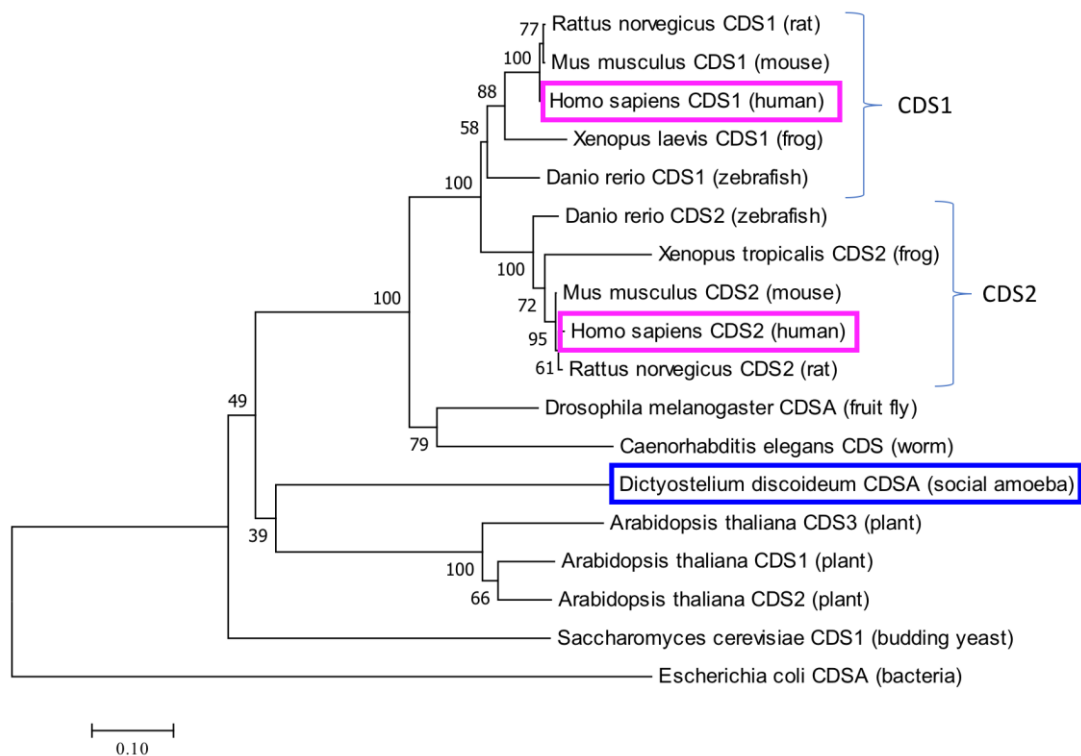


Figure 4.2. Phylogenetic analysis of CDS proteins within a range of kingdoms. The evolutionary relationship between CDS proteins is shown via a bootstrap consensus tree generated using the neighbour-joining method with bootstrap test (500 replicates) and the Poisson correction method computing the evolutionary distances from the Molecular Evolutionary Genetic Analysis (MEGA) 7 software. Numbers on the tree represent the percentage of replicate trees in which the associated taxa are clustered together. *E. coli* CDSA represents the root of the tree. *D. discoideum* CDSA is highlighted in blue and the two *H. sapiens* isoforms are shown in pink with the clustering of CDS1 and CDS2 shown by the 2 braces. Scale bar indicates the number of amino acid substitutions per site.

4.1.3 CDSA Sequence Alignment

Due to high sequence conservation in mammals, flies, yeast and bacteria, the CDS catalytic site has been predicted between amino acids 273-284 and 361-407 (Lykidis, et al., 1997). Therefore, sequence alignment analysis was employed in order to determine the conservation of this predicted catalytic site in *D. discoideum* and a range of other organisms (**Supplementary Figure S1**). A high degree of amino acid homology was observed around two sites in the sequence alignment, between amino acids 265-282 and 351-406; and 248-265 and 333-389 in *H. sapiens* CDS1 and CDS2 respectively, and amino acids 280-297 and 369-425 in *D. discoideum* (**Figure**

4.3). The high degree of homology within these two sites suggests the likely similarity of function of CDS in a range of organisms, consistent with a conserved cellular function.

Homo sapiens (human)	CDS1	265	TPLIKLSPKKTWEGFIG.	PFQIHSIALSTF	362
Homo sapiens (human)	CDS2	248	TPLIKLSPKKTWEGFIG.	PFQIHSIALSTF	345
Dictyostelium discoideum (social amoeba)	CDSA	280	TPLMKISPNKTWEGFIG.	PIQFHALVLALF	381
Mus musculus (mouse)	CDS1	265	TPLIKLSPKKTWEGFIG.	PFQIHSIALSTF	362
Mus musculus (mouse)	CDS2	247	TPLIKLSPKKTWEGFIG.	PFQIHSIALSTF	344
Danio rerio (zebrafish)	CDS1	254	TPLIKLSPKKTWEGFIG.	PFQIHSIALSSF	351
Danio rerio (zebrafish)	CDS2	247	TPLIKLSPKKTWEGFIG.	PFQIHSIALSSF	344
Drosophila melanogaster (fruit fly)	CDSA	262	TPLIKLSPKKTWEGFIG.	PFQIHSIALSLF	355
Xenopus tropicalis (frog)	CDS1	126	TPLIKLSPKKTWEGFIG.	PFQIHSIALSSF	223
Xenopus tropicalis (frog)	CDS2	269	TPLIKLSPKKTWEGFIG.	PFQIHSIALSTF	366
Caenorhabditis elegans (worm)	CDS	274	TPLIKLSPKKTWEGFIG.	PFV FHSIALSLF	372
Arabidopsis thaliana (plant)	CDS1	232	TPLIKLSPKKTWEGFIG.	PVQWHALCLGLF	326
Arabidopsis thaliana (plant)	CDS2	232	TPLIKLSPKKTWEGFIG.	PVQWHALCLGLF	326
Arabidopsis thaliana (plant)	CDS3	279	TPLIKLSPKKTWEGFIG.	PVQWHAFSLGLF	373
Saccharomyces cerevisiae (budding yeast)	CDS1	241	TKLIEISPKKTLGLFLG.	PIYFHALNLATF	338
Rhizophagus irregularis (fungi)	CDS	230	TPLIKLSPKKTWEGFVGL.	PLQWHVLMACF	334
Escherichia coli (bacteria)	CDSA	178	KLAPKVSFGKTKWQGFIG.	PVTL--LICSIV	226
Homo sapiens (human)	CDS1		ASLIGPFGGFFASGFKRAF	KIKDFANTIPG	392
Homo sapiens (human)	CDS2		ASLIGPFGGFFASGFKRAF	KIKDFANTIPG	375
Dictyostelium discoideum (social amoeba)	CDSA		GSLIAPFGGFFASGFKRAY	KVKDFDTIFPG	411
Mus musculus (mouse)	CDS1		ASLIGPFGGFFASGFKRAF	KIKDFANTIPG	392
Mus musculus (mouse)	CDS2		ASLIGPFGGFFASGFKRAF	KIKDFANTIPG	374
Danio rerio (zebrafish)	CDS1		ASLIGPFGGFFASGFKRAF	KIKDFADTIPG	381
Danio rerio (zebrafish)	CDS2		ASIMGPFGGFFASGFKRAF	KIKDFANTIPG	374
Drosophila melanogaster (fruit fly)	CDSA		SSIIGPFGGFFASGFKRAF	KIKDFGDMIPG	385
Xenopus tropicalis (frog)	CDS1		ASLIGPFGGFFASGFKRAF	KIKDFADTIPG	253
Xenopus tropicalis (frog)	CDS2		ASLIGPFGGFFASGFKRAF	KIKDFANTIPG	396
Caenorhabditis elegans (worm)	CDS		ASILGPFGGFFASGFKRAF	KIKDFGDVIPG	402
Arabidopsis thaliana (plant)	CDS1		ASIIAPFGGFFASGFKRAF	KIKDFGDSIPG	356
Arabidopsis thaliana (plant)	CDS2		ASIIAPFGGFFASGFKRAF	KIKDFGDSIPG	356
Arabidopsis thaliana (plant)	CDS3		ASIMAPFGGFFASGFKRAF	KIKDFGDSIPG	403
Saccharomyces cerevisiae (budding yeast)	CDS1		ASLIFAPFGGFFASGLKRTF	KVKDFGHSIPG	368
Rhizophagus irregularis (fungi)	CDS		ASLIAPFGGFFASGVKRAF	FNKDFGHSIPG	364
Escherichia coli (bacteria)	CDSA		AALASVLGDLTESMFKREAGI	KDSGHLIPG	256
Homo sapiens (human)	CDS1		HGGIMDRFDCQYLM		406
Homo sapiens (human)	CDS2		HGGIMDRFDCQYLM		389
Dictyostelium discoideum (social amoeba)	CDSA		HGGVTDRTDCQFIM		425
Mus musculus (mouse)	CDS1		HGGIMDRFDCQYLM		406
Mus musculus (mouse)	CDS2		HGGIMDRFDCQYLM		388
Danio rerio (zebrafish)	CDS1		HGGIMDRFDCQYLM		367
Danio rerio (zebrafish)	CDS2		HGGIMDRFDCQYLM		388
Drosophila melanogaster (fruit fly)	CDSA		HGGIMDRFDCQFLM		399
Xenopus tropicalis (frog)	CDS1		HGGIMDRSDCQYLM		266
Xenopus tropicalis (frog)	CDS2		HGGIMDRFDCQYLM		410
Caenorhabditis elegans (worm)	CDS		HGGIMDRFDCQLLM		416
Arabidopsis thaliana (plant)	CDS1		HGGITDRMDCQMVM		370
Arabidopsis thaliana (plant)	CDS2		HGGITDRMDCQMVM		370
Arabidopsis thaliana (plant)	CDS3		HGGFTDRMDCQMVM		417
Saccharomyces cerevisiae (budding yeast)	CDS1		HGGITDRVDCQFIM		382
Rhizophagus irregularis (fungi)	CDS		HGGITDRMDCQFLM		378
Escherichia coli (bacteria)	CDSA		HGGILDRIDSLTAA		270

Figure 4.3. Conservation of the CDS predicted catalytic site. Sequence alignment of the predicted catalytic site based on high amino acid conservation in a range of organisms. The names of the species used for comparison in the alignment are shown to the far left. The amino acid start position is shown to the left of the sequence and the end amino acid residue number of each line is shown to the right of the alignment. An intervening region is represented by ‘.’. Identical amino acids to the *D. discoideum* protein are highlighted in blue. The multiple sequence alignment was produced using Clustal Omega and Multiple Align Show (bioinformatics.org).

4.1.4 CDSA Domain Structure and Analysis

Due to the conservation of the CDS protein across a range of kingdoms, the domain structure of the *D. discoideum* CDSA protein was compared to that of the two human isoforms, CDS1 and CDS2 (**Figure 4.4**). The *D. discoideum* CDSA protein (479 amino acids) is of similar size to the two human isoforms (469 and 479 amino acids for CDS1 and CDS2 respectively). Domain structure analysis showed conservation of 6 transmembrane domains in both *D. discoideum* CDSA and the 2 *H. sapiens* isoforms, all of which comprise of 20 amino acids. High homology of two locations in the sequence alignment suggested the possible active site are in similar locations in both *D. discoideum* CDSA and the 2 *H. sapiens* isoforms, which comprises of 23 amino acids and 45 amino acids respectively. The final transmembrane domain is located within the second highly conserved area in all isoforms. The similarity in domain structure between the *H. sapiens* and *D. discoideum* isoforms is consistent with both enzymes having a related function.



Figure 4.4. Domain structure analysis of *D. discoideum* CDSA and *H. sapiens* CDS1 and CDS2. Schematic representation of the domain structure of CDS proteins in *D. discoideum* (UniProt ID: Q55D90) and *H. sapiens* (UniProt ID CDS1: Q92903 and CDS2: O95674). The domains shown are transmembrane domains (green) and the potential active site (red) with overlapping transmembrane domain and potential catalytic site is highlighted (yellow). The name of the organism and CDS isoform are shown to the left of the diagram and the protein length in amino acids (aa) is shown to the right of the alignment. There is an identical number of transmembrane domains in both organisms and the catalytic sites are located in similar locations.

4.2 CDIPT

4.2.1 CDIPT BLAST Analysis

The protein sequence of the single *D. discoideum* CDIPT protein was compared to the corresponding protein isoforms across other kingdoms. This was achieved by BLAST analysis, where the *D. discoideum* CDIPT (DDB_G0284857) protein sequence was compared against all sequenced genomes within the NCBI PSI-BLAST database. Homologous proteins were selected with E-values below 10^{-40} as previously described (Eichinger, et al., 2005). This analysis resulted in a number of CDIPT homologs from a range of species which had similar protein lengths (**Table 4.2**). CDIPT homologous proteins were found in fungi, invertebrates and vertebrates. Due to the high number of CDIPT homologs, it is suggested that there is a high degree of evolutionary conservation of the CDIPT protein, highlighting the importance of this enzyme.

Organism	Protein Name	Accession Number	Protein Length (aa)	Identity (%)	E-value
<i>Dictyostelium discoideum</i> (social amoeba)	CDIPT	XP_638368	207	100	0
<i>Homo sapiens</i> (human)	CDIPT	NP_006310.1	213	38	2e ⁻⁴³
<i>Papio anubis</i> (baboon)	CDIPT	XP_003918743	213	38	1e ⁻⁴¹
<i>Rattus norvegicus</i> (rat)	CDIPT	NP_620254.1	213	37	7e ⁻⁴²
<i>Mus musculus</i> (mouse)	CDIPT	NP_080914.1	213	37	2e ⁻⁴¹
<i>Danio rerio</i> (zebrafish)	CDIPT	NP_996971.1	213	36	3e ⁻⁴⁰
<i>Drosophila willistoni</i> (fruit fly)	CDIPT	XP_002075282.1	226	40	1e ⁻⁴⁰
<i>Anoplophora glabripennis</i> (beetle)	CDIPT	XP_018572854.1	217	39	3e ⁻⁴³
<i>Pogona vitticeps</i> (central bearded dragon)	CDIPT	XP_020654544.1	215	38	2e ⁻⁴¹
<i>Xenopus tropicalis</i> (frog)	CDIPT	NP_001072374.1	218	41	1e ⁻⁴⁹
<i>Pristionchus pacificus</i> (parasitic nematode)	CDIPT	PDM75564.1	216	38	4e ⁻⁴²
<i>Orbicella faveolata</i> (coral)	CDIPT	XP_020607792.1	217	41	5e ⁻⁴³
<i>Basidiobolus meristosporus</i> (fungus)	CDIPT	ORY03900.1	223	42	1e ⁻⁴⁸

Table 4.2. *D. discoideum* CDIPT protein homology search results identifying related proteins in other organisms. The accession numbers of related proteins are given and the name of the organism to which they relate. Protein length in number of amino acids are stated in addition to the percentage of identity relating to the *D. discoideum* protein. Statistical significance of a given pairwise alignment relating to the scoring system and size of the database used for comparison is shown by the E-value, with lower E-values indicating greater significance in homology. Results obtained using the NCBI PSI-BLAST database.

4.2.2 CDIPT Phylogenetic Analysis

The evolutionary conservation of CDIPT was determined via phylogenetic analysis. This involved using the neighbour-joining method of the MEGA 7 software, where the reliability of the tree nodes was measured using the bootstrap test of 500 replicates and the Poisson correction method to compute evolutionary distances (Kumar, Stecher and Tamura, 2016). Comparison of the entire CDIPT protein sequence across a range of organisms showed evolutionary conservation of the protein (**Figure 4.5**). At the first node there was a bootstrap value of 85, which separated eukaryotes and prokaryotes. The second node has a bootstrap value of 94 and separated multicellular organisms of the Animalia kingdom with single

celled eukaryotes and plants. The third node has a bootstrap value of 46, separating Fungi from Prosista, Plantae and yeast. *D. discoideum* CDIPT is located at the end of the fourth node where it is separated from plants and yeast, correlating with highest identity to *Basidiobolus meristosporus* (fungus). This phylogenetic analysis shows that CDIPT is conserved across a large range of kingdoms, with the *D. discoideum* protein showing weak correlation with plant and yeast isoforms.

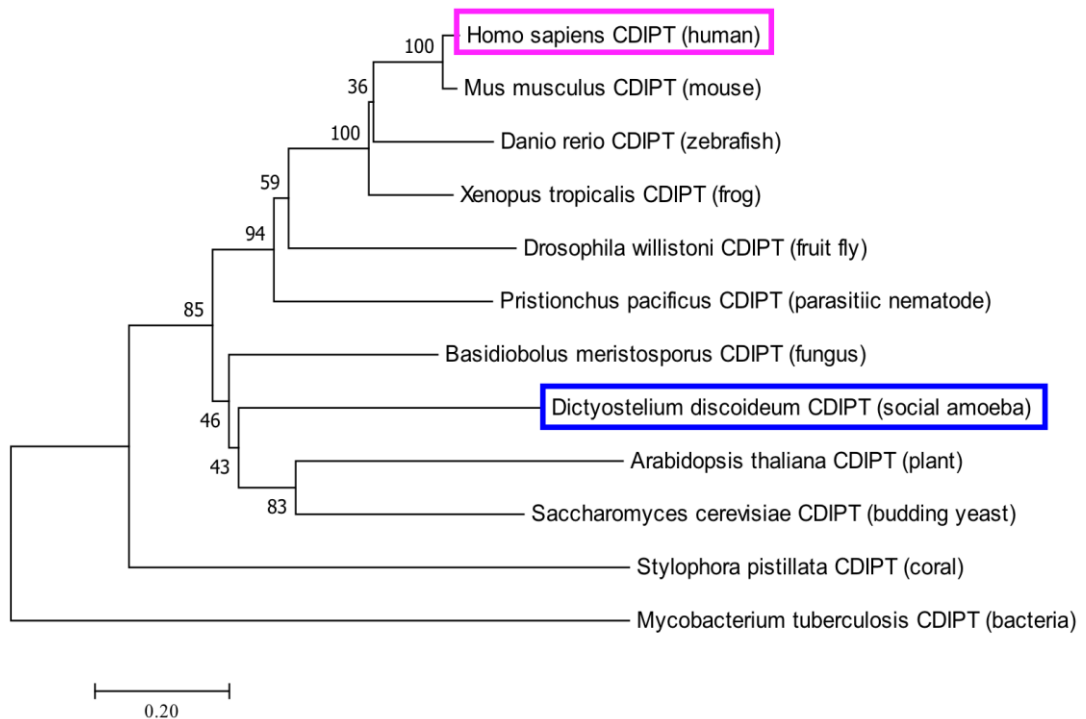


Figure 4.5. Phylogenetic analysis of CDIPT proteins within a range of kingdoms. The evolutionary relationship of CDIPT proteins is shown via a bootstrap consensus tree generated using the Molecular Evolutionary Genetic Analysis (MEGA) 7 software neighbour-joining method with bootstrap test (500 replicates) and the Poisson correction method to compute the evolutionary distances. Numbers on the tree represent the percentage of replicate trees in which the associated taxa are clustered together. *M. tuberculosis* CDIPT represents the root of the tree. *D. discoideum* CDIPT is highlighted in blue and the *H. sapiens* isoform in pink. Scale bar indicates the number of amino acid substitutions per site.

4.2.3 CDIPT Sequence Alignment

High homology across mammalian and yeast CDIPT proteins has previously been identified, suggesting conserved catalytic activity and regulatory role (Lykidis, et al., 1997). For this reason, the CDIPT protein sequence was aligned across a range of organisms to determine conservation of the protein (**Supplementary Figure S2**). A high degree of amino acid conservation was observed between CDIPT protein isoforms, particularly between amino acids 9-87 in *H. sapiens*, *D. discoideum*, *Mus musculus* (mouse), *Danio rerio* (zebrafish) and *Xenopus tropicalis* (frog), suggesting this may be the catalytic site (**Figure 4.6**). There is also conservation of 4 aspartic acid residues throughout all kingdoms which is required for magnesium ion binding and catalytic activity (Fischl, et al., 1986; Nogly, et al., 2014). The strong sequence homology within CDIPT proteins, in a broad range of organisms, suggests a widely conserved function for this enzyme.

Homo sapiens (human)	CDIPT	9	F	V	P	N	L	I	G	Y	A	R	I	V	F	A	I	S	F	Y	F	M	P	C	C	P	L	T	A	S	S	38	
Dictyostelium discoideum (social amoeba)	CDIPT	9	Y	V	P	N	I	I	G	Y	F	R	V	I	F	A	I	L	A	F	K	Y	S	H	D	E	Y	V	K	F	F	V	38
Mus musculus (mouse)	CDIPT	9	F	V	P	N	L	I	G	Y	A	R	I	V	F	A	I	S	F	Y	F	M	P	C	C	P	F	T	A	S	S	38	
Danio rerio (zebrafish)	CDIPT	9	F	V	P	N	L	I	G	Y	A	R	I	V	L	A	L	V	S	F	F	L	M	P	C	C	P	G	P	A	V	F	38
Drosophila willistoni (fruit fly)	CDIPT	12	F	V	P	N	I	I	G	Y	A	R	I	V	L	A	L	I	A	F	F	M	S	T	N	Y	V	I	A	G	W	41	
Xenopus tropicalis (frog)	CDIPT	9	F	V	P	N	L	I	G	Y	A	R	I	V	F	A	F	V	A	F	Y	F	M	P	T	S	P	V	L	A	S	T	38
Pristionchus pacificus (parasitic nematode)	CDIPT	14	F	W	P	N	I	I	G	Y	A	R	I	V	L	A	L	I	S	M	W	Y	F	P	S	A	P	V	T	A	M	F	43
Arabidopsis thaliana (plant)	CDIPT	17	Y	I	P	N	I	V	G	Y	M	R	V	L	L	N	C	V	A	F	A	V	C	F	S	N	K	P	L	S	V	46	
Saccharomyces cerevisiae (budding yeast)	CDIPT	18	Y	I	P	N	K	I	G	Y	V	R	V	I	T	A	A	L	S	F	F	V	M	K	N	H	P	T	A	F	T	W	47
Escherichia coli (bacteria)	CDIPT	31	D	V	V	T	I	L	G	T	T	A	S	V	A	G	A	L	T	L	F	P	M	G	K	L	F	A	G	A	C	V	60
Homo sapiens (human)	CDIPT		F	Y	L	L	S	G	L	L	D	A	F	D	G	H	A	A	R	A	L	N	Q	G	T	R	F	G	A	M	L	D	68
Dictyostelium discoideum (social amoeba)	CDIPT		F	Y	A	I	S	A	L	L	D	M	A	D	G	H	A	A	R	L	L	N	Q	S	Q	F	G	A	L	L	D	68	
Mus musculus (mouse)	CDIPT		F	Y	L	L	S	G	L	L	D	A	F	D	G	H	A	A	R	A	L	N	Q	G	T	R	F	G	A	M	L	D	68
Danio rerio (zebrafish)	CDIPT		C	Y	L	L	S	A	L	L	D	A	F	D	G	H	A	A	R	A	L	N	Q	G	T	K	F	G	A	M	L	D	68
Drosophila willistoni (fruit fly)	CDIPT		C	Y	I	S	A	L	L	D	A	V	D	G	H	A	A	R	A	F	N	Q	S	T	R	F	G	A	M	L	D	71	
Xenopus tropicalis (frog)	CDIPT		F	Y	L	L	S	G	L	L	D	A	F	D	G	H	A	A	R	L	L	N	Q	G	T	K	F	G	A	M	L	D	68
Pristionchus pacificus (parasitic nematode)	CDIPT		C	Y	A	L	S	A	V	L	D	A	F	D	G	W	A	A	R	T	Y	N	Q	S	S	R	F	G	A	M	L	D	73
Arabidopsis thaliana (plant)	CDIPT		L	Y	F	F	S	F	C	C	D	A	V	D	G	W	V	A	R	R	F	N	Q	V	S	T	F	G	A	V	L	D	76
Saccharomyces cerevisiae (budding yeast)	CDIPT		L	Y	S	T	S	C	L	L	D	A	L	D	G	T	M	A	R	K	Y	N	Q	V	S	S	L	G	A	V	L	D	77
Escherichia coli (bacteria)	CDIPT		-	V	W	F	F	V	L	F	D	M	L	D	G	A	M	A	R	E	R	G	G	T	R	F	G	A	V	L	D	89	
Homo sapiens (human)	CDIPT		M	L	T	D	R	C	S	T	M	C	L	L	V	N	L	A	L	L	Y											87	
Dictyostelium discoideum (social amoeba)	CDIPT		M	I	T	D	R	C	S	T	I	A	L	M	V	V	L	S	H	F	Y											87	
Mus musculus (mouse)	CDIPT		M	L	T	D	R	C	A	T	M	C	L	L	V	N	L	A	L	L	Y											87	
Danio rerio (zebrafish)	CDIPT		M	L	T	D	R	C	A	T	M	C	L	L	V	N	L	A	L	L	Y											87	
Drosophila willistoni (fruit fly)	CDIPT		Q	L	T	D	R	C	G	T	T	G	L	L	V	T	L	S	Y	F	Y											90	
Xenopus tropicalis (frog)	CDIPT		M	L	T	D	R	C	A	T	M	C	L	L	V	N	L	S	L	L	Y											87	
Pristionchus pacificus (parasitic nematode)	CDIPT		Q	L	T	D	R	C	A	L	L	S	L	V	M	T	L	C	V	L	Y											92	
Arabidopsis thaliana (plant)	CDIPT		M	V	T	D	R	V	S	T	A	C	L	L	V	I	L	S	Q	I	Y											95	
Saccharomyces cerevisiae (budding yeast)	CDIPT		M	V	T	D	R	S	S	T	A	G	L	M	C	F	L	C	V	Q	Y											96	
Escherichia coli (bacteria)	CDIPT		A	T	C	D	R	I	S	D	G	A	V	F	C	G	L	L	W	W	I											108	

Figure 4.6. Conservation of the CDIPT predicted catalytic site. Sequence alignment of the CDIPT protein in a region of high homology in a range of organisms. The names of the species used for comparison in the alignment are shown to the far left. The amino acid start position is shown to the left of the sequence and the end amino acid residue number of each line is shown to the right of the alignment. Identical amino acids to the *D. discoideum* protein are highlighted in blue with conserved aspartic acid residues shown in yellow. The multiple sequence alignment was produced using Clustal Omega and Multiple Align Show (bioinformatics.org).

4.2.4 CDIPT Domain Structure and Analysis

Since, CDIPT appeared to be well conserved across a range of kingdoms, the domain structure of the *D. discoideum* protein was compared to that of the *H. sapiens* isoform (**Figure 4.7**). The *D. discoideum* CDIPT protein (207 amino acids) is of similar size to the *H. sapiens* CDIPT isoform (213 amino acids). Domain structure analysis showed conservation of 4 transmembrane domains in *D. discoideum* CDIPT and 5 transmembrane domains within the *H. sapiens* isoform, all of which comprise of 16-20 amino acids. An area of high homology within the protein sequence alignment, possibly suggesting the location of the enzymes active site, is located in

identical positions in *D. discoideum* and *H. sapiens*, comprising of 39 amino acids in both organisms.

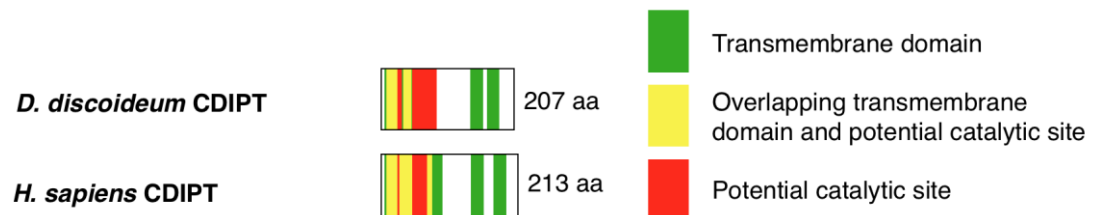


Figure 4.7. Domain structure analysis of *D. discoideum* and *H. sapiens* CDIPT. Schematic representation of the domain structure of CDIPT proteins in *D. discoideum* (UniProt ID: Q54P27) and *H. sapiens* (UniProt ID: O14735). The domains shown are transmembrane domains (green) and the potential active site (red), with overlapping transmembrane domain and potential catalytic site is highlighted (yellow). The name of the organism and CDIPT isoform are shown to the left of the diagram and the protein length in amino acids (aa) is shown to the right of the alignment. There is a similar number of transmembrane domains in both organisms and the catalytic site is in identical locations in both organisms.

4.3 DGKA

4.2.1 DGKA BLAST Analysis

The *D. discoideum* DGKA protein sequence (DDB_G0277223) was compared to other protein isoforms across all sequenced genomes within the NCBI PSI-BLAST database. Homologs were determined by having E-values below 10^{-40} as previously described (Eichinger, et al., 2005). BLAST analysis resulted in identification of a number of homologs to DGKA from a range of species which had similar protein lengths (**Table 4.3**). These DGKA homologous proteins were found mainly across the Animalia and Plantae kingdoms. These results suggest that there is a high degree of evolutionary conservation of DGK proteins, highlighting the importance of this enzyme.

Organism	Protein Name	Accession Number	Protein Length (aa)	Identity (%)	E-value
<i>Dictyostelium discoideum</i> (social amoeba)	DGKA	XP_642726.1	887	100	0
<i>Homo sapiens</i> (humans)	DGK α	AAH31870.1	735	31	1e ⁻⁶⁶
	DGK β	NP_001337634.1	804	33	5e ⁻⁷⁴
	DGK γ	BAA05132	791	31	2e ⁻⁶⁷
	DGK δ	BAC11809.2	1214	30	1e ⁻⁴⁴
	DGK ϵ	NP_003638	567	31	2e ⁻⁶¹
	DGK ζ	AAB60859	1117	29	2e ⁻⁵²
	DGK η	NP_821077	1220	32	2e ⁻⁴⁹
	DGK θ	NP_001338	942	37	3e ⁻⁵⁴
	DGK ι	NP_004708.1	1065	29	7e ⁻⁵⁰
	DGK κ	NP_001013764	1271	30	3e ⁻⁴³
<i>Mus musculus</i> (mouse)	DGK α	NP_058091	730	32	5e ⁻⁶⁷
	DGK β	NP_001348615	802	32	7e ⁻⁷⁵
	DGK γ	NP_619591.1	788	31	1e ⁻⁶⁷
	DGK δ	NP_808314.2	1220	30	9e ⁻⁴⁶
	DGK ϵ	NP_062378.1	564	29	5e ⁻⁶²
	DGK ζ	NP_612179.2	929	29	1e ⁻⁵³
	DGK η	NP_001074805	1180	32	5e ⁻⁵⁰
	DGK θ	NP_950176.1	934	36	1e ⁻⁵⁵
	DGK ι	NP_001074675.1	1071	29	3e ⁻⁵¹
	DGK κ	AAH75627.1	1118	31	1e ⁻⁴³
<i>Danio rerio</i> (zebrafish)	DGK α	NP_001038780	727	32	3e ⁻⁷⁶
	DGK β	XP_021322198.1	786	30	8e ⁻⁶¹
	DGK δ	XP_005172373	1074	31	4e ⁻⁴⁷
	DGK ϵ	NP_001165699.1	564	30	4e ⁻⁶⁰
	DGK ζ	XP_003201445.1	1300	31	2e ⁻⁶⁹
	DGK η	XP_021334551.1	1329	31	1e ⁻⁴⁷
	DGK ι	XP_009298312.1	968	27	4e ⁻⁵²
<i>Drosophila melanogaster</i> (fruit fly)	DGK1	BAA04135.1	1454	30	2e ⁻⁵⁹
<i>Xenopus tropicalis</i> (frog)	DGK β	NP_001096214.1	785	33	2e ⁻⁷¹
<i>Caenorhabditis elegans</i> (worm)	DGK	NP_001024382.1	794	35	2e ⁻⁵⁶
<i>Arabidopsis thaliana</i> (plant)	DGK1	NP_196409.1	728	32	5e ⁻⁵¹
	DGK2	NP_201182.1	712	38	9e ⁻⁶²
	DGK6	NP_194542.2	466	30	3e ⁻⁴⁰

Table 4.3. *D. discoideum* DGKA protein homology search results identifying related proteins in other organisms. The accession numbers of related proteins are given and the name of the organism to which they relate. Protein length in number of amino acids are stated in addition to the percentage of identity relating to the *D. discoideum* protein. Statistical significance of a given pairwise alignment relating to the scoring system and size of the database used for comparison is shown by the E-value, with lower E-values indicating greater significance in homology. Results obtained using the NCBI PSI-BLAST database.

4.2.2 DGKA Phylogenetic Analysis

Phylogenetic analysis was then used to determine the evolutionary conservation of DGK. To do this, MEGA 7 software was used to create a phylogenetic tree via the neighbour-joining method. Reliability of the tree nodes were measured using the bootstrap test of 500 replicates and evolutionary distances were computed using the Poisson correction method (Kumar, Stecher and Tamura, 2016). The resulting phylogenetic tree shows evolutionary conservation of DGK proteins present across a range of organisms, with distinct clusters grouping the different DGK types (1-5 (**Figure 4.8**). The first node has a bootstrap value of 19 which separated type 1 DGK (DGK- α , - β and - γ) from the remaining 4 groups, suggesting that between the DGK subtypes there is large sequence variation. The second node, which has a bootstrap value of 5 separates DGK types 2-4 with DGK type 5 and organisms with one protein isoform. Most likely, these low bootstrap values are a result of the characteristic domain structures of each group, which are missing in the other subtypes. The next node with a bootstrap value of 61 separates type 5 DGK (DGK- θ) and *A. thaliana* and *Caenorhabditis elegans* (worm) DGK-1 and -2 from *D. discoideum* DGKA and *A. thaliana* DGK-3-7. *D. discoideum* DGKA is separated from *A. thaliana* DGK 3-7 at the fourth clade, which has a bootstrap value of 35. This phylogenetic analysis suggests that the *D. discoideum* DGKA protein is closely related to the DGK- θ isoform present in a range of higher organisms, including *H. sapiens* and *M. musculus*.

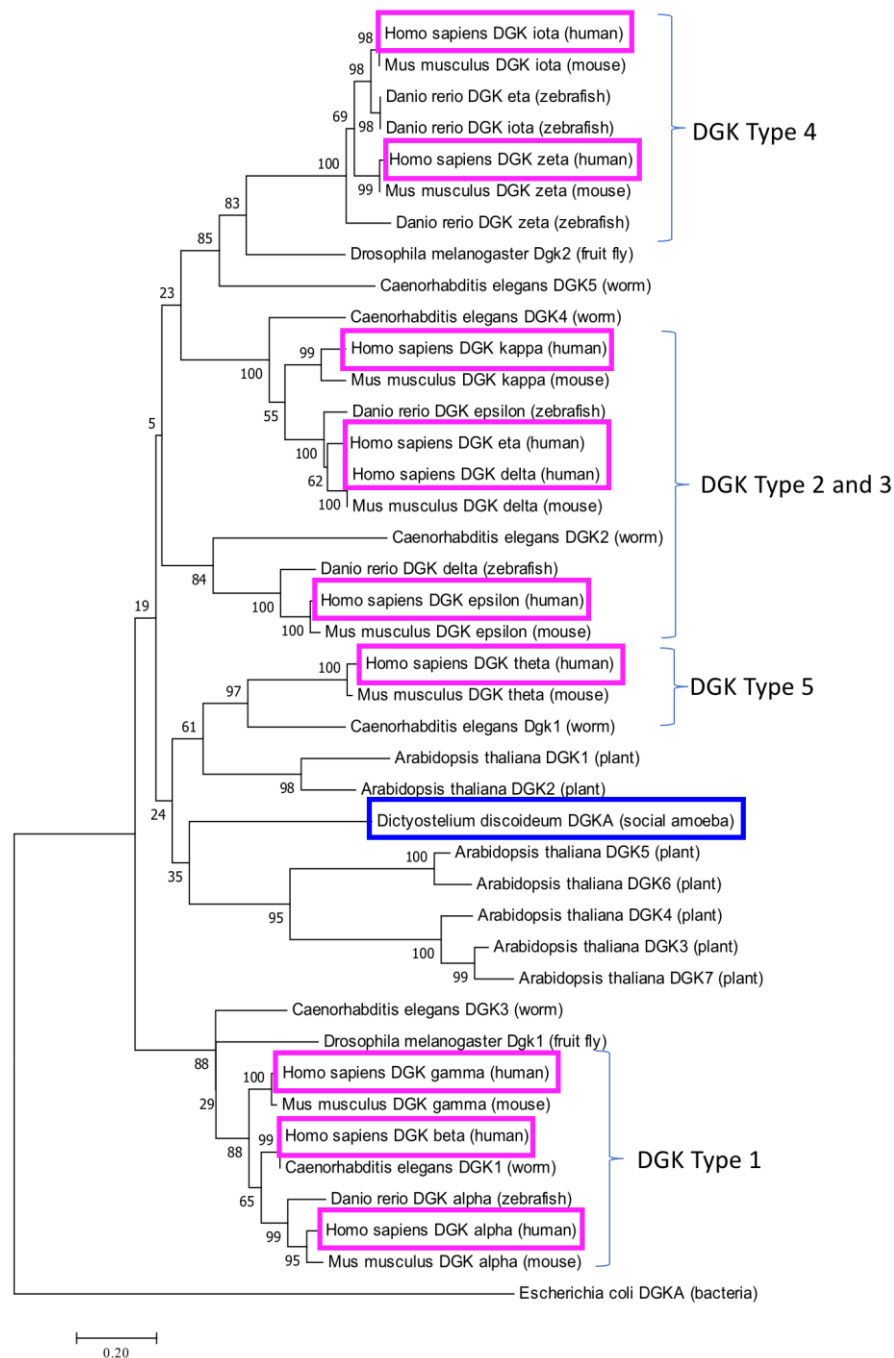


Figure 4.8. Phylogenetic analysis of DGK proteins within a range of kingdoms. A bootstrap consensus tree showing the evolutionary conservation of DGK generated using the Molecular Evolutionary Genetic Analysis (MEGA) 7 software neighbour-joining method with bootstrap test (500 replicates) and the Poisson correction method to compute the evolutionary distances. Numbers on the tree represent the percentage of replicate trees in which the associated taxa are clustered together. *E. coli* DGKA represents the root of the tree. *D. discoideum* CDSA is highlighted in blue and the two *H. sapiens* isoforms are shown in pink with the clustering of DGK types 1-5 shown by the 4 braces. Scale bar indicates the number of amino acid substitutions per site.

4.2.3 DGKA Sequence Alignment

To determine the conservation of the DGK catalytic site in *D. discoideum* compared with a range of other organisms (**Figure 4.9**), including all *H. sapiens* isoforms (**Figure 4.10**), amino acids within this region were aligned. A high degree of amino acid conservation across the catalytic site between a range of organisms and between the different *H. sapiens* isoforms was shown in the two sequence alignments. This confirms the similarity of function of the DGK protein in a range of organisms and between the different isoforms, thereby suggesting these proteins all have a similar function.

Homo sapiens (human)	DGK-theta	330	P	D	S	C	P	L	L	V	F	V	N	P	K	S	G	G	L	K	R	D	L	L	C	S	F	R	K	L	L	360	
Dictyostelium discoideum (social amoeba)	DGKA	584	M	P	E	K	V	L	F	V	F	V	N	S	K	S	G	G	Q	F	G	S	T	L	R	K	L	S	S	L	L	614	
Mus musculus (mouse)	DGK-theta	576	P	D	C	C	P	L	L	V	F	V	N	P	K	S	G	G	L	K	G	R	E	L	L	C	S	F	R	K	L	L	606
Danio rerio (zebrafish)	DGK-delta	323	S	C	S	S	P	L	L	V	L	V	N	S	K	S	G	D	N	Q	G	V	K	F	L	R	R	F	K	Q	L	L	353
Drosophila melanogaster (fruit fly)	DGKA	808	P	E	V	I	P	V	I	V	F	I	N	P	K	S	G	G	N	Q	G	H	K	L	L	G	K	F	Q	H	L	L	838
Arabidopsis thaliana (plant)	DGK-5	36	T	P	A	S	P	V	L	V	F	I	N	S	K	S	G	G	Q	L	G	G	E	L	I	L	T	Y	R	S	L	L	66
Homo sapiens (human)	DGK-theta		N	P	H	Q	V	F	D	I	T	N	-	G	G	P	L	P	G	L	H	L	F	S	-	-	-	-	-	-	-	-	381
Dictyostelium discoideum (social amoeba)	DGKA		N	P	L	Q	I	I	D	L	I	K	C	G	G	P	D	S	T	L	Q	M	I	N	R	Y	L	A	K	-	-	-	641
Mus musculus (mouse)	DGK-theta		N	P	H	Q	V	F	E	L	T	N	-	G	G	P	L	P	G	F	H	L	F	S	-	-	-	-	-	-	-	-	627
Danio rerio (zebrafish)	DGK-delta		N	P	A	Q	V	F	D	L	M	N	-	G	G	P	Q	L	G	L	R	L	F	Q	-	-	-	-	-	-	-	-	374
Drosophila melanogaster (fruit fly)	DGKA		N	P	R	Q	V	F	D	L	T	Q	-	G	G	P	K	M	G	L	D	M	F	R	-	-	-	-	-	-	-	-	859
Arabidopsis thaliana (plant)	DGK-5		N	H	N	Q	V	F	D	L	D	Q	-	E	T	P	D	K	V	L	R	R	I	Y	L	N	L	E	R	L	K	D	95
Homo sapiens (human)	DGK-theta		-	-	-	-	-	-	Q	V	P	C	F	R	V	L	V	C	G	G	D	G	T	V	G	W	V	L	G	A	L	E	405
Dictyostelium discoideum (social amoeba)	DGKA		-	-	-	H	P	E	Q	T	N	R	F	R	I	L	V	C	G	G	D	G	T	V	G	W	L	F	K	Q	M	T	668
Mus musculus (mouse)	DGK-theta		-	-	-	-	-	-	Q	V	P	S	F	R	V	L	V	C	G	G	D	G	T	V	G	W	V	L	A	A	L	E	651
Danio rerio (zebrafish)	DGK-delta		-	-	-	-	-	-	K	F	E	T	F	R	T	L	V	C	G	G	D	G	S	V	G	W	V	L	S	E	L	D	398
Drosophila melanogaster (fruit fly)	DGKA		-	-	-	-	-	-	K	A	P	N	L	R	V	L	A	C	G	G	D	G	T	V	G	W	V	L	S	V	L	D	883
Arabidopsis thaliana (plant)	DGK-5		D	D	F	A	R	Q	I	R	E	K	L	K	I	I	V	A	G	G	D	G	T	A	G	W	L	L	G	V	V	C	125
Homo sapiens (human)	DGK-theta		E	T	R	Y	R	L	A	-	C	P	E	P	S	V	A	I	L	P	L	G	T	G	N	D	L	G	R	V	L	R	434
Dictyostelium discoideum (social amoeba)	DGKA		K	H	L	V	-	-	-	P	S	T	I	P	I	G	I	I	P	L	G	T	G	N	D	L	A	R	S	L	G	694	
Mus musculus (mouse)	DGK-theta		E	T	R	R	H	-	L	A	C	P	E	P	S	V	A	I	L	P	L	G	T	G	N	D	L	G	R	V	L	R	680
Danio rerio (zebrafish)	DGK-delta		K	L	S	-	-	-	L	H	K	Q	C	Q	L	G	V	L	P	L	G	T	G	N	D	L	A	R	V	L	G	424	
Drosophila melanogaster (fruit fly)	DGKA		Q	I	Q	P	P	-	L	Q	P	A	P	A	V	G	V	L	P	L	G	T	G	N	D	L	A	R	A	L	G	911	
Arabidopsis thaliana (plant)	DGK-5		D	L	K	-	-	-	L	S	H	P	P	P	I	A	T	V	P	L	G	T	G	N	N	L	P	F	A	F	G	151	
Homo sapiens (human)	DGK-theta		W	G	A	G	Y	S	G	E	-	-	-	D	P	F	S	V	L	L	S	V	D	E	A	D	A	V	L	M	D	R	461
Dictyostelium discoideum (social amoeba)	DGKA		W	G	I	G	Y	D	G	E	-	-	-	K	L	I	E	I	L	K	S	I	N	E	A	K	T	I	Q	M	D	T	721
Mus musculus (mouse)	DGK-theta		W	G	A	G	Y	S	G	E	-	-	-	D	P	F	S	V	L	V	S	V	D	E	A	D	A	V	L	M	D	R	707
Danio rerio (zebrafish)	DGK-delta		W	G	G	L	C	D	D	D	A	-	-	Q	L	L	Q	I	L	E	K	L	E	R	A	T	T	K	M	L	D	R	452
Drosophila melanogaster (fruit fly)	DGKA		W	G	G	Y	T	D	E	P	-	-	I	G	-	K	I	L	R	E	I	G	M	S	Q	C	V	L	M	D	R	938	
Arabidopsis thaliana (plant)	DGK-5		W	G	K	K	N	P	G	T	D	R	T	A	V	E	S	F	L	E	Q	V	L	K	A	K	V	M	K	I	D	N	181
Homo sapiens (human)	DGK-theta		W	T	I	L	L	D	A																							468	
Dictyostelium discoideum (social amoeba)	DGKA		W	S	I	E	M	W	D																							728	
Mus musculus (mouse)	DGK-theta		W	T	I	L	L	D	A																							714	
Danio rerio (zebrafish)	DGK-delta		W	S	V	M	T	Y	E																							459	
Drosophila melanogaster (fruit fly)	DGKA		W	R	V	K	V	T	P																							945	
Arabidopsis thaliana (plant)	DGK-5		W	H	I	L	M	R	M																							188	

Figure 4.9. Conservation of the DGK catalytic site. Sequence alignment of the catalytic site of a number of organisms showing high amino acid homology. The names of the species used for comparison in the alignment are shown to the far left of the sequence. The amino acid start position is shown to the left of the sequence and the end amino acid residue number of each line is shown to the right of the alignment. Identical amino acids to the *D. discoideum* protein are highlighted in blue. The multiple sequence alignment was produced using Clustal Omega and Multiple Align Show (bioinformatics.org).

Dictyostelium discoideum (social amoeba) DGKA	Q T N R F R I L V C G G D G T V G W L F K Q M T K H L V --	418
Homo sapiens (human) DGK-alpha	D V P D S R I L V C G G D G T V G W I L E T I D K A N L --	451
Homo sapiens (human) DGK-beta	D V P D F R V L A C G G D G T V G W V L D C I E K A N V --	513
Homo sapiens (human) DGK-gamma	D T P D F R V L A C G G D G T V G W I L D C I D K A N F --	509
Homo sapiens (human) DGK-delta	K F D T F R I L V C G G D G S V G W V L S E I D S L N L --	396
Homo sapiens (human) DGK-epsilon	P Y Y S A R V L V C G G D G T V G W V L D A V D D M K I K G	298
Homo sapiens (human) DGK-zeta	K V H N L R I L A C G G D G T V G W I L S T L D Q L R L --	559
Homo sapiens (human) DGK-eta	K F D N F R I L V C G G D G S V G W V L S E I D K L N L --	407
Homo sapiens (human) DGK-theta	Q V P C F R V L V C G G D G T V G W V L G A L E E T R Y R L	665
Homo sapiens (human) DGK-iota	K V P N L R I L A C G G D G T V G W I L S I L D E L Q L --	451
Homo sapiens (human) DGK-kappa	N F A R F R I L V C G G D G S V S W V L S L I D A F G L --	566
Dictyostelium discoideum (social amoeba) DGKA	-- F S T I P I G I I P L G T G N D L A R S L G W G I G Y D	446
Homo sapiens (human) DGK-alpha	-- F V L P P V A V L P L G T G N D L A R C L R W G G G Y E	479
Homo sapiens (human) DGK-beta	-- G K H P P V A I L P L G T G N D L A R C L R W G G G Y E	541
Homo sapiens (human) DGK-gamma	-- A K H P P V A V L P L G T G N D L A R C L R W G G G Y E	537
Homo sapiens (human) DGK-delta	-- H K Q C Q L G V L P L G T G N D L A R V L G W G S A C D	424
Homo sapiens (human) DGK-epsilon	Q E K Y I P Q V A V L P L G T G N D L S N T L G W G T G Y A	328
Homo sapiens (human) DGK-zeta	-- K P P P F V A I L P L G T G N D L A R T L N W G G G Y T	587
Homo sapiens (human) DGK-eta	-- N K Q C Q L G V L P L G T G N D L A R V L G W G G S Y D	435
Homo sapiens (human) DGK-theta	A - C P E P S V A I L P L G T G N D L G R V L R W G G A G Y S	694
Homo sapiens (human) DGK-iota	-- S P Q P F V G V L P L G T G N D L A R T L N W G G G Y T	479
Homo sapiens (human) DGK-kappa	-- H E K C Q L A V I P L G T G N D L A R V L G W G A F W N	594
Dictyostelium discoideum (social amoeba) DGKA	G E - K L I E I L K S I N E A K T I Q M D T W S I E M W D -	474
Homo sapiens (human) DGK-alpha	G Q - N L A K I L K D L E M S K V V H M D R W S V E V I P -	507
Homo sapiens (human) DGK-beta	G E - N L M K I L K D I E N S T E I M L D R W K F E V I P -	569
Homo sapiens (human) DGK-gamma	G G - S L T K I L K D I E Q S P L V M L D R W H L E V I P -	565
Homo sapiens (human) DGK-delta	D D T Q L P Q I L E K L E R A S T K M L D R W S V M A Y - -	452
Homo sapiens (human) DGK-epsilon	G E I P V A Q V L R N V M E A D G I K L D R W K V Q V T N -	357
Homo sapiens (human) DGK-zeta	D E - P V S K I L S H V E E G N V V Q L D R W D L H A E P -	615
Homo sapiens (human) DGK-eta	D D T Q L P Q I L E K L E R A S T K M L D R W S I M T Y E -	464
Homo sapiens (human) DGK-theta	G E - D P F S V L L S V D E A D A V L M D R W T I L L D A -	722
Homo sapiens (human) DGK-iota	D E - P V S K I L C Q V E D G T V V Q L D R W N L H V E R N	508
Homo sapiens (human) DGK-kappa	K S K S P L D I L N R V E Q A S V R I L D R W S V M I R E -	623

Figure 4.10. Conservation of the DGK catalytic site between *D. discoideum* and the 10 *H. sapiens* isoforms. Sequence alignment of the catalytic site of *D. discoideum* DGKA and the 10 *H. sapiens* DGK isoforms. The names of the species and DGK isoforms used for comparison in the alignment are shown to the far left. The amino acid start position is shown to the left of the sequence and the end amino acid residue number of each line is shown to the right of the alignment. Identical amino acids to the *D. discoideum* protein are highlighted in blue. The multiple sequence alignment was produced using Clustal Omega and Multiple Align Show (bioinformatics.org).

4.2.4 DGKA Domain Structure and Analysis

Since DGK appears to be a well conserved enzyme across a range of kingdoms, the domain structure of the *D. discoideum* DGKA protein was compared to that of the 10 *H. sapiens* DGK isoforms, DGK- α , - β , - γ , - δ , - ϵ , - ζ , - η , - θ , - ι and - κ (**Figure 4.11**). The *D. discoideum* DGKA protein (887 amino acids) is of similar size to the 10 *H. sapiens* DGK isoforms (ranging 567-1271 amino acids). Domain structure analysis showed conservation of phorbol-ester/ DAG type 1 binding domains in all isoforms

ranging between 50 or 51 amino acids in *D. discoideum* and between 47-58 amino acids across the 10 *H. sapiens* isoforms. The phorbol-ester domains are followed by the catalytic site in all DGK isoforms and comprise of 143 amino acids in *D. discoideum* and between 134-141 amino acids in *H. sapiens*. The different DGK isoforms also have unique domains which are not present in *D. discoideum* DGKA and are characteristic of the 5 DGK subgroups.

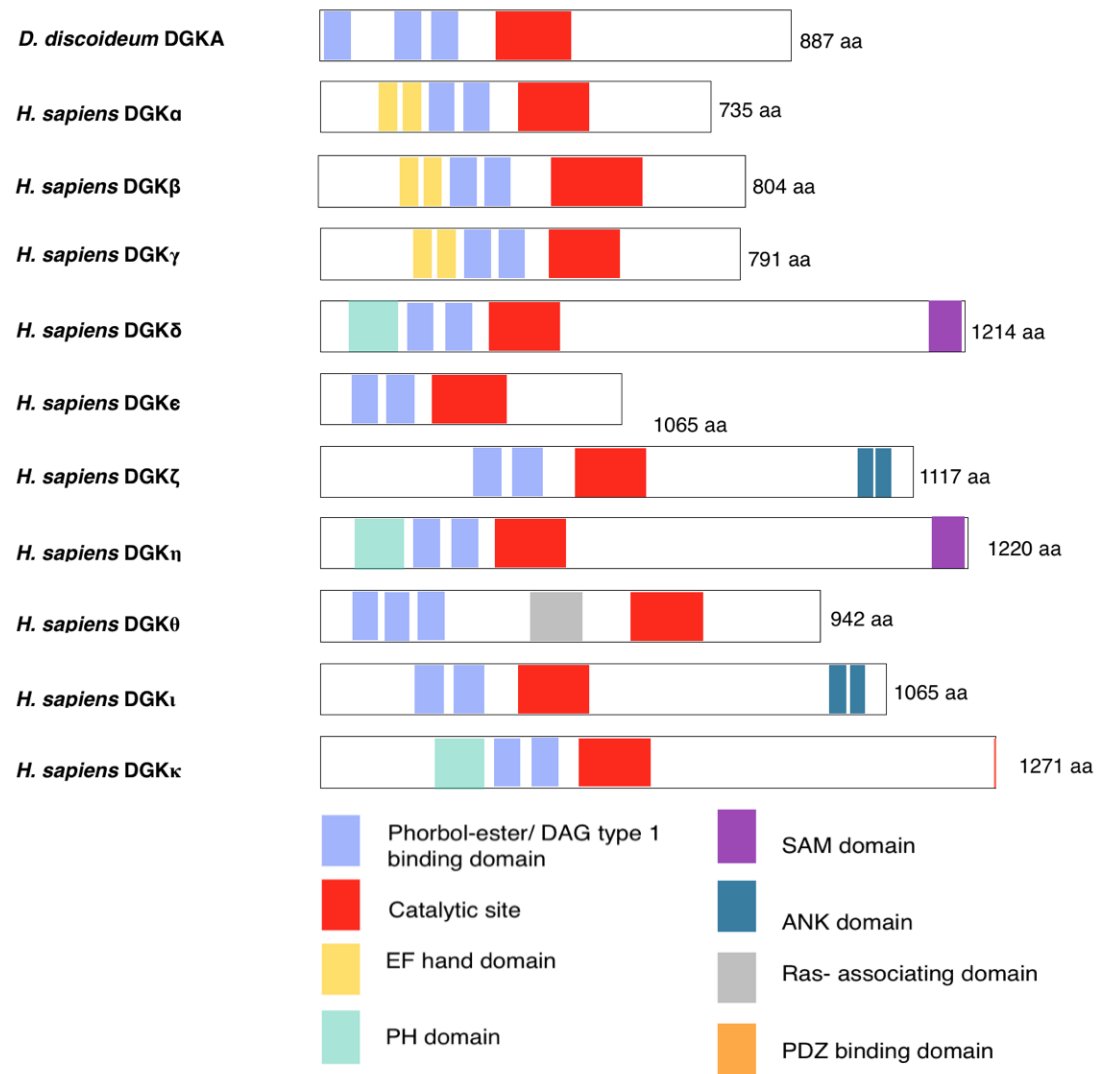


Figure 4.11. Domain structure analysis of *D. discoideum* DGKA and the 10 *H. sapiens* DGK isoforms. Schematic representation of the domain structure of DGK proteins in *D. discoideum* and *H. sapiens*. *H. sapiens* contain 10 DGK isoforms. *D. discoideum* DGKA protein (UniProt ID: P34125) was compared to that of the 10 human DGK isoforms, DGK- α (UniProt ID: P23743), DGK- β (UniProt ID: Q9Y6T7), DGK- γ (UniProt ID: P49619), DGK- δ (UniProt ID: P49619), DGK- ϵ (UniProt ID: P52429), DGK-zeta (UniProt ID: Q13574), DGK-eta (UniProt ID: Q86XP1), DGK- θ (UniProt ID: P52824), DGK-iota (UniProt ID: O75912) and DGK- κ (UniProt ID: Q5KSL6). The domains shown are the phorbol- ester/ DAG type 1 binding domain (blue), catalytic site (red), EF hand domain (yellow), PH domain (light green), SAM domain (purple), ANK domain (dark green), Ras- associating domain (grey) and PDZ binding domain (orange). The organism name and protein isoform is shown to the left of the diagram and the number of amino acids (aa) in the protein to the right.

4.4 Discussion

Previous studies researching the molecular target of VPA in regulating phosphoinositide and inositol phosphate signalling have been unable to identify a potential molecular target for this drug in *D. discoideum* (Chang, et al., 2012; Frej, et al., 2016). Identifying this target remains important, since similar effects on phosphoinositide levels have been identified using primary mammalian neurons and *in vivo* models (Williams, et al., 2002; Chang, et al., 2013). Therefore, finding a target of VPA to regulate these effects, which may be conserved in mammalian systems, is needed. In this chapter, *D. discoideum* PI salvage pathway proteins CDSA, CDIPT and DGKA are investigated using bioinformatic analysis for homology to mammalian proteins and to other kingdoms. *In silico* analysis included comparison of amino acid sequence conservation, domain structure and catalytic motifs across a range of organisms of these 3 proteins. These experiments suggest the *D. discoideum* proteins CDSA, CDIPT and DGKA are orthologues of the mammalian proteins with high conservation and so may retain common cellular functions from *D. discoideum* to mammals.

Bioinformatic analysis involved comparing *D. discoideum* proteins to isoforms present in other organisms and determining their evolutionary conservation. This began with BLAST analysis to identify significantly homologous proteins. This was achieved by setting the E-value threshold to a minimum of 10^{-40} . This E-value represents the number of expected matches from a random database, with lower values indicating higher significance since the value decreases exponentially as the number of matches increases. This was then followed by the construction of a phylogenetic tree to determine the evolutionary characteristics of *D. discoideum* and related protein isoforms from a range of organisms (taxa) based upon both similar and different genetic characteristics. The nodes of the tree represent common ancestors and the branches indicate groups of descendant taxa separated by species. Bootstrap values present on the phylogenetic tree represent a resampling analysis test to determine whether nodes are recovered in the same position if a single amino acid within the protein is removed across the whole

sequence. Therefore, the higher the bootstrap value, the more likely the species is located in the correct position. Analysis then continued with aligning the catalytic site of these proteins, as this domain will be highly conserved in proteins with similar functions. Where the location of the catalytic site is unknown, the whole protein sequence was aligned to predict this site from areas of high conservation as shown previously (Lykidis, et al., 1997). Finally, the locations of significant protein domains were aligned to determine whether these are conserved in both *D. discoideum* and *H. sapiens* isoforms.

Bioinformatic analysis revealed a number of significantly homologous proteins to *D. discoideum* CDSA in a range of organisms from mammals to plants and fungi. Identity values of all CDS isoforms ranged between 33-42 %, which is consistent with a previous study that found a functional link between a tomato pathogenesis related protein and a human glioma pathogenesis related protein where sequences were 35 % identical (Szyperski, et al., 1998). Strong conservation of CDS proteins is shown by the low E-values across a large range of species, suggesting CDS is highly conserved throughout evolution. CDS conservation is also highlighted in the phylogenetic tree, where there is clear clustering of CDS1, CDS2 (in *H. sapiens*, *Rattus norvegicus* (rat), *M. musculus*, *X. tropicalis* and *D. rerio*) and single CDS(A) isoforms (*C. elegans*, *D. discoideum* and *S. cerevisiae*), with the exception of *A. thaliana* and *Escherichia coli* (bacteria). These results suggest evolutionary conservation of CDS proteins, with distinct sequences in organisms with single CDS isoforms and the evolutionary changes between CDS1 and CDS2. Similarity in CDS proteins across a range of kingdoms is also supported by two areas of high sequence homology, which has previously been suggested as the catalytic site in mammals, flies, yeast and bacteria (between amino acids 273-284 and 361-407) (Lykidis, et al., 1997). Consistent with this previous work, 2 areas were identified with high protein sequence homology, between amino acids 265-282 and 351-406 (*H. sapiens* CDS1), 248-265 and 333-389 (*H. sapiens* CDS2) and 280-297 and 369-425 (*D. discoideum* CDSA). This result highlights the evolutionary preservation of the CDS catalytic site and therefore, the similarity in roles these proteins would conduct in the respective organisms. This was also supported by domain analysis,

where both *D. discoideum* and *H. sapiens* CDS protein isoforms have 2 potential catalytic sites and 5 transmembrane domains at similar locations, suggesting comparable protein structure between the two organisms. CDS transmembrane domains are important as they are involved in the synthesis of cardiolipin and PG at the inner matrix side of the mitochondria and for the production of PI at the cytoplasmic side of the endoplasmic reticulum (Thompson and MacDonald, 1975; Kuchler, Daum and Paltauf, 1986; Shen, et al., 1996; Henry, Kohlwein and Carman, 2012; Lilley, et al., 2014). This is of interest in epilepsy research as both CDP-DAG and PG accumulate following VPA treatment (Ju and Greenberg, 2003). Therefore, due to the highly conserved protein sequence and the similarity in domain structure, all CDS proteins most likely fulfil a common function in *D. discoideum* and mammals. Therefore, this could provide a common mechanism to regulate the effects of VPA in both *D. discoideum* and mammalian models.

Bioinformatic analysis was then conducted on CDIPT, where a number of significantly homologous proteins to the *D. discoideum* isoform were identified. The homologous proteins were identified in a range of kingdoms including mammals, reptiles, parasitic nematode and fungus. All of these homologous proteins had similar protein lengths (ranging 207-223 amino acids) and identity (ranging 36-42 %), suggesting conservation of the enzyme across a range of species. High sequence homology was also illustrated in the phylogenetic tree. Alignment of the *D. discoideum* and other homologous CDIPT protein sequences revealed a high degree of homology between amino acids 9-87 in *H. sapiens*, *D. discoideum*, *M. musculus* and *D. rerio*, suggesting the location of the CDIPT catalytic site. In all organisms, ranging from mammals to bacteria, there were 4 conserved aspartic acid residues. Aspartic acid residues are also conserved in PS synthase (catalyses the formation of PS from CDP-DAG) and PG synthase (catalyses the formation of PG from CDP-DAG) (Nikawa, Kodaki and Yamashita, 1987). The role of these aspartic acid residues in phosphotransferase enzymes is to direct magnesium or manganese ion binding, which is required for enzyme activity. These residues have also been suggested to be the inositol binding site (Fischl, et al., 1986; Nogly, et al., 2014). The areas of high sequence conservation across all organisms suggests that these CDIPT

proteins have a common ancestor and therefore, a similar role. Domain analysis also showed a comparable number of transmembrane domains in *D. discoideum* (4) and *H. sapiens* (5) which are located in similar positions, suggesting the two proteins are of similar structure. The transmembrane domains enable the enzyme to fold into a dimer and conduct its catalytic activity through substrate and magnesium or manganese ion binding (Nogly, et al., 2014). CDIPT is a protein of interest as a VPA target as the reaction product PI decreases during seizures (Yoshida, et al., 1987). The high conservation of CDIPT protein sequences in a range of organisms and the similarity in domain structure, suggests that all CDIPT proteins most likely have a common function in mammals and *D. discoideum*. Therefore, the mechanism of action of VPA is most likely conserved in both *D. discoideum* and mammalian models.

D. discoideum DGKA was the final protein bioinformatic analysis was conducted on. DGKA was a protein of interest as DGK- β (Ishisaka, et al., 2013), - δ (Leach, et al., 2007), and - ϵ (Rodriguez de Turco, et al., 2001) have been linked with epilepsy and VPA is known to alter DAG signalling (Yoshida, et al., 1987; Tokuoka, Saiardi and Nurrish, 2008). Proteins with significantly high homology to *D. discoideum* DGKA were determined by BLAST analysis and were identified within a range of organisms including mammals, worm and plants. There was a large range in protein lengths (ranging 466- 1454 amino acids) of related DGKA orthologues, due to the presence of 10 isoforms present in higher organisms. When comparing individual isoforms, e.g. DGK- α , protein lengths are similar. All proteins in a range of organisms had a similar identity to the *D. discoideum* DGKA (ranging 27-38 %), suggesting evolutionary conservation of this enzyme. This was supported by the phylogenetic tree. The tree nodes suggest common ancestors of DGK proteins. Groups of descendant taxa were separated by the branches of different species with clear clusters of DGK types 1-5, which are based upon different functional domains and therefore resulted in low bootstrap values. High sequence homology was then identified when aligning the catalytic sites of DGK- θ isoforms in *H. sapiens* and *M. musculus*, DGK- δ of *D. rerio*, DGK-5 of *A. thaliana* and DGKA of *D. discoideum* and *D.*

melanogaster and when aligning all 10 *H. sapiens* isoforms and *D. discoideum* DGKA. The high areas of sequence homology across all proteins, suggests a conserved function between all *H. sapiens* DGK isoforms and the single *D. discoideum* DGKA. Domain analysis followed, which confirmed the evolutionary conservation of 2 or 3 phorbol-ester/ DAG type 1 binding domains prior to the catalytic site. Each DGK subtype has specific domains. Type 1 (DGK- α , - β and - γ) isoforms have recovering homology domains and EF hand motifs. Type 2 (DGK- δ , - η , - κ) have pleckstrin homology domains. Type 3 (DGK- ϵ) isoforms have arachidonate- containing DAG domains. Type 4 (DGK- ζ and - ι) contain PDZ domains and ANK domains. Finally, type 5 (DGK- θ) have 3 phorbol-ester/ DAG type 1 binding domains and Ras associating domains. The recoverin homology domains and EF hand motifs of type 1 are involved in calcium binding, which initiates conformational changes in the enzymes tertiary structure. Calcium binding also initiates movement of the enzyme from the cytosol to the plasma membrane where the enzyme is functionally active (Sakane, et al., 1991; Yamada, et al., 1997). The type 2 DGKs pleckstein homology domains are responsible for the translocation of the enzyme from the cytosol to the plasma membrane by binding to intracellular PIP₂, thereby regulating the levels of this signalling molecule (Kume, et al., 2016). Type 3 DGKs have arachidonate- containing DAG domains which enables the catalysis of *sn*-2 arachidonoyl-DAG (Tang, et al., 1996; Lung, et al., 2009). The PDZ domains of DGK- κ and type 4 DGKs bind gamma-1-syntrophin within the cytoplasm, causing the translocation of the enzyme to the nucleus (Hogan, et al., 2001). The ANK domains are used for protein- protein interactions to enable the translocation of the enzyme from the cytosol to plasma membrane (Santos, et al., 2002). The type 5 Ras associating domain is responsible for the binding of RhoA, a homolog of Ras, which inhibits DGK enzyme activity (Houssa, et al., 1999). Therefore, as the amino acid sequence and the core domain structures in DGKA is highly conserved among a range of organisms, all DGK proteins are likely to have a common function in both *D. discoideum* and mammalian models. Therefore, *D. discoideum* could be used as a biomedical model to investigate DGK as a potential target to VPA.

4.5 Summary

In this chapter, bioinformatic analysis has identified evolutionary conservation of CDS, CDIPT and DGK proteins across a number of organisms, including *D. discoideum* and *H. sapiens*. There is clear separation of organisms with single and multiple protein isoforms, highlight the evolutionary conservation and differences within the protein sequences. The data suggests a similar function of all 3 proteins within *D. discoideum* and *H. sapiens* homologs, with conservation of key protein sequences and domains, suggesting all of the protein isoforms have a similar function in both *D. discoideum* and mammalian models.

Chapter 5

Analysis of CDSA as a Target of VPA

5. Analysis of CDSA as a Target of VPA

The PI salvage pathway enzyme CDS catalyses a condensation reaction between PA and CTP to produce CDP-DAG and pyrophosphate (**Figures 1.4** and **5.1**). CDP-DAG is an important branch point intermediate as it acts as a precursor for PI through the PI salvage pathway and cardiolipin, PG, PS, PE and PC via the CDP-DAG pathway (Thompson and MacDonald, 1975; Shen, et al., 1996; Henry, Kohlwein and Carman, 2012; Lilley, et al., 2014). CDS is predominantly present within the endoplasmic reticulum and mitochondria (Raetz and Kennedy, 1973), where the enzyme regulates rapid PI turnover and signalling in a rate-limiting step due to the small size of the CDP-DAG pool (Nickels, Buxeda and Carman, 1994; Lykidis, et al., 1997). CDS is investigated here as a target of VPA due to CDP-DAG being a precursor of a large range of signalling molecules and for its role within the PI salvage pathway.

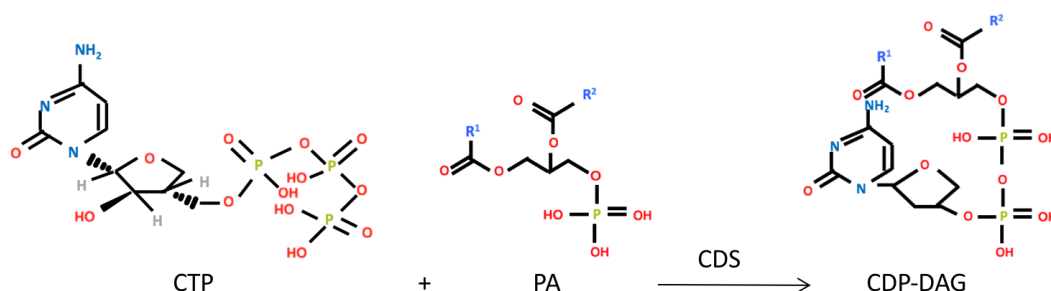


Figure 5.1. The catalytic activity of cytidine diphosphate diacylglycerol synthase. A condensation reaction converts phosphatidic acid (PA) and cytidine triphosphate (CTP) into cytidine diphosphate- diacylglycerol (CDP-DAG), catalysed by CDP-DAG synthase (CDS).

D. discoideum has a single *Cds* gene, *CdsA* (DDB_G0269742), which has a length of 3688 bp. This includes three introns and encodes a protein of 479 amino acids.

D. discoideum *CdsA* is expressed during the vegetative phase of the life cycle (Stajdohar, et al., 2015). The *D. discoideum* CDSA protein shares 35 % and 34 % identity to *H. sapiens* CDS1 and CDS2 orthologues respectively (**Chapter 4**), implying a similar catalytic role of the enzymes in both organisms. This chapter, therefore, describes the creation of a CDSA knockout construct and subsequent attempts to ablate the gene in *D. discoideum*. In addition, an RFP-*cdsA* overexpression construct

was created. The resulting WT::RFP-*cdsA* overexpressing cells were phenotypically characterized during *D. discoideum* growth and development, in both the absence and presence of anti-seizure compounds, including VPA and the BD treatment LiCl.

5.1 Construction of *CdsA* Knockout Vector

A *CdsA* knockout vector was created using the pLPBLP (Faix et al., 2004) background. To this vector, two distal PCR amplified regions of the *CdsA* gene were inserted on either side of a blasticidin resistance cassette (**Figures 5.2A and 5.2B**). The 490 bp 5' fragment started 64 bp within the open reading frame and contained no introns. The 508 bp 3' fragment within the coding sequence contained one intron, removing a total of 584 bp of coding sequence, resulting in the cloning of 899 bp of exon sequence. Restriction mapping (**Figure 5.2C**) was used to confirm the presence of the four restriction sites used for cloning (*Bam*HI, *Pst*I, *Hind*III and *Kpn*I) the two *CdsA* fragments into the *CdsA* knockout vector. Single digests resulted in a single band corresponding to the *CdsA* knockout vector at approximately 5500 bp. The presence of the two distal fragments within the *CdsA* knockout vector were excised by double digests which produced two bands, one at either 490 bp or 510 bp, indicating the presence of the *cdsA* 5' and 3' fragments respectively. The second band (5000 bp confirmed the 5' region and 4900 bp for the 3' fragment) corresponded to the remaining *CdsA* knockout plasmid. The knockout cassette (approximately 2560 bp) contained the two *cdsA* gene fragments and the blasticidin resistance cassette, which was excised from the recombinant plasmid (approximately 2900 bp) by a further digest using the enzymes *Bam*HI and *Kpn*I.

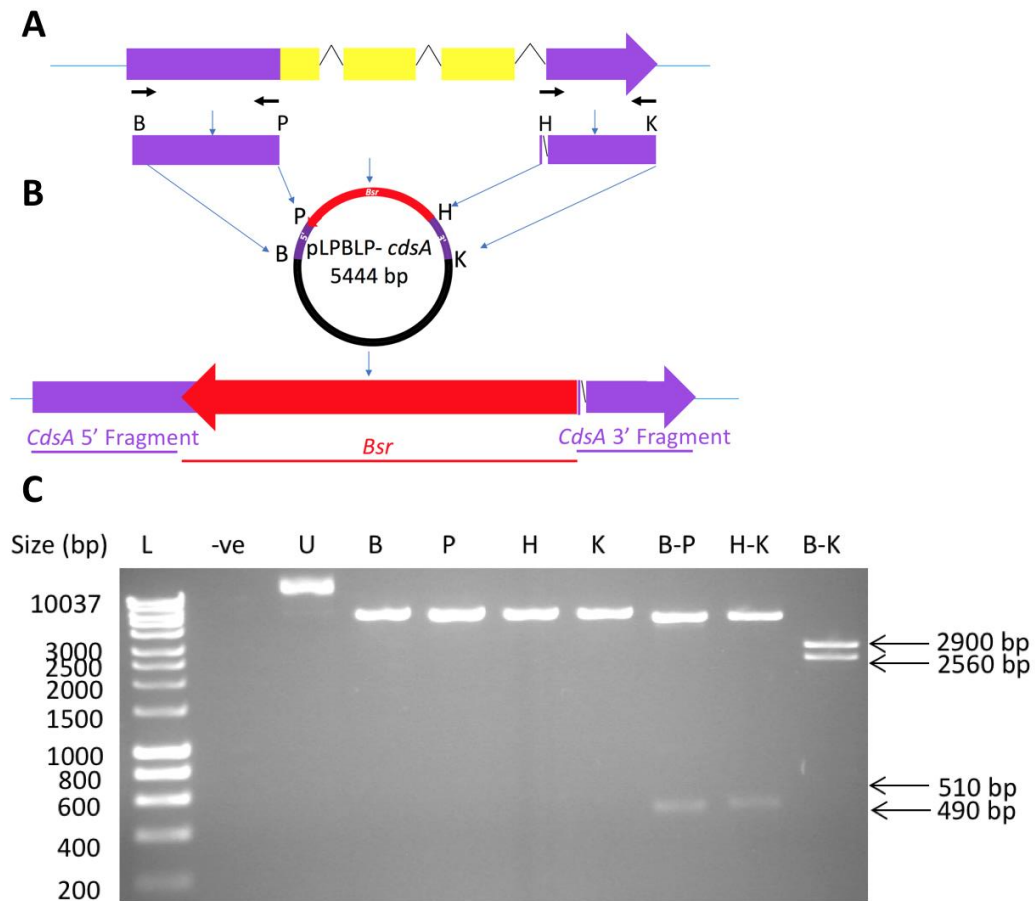


Figure 5.2. Confirmation of the *CdsA* knockout construct. **(A)** *CdsA* genomic DNA with the region to be removed shown in yellow. The arrows indicate the locations of the primers used to amplify the 5' and 3' genomic DNA fragments and the cut sites *Bam*HI (B), *Pst*I (P), *Hind*III (H) and *Kpn*I (K) which were added onto these fragments. **(B)** Plasmid map of pLPBLP-*cdsA* containing the two *CdsA* fragments located on either side of the blasticidin resistance cassette (*Bsr*). **(C)** Restriction mapping of the *CdsA* knockout vector by single and double digests visualised following gel electrophoresis with a ladder (L), negative control with no vector (-ve), uncut knockout vector (U), single digests to confirm individual enzyme activity of *Bam*HI (B), *Pst*I (P), *Hind*III (H) and *Kpn*I (K) and double digests to confirm the 5' and 3' fragments within the vector using *Bam*HI-*Pst*I (B-P) and *Hind*III-*Kpn*I (H-K) and the linearized knockout cassette used for electroporation with *Bam*HI-*Kpn*I (B-K). Molecular weights of the DNA ladder are indicated on the left of the gel image (10037 bp- 200 bp) and the expected plasmid insert sizes are provided (arrows) to the right of the image.

5.2 Screening of Potential *cdsA*⁻ *D. discoideum* Cells

To create *cdsA*⁻ *D. discoideum* cells, the *CdsA* knockout cassette (**Figure 5.2**) was excised from the *CdsA* knockout construct and electroporated into WT cells. Transformant cells were selected for resistance to blasticidin during growth which was added to the media. Surviving colonies were screened by PCR for homologous integration of the knockout cassette into genomic DNA, thereby creating *cdsA*⁻ cells. Homologous recombinant cells were then determined by PCR screening. This involved designing primers which confirmed the presence of the two distal *CdsA* gene fragments by amplifying genomic DNA from outside to within the fragment (genomic control), resulting in a 530 bp and 510 bp band for the 5' and 3' terminus respectively. Primers also amplified from within the fragment into the vector blasticidin resistance cassette (vector control) at the 5' (590 bp) and 3' (600 bp) terminus. Knockout diagnostic primers confirmed homologous recombination by using the genomic control primer located outside of the fragment and the primer located within the blasticidin resistance cassette (650 bp for the 5' terminus and 710 bp for the 3' terminus).

Numerous attempts were made to create and identify a *cdsA*⁻ mutant using the *CdsA* knockout cassette. In the event of the mutant being an auxotroph, *cdsA*⁻ cells were grown in the presence of the products CDP-DAG is a substrate for, PI and PG. After 16 electroporations, 329 blasticidin resistant colonies were screened. 195 of the 329 blasticidin resistant colonies were grown in the presence of PI (100 µM), 117 in media containing PG (100 µM) and 17 were grown in the presence of PI (100 µM) and PG (100 µM). However, no *cdsA*⁻ cells were identified. This approach was taken as previous studies have shown CDSA to be essential in organisms with one protein isoform (Shen and Dowhan, 1996; Sato, et al., 2000; Ganong and Raetz, 1982).

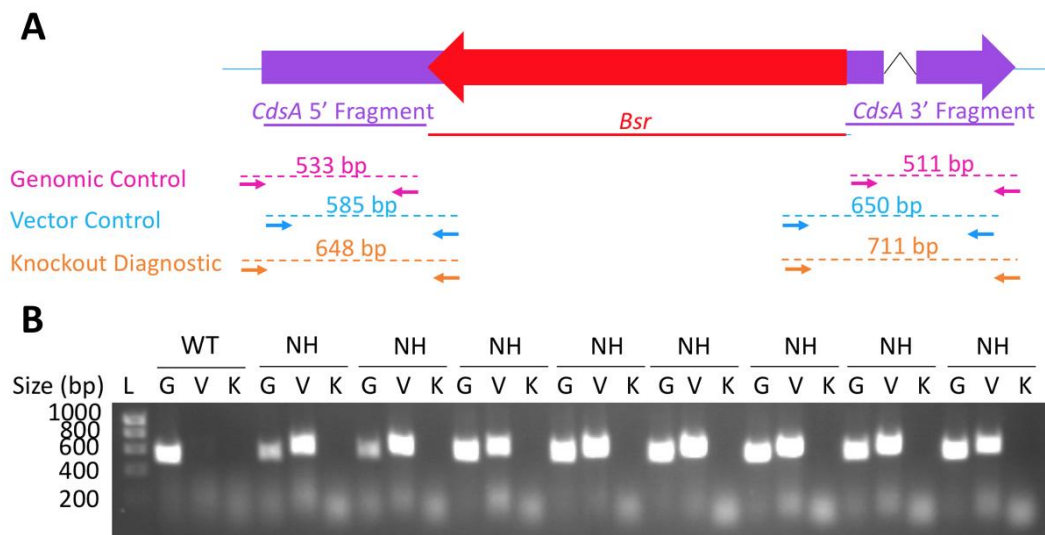


Figure 5.3. PCR screening of potential *cdsA*⁻ transformant cells. (A) Schematic representation of the *CdsA* knockout construct and the locations of the screening primers (arrows) and corresponding PCR product (dotted line) used for determining homologous integration- genomic (pink), vector (blue) and knockout diagnostic (yellow) primers and the predicted sizes of these products. **(B)** 5'-terminal PCR screening of WT and blasticidin-resistant cells with genomic control (G), vector control (V) and knockout diagnostic (K). PCR products are shown where the genomic control (G) band is amplified from WT DNA, genomic (G) and vector (V) control bands are amplified from non-homologous integrant (NH) DNA and all 3 bands (G, V and knockout diagnostic (K)) are amplified from the potential knockout (*cdsA*⁻) DNA. DNA ladder and the corresponding molecular weights are indicated on the left of the gel image (1000 bp- 200 bp).

5.3 Preparing a *CdsA* Overexpression Construct

To overexpress CDSA, WT::RFP-*cdsA* cells were created by PCR amplifying *CdsA* cDNA and inserting the resulting PCR fragment into a 5' RFP tagged overexpression construct (389-19 mRFPmars) (Basu, et al., 2013; Fey, et al., 2013) (**Figure 5.4**).

Primers were designed which amplified the whole *CdsA* cDNA (1440 bp) to which 5' *Bam*HI and 3' *Eco*RI cut sites were added and this PCR product was cloned into the 5' RFP overexpression construct. The presence of the two restriction sites used for cloning (*Bam*HI and *Eco*RI) were confirmed by restriction mapping and produced a single band at approximately 7340 bp. Insertion of the *CdsA* cDNA PCR fragment

was confirmed by a double restriction digest using the same two enzymes which produced one band at 1440 bp corresponding to the PCR amplified CDSA cDNA and the RFP-plasmid band at 3900 bp. The construct was sequenced to ensure that no mutations were present in the inserted PCR product. The 5' RFP tagged *CdsA* overexpression construct was then electroporated into *D. discoideum* cells and selected by growth in the presence of neomycin (G418), creating WT::RFP-*cdsA* cells.

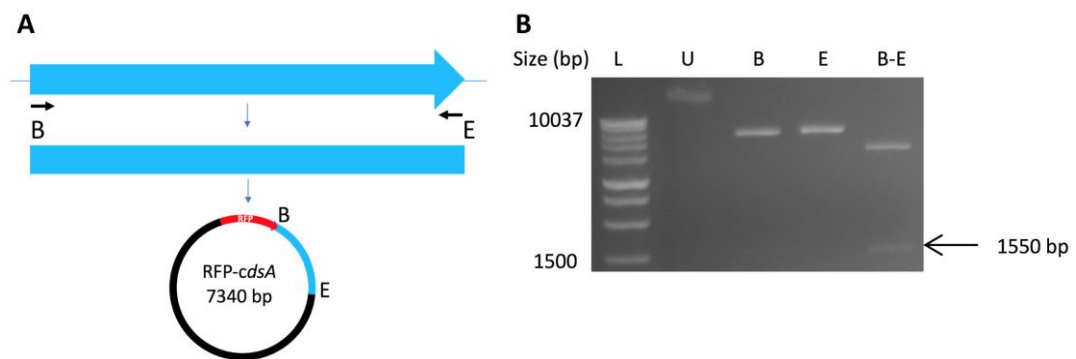


Figure 5.4. Confirmation of the RFP-*cdsA* overexpression construct. (A) Schematic representation of *CdsA* cDNA with the arrows indicating the locations of the primers used for PCR amplification and the cut sides of *Bam*HI (B) and *Eco*RI (E) used for cloning the *CdsA* cDNA into the 5' RFP expression vector. (B) Confirmation of the inserted *CdsA* cDNA into the RFP expression vector by a series of single and a double restriction digest visualised following gel electrophoresis with a ladder (L), uncut vector (U), single digests to confirm individual enzyme activity of *Bam*HI (B) and *Eco*RI (E) and a double digest using *Bam*HI-*Eco*RI (B-E) to confirm the presence of *CdsA* PCR fragment. To the left of the gel image is the DNA ladder molecular weights (10037 bp-1000 bp) and to the right is the expected PCR fragment insert size (arrow).

Western blotting was used to confirm RFP-CDSA expression in WT::RFP-*cdsA* cells, by comparison with WT cells using MccA (also Mccc1) as a protein loading control (Davidson, King and Insall, 2013). WT cells had no expression of RFP, whereas the neomycin resistant WT::RFP-*cdsA* cells had a band corresponding to RFP-CDSA expression at the expected size (83 kDa) (Figure 5.5A). RFP expression was also

verified by fluorescence microscopy, which showed RFP localized within the cytosol in both WT::RFP and WT::RFP-*cdsA* cells (**Figure 5.5B**).

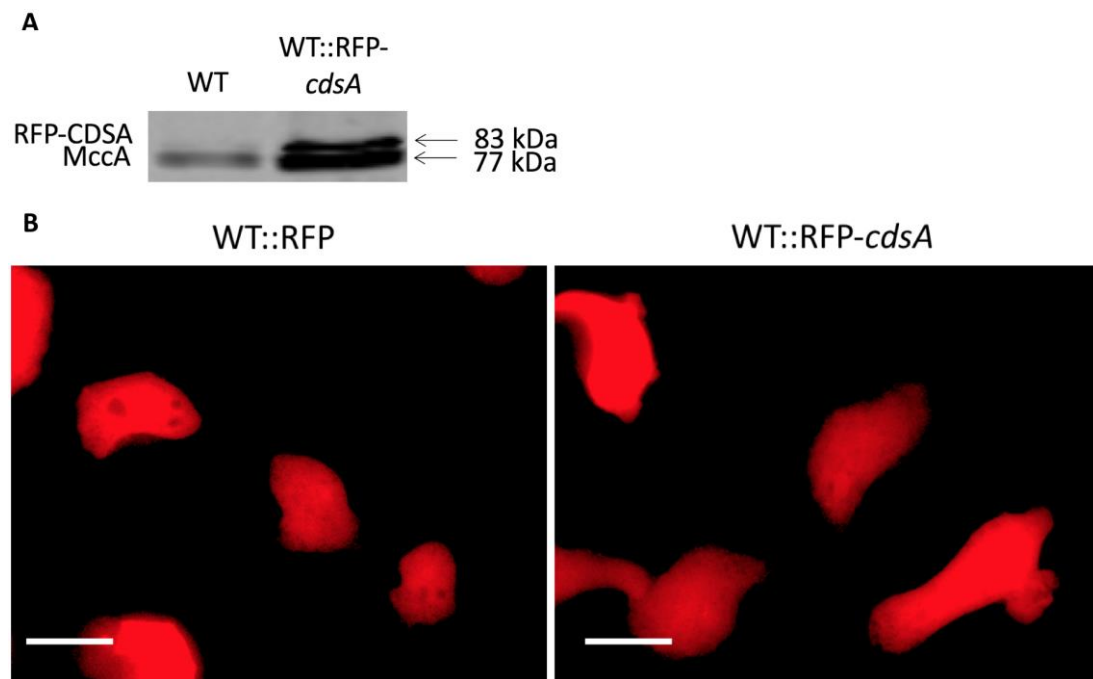


Figure 5.5. CDSA expression and localization. (A) Western blot showing WT cells expressing the loading control MccA only and WT::RFP- *cdsA* cells expressing MccA and RFP-CDSA. (B) WT::RFP and WT::RFP-*cdsA* cells visualized using fluorescence microscopy with RFP localized within the cytosol in both cell lines. Scale bars represent 10 μ m.

5.4 Phenotypic Characterization of WT::RFP-*cdsA* Cells

WT::RFP-*cdsA* cells were then phenotypically characterized through a series of experiments and compared with WT::RFP cells in both the absence and presence of VPA during cell growth and development. WT::RFP-*cdsA* cells were then characterized in the presence of a range of anti-seizure compounds and the BD treatment LiCl during *D. discoideum* development.

5.4.1 Analysis of WT::RFP-*cdsA* Cell Growth in the Presence of VPA

Cell growth was investigated on WT::RFP-*cdsA* cells in both the absence and presence of VPA as the drug is known to have a dose-dependent effect on WT cell

proliferation (Terbach, et al., 2011). WT::RFP and WT::RFP-*cdsA* cells were grown in the presence of increasing VPA concentrations (ranging between 0.01 mM-2 mM), including therapeutic concentrations (0.3 mM-0.6 mM) (Kanner, 2003; Vázquez-Calvo, et al., 2013), for 168 hours (**Figure 5.6**). In the absence of VPA there was no significant difference in cell growth between WT::RFP and WT::RFP-*cdsA* cells (**Figure 5.6A** and **5.6B**). In the presence of increasing VPA concentrations, both cell lines showed a dose-dependent reduction in cell growth, with no significant differences in cell number between the two cell lines. This result suggests the growth-inhibitory effect of VPA is not dependent on CDSA overexpression. This was additionally shown in a secondary plot which compared the rate of cell growth against log VPA concentration (**Figure 5.6C**). The calculated IC₅₀ value for WT::RFP was 0.5 ± 0.05 mM and for WT::RFP-*cdsA* was 0.3 ± 0.09 mM, highlighting VPA growth inhibition at similar concentrations.

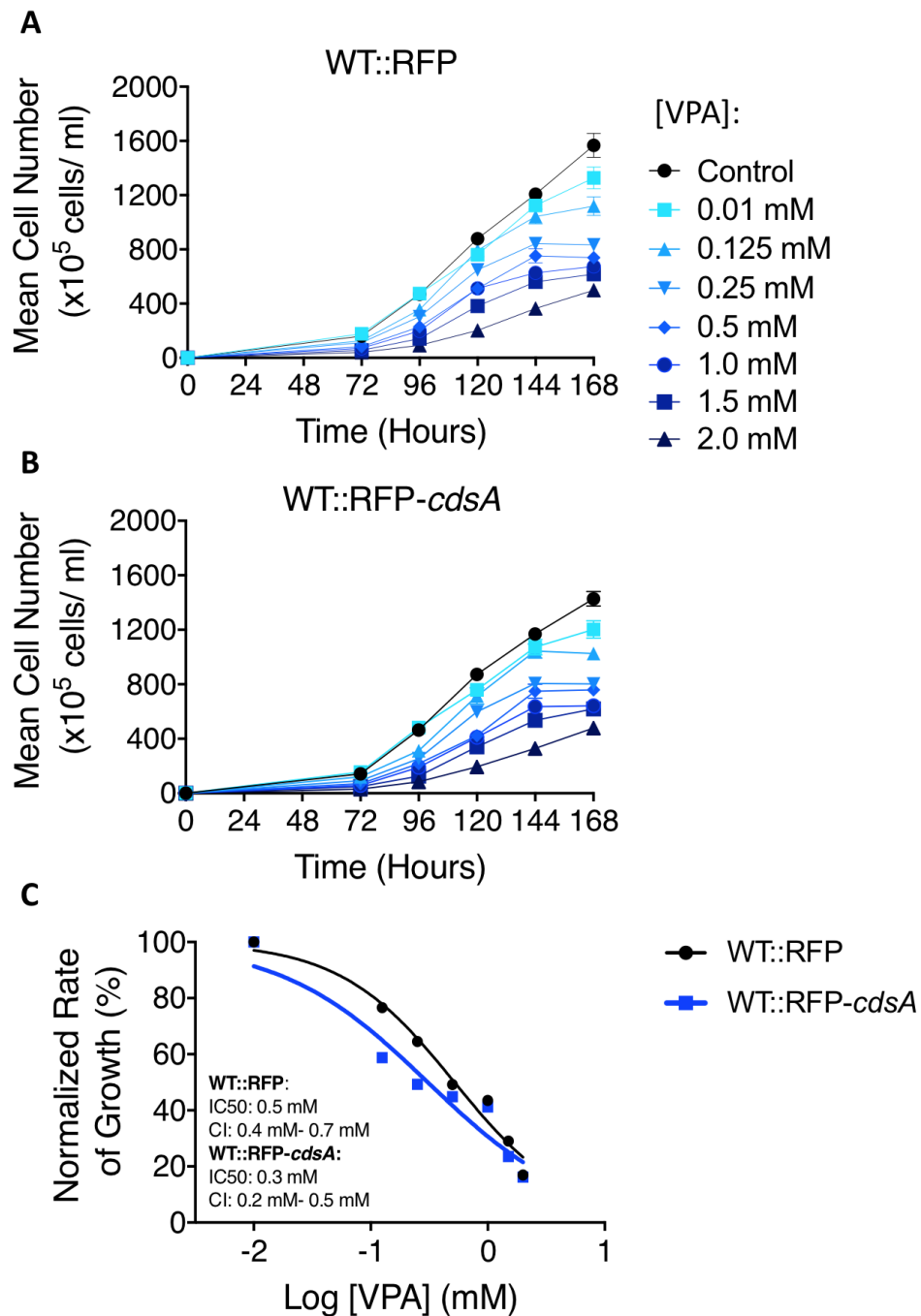


Figure 5.6. WT::RFP and WT::RFP-*cdsA* growth in both the absence and presence of VPA.

(A) WT::RFP and **(B)** WT::RFP-*cdsA* cell proliferation was determined in both the absence (control, black) and presence of VPA at the indicated concentrations (of increasing shades of blue) for 168 hours. **(C)** A secondary plot comparing the normalized change in the rate of cell growth between 96 and 144 hours plotted against log VPA concentration for WT::RFP and WT::RFP-*cdsA* cells. No significant differences in cell proliferation was identified under control conditions or in the presence of VPA using the Kruskal- Wallis test and Dunns post hoc test. Data presented as mean (+/- SEM). $n = 6$.

5.4.2 Analysis of WT::RFP-*cdsA* Cell Development in the Presence of VPA

When *D. discoideum* cells are starved, they enter the developmental cycle, whereby single cells migrate together to form multicellular fruiting bodies after 24 hours (**Figure 1.6**). VPA is known to inhibit this developmental cycle (Williams, et al., 2002). *D. discoideum* development was investigated using WT::RFP and WT::RFP-*cdsA* cells in both the absence (control) and presence of VPA (0.3 mM-1 mM) (**Figure 5.7**). Under control conditions, both cell lines were able to develop into multicellular fruiting bodies of similar size and shape, containing a basal disc, stalk and spore head. In the presence of 0.3 mM and 0.5 mM VPA, both cell lines developed into finger structures. When exposed to 1 mM VPA, both cell lines developed to the mound stage. These results suggest that elevating CDSA levels has no impact on the inhibitory effects of VPA during *D. discoideum* development.

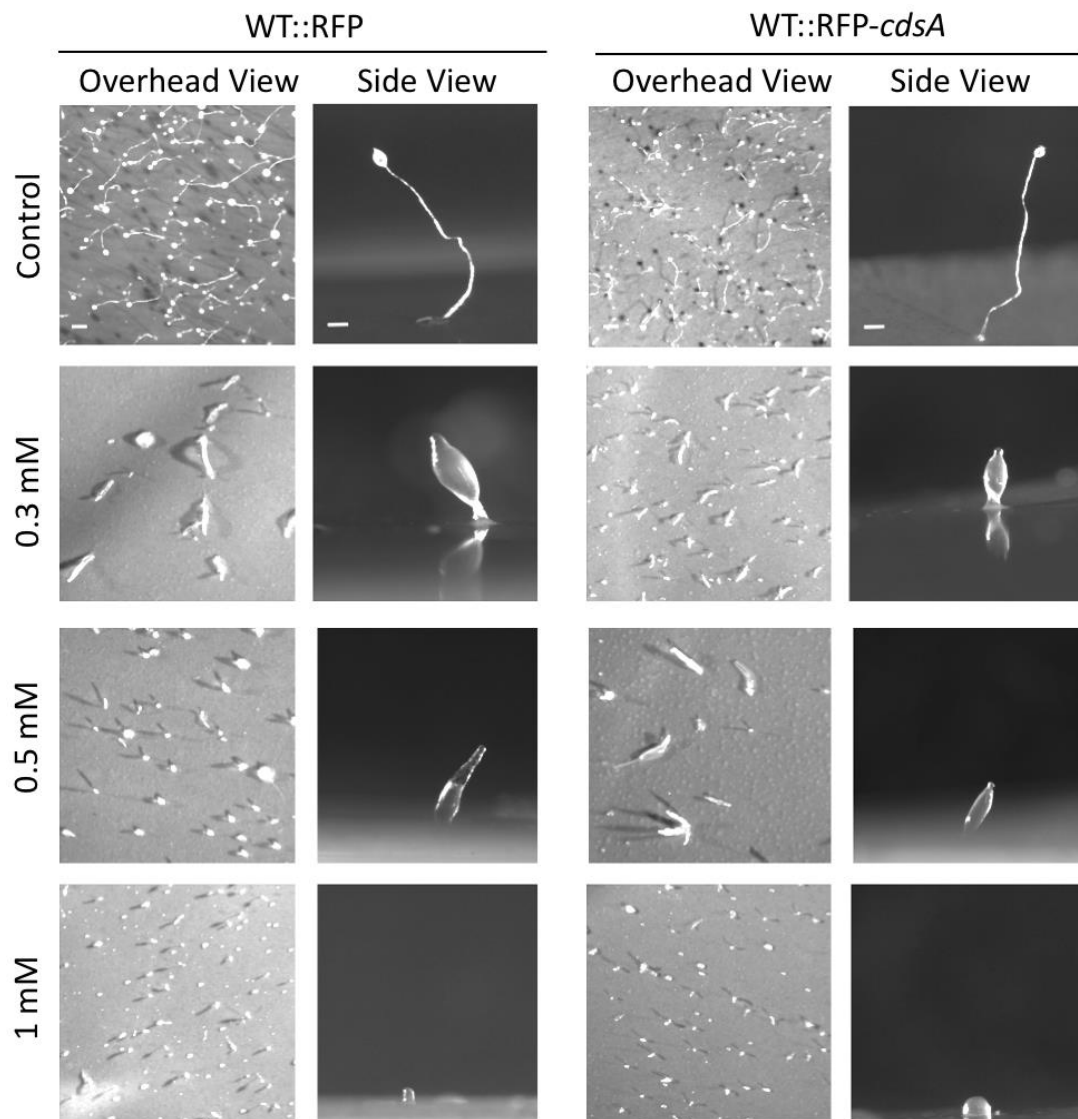


Figure 5.7. WT::RFP and WT::RFP-*cdsA* development in both the absence and presence of VPA. WT::RFP (left) and WT::RFP-*cdsA* (right) cells were developed on nitrocellulose membranes in both the absence (top row) and presence (descending rows) of 0.3 mM, 0.5 mM and 1 mM VPA for 24 hours. Images were then taken of an overhead view (left) of the whole membrane and of a single fruiting body (right). Both cell lines produced fruiting bodies in the absence of VPA and developed into fingers in the presence of 0.3 mM and 0.5 mM and into a mound in the presence of 1mM VPA. $n = 3$. Scale bar of the overhead view represents 0.5 mm and of the side view 0.1 mm.

5.4.3 Analysis of WT::RFP-*cdsA* Cell Development in the Presence of Anti-Seizure Compounds and LiCl

It was then assessed whether CDSA overexpression was a target for other anti-seizure compounds and the BD treatment LiCl. The compounds tested have previously been shown to have an effect on *D. discoideum* cell growth, development, alter phosphoinositide and inositol phosphate levels; and effect *in vivo* epilepsy model epileptic discharges (Williams, et al., 1999; Williams, et al., 2002; Eickholt, et al., 2005; Ludtmann, Boeckeler and Williams, 2011; Elphick, et al., 2012; Chang, et al., 2012; Chang, et al., 2013; Chang, et al., 2015; Chang, et al., 2016). Cells were starved on nitrocellulose filters for 24 hours to induce development in both the absence (control) and presence of a range of compounds at concentrations which blocked fruiting body formation in WT cells (**Figure 5.8**). VPA structurally related compounds VPD (6.5 mM) and PIA (1.4 mM) (Eickholt, et al., 2005; Elphick, et al., 2012) were tested, along with DA (1.65 mM) and OA (0.22 mM) which are key components of the MCT diet (Chang, et al., 2012; Chang, et al., 2013; Chang, et al., 2015; Chang, et al., 2016). A branched chain compound with seizure control and neuroprotective effects, 4-EOA (0.5 mM) (Chang, et al., 2013; Chang, et al., 2015), was also tested. As a negative control, 2-MHA (0.5 mM) which was used as it has not been shown to have activity in *D. discoideum* nor in seizure prevention (Chang, et al., 2012). Both WT::RFP and WT::RFP-*cdsA* cells were able to develop into mature fruiting bodies after 24 hours under control conditions. In the presence of all the compounds tests, WT::RFP and WT::RFP-*cdsA* cells developed to the finger or mound stage. These results suggest that the mechanism of action of these compounds does not involve elevating the activity of CDSA.

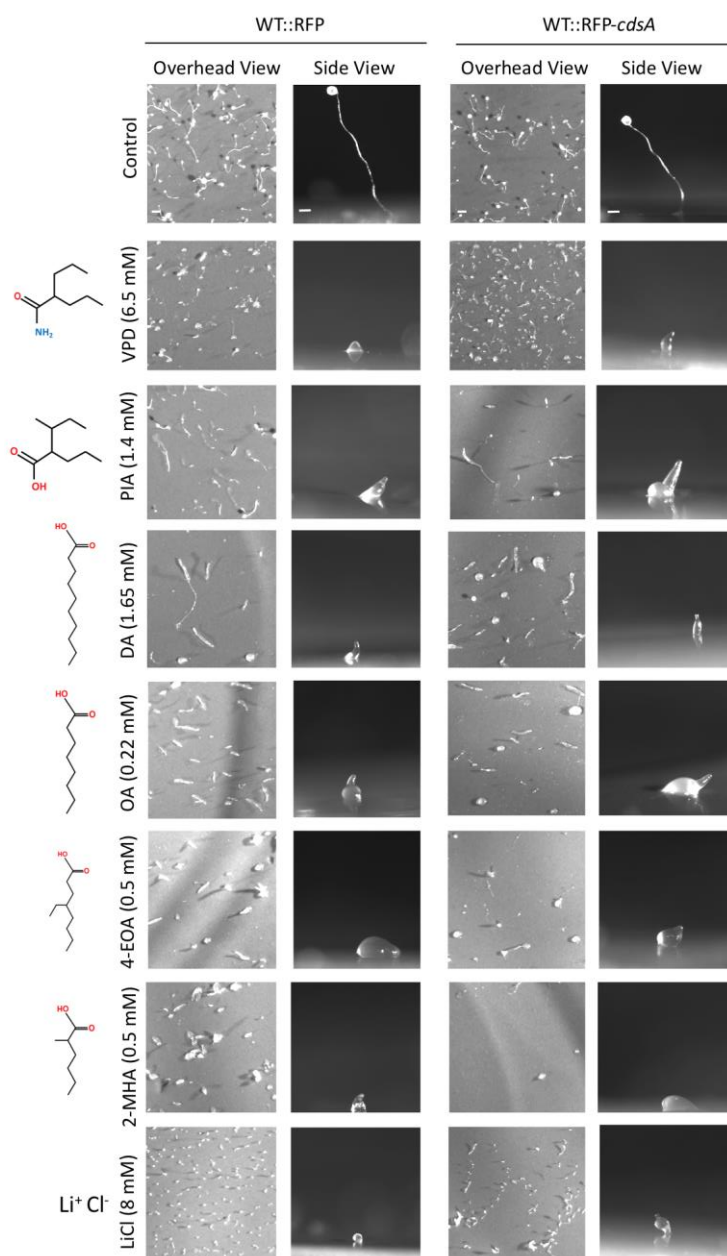


Figure 5.8. WT::RFP and WT::RFP-*cdsA* development in both the absence and presence of a range of other compounds. WT::RFP (left) and WT::RFP-*cdsA* (right) cells were developed on nitrocellulose membranes for 24 hours in both the absence (top row) and presence (descending rows) of VPD, PIA, DA, OA, 4-EOA, 2-MHA and LiCl at the stated concentrations to the left of the development images. Images were taken of an overhead view of the whole membrane (left) and of a single fruiting body (right). Both cell lines developed into fruiting bodies in the absence of any compound. In the presence of VPD, PIA, DA, OA, 4-EOA, 2-MHA and LiCl both WT::RFP and WT::RFP-*cdsA* cells developed to the finger or mound stage. $n = 3$. Scale bar of the overhead view represents 0.5 mm and of the side view 0.1 mm.

5.5 Discussion

D. discoideum phosphoinositide levels are reduced in a dose-dependent manner in the presence of VPA (Chang, et al., 2012). To determine the mechanism of action of VPA, a range of proteins have previously been investigated as molecular targets of the drug. These studies resulted in the elimination of *de novo* inositol production, *de novo* inositol biosynthesis, inositol recycling and PI3K activity (Chang, et al., 2012; Frej, et al., 2016). This leaves the PI salvage pathway as potentially containing the molecular target of VPA in reducing phosphoinositide levels. This chapter has, therefore, reported several attempts to ablate the encoding gene (**Figures 5.2 and 5.3**), the creation of CDSA overexpression cells (**Figure 5.4 and 5.5**) and their characterization in both the absence and presence of anti-seizure compounds, including VPA and the BD treatment LiCl (**Figures 5.6-5.8**).

To ablate CDSA from *D. discoideum*, a knockout vector was created and used to transform cells. Previous studies have shown CDS ablation is lethal in organisms which only contain one CDS gene, including yeast (Shen and Dowhan, 1996), cyanobacteria (Sato, et al., 2000) and *E. coli* (Ganong and Raetz, 1982). However, CDS null cyanobacteria cells were created by supplementing media with PG liposomes (Sato, et al., 2000) and it is known that *D. discoideum* can uptake endogenous fatty acids (Elphick, et al., 2012). Therefore, *D. discoideum* media was supplemented with PI, PG or a combination of PI and PG. However, this resulted in no *cdsA*⁻ cells. Lethality is also seen when ablating PS synthase, another component of the CDP-DAG pathway, and mutants only survive when media is supplemented with ethanolamine or choline (Atkinson, et al., 1980). Research conducted using *E. coli* suggests that the inviable nature of *cds* null cells is due to an increase in cellular pH, to above pH 8, which is a result of the build-up of the substrate PA (Ganong and Raetz, 1982). PA is able to accumulate within cells due to the larger size of the PA pool compared with the CDP-DAG pool (Raetz and Kennedy, 1973). The PA pool is approximately 20 times higher compared with CDP-DAG in *E. coli* (Raetz and Kennedy, 1973) and 99 % larger than CDP-DAG in bovine brain (Thompson and MacDonald, 1976). However, when CDSA was ablated in *D. melanogaster*, the

resulting phenotype was of significant accumulation of neutral lipids with reduced cell and organ size which was rescued with CDSA overexpression (Liu, et al., 2014). In yeast, a point mutation in CDS caused a reduction of enzyme activity and resulted in inositol excretion into growth medium (Shen and Dowhan, 1996).

An overexpression approach was then taken. The overexpressing N-terminal tagged CDSA cells, WT::RFP-*cdsA*, was created and initially characterized by Western blotting, which confirmed RFP-CDSA expression. Protein localization was then investigated by fluorescence microscopy which showed RFP localization within the cytosol in WT::RFP and WT::RFP-*cdsA* cells, which is comparable with CDSA overexpression in HeLa cells (Qi, et al., 2016). In yeast, enzyme activity of CDSA is within the mitochondria and endoplasmic reticulum (Nickels, Buxeda and Carman, 1994). These findings suggest that CDSA may reside in the cytosol and translocate to specific organelles for activity in *D. discoideum*. Translocation of enzymes from one site of the cell to another is demonstrated by a number of enzymes, e.g. sphingosine kinase 1 which moves from the cytoplasm to the plasma membrane (Jarman et al., 2010) and cytidine triphosphate:phosphocholine cytidyltransferase- α which is soluble in an inactive state within the cytosol and insoluble on activation (Aitchison, Arsenault and Ridgway, 2015) where it becomes membrane bound (Morand and Kent, 1989; Ridsdale, et al., 2001). However, it cannot be ruled out that the fusion of RFP to CDSA may affect the localization and function of this enzyme, potentially resulting in an inactive enzyme.

The effects of VPA on WT::RFP-*cdsA* cell growth was then investigated. Both the control cells WT::RFP and WT::RFP-*cdsA* had similar rates of cell growth in the absence of VPA, with no significant differences between the two cell lines identified. This result is consistent with previous work where overexpression of human CDS1 within primate cells had no effect on the rate of PI synthesis, a downstream regulator of the cell cycle (Deguchi, et al., 2002). A second study showed the levels of CDP-DAG remained constant within native COS-7 monkey fibroblast-like cells and overexpressing CDS1 cells (Lykidis et al., 1997). These results suggest that even with abundant enzyme, the rate of PA conversion into

CDP-DAG remains constant, and therefore no effect on cell growth would be expected as CDS activity would be equal in both control and overexpressing cells. During chronic VPA treatment, both WT::RFP and WT::RFP-*cdsA* cells exhibited a dose-dependent reduction of cell growth with increasing VPA concentration. The similarity in cell growth between the two cell lines in response to VPA suggests that the mechanism of action of the drug is independent of CDSA activity in *D. discoideum*. CDSA was investigated as a potential VPA target as depression is well characterized in epilepsy patients (Schmitz, Robertson and Trimble, 1999), effecting 9-37 % of patients (Kwon and Park, 2014). Depression has been associated with a reduction in CDP-DAG levels, where anti-depressant medications, such as maprotiline, paroxetine and imipramine, counteracting this reduction (Tyeryar, Vongtau and Undieh, 2008; Aboukhatwa and Undieh, 2010). Interestingly, some AEDs, including VPA, also have mood stabilizing effects as well as treating seizures, with Lamotrigine also being used as a treatment for depression (Kwon and Park, 2014). This suggests the regulation of CDP-DAG and other PI salvage pathway components is important in both seizure control and mood stabilization. For this reason, VPA was investigated as a potential activator of CDSA during cell growth, when the gene is highly expressed (Stajdohar, et al., 2015), to counteract the reduction in CDP-DAG levels which is associated with depression.

WT::RFP and WT::RFP-*cdsA* cell development was then investigated in both the absence and presence of VPA. Under control conditions, both cell lines developed into similar sized fruiting bodies. In the presence of VPA, CDSA overexpression did not alter VPA-sensitivity, where both cell lines developed to the finger and mound stages. These results suggest that CDSA activity is not enhanced by VPA during the *D. discoideum* developmental cycle. It has previously been found that 30 minutes of VPA treatment results in a significant increase in CDP-DAG and PG, suggesting the mechanism of action of VPA involves accumulation of CDP-DAG (Ju and Greenberg, 2003). It was, therefore, investigated here whether chronic VPA treatment for 24 hours would alter fruiting body development. Although CDP-DAG can only be synthesised by CDSA, the results investigating overexpressed CDSA within *D.*

discoideum show VPA sensitivity, suggesting CDSA is not regulated by VPA during the developmental cycle.

A range of anti-seizure compounds were then investigated on WT::RFP and WT::RFP-*cdsA* cell development. These compounds included a range of VPA structurally related compounds, active components of the MCT diet and the BD treatment LiCl. In the presence of all of these compounds (VPD, PIA, DA, OA, 4-EOA, 2-MHA and LiCl) WT::RFP and WT::RFP-*cdsA* cells developed to the finger or mound stage. These results suggest, that like VPA, the mechanism of action of these compounds does not involve elevation of CDSA activity in *D. discoideum*.

Interestingly, in a similar way to VPA, which is used to treat both epilepsy and BD, the common BD treatment lithium also results in an accumulation of CDP-DAG, by approximately 10-fold (Stubbs Jr. and Agranoff, 1993). Accumulation of CDP-DAG from lithium treatment has been demonstrated numerous times using human SK-N-SH neuroblastoma cells (Stubbs Jr. and Agranoff, 1993), human neutrophils (Stubbs Jr., et al., 1992) and human platelets (Watson, Shipman and Godfrey, 1990). These results suggest VPA and lithium have similar mechanisms of action, independent of elevating CDSA activity in *D. discoideum*.

5.6 Summary

In *D. discoideum* it is probable that CDSA is essential for cell survival, consistent with previous work in other species containing one CDS isoform. In an attempt to overcome the challenges of creating *cdsA*⁻ cells, media was supplemented with PI, PG or a combination of the two, however, this was not successful. Therefore, an overexpression approach was taken. Western blot analysis identified RFP-CDSA within WT::RFP-*cdsA* cells, with expression localized within the cytosol. WT::RFP-*cdsA* cells were sensitive to VPA at similar concentrations to WT::RFP cells, indicating CDSA is not involved in the inhibitory effects of VPA on *D. discoideum* growth and development. Additionally, WT::RFP-*cdsA* cells were also sensitive to other anti-seizure compounds and to the BD treatment LiCl. However, as there was

no change in cellular phenotype compared with WT cells, it is unknown whether the RFP-*cdsA* protein has active enzymatic activity.

Chapter 6

Analysis of CDIPT as a Target of VPA

6. Analysis of CDIPT as a Target of VPA

CDIPT (also known as PI synthase) is the enzyme responsible for the production of PI from the condensation reaction of CDP-DAG and *myo*-inositol within the PI salvage pathway (**Figures 1.4** and **6.1**). PI is an essential phospholipid, forming 2-12 % of the total phospholipids in eukaryotic cells (Flint, et al., 1986). Phosphorylation of the inositol head group of PI results in PI- polyphosphates which regulate G-protein coupled receptors, tyrosine kinases (Lykidis, et al., 1997), membrane anchoring and calcium/ PKC signal transduction pathways (Antonsson, 1997; Bankaitis and Grabon, 2011). CDIPT is a protein of interest as a target of VPA due to the essential nature of PI and its role in calcium signalling which is altered in BD patients during manic episodes (Carman and Wyatt, 1979; Cipriani, et al., 2016).

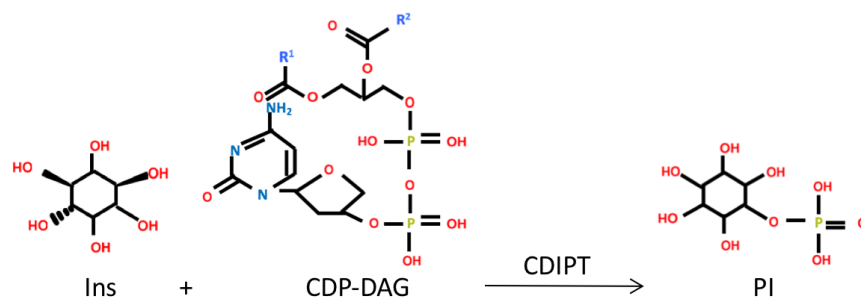


Figure 6.1 The catalytic activity of cytidine diphosphate-diacylglycerol-inositol 3 phosphatidyltransferase. Cytidine diphosphate- diacylglycerol (CDP-DAG) and inositol (Ins) are converted into phosphatidylinositol (PI) by cytidine diphosphate-diacylglycerol-inositol 3 phosphatidyltransferase (CDIPT) via a condensation reaction in the phosphatidylinositol salvage pathway in *D. discoideum*.

The *D. discoideum* *Cdipt* gene (DDB_G0284857) has a length of 2735 bp, which includes one intron and encodes a protein of 207 amino acids. *D. discoideum* has one CDIPT isoform, which is expressed during the vegetative phase of the *D. discoideum* life cycle (Stajdohar, et al., 2015). *D. discoideum* CDIPT has similar homology to the *H. sapiens* orthologue (38 % identity) (**Chapter 4**), suggesting a similar catalytic role for both proteins. This chapter reports the creation of two

knockout constructs to interrupt and ablate *Cdipt* and an RFP-*cdipt* expression construct to overexpress the gene. This chapter then describes the phenotypic characterization of these overexpressing cells, WT::RFP-*cdipt*, during cell growth and development in both the absence and presence of anti-seizure compounds, including VPA and the BD treatment LiCl.

6.1 Construction of *Cdipt* Knockout Vector Part 1

A *Cdipt* knockout vector was created which contained two distal *Cdipt* gene fragments produced by PCR, which were inserted into a pLPBLP vector (Faix et al., 2004) on either side of a blasticidin resistance cassette (**Figure 6.2A** and **6.2B**). The 5' fragment consisted of 463 bp, starting 19 bp outside of the open reading frame and contained one intron. The 3' fragment consisted of 350 bp with no introns and 170 bp of regulatory sequence past the stop codon, resulting in the cloning of 532 bp of exon sequence. The construct had 110 bp removed from the coding sequence. Restriction mapping (**Figure 6.2C**) was used to confirm the presence of the four restriction sites used for cloning in the two distal gene fragments into the pLPBLP vector (*Bam*HI, *Pst*I, *Nco*I and *Kpn*I). Single restriction digests resulted in a single band at approximately 5250 bp which corresponds to the size of the pLPBLP plasmid and the additional two *Cdipt* fragments. Restriction mapping was then used to show the correct sized fragments within the knockout construct at approximately 460 bp for the 5' and 350 bp for the 3' regions. There was also a second larger band corresponding to the remaining recombinant plasmid (4800 bp and 5000 bp confirming the 5' and 3' regions respectively). A further digest using *Bam*HI and *Kpn*I was conducted to excise the knockout cassette, which contained the 5' and 3' *Cdipt* gene fragments flanking either side of a blasticidin resistance gene, from the recombinant *Cdipt* knockout plasmid. Two bands were obtained, one at 2400 bp which corresponded to the knockout cassette and the second at 2900 bp of the remaining pLPBLP plasmid.

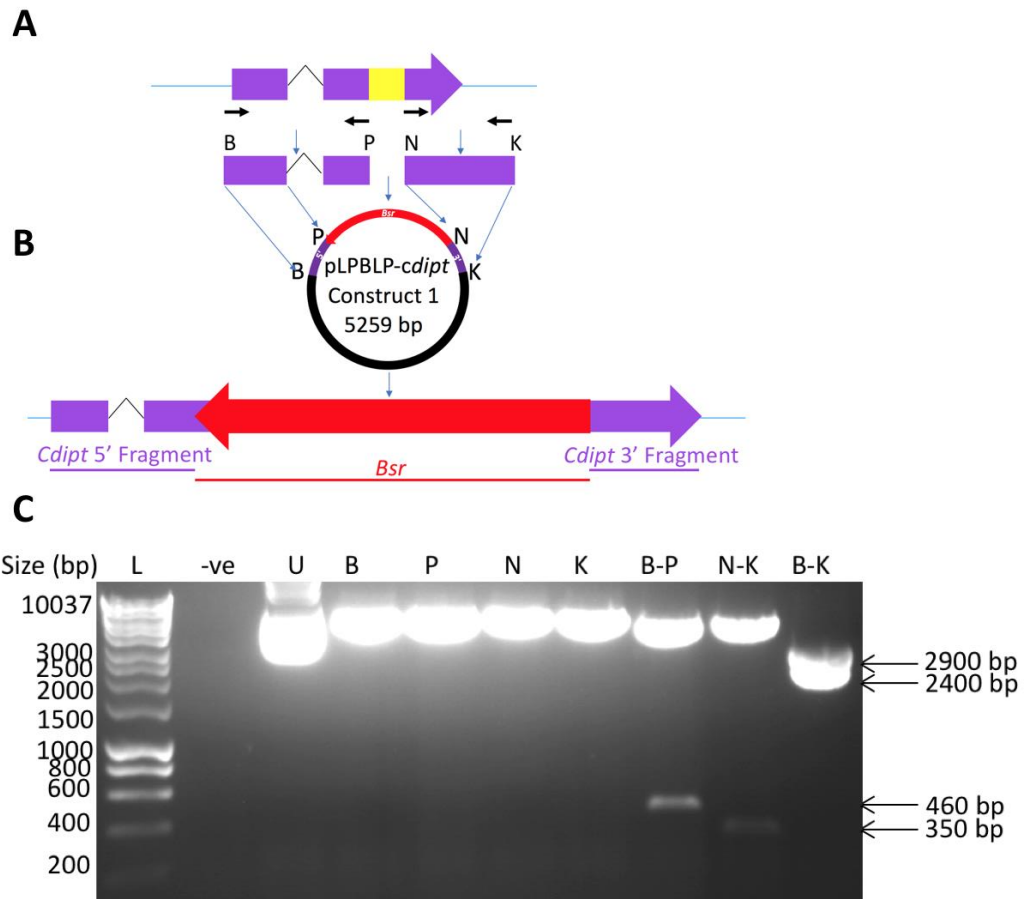


Figure 6.2 Confirmation of the *Cdipt* knockout construct 1. (A) *Cdipt* genomic DNA with the yellow box showing the region to be knocked out and the arrows indicating the 5' and 3' genomic DNA fragments which were PCR amplified using primers containing cut sites for *Bam*HI (B), *Pst*I (P), *Nco*I (N) and *Kpn*I (K). (B) Plasmid map of pLPBLP-*cdipt* containing the 5' and 3' *Cdipt* fragments cloned on either side of the blasticidin resistance cassette by *Bam*HI (B), *Pst*I (P), *Nco*I (N) and *Kpn*I (K). (C) Confirmation of the *Cdipt* inserts within the pLPBLP vector by a series of single and double restriction digests visualised following gel electrophoresis with a ladder (L), negative control without any plasmid (-ve), uncut knockout vector (U), single digests confirming individual enzyme activity of *Bam*HI (B), *Pst*I (P), *Nco*I (N) and *Kpn*I (K) and double digests to confirm the presence of the 5' and 3' CDIPT fragments using *Bam*HI-*Pst*I (B-P) and *Nco*I-*Kpn*I (N-K) and the linearized knockout cassette used for electroporation with *Bam*HI-*Kpn*I (B-K). Molecular weights of the DNA ladder are indicated on the left of the gel image (10037 bp- 200 bp) and the expected plasmid insert sizes are given (arrows) to the right of the image.

6.2 Screening Potential *cdipt*⁻ *D. discoideum* Cells Part 1

To ablate the *Cdipt* gene in *D. discoideum*, the *Cdipt* knockout cassette (**Figure 6.2**) was electroporated into WT cells and selected by growth in the presence of blasticidin. PCR screening of surviving colonies was then conducted to identify transformant cells which had the knockout cassette integrated into the *Cdipt* gene, thereby creating *cdipt*⁻ cells. For PCR screening (**Figure 6.3A**), primers were designed around the 5' and 3' regions of the blasticidin resistance cassette which amplified a product from the endogenous gene (genomic control), resulting in a 5' (500 bp) and 3' (450 bp) band for both WT and transformant cells. A second primer set amplified a product from the gene fragment into the vector sequence (vector control), which resulted in a 530 bp or 500 bp band for the 5' and 3' screen only in transformant cells. Finally, homologous recombinant cells were identified by amplifying a region that will be produced (560 bp and 530 bp band for the 5' and 3' *Cdipt* fragments respectively) only in *cdipt*⁻ cells covering the endogenous gene fragment and the blasticidin resistance cassette (knockout diagnostic).

Numerous attempts were made to identify a *cdipt*⁻ mutant using the *Cdipt* knockout cassette. A total of 6 electroporations yielded 293 independent blasticidin resistant mutants that were individually screened (**Figure 6.3B and 6.3C**). From this work, no *cdipt*⁻ cells were identified. Around 28 transformants were additionally grown in the presence of PI (100 µM) in case the null mutant was an auxotroph. This approach was taken as CDIPT has been shown to be essential in other organisms with one protein isoform (Nikawa, Kodaki and Yamashita, 1987; Wang and Montell, 2006).

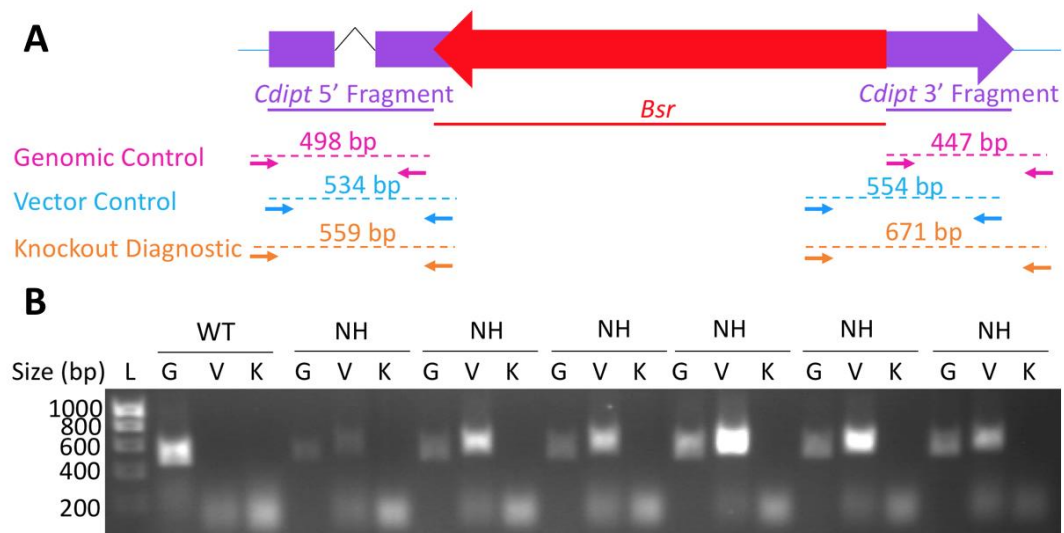


Figure 6.3 PCR screening of potential *cdipt* transformant cells using knockout cassette 1.

(A) Schematic representation of the *Cdipt* gene containing the homologous integrated knockout construct. The locations of the screening primers (arrows) and the corresponding PCR product (dotted line) used for determining homologous integration are shown for genomic (pink), vector (blue) and knockout diagnostic (yellow) primers and the predicted sizes of these products. **(B)** 5'-terminal PCR screening of blasticidin-resistant cells with genomic control (G), vector control (V) and knockout diagnostic (K). PCR products are shown where the genomic control (G) band is amplified from WT DNA, genomic (G) and vector (V) control bands are amplified from non-homologous integrant (NH) DNA and all 3 bands are (G, V and knockout diagnostic (K)) are amplified from the potential knockout (*cdipt*) DNA. Molecular weights of the DNA ladder are indicated on the left of the gel image (1000 bp- 200 bp).

6.3 Construction of *cdipt* Knockout Vector Part 2

To overcome the unsuccessful creation of *cdipt* *D. discoideum* cells, a second *Cdipt* knockout plasmid was produced. This second knockout plasmid had an increased size of exon sequence (from 532 bp to 563 bp) and reduced number of base pairs being deleted (from 110 bp to 5 bp), to increase the likelihood of homologous integration (**Figure 6.4A**). The second *Cdipt* recombinant plasmid was produced in the same way as the first, whereby two *Cdipt* PCR amplified DNA fragments (317 bp and 357 bp for the 5' and 3' fragments respectively) located within the coding sequence were inserted on either side of a blasticidin resistance gene. Restriction

mapping (**Figure 6.4C**) was used to confirm the presence of the four restriction enzyme cut sites used for cloning (*Bam*HI, *Pst*I, *Hind*III and *Kpn*I) by a single digest, resulting in one band at 5000 bp. The presence of the *Cdipt* 5' (320 bp) and 3' (360 bp) fragments within the knockout vector were confirmed by double restriction digests, whereby two bands were obtained, one whose size confirmed the correct insertion of the *Cdipt* fragment and the second being the remaining recombinant plasmid (4900 bp and 5000 bp for 5' and 3' gene fragments respectively). The knockout cassette was excised from the vector using the enzymes *Bam*HI and *Kpn*I, which produced a band at 2600 bp, with the remaining plasmid band at 2900 bp.

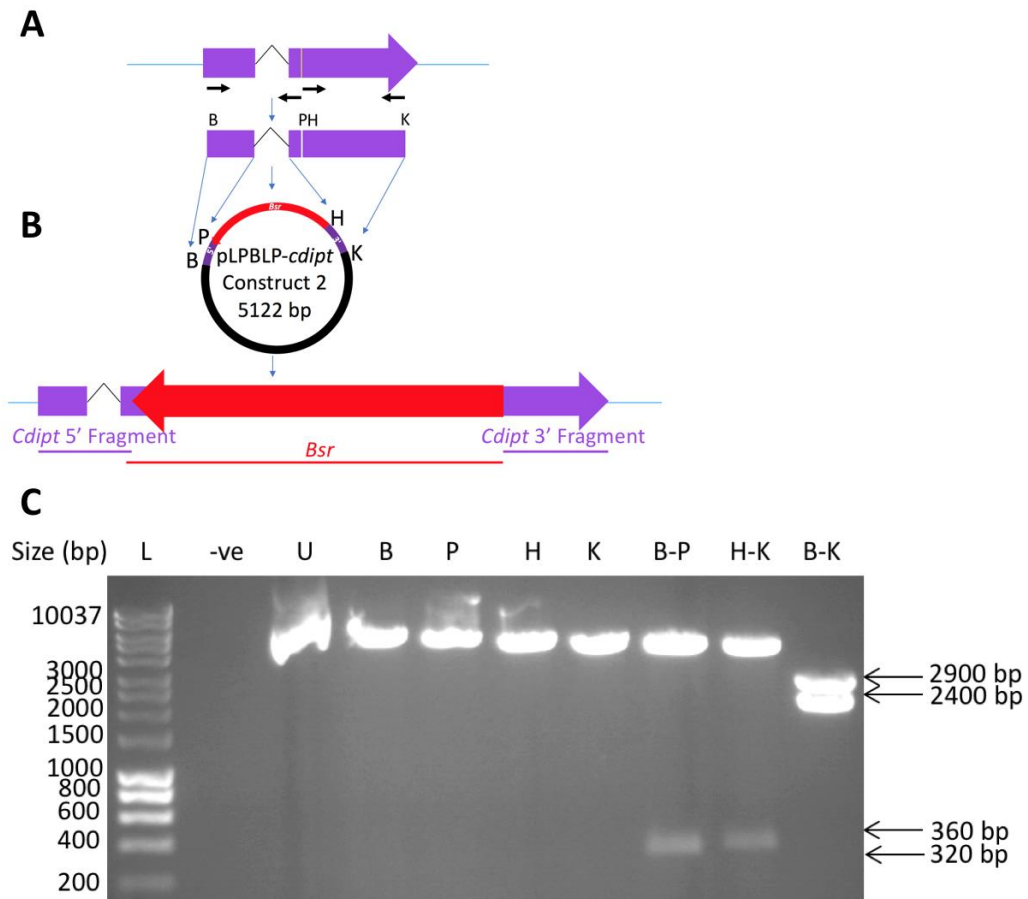


Figure 6.4 Confirmation of the *Cdipt* knockout construct 2. **(A)** *Cdipt* genomic DNA with the region to be knocked out highlighted in yellow and the 5' and 3' genomic DNA fragments which were PCR amplified using primers containing cut sites for *Bam*HI (B), *Pst*I (P), *Hind*III (H) and *Kpn*I (K). **(B)** pLPBLP-*cdipt* plasmid map containing the 5' and 3' *Cdipt* fragments cloned into either side of the blasticidin resistance cassette. **(C)** Confirmation of the *Cdipt* inserts in the pLPBLP vector by a series of single and double restriction digests visualised following gel electrophoresis with a ladder (L), negative control with no plasmid (-ve), uncut knockout vector (U), single digests confirming individual enzyme activity of *Bam*HI (B), *Pst*I (P), *Hind*III (H) and *Kpn*I (K) and double digests confirming the presence of the 5' and 3' fragments using *Bam*HI-*Pst*I (B-P) and *Hind*III-*Kpn*I (H-K) and the linearized knockout cassette used for electroporation excised with *Bam*HI-*Kpn*I (B-K). To the left of the gel image are the molecular weights of the DNA ladder (10037 bp- 200 bp) and to the right are the expected plasmid insert sizes (arrows).

6.4 Screening and Confirmation of Potential *cdipt*⁻ *D. discoideum* Cells Part 2

The second *Cdipt* knockout cassette was then digested and electroporated into WT *D. discoideum* cells (**Figure 6.4**). Transformant cells were selected by growth in the presence of blasticidin. Surviving colonies were screened by PCR to identify *cdipt*⁻ homologous recombinants. For this vector, new screening primers for the genomic control, which amplified DNA from outside to within the fragment of interest at the 5' (330 bp) and 3' (370 bp) region were produced, where a band for this control was expected in both WT and transformant cells. New vector control primers were also produced which confirmed the 5' (390 bp) and 3' (280 bp) *Cdipt* fragments were located on either side of the blasticidin resistance cassette and so a band would only be amplified from transformant cell DNA containing the blasticidin resistance cassette (**Figure 6.5A**). Potential homologous recombinant cells were identified using the knockout diagnostic primers where DNA was amplified from outside the inserted fragment to within the blasticidin resistance cassette, with expected PCR products of 450 bp for the 5' fragment and 590 bp for the 3' fragment.

Numerous attempts were again made to identify a *cdipt*⁻ mutant using the second *Cdipt* knockout vector. Transformation of the second *Cdipt* knockout cassette resulted in 427 blasticidin resistant colonies, of which 232 colonies were grown in media supplemented only with blasticidin and 195 colonies were grown in media supplemented with blasticidin and PI (100 µM) (the product of CDIPT). Whilst screening transformant colonies grown in media containing PI and blasticidin, 8 independent colonies were identified which contained a PCR fragment amplified using the 3' knockout diagnostic primers. However, this band was smaller than expected (approximately 140 bp). When the 5' terminus was screened, 3 of these 8 independent colonies also amplified a 5' knockout diagnostic band of the expected size (**Figure 6.5B** and **6.5C**). To determine whether these 3 transformant colonies which amplified both the 5' and 3' knockout diagnostic band were *cdipt*⁻ cells, the PCR fragment produced using the 3' knockout diagnostic primers for each transformant was cloned into TA and sequenced. Sequencing confirmed that these

colonies contained the *Cdipt* 3' fragment, however, a loop had formed, resulting in part of the sequence being lost (**Figure 6.5D**) and thereby resulted in a larger number of base pairs being deleted from the *Cdipt* gene within these 3 colonies. In the subsequent process of isolating isogenic cell lines of these 3 independent transformants, all the cell lines ceased to grow.

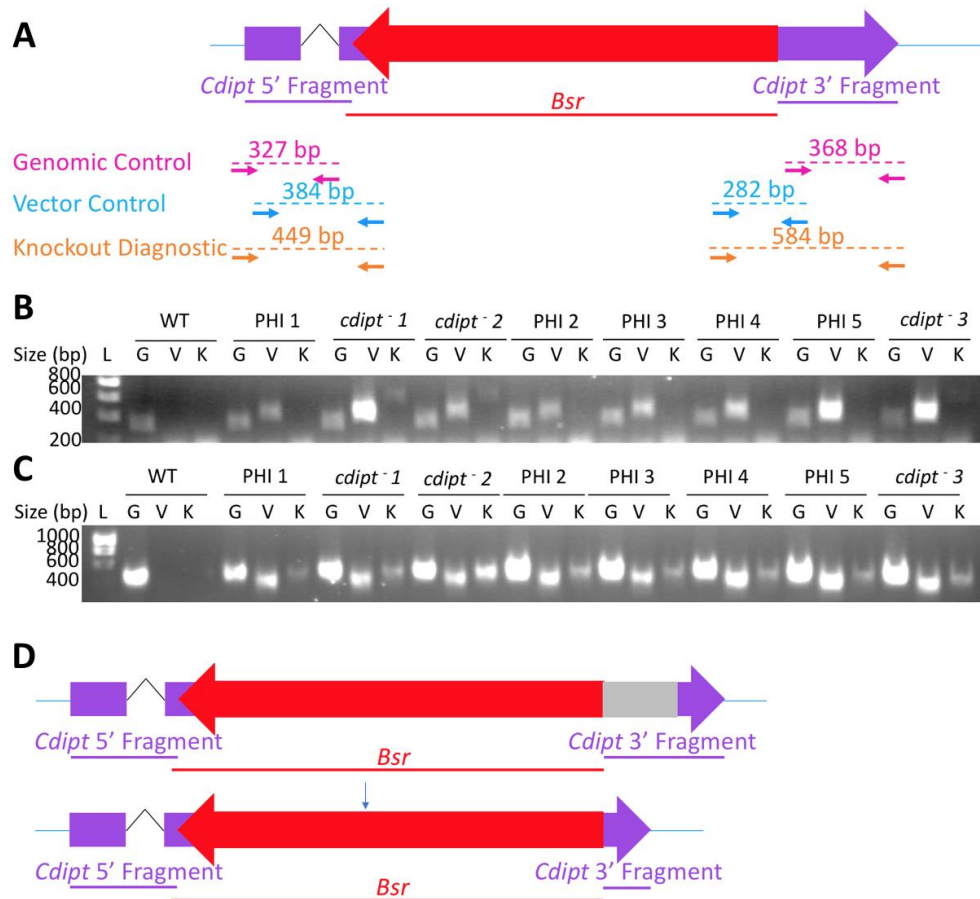


Figure 6.5. PCR screening of potential *cdipt*⁻ transformant cells using knockout cassette 2.

(A) Schematic representation of the *Cdipt* gene containing the homologous integrated knockout construct. The locations of the screening primers (arrows) and the corresponding PCR product (dotted line) used for determining homologous integration are shown—genomic (pink), vector (blue) and knockout diagnostic (yellow) primers along with the predicted sizes of the products. **(B)** 3'- and **(C)** 5' PCR screening of transformant cells showing the genomic control (G), vector control (V) and knockout diagnostic (K). PCR products are shown where the genomic control (G) band is amplified from WT DNA, genomic (G) and vector (V) control bands are amplified from non-homologous integrant (NH) DNA and all 3 bands are (G, V and knockout diagnostic (K)) are amplified from the potential knockout (*cdipt*⁻) DNA. **(D)** Illustration of the 3' knockout diagnostic PCR fragment taken from sequencing results where the region in grey indicates the size of the 3' fragment sequence which formed a loop and was additionally knocked out, resulting in a smaller 3' fragment adjacent to the blasticidin resistance cassette. Molecular weights of the DNA ladder (1000 bp-200 bp) are indicated on the left of the gel image.

6.5 Preparing a *Cdipt* Overexpression Construct

To create WT::RFP-*cdipt* *D. discoideum* cells, an 5' RFP tag overexpression construct (389-19 mRFPmrs) (Basu, et al., 2013; Fey et al., 2013) containing PCR amplified *Cdipt* cDNA was created (**Figure 6.6A**). *Cdipt* cDNA (624 bp) was amplified using primers containing cut sites for the restriction enzymes *Bam*HI and *Eco*RI and this fragment was cloned into the 5' RFP tagged overexpression construct. Restriction mapping was used to confirm the presence of the two restriction sites used for cloning (*Bam*HI and *Eco*RI), which produced a single band at approximately 6500 bp. A double digest using the same two restriction enzymes confirmed the insertion of the *Cdipt* cDNA PCR amplified product with a band at approximately 620 bp and a second band at 5900 bp corresponding to the RFP plasmid (**Figure 6.6B**). This construct was sequenced to ensure that there were no mutations in the inserted PCR product. WT::RFP-*cdipt* *D. discoideum* cells were then created by electroporating the 5' RFP tagged-*cdipt* overexpression construct into WT cells and selecting cells by growth in the presence of neomycin (G418).

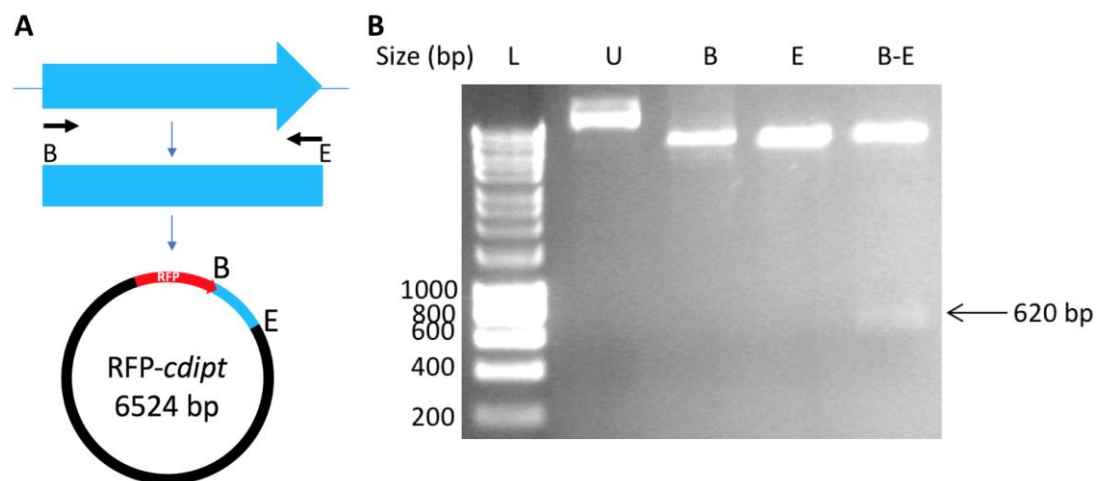


Figure 6.6 Confirmation of the RFP-*cdipt* overexpression construct. (A) Schematic representation of *Cdipt* cDNA showing the primer locations (arrows) used for PCR amplification and the cut sites *Bam*HI (B) and *Eco*RI (E) used for cloning the *Cdipt* cDNA into the 5' RFP- expression vector. **(B)** Confirmation of *Cdipt* cDNA inserted into the RFP- expression vector by a series of single and a double restriction digest visualised following gel electrophoresis with a ladder (L), uncut vector (U), single digests confirming individual enzyme activity of *Bam*HI (B) and *Eco*RI (E) and a double digest to confirm the presence of *Cdipt* PCR fragment using *Bam*HI-*Eco*RI (B-E). DNA ladder molecular weights (1000 bp-200 bp) are indicated on the left of the gel image and to the right is the expected PCR fragment insert size (arrow).

CDIPT expression within WT::RFP-*cdipt* cells was examined by Western blotting. Comparison was made to WT cells and protein loading was identified by comparing with MccA (also known as Mccc1) expression (Davidson, King and Insall, 2013). As expected, there was no expression of RFP in WT cells and surprisingly there was low RFP-CDIPT expression in the neomycin resistant WT::RFP-*cdipt* cells at the expected size (77 kDa) (**Figure 6.7A**). Fluorescence microscopy was then used to confirm RFP localization in WT::RFP and WT::RFP-*cdipt* cells. In these experiments WT::RFP cells showed fluorescence with no specific localization, consistent with the RFP protein being present in the cytosol. In contrast, WT::RFP-*cdipt* cells showed fluorescence at low level within the cytosol and high levels of fluorescence localized within puncta (**Figure 6.7B**). As CDIPT has transmembrane domains, the puncta staining could be a

membrane compartment, with the possibility of vesicles. The cytosolic RFP signal could be a result of cleavage of the fluorescent tag from the full-length protein.

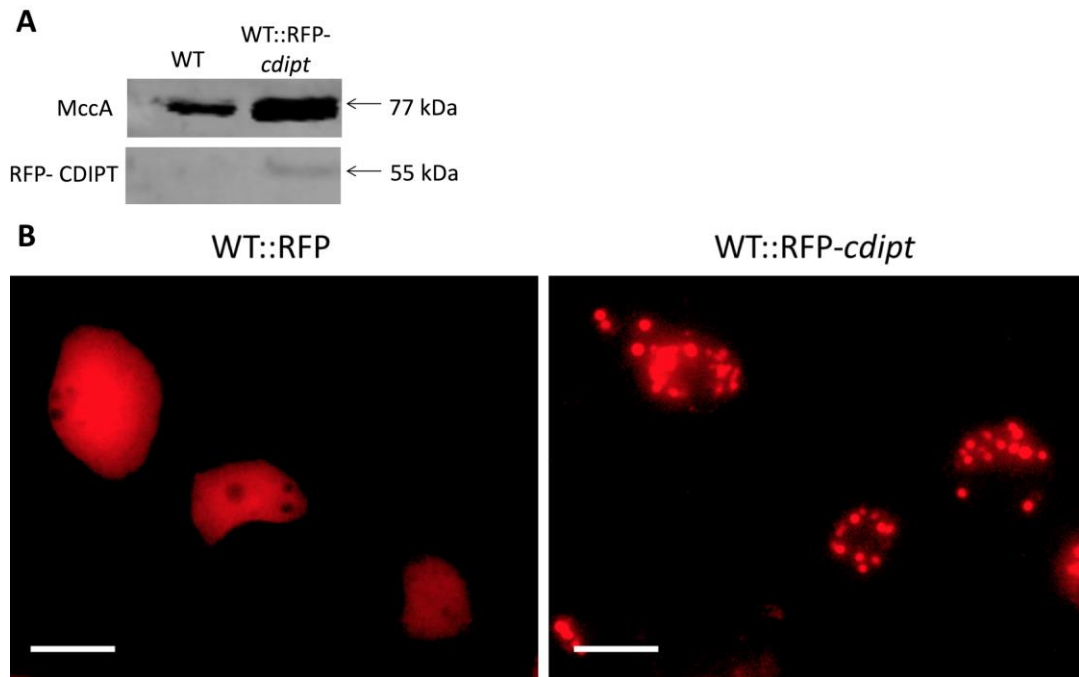


Figure 6.7. CDIPT expression and localization. (A) Western blot of WT cells expressing no RFP and WT::RFP-*cdipt* cells showing a control MccA band to compare protein loading between the two cell lines and a weak RFP-CDIPT band in WT::RFP-*cdipt* cells. **(B)** WT::RFP and WT::RFP-*cdipt* cells were visualized using fluorescence microscopy. RFP in WT cells showed cytosolic localization whereas RFP-CDIPT appears to be mainly localized within membrane bound vesicles and at low levels within the cytosol. Scale bars represent 10 μ m.

6.6 Phenotypic Characterization of WT::RFP-*cdipt* Cells

Since CDIPT ablation appeared to be lethal, an overexpression approach was taken to manipulate levels of the enzyme. Phenotypic changes caused by the overexpression of CDIPT in WT::RFP-*cdipt* cells were investigated through a series of experiments by comparison with WT::RFP cells. These experiments involved determining the effects of VPA on growth and development in these two cell lines. WT::RFP-*cdipt* cells were then exposed to a range of anti-seizure compounds and the BD treatment LiCl during *D. discoideum* development.

6.6.1 Analysis of WT::RFP-*cdipt* Cell Growth in the Presence of VPA

Since WT::RFP-*cdipt* cells had the RFP-CDIPT protein mainly localized within membrane bound vesicles, these cells were assessed for altered susceptibility to VPA during growth. Cell growth was initially investigated as VPA inhibits *D. discoideum* cell proliferation in a dose-dependent manner (Terbach, et al., 2011). WT::RFP and WT::RFP-*cdipt* cells were grown for 168 hours in a range of VPA concentrations (0.01 mM-2 mM), widely spanning the therapeutic (plasma) concentration of 0.3 mM-0.6 mM (Kanner, 2003; Vázquez-Calvo, et al., 2013) (**Figure 6.8**). Under control conditions, in the absence of VPA, no difference in cell growth between the two cell lines was identified. In the presence of VPA, however, WT::RFP cells showed a dose-dependent reduction on cell growth (**Figure 6.8A**), whereas WT::RFP-*cdipt* cells appeared to be less sensitive to VPA at 0.125 mM and 0.25 mM. At 0.5 mM VPA there was a statistically significant difference (P value 0.0005) using the Kruskal- Wallis test between the two cell lines, suggesting altering CDIPT expression reduces VPA-sensitivity during cell growth (**Figure 6.8B**). The IC₅₀ values for the two cell lines also illustrated WT::RFP-*cdipt* cell resistance to VPA during chronic exposure, with IC₅₀ values of 0.5 ± 0.08 mM VPA for WT::RFP cells and 1.1 ± 0.02 mM for WT::RFP-*cdipt* cells (**Figure 6.8C**).

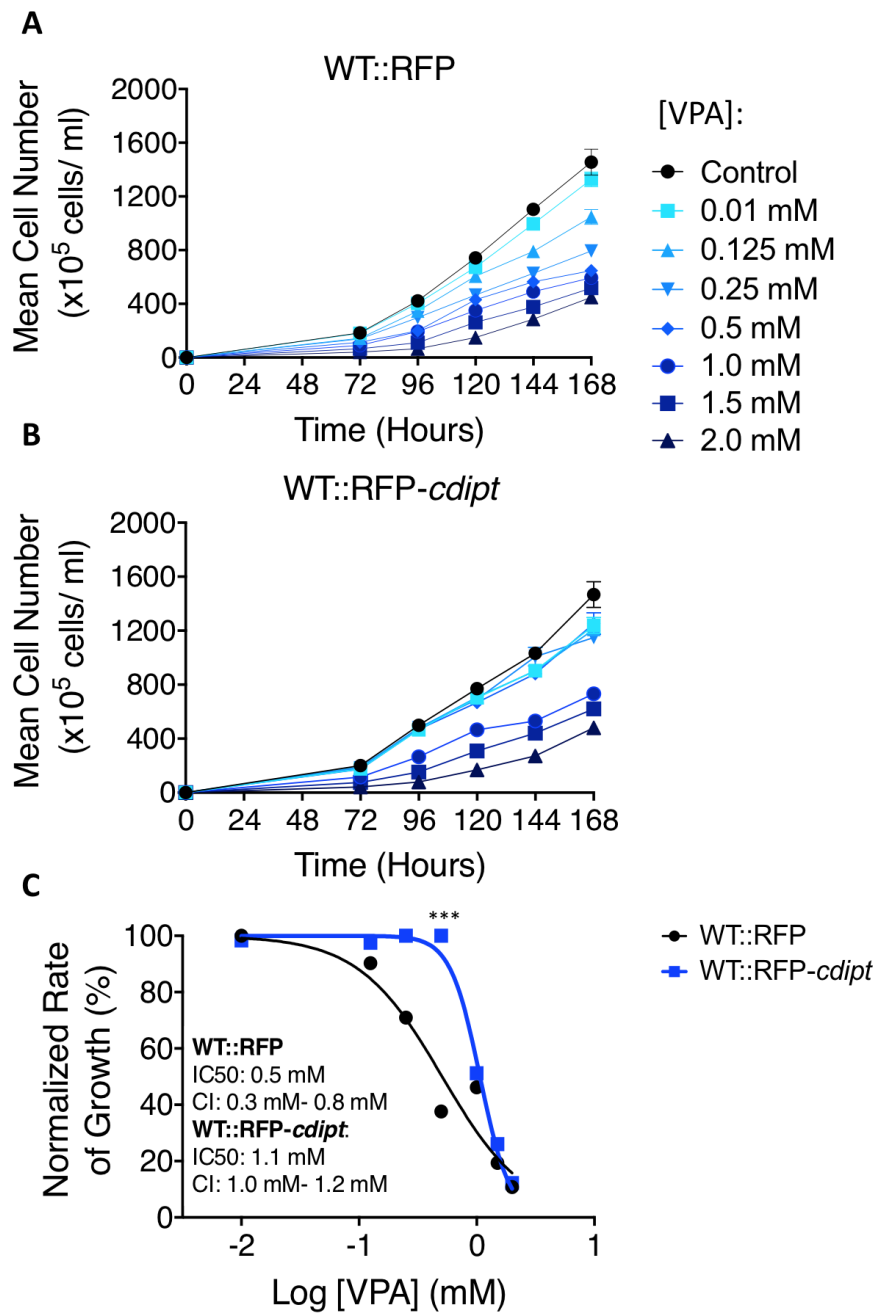


Figure 6.8. WT::RFP and WT::RFP-*cdipt* growth in both the absence and presence of VPA.

(A) WT::RFP and **(B)** WT::RFP-*cdipt* cell proliferation was determined in both the absence (control, black) and presence of VPA at indicated concentrations (at increasing shades of blue) VPA for 168 hours. **(C)** A secondary plot illustrating the normalized change in the rate of cell growth between 96 and 144 hours plotted against log VPA concentration for WT::RFP and WT::RFP-*cdipt* cells. Statistically significant differences in cell proliferation were identified at 0.5 mM VPA tested between the two cell lines using the Kruskal- Wallis test and Dunns post hoc test. Data presented as mean (\pm SEM). $n = 6$. *** P value = 0.0005.

6.6.2 Analysis of WT::RFP-*cdipt* Cell Development in the Presence of VPA

The *D. discoideum* developmental cycle results from starvation and involves single cells migrating together to form a fruiting body (**Figure 1.6**). Previous work using *D. discoideum* has shown VPA to inhibit fruiting body formation (Williams, et al., 2002). In order to investigate the effects of VPA on WT::RFP and WT::RFP-*cdipt* cell development, cells were starved for 24 hours on nitrocellulose filters to induce development in both the absence (control) and presence of 0.3 mM, 0.5 mM and 1 mM VPA (**Figure 6.9**). Both cell lines in the absence of VPA were able to develop into fruiting bodies containing a basal disc, stalk and spore head of similar size, showing that an altering CDIPT activity does not effect *D. discoideum* development. In the presence of 0.3 mM and 0.5 mM VPA, WT::RFP cells developed to the finger stage. In contrast, WT::RFP-*cdipt* cells developed into multicellular fruiting bodies resembling control conditions in the presence of 0.3 mM and 0.5 mM VPA. This data suggests that altering CDIPT levels in *D. discoideum* causes resistance to VPA dependent inhibition during development.

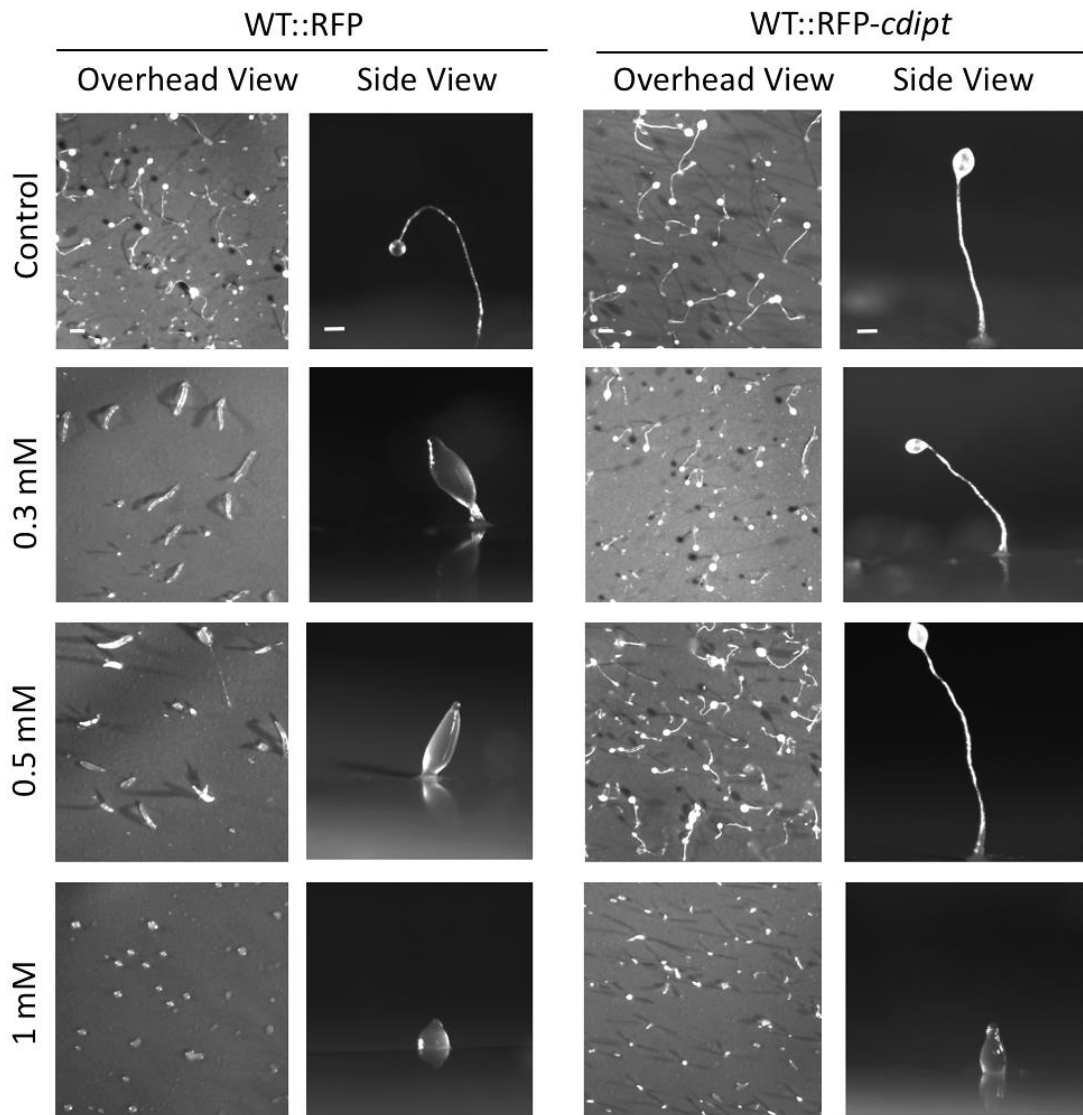


Figure 6.9. WT::RFP and WT::RFP-*cdipt* development in both the absence and presence of VPA. WT::RFP (left) and WT::RFP-*cdipt* (right) cells were developed on nitrocellulose membranes for 24 hours both in the absence (top row) and presence (descending rows) of 0.3 mM, 0.5 mM and 1 mM VPA. Images were taken of an overhead view (left) of the whole membrane and of a single fruiting body (right). Both cell lines developed into mature fruiting bodies in the absence of VPA. WT::RFP cells in the presence of 0.3 mM and 0.5 mM developed to the finger stage and when exposed to 1 mM VPA into a mound after 24 hours. In contrast, WT::RFP-*cdipt* cells were resistant to the effects of VPA and continued to develop into mature fruiting bodies when exposed to 0.3 mM and 0.5 mM VPA and into a mound in the presence of 1 mM VPA. $n = 3$. Scale bar of the overhead view represents 0.5 mm and of the side view 0.1 mm.

6.6.3 Analysis of WT::RFP-*cdipt* Cell Development in the Presence of Anti-Seizure Compounds and LiCl

WT::RFP-*cdipt* cells were also investigated as a potential target of other anti-seizure compounds and a BD treatment due to the use of VPA in both disorders. The compounds chosen for analysis have previously been shown to have an effect on growth, development and inositol phosphate and phosphoinositide signalling in *D. discoideum* and in mammalian epilepsy models (Williams, et al., 1999; Williams, et al., 2002; Eickholt, et al., 2005; Ludtmann, Boeckeler and Williams, 2011; Elphick, et al., 2012; Chang, et al., 2012; Chang, et al., 2013; Chang, et al., 2015; Chang, et al., 2016). Cells were starved for 24 hours on nitrocellulose filters to induce development in both the absence (control) and presence of a range of anti-seizure compounds at concentrations which blocked WT development (**Figure 6.10**). VPD (6.5 mM) and PIA (1.4 mM) were selected as they are structurally related to VPA (Eickholt, et al., 2005; Ludtmann, Boeckeler and Williams, 2011; Elphick, et al., 2012) and DA (1.65 mM) and OA (0.22 mM) were chosen as they are key components of the MCT diet, used for the treatment of drug-resistant epilepsy (Chang, et al., 2012; Chang, et al., 2013; Chang, et al., 2016). Branched chain fatty acids were also investigated, including 4-EOA (0.5 mM) which has proven anti-seizure and neuroprotection effects and 2-MHA (0.5 mM) which tested as a negative control as it has no activity in *D. discoideum* nor does it have an effect on preventing seizures (Chang, et al., 2012; Chang, et al., 2013; Chang et al., 2015). As shown previously, both cell lines under control conditions were able to develop into mature fruiting bodies with a basal disc, stalk and spore head. In the presence of VPD, DA, OA, 4-EOA, 2-MHA or LiCl neither WT::RFP and WT::RFP-*cdipt* developed into mature fruiting bodies, suggesting that the mechanism of action of these compounds does not involve altering CDIPT levels. However, in the presence of PIA, WT::RFP cells developed to the mound stage whereas WT::RFP-*cdipt* cells developed into mature fruiting bodies after 24 hours resembling control conditions. This result suggests that the mechanism of action of PIA does involve regulating CDIPT during *D. discoideum* development.

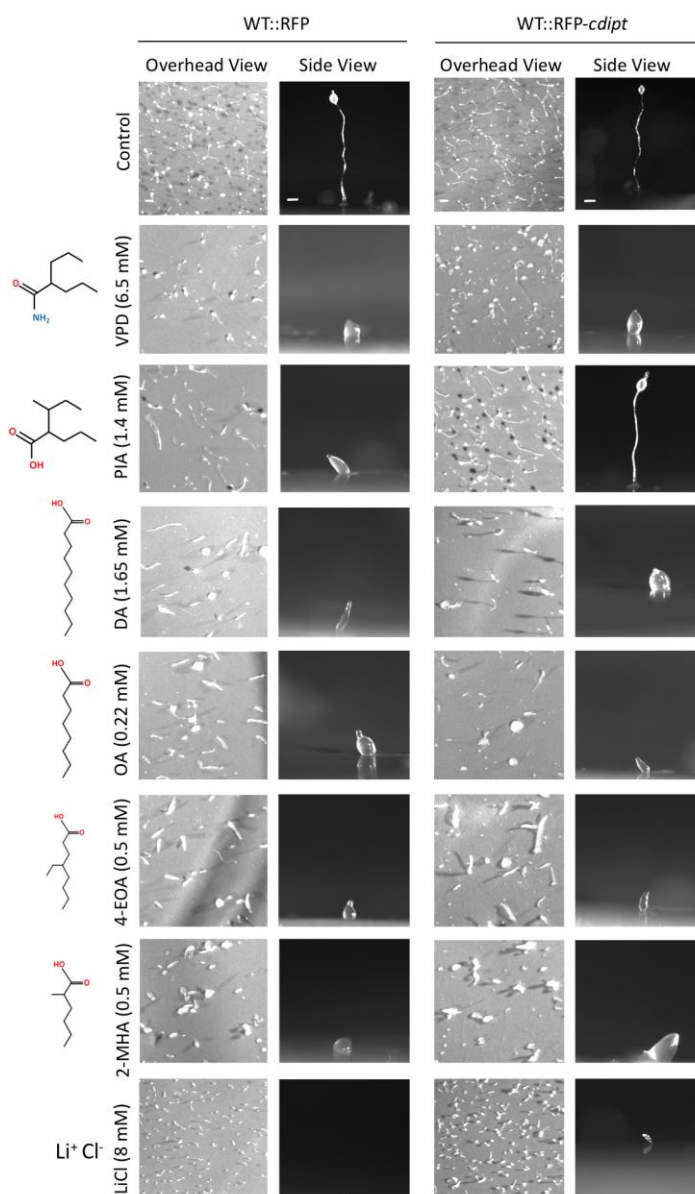


Figure 6.10. WT::RFP and WT::RFP-*cdipt* development in both the absence and presence of a range of other compounds. WT::RFP (left) and WT::RFP-*cdipt* (right) cells were developed on nitrocellulose membranes for 24 hours both in the absence (top row) and presence (descending rows) of VPD, PIA, DA, OA, 4-EOA, 2-MHA and LiCl at the stated concentrations to the left of the development images. Images were taken of an overhead view of the whole membrane (left) and of a single fruiting body (right). Both cell lines produced fruiting bodies in the absence of any compound. In the presence of VPD, DA, OA, 4-EOA, 2-MHA and LiCl both WT::RFP and WT::RFP-*cdipt* cells developed to the mound stage. However, in the presence of 1.4 mM PIA, WT::RFP-*cdipt* cells were able to develop into mature fruiting bodies at concentrations where WT::RFP developed into mounds. $n = 3$. Scale bar of the overhead view represents 0.5 mm and of the side view 0.1 mm.

6.7 Discussion

VPA has been shown to reduce *D. discoideum* phosphoinositide levels (Chang, et al., 2012). To investigate targets for this effect, a range of mutants were assessed, enabling the elimination of PI3K activity, inositol recycling, *de novo* inositol biosynthesis and *de novo* inositol production (Chang, et al., 2012; Frej, et al., 2016) as a mechanism of action of VPA. One remaining unexplored option is the PI salvage pathway. For this reason, this chapter has investigated CDIPT, the enzyme responsible for the deAMPylation of CDP-DAG and *myo*-inositol into PI. This chapter has described attempts to ablate the encoding gene (**Figures 6.2- 6.5**), the overexpression of CDIPT (**Figure 6.6 and 6.7**) and characterization of this mutant in both the absence and presence of a range of anti-seizure compounds including VPA and LiCl, a BD treatment (**Figures 6.8-6.10**).

In order to ablate CDIPT from *D. discoideum* cells, two *cdipt* knockout constructs were created using the pLPBLP vector (Faix, et al., 2004). The first knockout cassette contained targeting regions including non-coding sequence and deleted a large region of the open reading frame. The second construct contained more exon sequence in the targeting region to increase the likelihood of homologous integration but deleted only a small central region of the gene. Using the second construct, 3 independent *cdipt*⁻ cell lines were identified, however, all 3 cell lines died shortly after isolation. From this result, it may be the case that CDIPT is vital in *D. discoideum*. This is supported by studies in other organisms including yeast (Nikawa, Kodaki and Yamashita, 1987), *T. brucei* (Martin and Smith, 2006) and *Drosophila* (Wang and Montell, 2006). For this reason, potential *cdipt*⁻ cells were grown in media supplemented with the enzyme product PI to increase the chances of identifying a knockout cell line as it has previously been shown that *D. discoideum* cells can take up exogenous fatty acids (Elphick, et al., 2012). A rationale for this vital function may be that CDIPT is a downstream regulator of the cell cycle G1 phase and therefore, removal of this protein would prevent cells progressing into the cell cycle (Deguchi, et al., 2002).

Since ablation of CDIPT did not provide a practical approach, the protein was overexpressed with an N-terminal RFP-tag, resulting in WT::RFP-*cdipt* cells. Characterization of the resulting mutant initially involved Western blotting to ensure the presence of the entire RFP-CDIPT in WT::RFP-*cdipt* cells. Unfortunately, low levels of soluble RFP-CDIPT was detected in the WT::RFP-*cdipt* neomycin resistant cells by Western blotting. As the WT::RFP-*cdipt* cells were resistant to the selection marker neomycin, and should be expressing the protein, cells were examined using fluorescence microscopy. WT::RFP cells were used as a control which showed RFP present in the cytosol. In contrast, WT::RFP-*cdipt* cells showed RFP-CDIPT mainly localized within puncta. Due to the transmembrane domains present within the CDIPT protein structure there is a high chance the puncta staining is a membrane compartment, such as a vesicle. The low RFP-CDIPT expression within the cytosol suggests the protein is slightly overexpressed or the RFP tag has been cleaved from the full length protein. This localization was inconsistent with other models, where the protein has been found to localize within the endoplasmic reticulum in mammals (Deguchi, et al., 2002; Williamson and Morré, 1976) and plants (Carman and Dougherty, 1980; Löfke, et al., 2008), although it has also been detected within the Golgi and plasma membrane (Williamson and Morré, 1976). This resistant phenotype is unusual when the soluble protein is expressed in the cytosol at low levels, suggesting these cells could be overexpressing CDIPT or CDIPT is knocked-down. In order to determine whether these cells are overexpressing or have CDIPT knockdown, Western blotting using a CDIPT specific antibody would need to be conducted and CDIPT expression within WT and WT::RFP-*cdipt* cells would need to be compared. If the amount of CDIPT is higher in WT::RFP-*cdipt* cells, this mutant is overexpressing CDIPT. However, if there is a reduction in CDIPT, then the cells are a knockdown. Other approaches that can be taken are thin layer chromatography to quantify production of PI (Chang, et al., 2012) and thereby determine enzyme activity or by conducting PI: inositol exchange reactions (Lykidis, et al., 1997).

There are two possible reasons for this puncta staining. The first is simply that aggregation of the overexpressed protein into membrane bound vesicles is due to

the tight regulation of the CDP-DAG pool, the substrate of CDIPT, which has been reported previously (Lykidis et al., 1997) and therefore, maintains near WT levels of PI. The second explanation is that CDIPT overexpression results in the sequestering of the overexpressed and endogenous protein, resulting in a knockdown of CDIPT. When proteins are tightly regulated the cell prevents toxicity by packing excess protein into storage vesicles in a process shown in mammalian models during drug-induced phospholipidosis (Yamamoto, et al., 1971; Seiler and Wassermann, 1975). Phospholipidosis can be caused by cationic amphiphilic drugs which result in increased production of PI, leading to accelerated formation of membrane bound vesicles as shown by the malarial drug chloroquine (Matsuzawa and Hostetler, 1980). These vesicles may then be acting as autophagosomes to enable the excess protein to be degraded by lysosomes, as it is known that early structures of autophagy are formed close to the endoplasmic reticulum (Axe, et al., 2008), mitochondria (Hamasaki, et al., 2013) and Golgi (Ge, et al., 2013). The reason for this is that the Unc-51 autophagy activating kinase localizes first to CDIPT enriched subdomains in order for punctate autophagosome structures to be formed from PI (Nishimura, et al., 2017).

Despite the low level of expression and the cellular localization of CDIPT, cell growth was compared between WT::RFP and WT::RFP-*cdipt* cells in both the absence and presence of VPA. WT::RFP-*cdipt* cells grew at a similar rate to WT::RFP cells, with no significant differences identified under control conditions. In *Arabidopsis* when the two CDIPT isoforms were overexpressed, the resulting plants had decreased leaf size area compared with control (Löfke, et al., 2008), suggesting CDIPT overexpression results in reduced cell growth. However, this was not seen in WT::RFP-*cdipt* cells, where the protein is located within puncta and so differences between cell growth of CDIPT overexpressed in plants and *D. discoideum* were not unexpected.

Chronic VPA treatment on cell growth resulted in a dose-dependent reduction in cell number for WT::RFP cells. In contrast, WT::RFP-*cdipt* cells were resistant to VPA at physiological concentrations (0.3 mM- 0.6 mM) (Kanner, 2003; Vázquez-Calvo et

al., 2013). These results suggest that the mechanism of action of VPA relies on altering the activity of CDIPT and thus the levels of PI. This theory supports work published in 1987 which found the levels of PI to decrease during seizures in association with increased free fatty acids and DAG (Yoshida, et al., 1987). In this study a number of salvage pathway components were measured (PI, PIP, PIP₂, DAG and PA) as well as free fatty acids from forebrain tissue of rats at 1, 20 and 60 minutes after seizure induction by bicuculline. During the 60 minutes, DAG levels increased alongside a progressive reduction in PI whilst PIP, PIP₂ and PA did not change. At the start of the seizure the levels of free fatty acids increased but dropped during seizure progression as the free fatty acids were converted into triglycerides (Yoshida et al., 1987). The mechanism of action of VPA, therefore, may be in regulating PI levels during *D. discoideum* cell growth.

The *D. discoideum* developmental cycle was also investigated. WT::RFP and WT::RFP-*cdipt* cells developed into mature fruiting bodies of similar size under control conditions. In the presence of 0.3 mM- 1 mM VPA, WT::RFP cell development was delayed at the finger and mound stage. In contrast, WT::RFP-*cdipt* cells were resistant to the effect of VPA at therapeutic concentrations (0.3 mM and 0.5 mM) and continued to develop into mature fruiting bodies, although 1 mM VPA blocked development. In *D. discoideum* it is likely that distorted levels of CDIPT and PI are responsible for VPA resistance. VPA resistance in this mutant is key as this drug is used to control seizures in epilepsy patients. Both epileptogenesis and seizures are generated from calcium-dependent signalling pathways, where prolonged seizures rely on a constant supply of PIP₂, whose hydrolysis into IP₃ releases stored calcium (Alswied and Parekh, 2015). The supply of PIP₂ relies on PI synthesis and phosphorylation, suggesting PI is important in seizure generation and progression. Therefore, if the mode of action of VPA relies on altering PI levels, this will in turn effect calcium signalling. Of interest, calcium-dependent signalling pathways are being used as targets for new AEDs, e.g. levetiracetam whose mode of action in part modulates the influx of calcium (Niespodziany, Klitgaard and Margineanu, 2001; Steinlein, 2014).

A range of anti-seizure compounds, including those structurally related to VPA and components of the MCT diet and the BD treatment LiCl, were also investigated during *D. discoideum* development. In the presence of VPD, DA, OA, 4-EOA, 2-MHA and LiCl both WT::RFP and WT::RFP-*cdipt* developed to the finger or mound stage. However, in the presence of 1.4 mM PIA, at a concentration where WT::RFP development was inhibited, WT::RFP-*cdipt* cells developed into mature fruiting bodies resembling control conditions. In *D. discoideum*, therefore, it is likely that distorted levels of CDIPT are responsible for PIA resistance, suggesting VPA and PIA regulate the same targets. Sensitivity of WT::RFP-*cdipt* cells to VPD was not unexpected as previous studies have shown VPD and VPA work through a similar target, but through altered pathways (Ludtmann, Boeckeler and Williams, 2011). In this study, both VPA and LiCl were found to increase pERK2 levels, whereas, this is only partially achieved with VPD treatment in *D. discoideum* (Ludtmann, Boeckeler and Williams, 2011). This suggests a similar mode of action of VPA and VPD, however altering CDIPT levels is not common to both treatments.

6.8 Summary

In *D. discoideum* it is likely that CDIPT expression is essential for cell survival, consistent with previous studies in models containing one protein isoform. This is also the case when media is supplemented with the reaction product PI. This function made gene ablation complex, and so an overexpression approach was employed. Western blot analysis identified low levels of soluble RFP-CDIPT in WT::RFP-*cdipt* cells, with fluorescence microscopy showing RFP-CDIPT localized within membrane bound vesicles. WT::RFP-*cdipt* cells showed resistance to VPA during both growth and development at therapeutic concentrations, indicating a role for CDIPT in VPA cellular function. WT::RFP-*cdipt* cells were also resistant to the effect of PIA, suggesting this drug has a similar mode of action to VPA. It remains to be determined if this VPA-resistance is derived from slightly elevated or depleted CDIPT levels.

Chapter 7

Analysis of DGKA as a Target of VPA

7. Analysis of DGKA as a Target of VPA

DGK is the enzyme responsible for the phosphorylation of DAG to form PA within the PI salvage pathway (**Figure 1.4** and **Figure 7.1**). Both DAG and PA are important signalling molecules, where DAG is involved in the signalling of PKC (van Baal, et al., 2005), synaptic plasticity (Lee, Kim and Tanaka-Yamamoto, 2016) and the synthesis of triglycerides and PC and PE via the Kennedy pathway (Kennedy and Weiss, 1956; Gibellini and Smith, 2010). PA has a role in cell growth (Banfić, et al., 1993), lipid regulation (Cerbón, et al., 2005) and calcium signalling (Carpio and Dziak, 1998). DGK is a protein of interest as a VPA target due to the number of signalling pathways both DAG and PA regulate. A previous study using *C. elegans* has shown VPA effects DAG signalling (Tokuoka, Saiardi and Nurrish, 2008). Additionally, knockout studies have linked DGK- δ (Leach, et al., 2007), - ε (Rodriguez de Turco, et al., 2001) and - β to epilepsy and DGK- β (Ishisaka, et al., 2013) and - η to BD (Baum, et al., 2008; Squassina, et al., 2009; Kakefuda, et al., 2010).

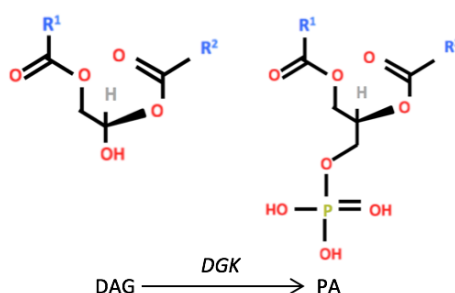


Figure 7.1. The catalytic activity of diacylglycerol kinase. Diacylglycerol (DAG) is phosphorylated into phosphatidic acid (PA) by diacylglycerol kinase (DGK) in the phosphatidylinositol salvage pathway.

In *D. discoideum* there is only one DGK gene, *DgkA* (DDB_G0277223) of 4751 bp with one intron, which encodes a protein of 887 amino acids. This gene is expressed during the developmental cycle, with peak expression at 8 hours and 24 hours after induction of starvation (Parikh, et al., 2010; Stajdohar, et al., 2015). *D. discoideum* DGKA has similar homology to all 10 *H. sapiens* orthologues (ranging from 27-33 % identity), with highest identity to *H. sapiens* DGK- θ (37 % identity) (**Chapter 4**). This

suggests that the *D. discoideum* DGKA may act as a generic DGK, thereby regulating the same pathways as the 10 *H. sapiens* DGKs.

Studies researching *D. discoideum* DGKA have previously been undertaken. In 1996, Abu- Elneel, Karchi and Ravid created a cell line in parental JH10 which they believed to have ablated MHC-PKC. However, in 2002, De La Roche et al., published work reporting the mislabelling of this MHC-PKC mutant to be the single DGK in *D. discoideum*, *dgkA*. Abu- Elneel, Karchi and Ravid (1996) investigated the localization of MHC, where protein expression was identified at the cell membrane in WT (JH10) cells, but this was impaired in *dgkA*⁻ (JH10) cells. The authors also found a delay in development of mature fruiting bodies in *dgkA*⁻ (JH10) cells from 24 hours to 44-48 hours with upward extensions from the spore fruiting body head compared with WT (JH10) cells (Abu-Elneel, Karchi and Ravid, 1996).

This chapter, therefore, describes the ablation of *DgkA* via a knockout construct in the Ax2 background and the creation of a rescue cell line. Phenotypic characterization of both the ablated *dgkA*⁻ and rescue *dgkA*^{-/+} cells are described. Phenotypic characterization involved investigating the localization of MHC in the *dgkA*⁻ cells. The effects of VPA were then investigated during growth, acute cell behaviour and development of *dgkA*⁻ cells with resistant phenotypes being rescued on the reintroduction of the gene in *dgkA*^{-/+} cells. The effects of other anti-seizure compounds and the BD treatment LiCl were also investigated on *dgkA*⁻ and *dgkA*^{-/+} cell development. DAG levels were then quantified by an ELISA assay in both the absence and presence of all compounds tested.

7.1 Confirmation of *DgkA* Knockout Vector

A previously made recombinant pLPBLP plasmid (Faix, et al., 2004) containing two distal PCR amplified *DgkA* gene fragments inserted on either side of a blasticidin resistance cassette was initially examined to verify the presence of the two *DgkA* fragments (**Figure 7.2A** and **7.2B**). The 5' fragment was 556 bp which started 173 bp within the open reading frame and contained no introns. Similarly, the 3' fragment

was 484 bp and only consisted of coding sequence with no introns, resulting in the cloning of 729 bp exon sequence. The construct would, therefore, remove 1562 bp of coding sequence. Restriction mapping (**Figure 7.2C**) confirmed the presence of the four restriction sites used for cloning the two distal *DgkA* PCR fragments into the pLPBLP vector (*Bam*HI, *Pst*I, *Nco*I and *Hind*III). A series of single restriction digests resulted in a single band at approximately 5500 bp, corresponding to the two *DgkA* fragments inserted into the pLPBLP plasmid. Restriction mapping also confirmed the insertion of the correct sized *DgkA* fragments within the knockout plasmid, producing two bands of 560 bp for the 5' gene fragment and the remaining plasmid at 4900 bp. The 3' fragment was identified at 480 bp with the remaining plasmid at 5000 bp. The knockout cassette containing the 5' and 3' *DgkA* gene fragments located on either side of the blasticidin resistance cassette were then excised from the pLPBLP-*dgkA* recombinant plasmid using the enzymes *Bam*HI and *Hind*III. Two bands were obtained, one at 2570 bp consistent with the size of the *DgkA* knockout cassette and the second of the remaining pLPBLP plasmid at 2900 bp.

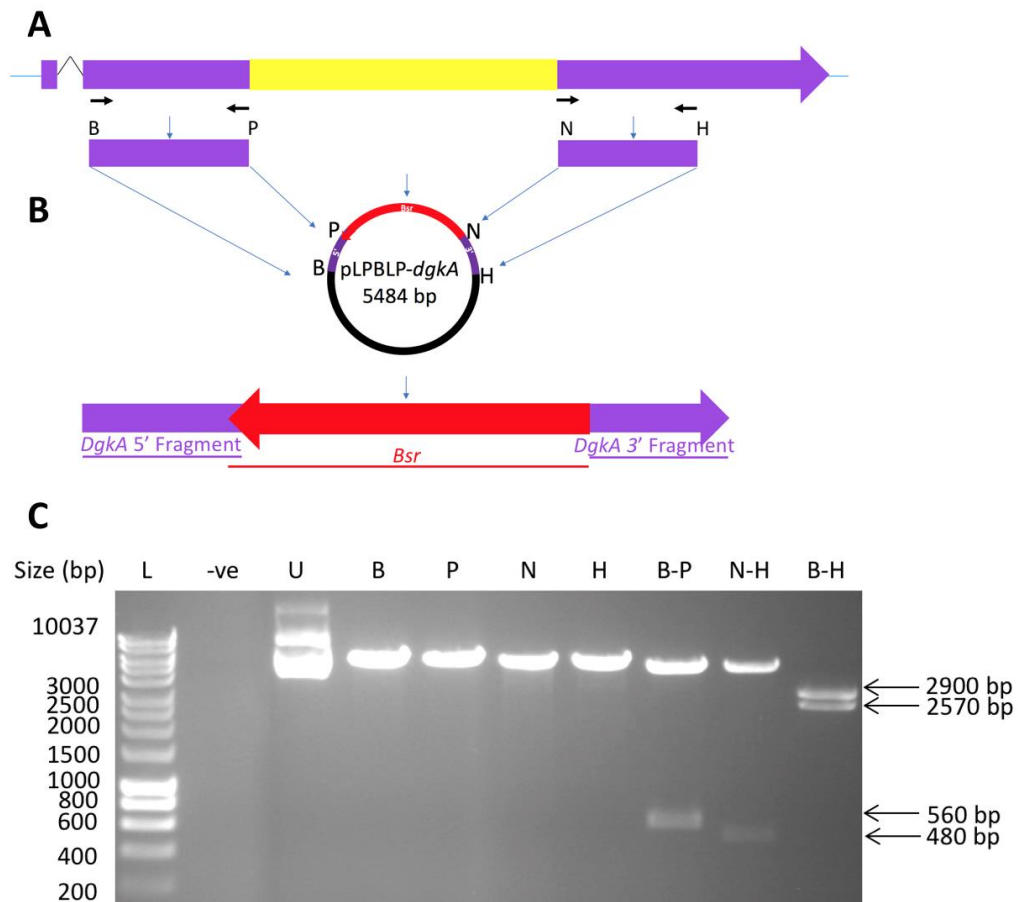


Figure 7.2. Confirmation of the *DgkA* knockout construct. **(A)** *DgkA* genomic DNA with the yellow box indicating the region knocked out and the arrows indicating the 5' and 3' genomic DNA fragments which were PCR amplified using primers containing cut sites for *Bam*HI (B), *Pst*I (P), *Nco*I (N) and *Hind*III (H). **(B)** Plasmid map of pLPBLP-*DgkA* containing the 5' and 3' *DgkA* fragments cloned into the plasmid on either side of the blasticidin resistance cassette by *Bam*HI (B), *Pst*I (P), *Nco*I (N) and *Hind*III (H). **(C)** Confirmation of the *DgkA* inserts within the pLPBLP-*dgkA* vector by a series of single and double restriction digests visualised following gel electrophoresis with a ladder (L), negative control without plasmid (-ve), uncut knockout vector (U), single digests confirming individual enzyme activity of *Bam*HI (B), *Pst*I (P), *Nco*I (N) and *Hind*III (H) and double digests confirming the presence of the 5' and 3' fragments using *Bam*HI-*Pst*I (B-P) and *Nco*I-*Hind*III (N-H) and the linearized knockout cassette used for electroporation with *Bam*HI- *Hind*III (B-H). Molecular weights of the DNA ladder are indicated on the left of the gel image (10037 bp- 200 bp) and the expected plasmid insert sizes are given (arrows) to the right of the image.

7.2 Screening Potential *dgkA*⁻ *D. discoideum* Cells

To ablate *DgkA* from *D. discoideum*, the *DgkA* knockout cassette (**Figure 7.2**) was electroporated into WT cells and selected for resistance to blasticidin during cell growth. Surviving colonies were screened by PCR to identify transformant cells which had the knockout cassette integrated into the *DgkA* gene, creating *dgkA*⁻ cells. PCR screening involved designing primers around the two *dgkA* fragments and the blasticidin resistance gene to amplify a region from outside to inside the targeting fragment of the 5' (520 bp) and 3' (540 bp) terminal (genomic control). Primers were also designed to amplify a region from within the targeting fragment into the blasticidin resistance gene (product size expected at 660 bp for the 5' region and 680 bp for the 3' region in transformant colonies only) (vector control). Finally, primers were used which amplified outside the targeting fragment into the blasticidin resistance gene (knockout diagnostic), which had a product size expected at 730 bp for both the 5' and 3' regions (**Figure 7.3A**).

Numerous attempts were made to identify *dgkA*⁻ mutants using the *DgkA* knockout cassette. A total of 5 electroporations resulted in 206 blasticidin resistant colonies which were individually screened (**Figure 7.3B** and **7.3C**). This approach identified 7 *dgkA*⁻ homologous integrants. Single isogenic lines of 3 of these homologous integrants were obtained by inoculating cells from an individual colony grown on each of the 3 *R. planticola* plates.

To ensure the potential *dgkA*⁻ mutants had lost part of the coding region in these 3 cell lines, complementary cDNA was synthesised and analysed by RT-PCR. Since *DgkA* is expressed following starvation (Parikh, et al., 2010; Stajdohar, et al., 2015), cells which had developed for 8 hours were used for analysis. Loss of part of the *DgkA* gene was confirmed using primers which annealed to the region deleted in the potential *dgkA*⁻ cells. RT-PCR resulted in a 529 bp product only in WT cells, confirming the 3 homologous integrants as *dgkA*⁻ cells. Control primers for the housekeeping gene *Ig7* (which produces mitochondrial large subunit ribosomal

RNA) was also amplified (approximately 540 bp) as a control to confirm the PCR was working (**Figure 7.3.D** and **7.3E**).

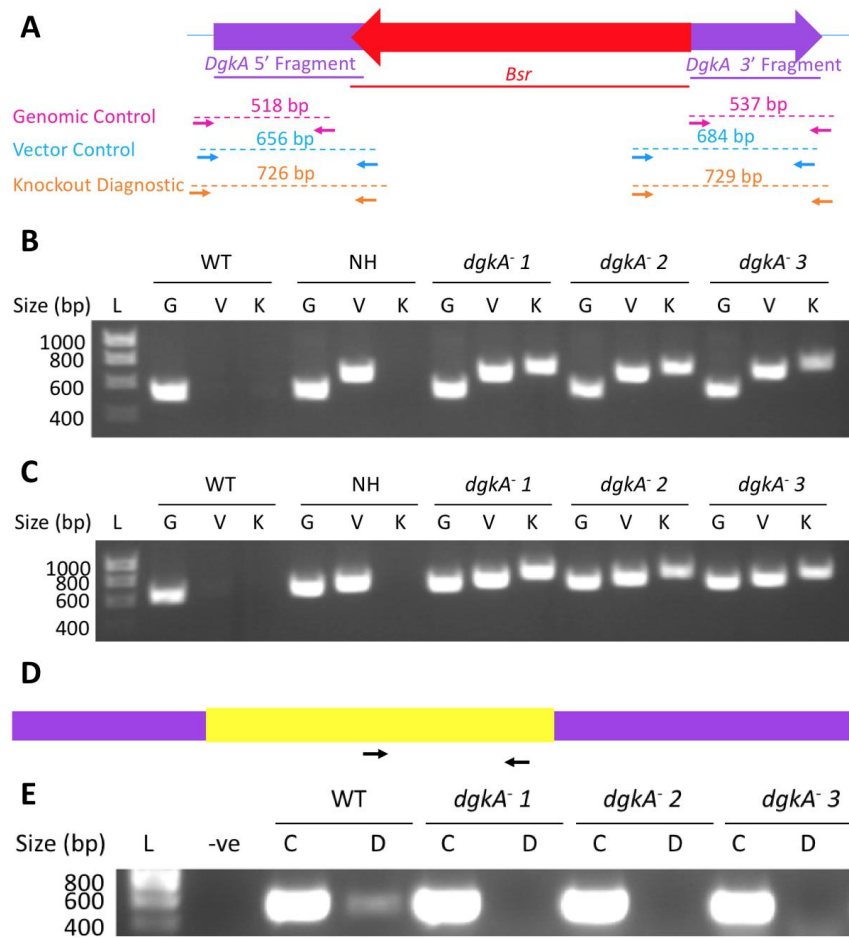


Figure 7.3. PCR screening of *dgkA*⁻ isogenic transformant cell lines. **(A)** Schematic representation of the *DgkA* gene containing the homologous integrated knockout construct. The locations of the screening primers (arrows) and the corresponding PCR product (dotted line) used for determining homologous integration- genomic (pink), vector (blue) and knockout diagnostic (yellow) primers and the predicted sizes of the products are shown. **(B)** 5'- and **(C)** 3'- PCR screening of blasticidin-resistant cells with genomic control (G), vector control (V) and knockout diagnostic (K). PCR products are shown where the genomic control (G) band is amplified from WT DNA, genomic (G) and vector (V) control bands are amplified from non-homologous integrant (NH) DNA and all 3 bands are (G, V and knockout diagnostic (K)) are amplified from the potential knockout (*dgkA*⁻) DNA. **(D)** Schematic representation of the *DgkA* gene with the yellow box indicating the region deleted from the gene with the arrows indicating the locations of the two RT-PCR primers. **(E)** RT-PCR of control *Ig7* (C) and *DgkA* primers within the deleted region (D) PCR products where cDNA from WT provides products for both control and the deleted *DgkA* region and *dgkA*⁻ cell lines only have a control *Ig7* PCR product. Molecular weights of the DNA ladder are indicated on the left of the gel image (1000 bp- 200 bp).

7.3 Confirming the *DgkA* Insert Within the Overexpression Construct

This was followed by creating *dgkA*^{-/+} rescue cells. A pTX-DGK (GFP-*DgkA*) expression plasmid was kindly provided by T. Egelhoff (De La Roche, et al., 2002). On obtaining this plasmid, restriction mapping verified the presence of the *DgkA* PCR fragment. Single digests with *Xba*I or *Sal*I linearized the plasmid and resulted in a single band at approximately 10000 bp. A double digest using the same two restriction enzymes was used to excise the *DgkA* fragment (approximately 2550 bp) from the remaining GFP plasmid (approximately 9000 bp) (**Figure 7.4**). The GFP-*dgkA* expression construct was then electroporated into *dgkA*⁻ cells and selected for by growth in the presence of blasticidin and neomycin (G418).

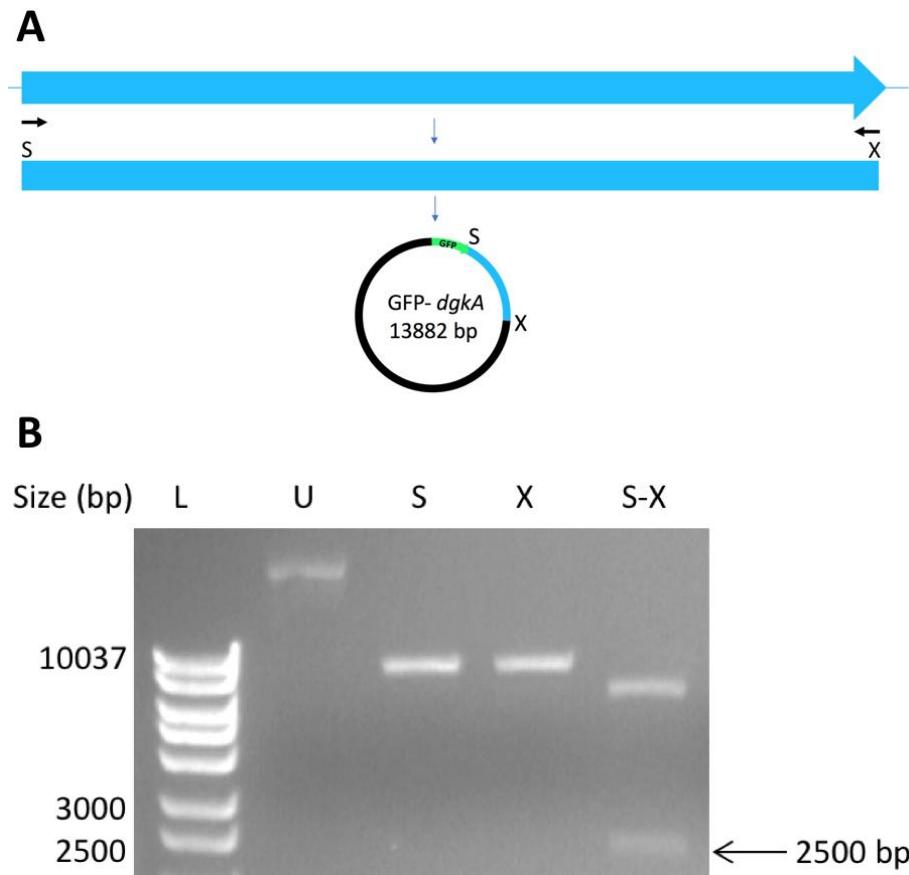


Figure 7.4. Confirming the *DgkA* insert within the GFP-*dgkA* overexpression construct. (A)

Schematic representation of *DgkA* cDNA with the arrows indicating the locations of the primers used for PCR amplification and the cut sites *Sall* (S) and *XbaI* (X) used for excising the *DgkA* PCR fragment from the 5' GFP-*dgkA* expression vector. **(B)** Confirmation of the inserted *DgkA* cDNA PCR fragment into the GFP-*DgkA* expression vector by a series of single and a double restriction digest visualised following gel electrophoresis with a ladder (L), uncut vector (U), single digests confirming cut sites of *Sall* (S) and *XbaI* (X) and a double digest using *Sall*-*XbaI* (S-X) confirming the presence of *DgkA* PCR fragment. To the left of the gel is the DNA ladder molecular weights (10037 bp-2500 bp) and to the right is the expected PCR fragment insert size (arrow).

Western blotting was used to confirm the expression of GFP-DGKA within *dgkA*^{-/+} cells, which was compared with WT and *dgkA*⁻ cells. Expression of the protein Mcca (also Mccc1) (Davidson, King and Insall, 2013) was used as a loading control. WT and *dgkA*⁻ cells did not express GFP as expected, whereas *dgkA*^{-/+} cells displayed GFP-DGKA expression at the expected size (126 kDa) (**Figure 7.5A**), confirming

reintroduction of the protein. DGKA localization was also investigated by fluorescence microscopy, where GFP-DGKA was localized to the cytosol (**Figure 7.5B**).

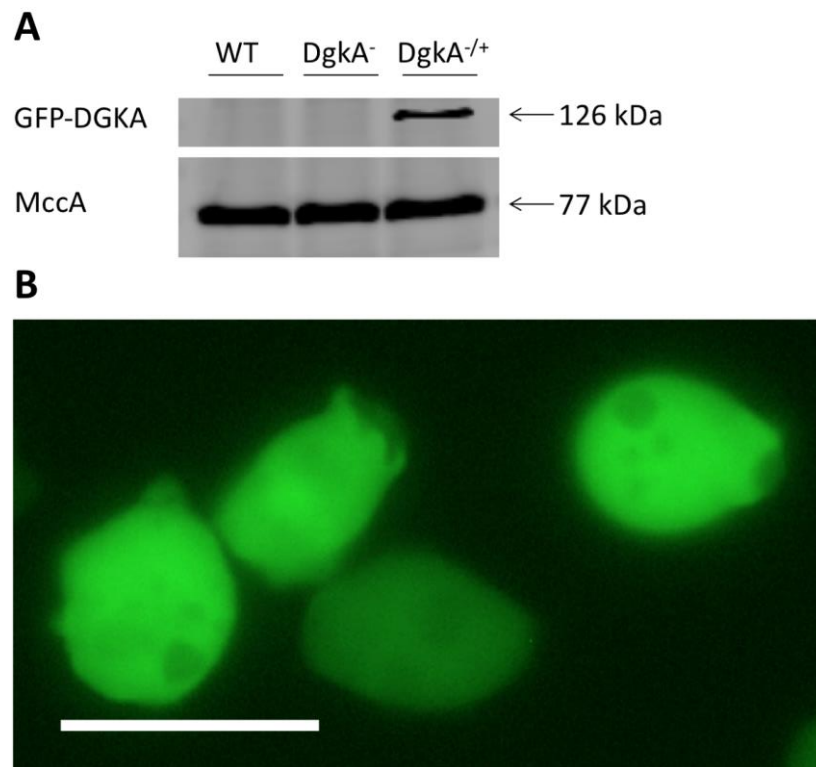


Figure 7.5. GFP-DGKA expression and localization. (A) Western blot showing WT and *dgkA*⁻ cells expressing no GFP and *dgkA*^{-/+} cells showing GFP-DGKA expression with protein loading for all 3 cells being shown by the control MccA. **(B)** *dgkA*^{-/+} cells were visualized using fluorescence microscopy. GFP-DGKA showed cytosolic localization. Scale bar represents 10 μ m.

7.4 Phenotypic Characterization of *dgkA*⁻ and *dgkA*^{-/+} Cells

In order to investigate DGK as a target of VPA, a range of experiments were conducted using WT, *dgkA*⁻ and *dgkA*^{-/+} cells. Characterization involved investigating the localization of the MHC protein and the phenotypic changes in both the absence and presence of VPA during cell growth, acute cell behaviour and development by comparing WT, *dgkA*⁻ and *dgkA*^{-/+} cells. DGKA was then investigated as to whether it was a target of other anti-seizure compounds or the BD treatment LiCl by

development assays. To determine changes in molecular DAG levels, an ELISA assay was conducted in both the absence and presence of all compounds tested.

7.4.1 Localization of MHC in $dgkA^-$ Cells During the Vegetative Phase

Immunohistochemistry was used to investigate the localization of the MHC since this was altered in the $dgkA^-$ (JH10) cells when compared with WT (JH10) (Abu-Elneel, Karchi and Ravid, 1996). In WT (JH10) cells, the MHC protein was present as a loose fibrous network within the cytoplasm, but this was altered in $dgkA^-$ (JH10) cells where MHC formed a dense cortical ring. To determine MHC localization within $dgkA^-$ (Ax2) cells, immunohistochemistry was conducted by fixing cells to coverslips using paraformaldehyde (**Figure 7.6**). WT (Ax2) and $dgkA^-$ (Ax2) cells were stained with antibodies either for calreticulin (control) or MHC. Both WT (Ax2) and $dgkA^-$ (Ax2) cells showed a similar staining of calreticulin within the endoplasmic reticulum. In both vegetative WT (Ax2) and $dgkA^-$ (Ax2) cells, MHC was located within the cytoplasm as a loose fibrous network with clear adhesion sites, consistent with the location of MHC previously reported and from other studies (Abu-Elneel, Karchi and Ravid, 1996; Heid, et al., 2004).

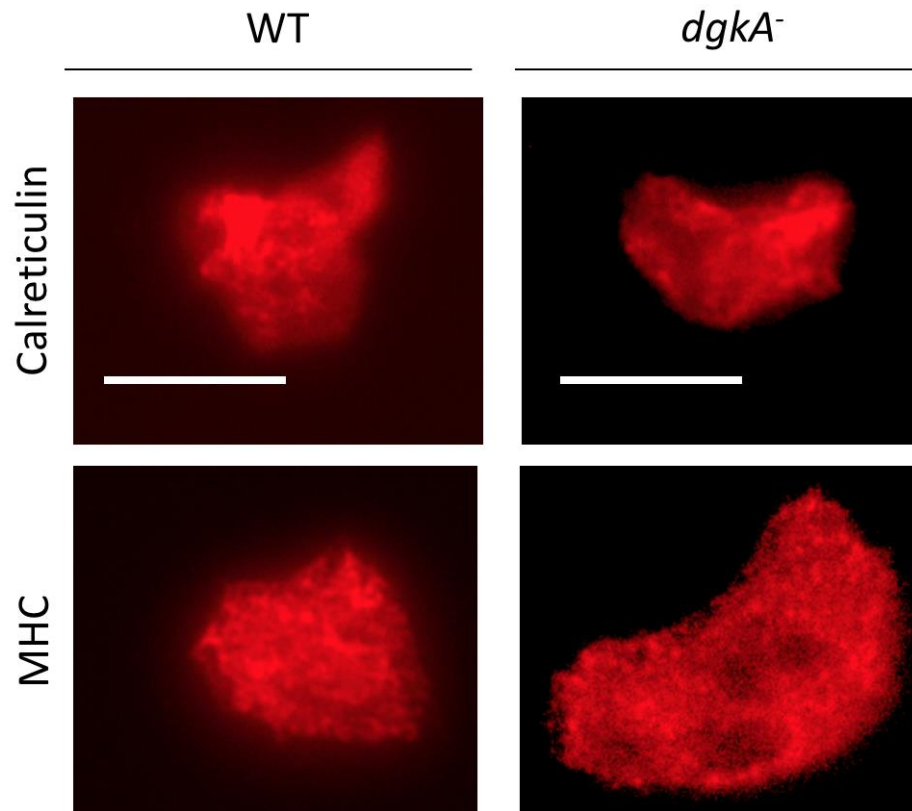


Figure 7.6. Comparison of myosin II heavy chain localization in WT and *dgkA*⁻ cells. WT and *dgkA*⁻ cells visualized using immunofluorescence. WT and *dgkA*⁺ cells show cytoplasmic localization of myosin II heavy chain (MHC). Scale bars represent 10 μ m.

7.4.3 Analysis of MHC Movement in Response to cAMP

Since there was no apparent gross difference in MHC localization between WT (Ax2) and *dgkA*⁻ (Ax2) growing cells, early development was induced by starvation in the presence of pulsate cAMP. Following induction of early development, cells were washed and stimulated with a single pulse of cAMP and images were recorded at regular intervals over 120 seconds. Both WT (Ax2) and *dgkA*⁻ (Ax2) cells were electroporated with GFP- tagged fluorescent constructs. This enabled the visualisation of F-actin-GFP from cells electroporated with the LB150B construct (control) (Kortholt, et al., 2011) or MHC-GFP from cells containing the pBIGGFPmyo construct (Keizer-Gunnink, Kortholt and van Haastert, 2007) kindly provided by Arjan Kortholt. Under control conditions, F-actin-GFP was transient to the cell membrane in both cell lines (**Figure 7.7**). In response to cAMP, no difference in F-actin localization was shown between WT (Ax2) or *dgkA*⁻ (Ax2) cells. MHC was

localized within the cytosol under control conditions in both WT (Ax2) and *dgkA*⁻ (Ax2) cells. In response to cAMP stimulation, WT (Ax2) cell MHC was located within the cytoplasm. In contrast, in *dgkA*⁻ (Ax2) cells, MHC localized to the cell cortex as a dense cortical ring within 30 seconds of cAMP stimulation, consistent with *dgkA*⁻ (JH10) cells (Abu-Elneel, Karchi and Ravid, 1996).

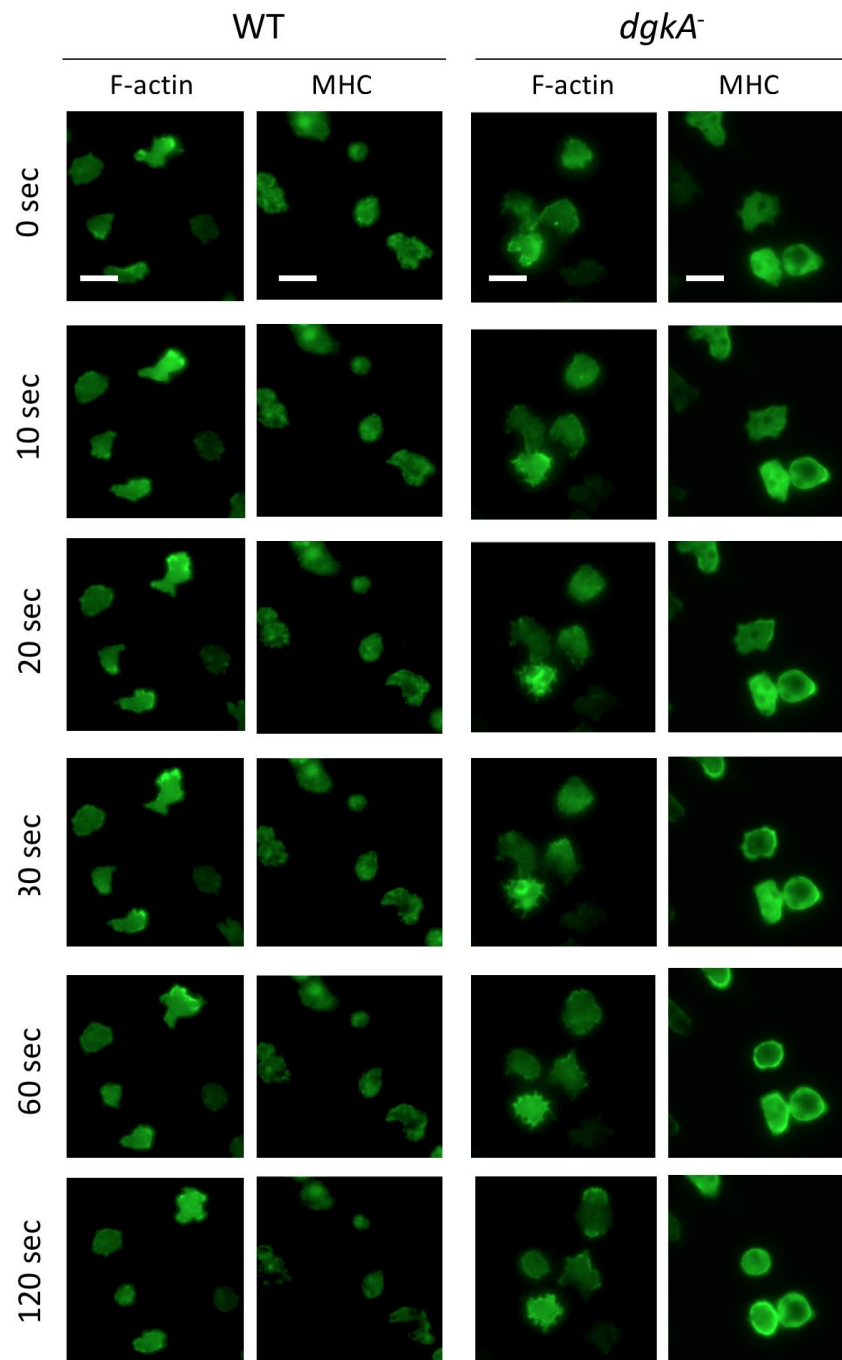


Figure 7.7. F-actin- GFP and myosin II heavy chain-GFP localization in response to cAMP stimulation. GFP tagged F-actin and myosin II heavy chain (MHC) localization in WT (Ax2) and *dgkA*⁻ (Ax2) cells containing the F-actin-GFP tagged plasmid or the MHC-GFP tagged plasmid. Cells were visualized using fluorescence microscopy with images taken at the started times to the left of the image after cAMP stimulation. WT and *dgkA*⁻ cells show no difference in F-actin localization after cAMP stimulation, with cAMP stimulation causing MHC localization within the cytoplasm in WT cells and in contrast, to the cell cortex in *dgkA*⁻ cells. *n*= 7-10. Scale bars represent 10 μ m.

7.4.4 4 Analysis of DGKA on Cell Growth in the Presence of VPA

The effects of VPA on cell growth were then investigated. Cell growth was investigated as previous work has shown VPA to cause a dose-dependent inhibition in *D. discoideum* (Terbach, et al., 2011). WT and *dgkA*⁻ cells were grown in the presence of increasing VPA concentrations (ranging 0.01 mM- 2 mM) spanning the therapeutic concentration (Kanner, 2003; Vázquez-Calvo, et al., 2013) for 168 hours (**Figure 7.8**). In the absence of VPA, WT and *dgkA*⁻ cells grew at a similar rate (**Figure 7.8A** and **7.8B**). In the presence of VPA, both WT and *dgkA*⁻ cells showed a dose-dependent reduction on cell growth, with no significant differences being identified. Comparison of the rate of cell growth between WT and *dgkA*⁻ cells when exposed to differing VPA concentrations is displayed in a secondary plot (**Figure 7.8C**) with the corresponding calculated IC₅₀ values. For WT cells the VPA IC₅₀ value was 0.7 mM and for *dgkA*⁻ cells 0.5 mM. These results suggest DGKA is not a target of VPA during the vegetative phase of *D. discoideum* cells.

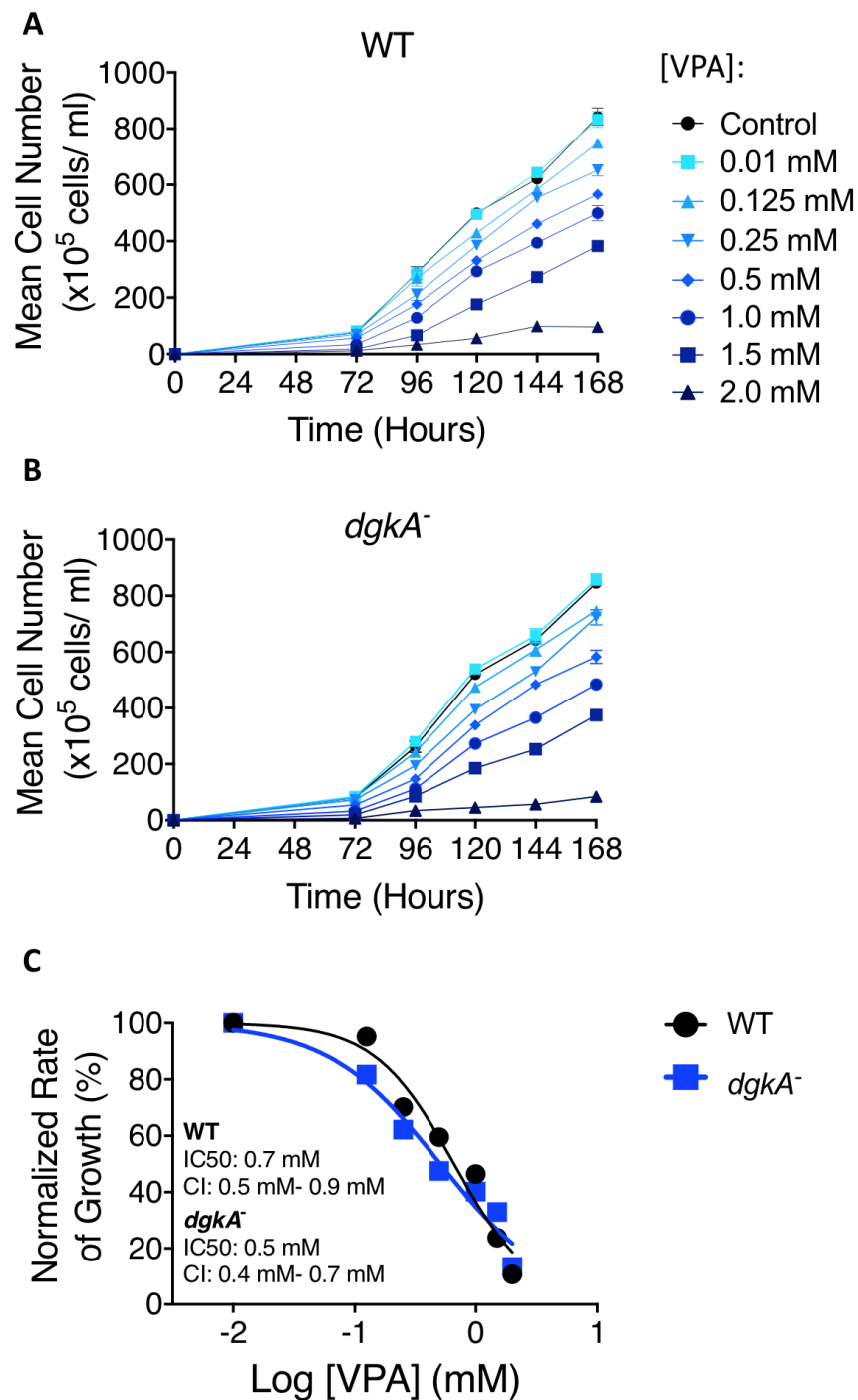


Figure 7.8. WT and *dgkA*⁻ growth in both the absence and presence of VPA. (A) WT and (B) *dgkA*⁻ cell proliferation was determined both in the absence (control, black) and presence of VPA at the indicated concentrations for 168 hours. (C) A secondary plot comparing the normalized change in the rate of cell growth between 96 and 144 hours plotted against log VPA concentration for WT and *dgkA*⁻ cells. No significant differences in cell proliferation was identified under control conditions or in the presence of VPA using the Kruskal- Wallis test and Dunns post hoc test. Data presented as mean (+/- SEM). *n* = 6.

7.4.5 Analysis of DGKA on Acute Cell Behaviour in the Presence of VPA

Since loss of DGKA did not alter the effect of VPA on cell growth, the *D. discoideum* developmental cycle was then investigated. In these experiments, acute cell behaviour was investigated using cells in early development as this is when *DgkA* is most highly expressed and cells are chemotactically competent (Xu, et al., 2007). This assay was employed since VPA inhibits *D. discoideum* movement and causes loss of cell shape from amoeboid to round (Xu, et al., 2007). Experiments initially involved imaging cells prior to and 10 minutes following 0.5 mM VPA treatment to determine any differences between WT and *dgkA*⁻ cells. In WT cells, exposure to 0.5 mM VPA resulted in cells halting movement and becoming circular in shape (**Figure 7.9A**). In contrast, *dgkA*⁻ cells in the presence of 0.5 mM VPA continued moving and remained amoeboid in shape, thereby showing resistance to VPA at this concentration (**Figure 7.9B**).

VPA dependent changes in cell behaviour were then quantified using time-lapse microscopy. Computer-generated cell outlines were used to detect variations in the shortest distance individual cells travelled (displacement), cell shape (circularity, with round cells given an arbitrary value of “1”), membrane protrusions and speed of cell speed (motility) (**Figure 7.9C**). A control period of 225 seconds was used to establish any differences in cell behaviour between WT, *dgkA*⁻ and *dgkA*^{-/+} cells before being exposed to a range of VPA concentrations (0.1 mM- 0.7 mM), including the therapeutic concentration, for 525 seconds (**Table 7.1** and **Figure 7.9D- 7.9G**). During control conditions with no VPA exposure, there was no change in WT, *dgkA*⁻ or *dgkA*^{-/+} cell behaviour with regard to cell displacement, circularity, membrane protrusions and motility. No significant differences were identified between the 3 cell lines in the absence of VPA. However, in the presence of 0.5 mM VPA upwards, WT cells had a near block in all cell behaviour criteria measured, whereas *dgkA*⁻ behaved in a similar way to control conditions and therefore resistant to VPA at this concentration. VPA sensitivity was then restored in *dgkA*^{-/+} cells. Significant differences were identified between WT and *dgkA*⁻, and *dgkA*⁻ and *dgkA*^{-/+} cells at either or both 0.3 mM and 0.5 mM VPA for displacement (P values ranging between 0.0230- 0.0403), circularity (P value ranging between ≤0.0001-

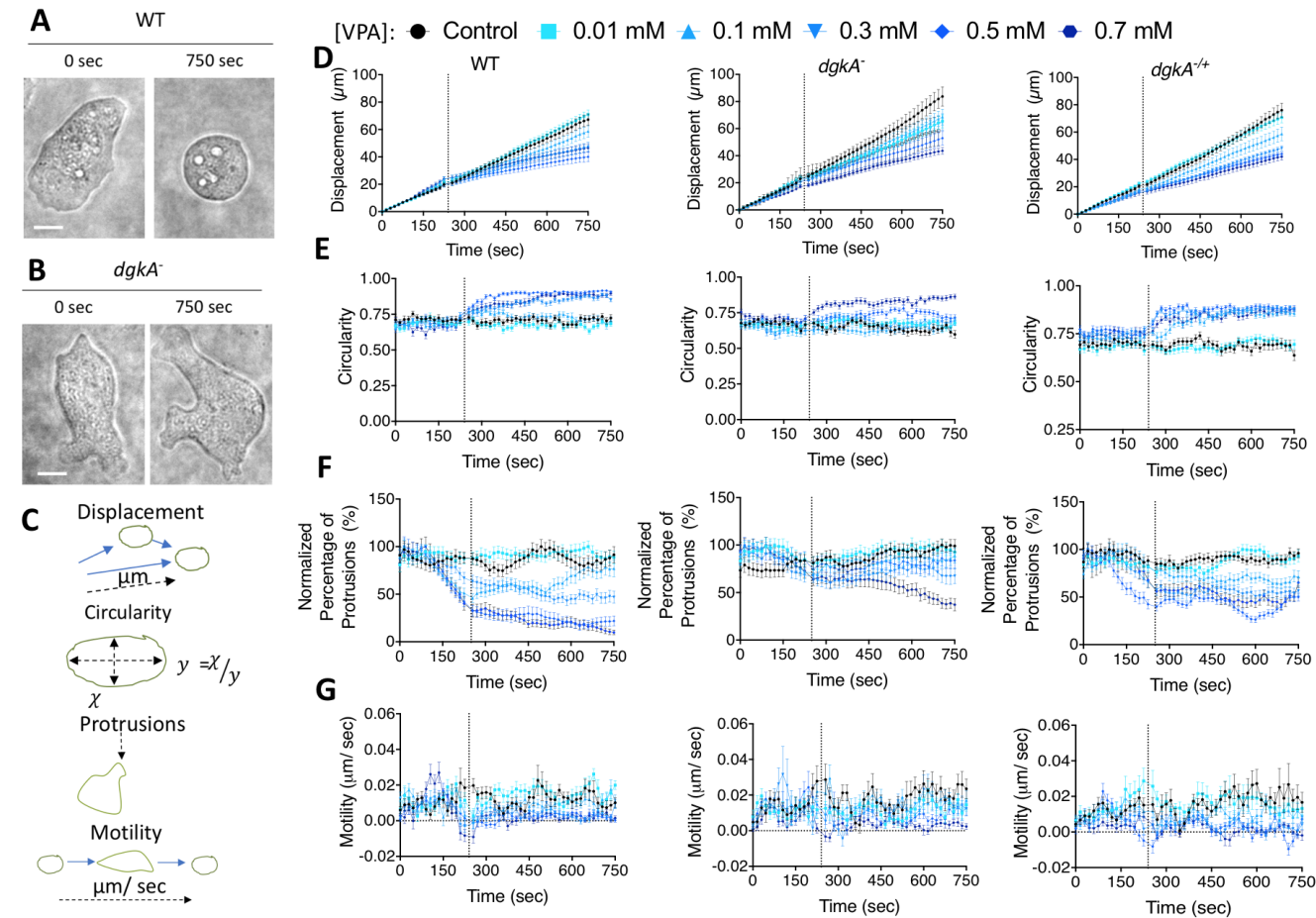
0.0006), membrane protrusions (P value ranging between ≤ 0.0001 -0.0129) and motility (P values ≤ 0.0001).

<u>Cell Line</u>	[VPA] (mM)						VPA IC₅₀ Value (mM)
	Control	0.01	0.1	0.3	0.5	0.7	
<i>Displacement (μm)</i>							
WT	67.2 ± 4.2	70.9 ± 3.2	58.7 ± 4.3	47.3 ± 3.4	40.0 ± 3.5	46.5 ± 2.9	0.4 ± 0.08
<i>dgkA</i> ⁻	83.7 ± 7.1	65.5 ± 4.8	68.6 ± 5.7	64.9 ± 6.0	53.0 ± 5.1	43.6 ± 2.5	0.8 ± 0.06
<i>dgkA</i> ^{+/-}	76.1 ± 5.1	70.9 ± 3.8	58.7 ± 4.9	56.0 ± 3.6	56.0 ± 1.7	54.0 ± 2.8	-
<i>Circularity</i>							
WT	0.71 ± 0.004	0.67 ± 0.004	0.73 ± 0.004	0.85 ± 0.004	0.90 ± 0.001	0.88 ± 0.004	-
<i>dgkA</i> ⁻	0.63 ± 0.004	0.67 ± 0.003	0.64 ± 0.004	0.67 ± 0.004	0.74 ± 0.004	0.83 ± 0.004	-
<i>dgkA</i> ^{+/-}	0.68 ± 0.004	0.70 ± 0.004	0.85 ± 0.003	0.87 ± 0.003	0.88 ± 0.002	0.86 ± 0.003	-
<i>Protrusions</i>							
WT	8.7 ± 0.13	9.0 ± 0.07	5.8 ± 0.17	3.6 ± 0.05	1.5 ± 0.06	1.7 ± 0.07	0.2 ± 0.05
<i>dgkA</i> ⁻	10.1 ± 0.10	8.6 ± 0.05	7.3 ± 0.05	7.7 ± 0.07	6.2 ± 0.04	3.6 ± 0.14	0.6 ± 0.04
<i>dgkA</i> ^{+/-}	7.1 ± 0.04	8.5 ± 0.12	4.6 ± 0.05	4.1 ± 0.04	2.7 ± 0.12	1.8 ± 0.05	0.2 ± 0.11
<i>Motility (μm/sec)</i>							
WT	0.013 ± 0.0009	0.016 ± 0.0009	0.010 ± 0.0005	0.004 ± 0.006	0.003 ± 0.0002	0.002 ± 0.0003	0.2 ± 0.03
<i>dgkA</i> ⁻	0.019 ± 0.0011	0.012 ± 0.0011	0.014 ± 0.0007	0.015 ± 0.0007	0.008 ± 0.0006	0.004 ± 0.0004	0.5 ± 0.04
<i>dgkA</i> ^{+/-}	0.020 ± 0.0010	0.016 ± 0.0007	0.011 ± 0.0006	0.003 ± 0.0005	0.002 ± 0.0009	0.001 ± 0.0005	0.2 ± 0.02

Table 7.1. WT, *dgkA*⁻ and *dgkA*^{+/-} changes in acute cell behaviour in both the absence and presence of VPA. Comparison of WT, *dgkA*⁻ and *dgkA*^{+/-} acute cell behaviour values of total displacement during the assay and average circularity, protrusions and motility within the final 300 seconds. The calculated IC₅₀ values are shown to the right of the table for each cell line for displacement, number of protrusions and motility. Data presented as mean (+/- SEM). *n* = 30.

Detailed analysis of cell behaviour in these experiments was then conducted. Analysis of displacement (**Figure 7.10A**), circularity (**Figure 7.10B**), membrane protrusions (**Figure 7.10C**) and motility (**Figure 7.10D**) at 750 seconds, or within the final 300 seconds, showed a shift in the curve to the right for the *dgkA*⁻ cells. This shift highlights *dgkA*⁻ cells partial resistance to VPA. The curve returned closer towards WT for *dgkA*^{-/+} cells, highlighting restoration of VPA sensitivity. This partial resistance of *dgkA*⁻ cells is also illustrated in the IC₅₀ values calculated for each condition (**Table 7.1**). An IC₅₀ could not be calculated for circularity due to the data points increasing with higher VPA concentrations rather than decreasing, therefore, drug inhibition cannot be measured. VPA partial resistance of *dgkA*⁻ cells is also shown by the IC₅₀ values being at least double that of WT and *dgkA*^{-/+} cells. Statistically significant differences between WT, *dgkA*⁻ and *dgkA*^{-/+} cells also highlights *dgkA*⁻ cell resistance to VPA. From these results, it can be suggested that DGKA is a target of VPA during *D. discoideum* acute cell behaviour.

Chapter 7



Analysis of DGKA as a Target of VPA

Figure 7.9. WT, *dgkA*⁻ and *dgkA*^{-/-} acute cell behaviour in both the absence and presence of VPA primary plots. (A) WT and (B) *dgkA*⁻ cell shape at 0 seconds and 750 seconds after addition of 0.5 mM VPA where WT cells were circular 750 seconds after drug addition and *dgkA*⁻ cells were amoeboid. (C) Schematic of the quantitative measurements taken during the assay where the black dashed arrows represent the measurement being taken for the primary data for (D) displacement, (E) circularity, (F) membrane protrusions and (G) motility for WT cells (left), *dgkA*⁻ (middle) and *dgkA*^{-/-} cells. Data presented as mean (+/- SEM) $n=30$ cells. Scale bar represents 12 μm .

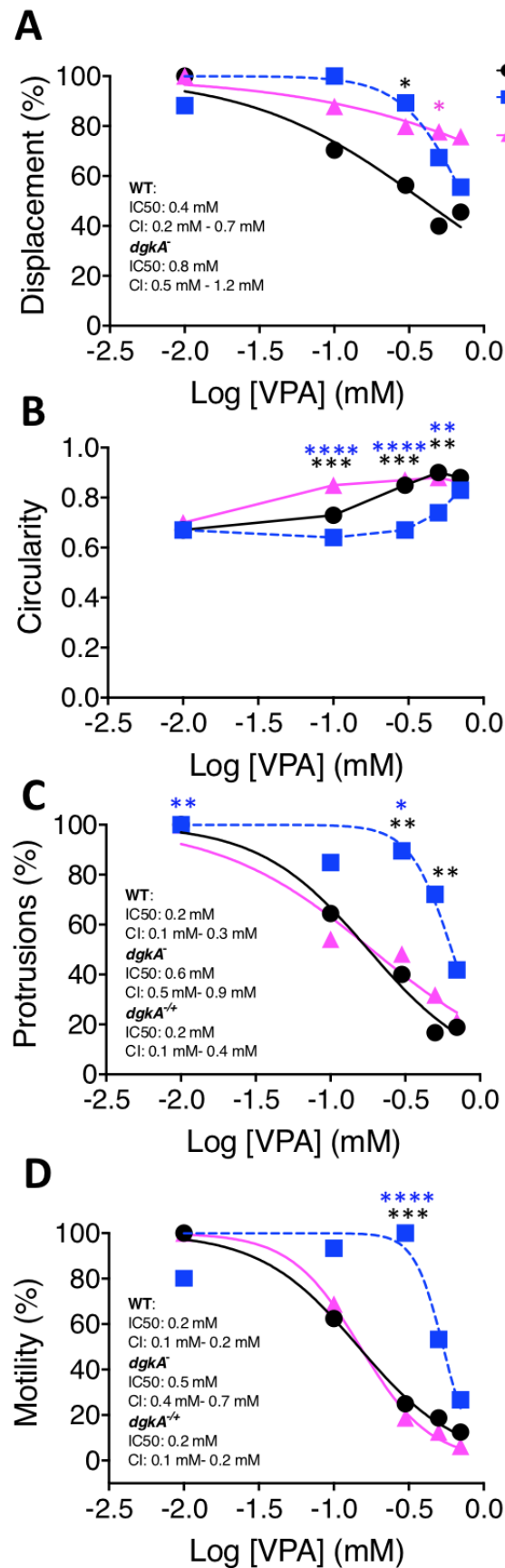


Figure 7.10. WT, *dgkA*⁻ and *dgkA*^{-/+} acute cell behaviour in the presence of VPA secondary plots. (A) Displacement, (B) circularity, (C) membrane protrusions and (D) motility secondary plots for WT (black circles), *dgkA*⁻ (blue squares) and *dgkA*^{-/+} (pink triangles) comparing the total displacement at 750 seconds or comparing average circularity, membrane protrusions or motility between 450 seconds and 750 seconds between the 3 cell lines with calculated IC₅₀ stated in the graphs which show *dgkA*⁻ partial resistance to VPA up to 0.5 mM compared with WT and the restoration of VPA sensitivity in *dgkA*^{-/+} cells. Significant differences between WT and *dgkA*⁻ cells are shown by black stars, between WT and *dgkA*^{-/+} cells with a pink star and between *dgkA*⁻ and *dgkA*^{-/+} with blue stars using the Kruskal-Wallis test and Dunns post hoc test. *P* value: * *P* value = ≤0.05, ** *P* value = ≤0.01 and * *P* value = ≤0.001. Data presented as mean (+/- SEM) *n* = 30 cells.**

7.4.6 Analysis of DGKA Cell Development in the Presence of VPA

The *DgkA* gene is expressed during the *D. discoideum* developmental phase and VPA is known to block fruiting body formation (Williams, et al., 2002). For these reasons, the effect of VPA was investigated on WT, *dgkA*⁻ and *dgkA*^{-/+} fruiting body formation by starving cells on nitrocellulose filters for 24 hours in both the absence and presence VPA (0.3 mM, 0.5 mM and 1 mM) (**Figure 7.11**). WT cells developed into typical fruiting bodies containing a basal disc, stalk and spore head under control conditions (**Figure 7.11A**). The *dgkA*⁻ cells were also able to develop into fruiting bodies containing a basal disc, stalk and spore head, however, the fruiting bodies which developed were smaller than WT, consistent with the previous report of *DgkA* ablation in JH10 cells (Abu-Elneel, Karchi and Ravid, 1996). WT fruiting body size was restored on reintroduction of *DgkA* within *dgkA*^{-/+} cells. In the presence of 0.3 mM and 0.5 mM VPA, WT cells developed into finger structures. In contrast, *dgkA*⁻ cells continued to develop into full fruiting bodies resembling control conditions in the presence of 0.3 mM and 0.5 mM VPA (**Figure 7.11B**). Sensitivity of 0.3 mM and 0.5 mM VPA was restored in *dgkA*^{-/+} cells which developed into finger structures. In the presence of 1 mM VPA, WT, *dgkA*⁻ and *dgkA*^{-/+} cells developed into mounds after 24 hours. These results suggest that DGKA is a target, or is regulated by VPA at therapeutic concentrations during *D. discoideum* development.

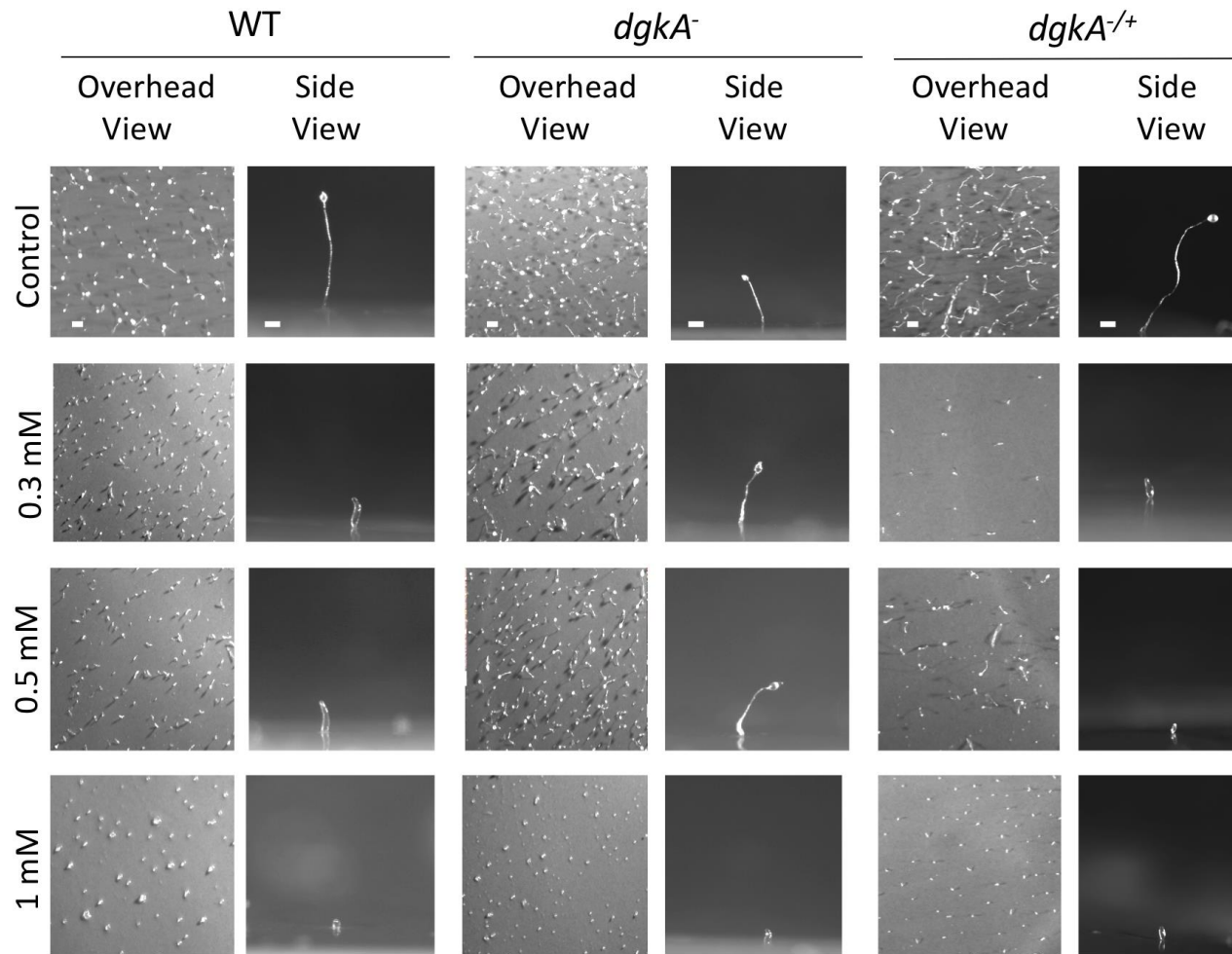
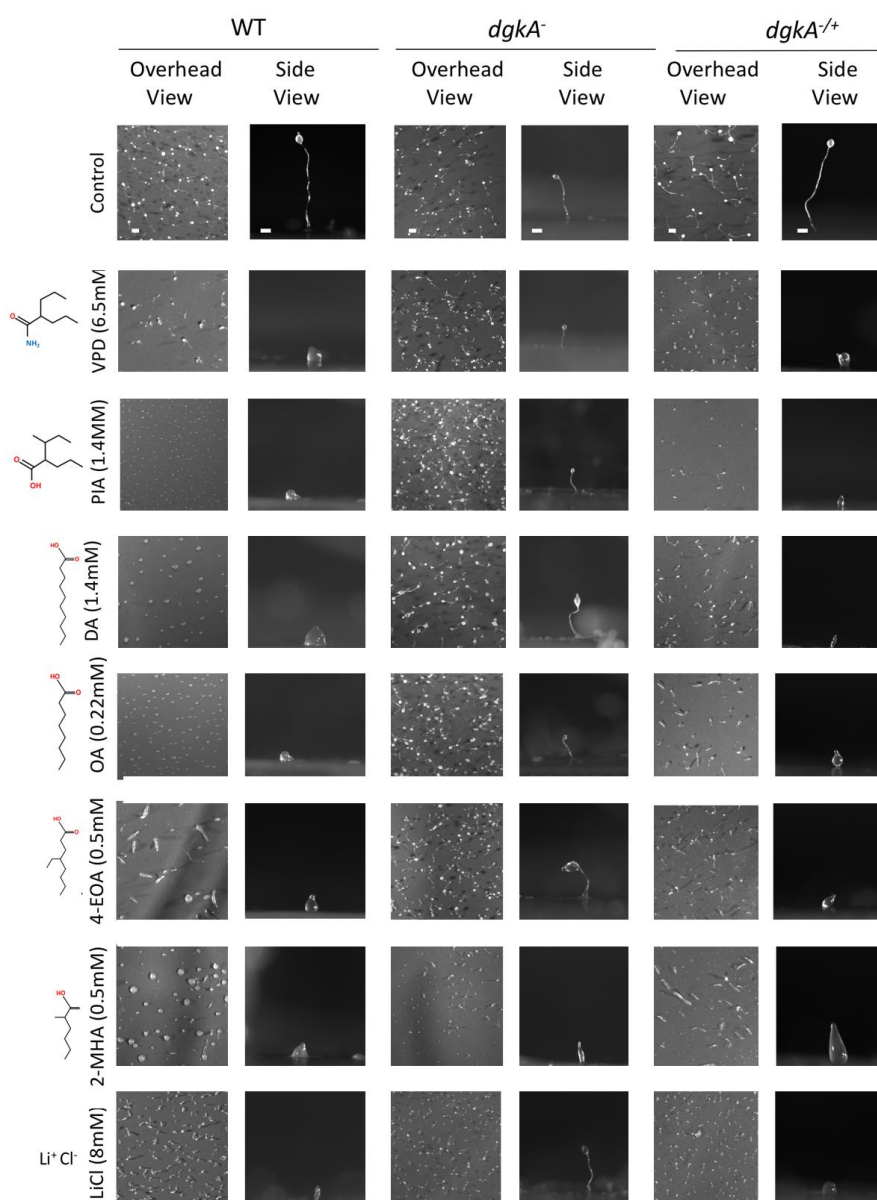


Figure 7.11. WT, *dgkA*⁻ and *dgkA*^{-/+} development in both the absence and presence of VPA. WT (left), *dgkA*⁻ (middle) and *dgkA*^{-/+} (right) cells were developed on nitrocellulose membranes for 24 hours in both the absence (top row) and presence (descending rows) of 0.3 mM, 0.5 mM and 1 mM VPA and images were taken of an overhead view (left) of the whole membrane and of a single fruiting body (right). All cells produced fruiting bodies in the absence of VPA, though the *dgkA*⁻ cells developed into smaller fruiting bodies compared with control which was rescued in *dgkA*^{-/+} cells. WT and *dgkA*^{-/+} cells in the presence of 0.3 mM and 0.5 mM developed to the finger stage and at 1 mM VPA developed into a mound after 24 hours. In contrast, *dgkA*⁻ cells were resistant to VPA and still able to develop into mature fruiting bodies when exposed to 0.3 mM and 0.5 mM VPA and to a mound in the presence of 1 mM VPA. *n* = 3. Scale bars of the overhead view indicates 0.5 mm and side view 0.1 mm.

7.4.7 Analysis of DGKA Cell Development in the Presence of Anti-Seizure Compounds and LiCl

DGKA was then investigated as a potential target for other anti-seizure compounds and the BD treatment LiCl. The anti-seizure compounds selected have previously been shown to have an active effect on both *D. discoideum* and in *in vivo* epilepsy models (Williams, et al., 1999; Williams, et al., 2002; Eickholt, et al., 2005; Chang, et al., 2012; Elphick, et al., 2012; Chang, et al., 2013; Chang, et al., 2015; Chang, et al., 2016). These experiments repeated the format of VPA analysis, with cells plated on nitrocellulose filters for 24 hours in the absence (control) and presence of a range of anti-seizure compounds and the BD drug LiCl at concentrations which blocked formation of fruiting bodies in WT cells (**Figure 7.12**). The compounds tested were VPD (6.5 mM) (Eickholt, et al., 2005) and PIA (1.4 mM) (Elphick, et al., 2012) which are structurally related to VPA. DA (1.65 mM) and OA (0.22 mM) were also tested which are key components of the MCT diet (Chang, et al., 2012; Chang, et al., 2013; Chang, et al., 2016). Branched compounds 4-EOA (0.5 mM) (Chang, et al., 2013; Chang, et al., 2015), which has been shown to control seizures and has neuroprotective effects was also tested, along with 2-MHA (0.5 mM) as a negative control as it is not active in *D. discoideum* nor in seizure control (Chang, et al., 2012). Under control conditions, WT, *dgkA*⁻ and *dgkA*^{+/-} cells were able to develop into mature fruiting bodies after 24 hours. In the presence of VPD, PIA, DA, OA, 4-EOA and LiCl at concentrations where WT cells developed into fingers or mounds, *dgkA*⁻ cells continued to develop into mature fruiting bodies resembling control conditions. The resistant phenotype shown to these compounds was restored back to that of WT in *dgkA*^{+/-} cells. In the presence of 2-MHA, WT, *dgkA*⁻ and *dgkA*^{+/-} cells developed into mounds after 24 hours. These results suggest that the compounds VPD, PIA, DA, OA and 4-EOA have a similar mechanism of action as VPA in regulating DGKA during *D. discoideum* development. Interestingly, the structurally unrelated compound LiCl also appears to target DGKA in *D. discoideum*, suggesting a conserved mechanism of action in the treatment of both epilepsy and BD.



7.12. WT, *dgkA*⁻ and *dgkA*^{-/+} development in both the absence and presence of a range of other compounds. WT (left), *dgkA*⁻ (middle) and *dgkA*^{-/+} (right) cells were developed on nitrocellulose membranes for 24 hours in the absence (top row) and presence (descending rows) of VPD, PIA, DA, OA, 4-EOA, 2-MHA and LiCl at the stated concentrations to the left of the development images. Images were taken as an overhead view of the whole membrane and of a single fruiting body (right). All cells developed into fruiting bodies in the absence of any compound. In the presence of VPD, PIA, DA, OA, 4-EOA and LiCl at concentrations which inhibited WT development, *dgkA*⁻ cells developed into mature fruiting bodies and compound sensitivity was restored in the *dgkA*^{-/+} cells. In the presence of 2-MHA, WT, *dgkA*⁻ and *dgkA*^{-/+} cells developed to the mound stage. $n = 3$. Scale bar for overhead view represents 0.5 mm and of the side view 0.1 mm.

7.4.8 Analysis of DAG Levels in *dgkA*⁻ and *dgkA*^{-/+} Cells in Response to Other Compounds

As the *dgkA*⁻ mutant was resistant to both VPA, a range of other anti-seizure compounds and LiCl, these compounds were also assessed for their effect on DAG levels. In these experiments, cells were pulsed with cAMP for 5 hours to allow cells to enter early development prior to being exposed to a range of compounds for 10 minutes (**Figure 7.13**). It was previously demonstrated during the acute cell behaviour assays that 10 minutes is enough time for cells to respond to VPA. Under control conditions, WT cells had an average DAG level of 0.17 ± 0.06 ng per 5×10^6 cells. The *dgkA*⁻ cells had an approximate 89 % reduction in levels of DAG (average 0.02 ± 0.01 ng per 5×10^6 cells) compared with WT cells. The levels of DAG in *dgkA*^{-/+} cells were not restored back to that of WT but were slightly increased by approximately 2-fold (average 0.04 ± 0.03 ng per 5×10^6 cells) compared with *dgkA*⁻ cells.

DAG levels were then quantified in WT, *dgkA*⁻ and *dgkA*^{-/+} cells following exposure to VPA. DAG levels increased by approximately 2.3-fold and 1.8-fold in WT cells (to 0.39 ± 0.17 ng per 5×10^6 cells and to 0.31 ± 0.09 ng per 5×10^6 cells) and by 3.5-fold and 5.0-fold in *dgkA*^{-/+} (to 0.14 ± 0.03 ng per 5×10^6 cells and to 0.20 ± 0.08 ng per 5×10^6 cells) when treated with 0.3 mM or 0.5 mM VPA respectively (**Figure 7.13A**). In the presence of 0.3 mM VPA, there was minute change in DAG levels in *dgkA*⁻ cells (to 0.01 ± 0.01 ng per 5×10^6 cells) and no detectable DAG when cells were exposed to 0.5 mM VPA. Statistically significant differences in DAG levels were identified between WT and *dgkA*⁻ cells (P value ≤ 0.01) and between *dgkA*⁻ and *dgkA*^{-/+} cells (P value ≤ 0.05). No statistically significant changes were identified between WT and *dgkA*^{-/+}. These results suggest that the mode of action of VPA involves increasing DAG levels. An increase in DAG levels, therefore, appears to inhibit *D. discoideum* acute cell behaviour (displacement, membrane protrusions and motility) and development.

DAG levels were then quantified in WT, *dgkA*⁻ and *dgkA*^{-/+} cells following exposure to LiCl. A similar effect was seen in the presence of LiCl, where WT DAG levels were raised approximately 2.8-fold (to an average of 0.48 ± 0.13 ng per 5×10^6 cells) and *dgkA*^{-/+} 5.5-fold to an average of 0.22 ± 0.11 ng per 5×10^6 cells) compared with control (**Figure 7.13A**). As with VPA treatment, *dgkA*⁻ cells had no detectable DAG when exposed to LiCl, with statistically significant differences being detected between WT and *dgkA*⁻ cells (P value ≤ 0.01) and *dgkA*⁻ cells with *dgkA*^{-/+} (P value ≤ 0.05). These results suggest that VPA and LiCl have a similar mode of action in *D. discoideum*.

DAG levels in WT cells was then investigated following exposure to the anti-seizure compounds which the *dgkA*⁻ cells were resistant. The *dgkA*⁻ cells were not tested in the presence of these compounds as there was low levels of DAG under control conditions which was abolished with VPA and LiCl treatment. In the presence of all compounds tested, statistically significant increases in DAG levels were identified compared with control conditions (P value ≤ 0.05) (**Figure 7.13B**). In the presence of the VPA structurally related compounds, DAG levels increased by approximately 11-fold (to 1.91 ± 0.45 ng per 5×10^6 cells) and 13-fold (to 2.17 ± 0.22 ng per 5×10^6 cells) when exposed to VPD and PIA respectively. When treated with DA and OA, the main components of the MCT diet, DAG levels increased 10.6-fold (to 1.81 ± 0.24 ng per 5×10^6 cells) and 11-fold (to 1.88 ± 0.51 ng per 5×10^6 cells) respectively. When treated with 4-EOA, a branch chain fatty acid, DAG levels 11-fold (to 1.90 ± 0.13 ng per 5×10^6 cells). These results suggest that VPD, PIA, DA, OA and 4-EOA all have a similar mode of action by raising DAG levels in *D. discoideum*.

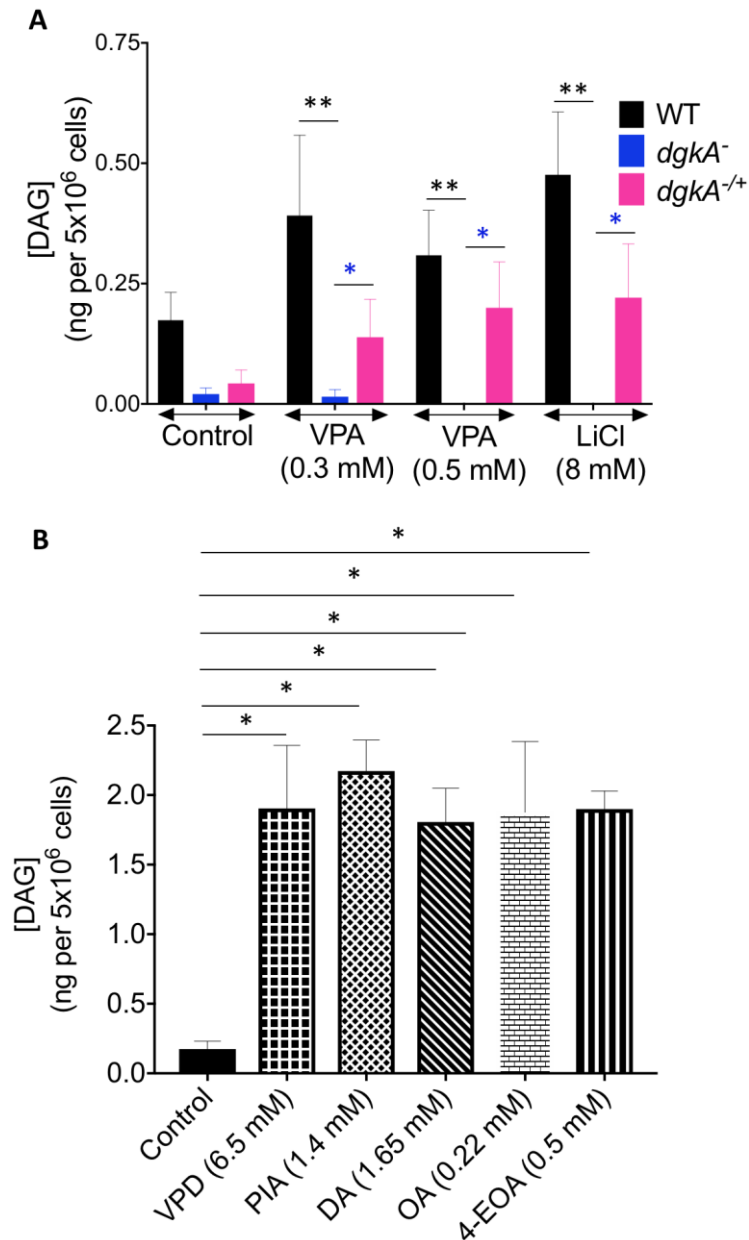


Figure 7.13. WT, *dgkA*⁻ and *dgkA*^{-/+} analysis of DAG levels in response to anti-seizure compounds and a bipolar disorder treatment. (A) WT (black), *dgkA*⁻ (blue) and *dgkA*^{-/+} (pink) DAG levels in the absence (control) of any treatment and in the presence of VPA (0.3 mM and 0.5 mM) and LiCl (8 mM) was increased in WT and *dgkA*^{-/+} cells in response to treatment, however, DAG levels were abolished in the *dgkA*⁻ following treatment. **(B)** DAG levels in WT cells when exposed to VPD (6.5 mM, black squares), PIA (1.4 mM, black diamonds), DA (1.65 mM, black and white lines), OA (0.22 mM, white bricks) and 4-EOA (0.5 mM, black and white vertical lines) increased significantly compared with control conditions. Data presented as mean (+/- SEM) *n* =4-7. Significant differences between WT and *dgkA*⁻ are shown by a black star and between *dgkA*⁻ and *dgkA*^{-/+} by a blue star using the Mann-Whitney test. *P* value: * *P* value = ≤0.05 and ** *P* value = ≤0.01.

7.5 Discussion

VPA treatment has been shown to reduce *D. discoideum* phosphoinositide levels in both a time and dose dependent manner (Chang, et al., 2012). Therefore, proteins involved in regulating phosphoinositide synthesis and breakdown have previously been investigated for VPA resistance or sensitivity. It has been suggested that the target of VPA in this effect is unlikely to function within pathways for *de novo* inositol biosynthesis, PI3K activity, inositol recycling and *de novo* inositol production (Chang, et al., 2012; Frej, et al., 2016). Therefore, proteins within the PI salvage pathway have been studied. Within this chapter, DGKA, the enzyme responsible for the phosphorylation of DAG into PA has been investigated. This chapter has described the ablation of the encoding DGKA gene (**Figures 7.2 and 7.3**) and the re-expression of DGKA in *dgkA*⁻ cells (**Figures 7.4 and 7.5**). Both *dgkA*⁻ and *dgkA*^{-/+} cells were phenotypically characterized in both the absence and presence of VPA, other anti-seizure compounds and the BD treatment LiCl (**Figures 7.6- 7.13**).

DGKA was ablated from Ax2 *D. discoideum* cells using a *dgkA* knockout construct previously created using the pLPBLP vector (Faix, et al., 2004). Isogenic *dgkA*⁻ cells were confirmed by RT-PCR and used for characterization in both the absence and presence of VPA. Ablation of *DgkA* is possible in *D. discoideum* as the gene has previously been ablated in *D. discoideum* JH10 cells (Abu-Elneel, Karchi and Ravid, 1996). In this work, the authors believed they were ablating MHC-PKC, however, it was later found that the gene was in fact the single *DgkA* (De La Roche, et al., 2002). Misinterpretation of the MHC-PKC was explained by the various DGK isoforms not being recognised as a kinase enzyme and from errors in the original DNA sequence at the time of cloning (De La Roche, et al., 2002). DGK has also been ablated in other organisms with one isoform, including yeast, suggesting that this protein is not essential for survival (Han, et al., 2008). The reason for the non-essential nature of DGKA is that DAG can be converted into PE and PC via the Kennedy pathway and then reintroduced into the PI salvage pathway via the formation of PA from PC (Kennedy and Weiss, 1956; Gibellini and Smith, 2010). This

reaction bypasses the phosphorylation of DAG into PA via DGK within the PI salvage pathway.

DGKA rescue cells (*dgkA*^{-/+}) were also created where the gene was reintroduced into *dgkA*⁻ cells. Characterization of *dgkA*^{-/+} cells initially involved Western blotting to ensure expression of GFP-DGKA. Fluorescence microscopy was conducted to determine the localization of GFP-DGKA. Consistent with previous work, GFP-DGKA was localized within the cytosol in vegetative cells and migrated to the cell cortex on cAMP stimulation where its enzyme activity is conducted (De La Roche, et al., 2002). A similar effect to DGKA translocation from the cytosol to the plasma membrane has been shown for DGK- θ in rat arteries, where the enzyme migrates to the plasma membrane following noradrenaline stimulation (Walker, et al., 2001). In a transgenic mouse model, DGK- α is activated by a Ras-nucleotide- releasing protein, resulting in enzyme translocation to the plasma membrane (Sanjuan, et al., 2003). Future work could investigate the effect of VPA on DGKA localization to determine whether the drug inhibits DGKA movement from the cytosol to the plasma membrane.

MHC localization was first investigated since the localization of this protein was disrupted in the *dgkA*⁻ (JH10) cells (Abu-Elneel, Karchi and Ravid, 1996). MHC localization was investigated in both vegetative and starved *dgkA*⁻ cells. Vegetative cells were fixed and stained with an MHC antibody, or *dgkA*⁻ cells containing a plasmid driving expression of a GFP fluorescently tagged MHC were starved and pulsed with cAMP to enter the developmental phase. In agreement with previous work, MHC was localised to the cytosol as shown by punctate staining in vegetative *dgkA*⁻ (Ax2) cells (Fukui, 1990; Abu-Elneel, Karchi and Ravid, 1996; Sabry, et al., 1997; Heid, et al., 2004). In *dgkA*⁻ (Ax2) starved cells, which had entered the developmental cycle, cytosolic MHC moved from the cytosol to the cell cortex, forming a dense cortical ring approximately 30 seconds post cAMP stimulation, consistent with the *dgkA*⁻ (JH10) mutant (Abu-Elneel, Karchi and Ravid, 1996). No change in MHC localization was seen between WT (Ax2) and *dgkA*⁻ (Ax2) cells during the vegetative phase, consistent with *DgkA* being expressed approximately 8

and 24 hours into the developmental cycle (Parikh, et al., 2010; Stajdohar, et al., 2015). Dysregulation of MHC in *dgkA*⁻ (Ax2) cells was of interest since the binding of cAMP to cell surface receptors initiates PIP₂ hydrolysis into IP₃ and DAG. DAG activates PKC (Kishimoto, et al., 1980; van Baal, et al., 2005) which initiates its movement to the site of stimulation. Meanwhile, IP₃ initiates an influx of calcium to activate DGK (Hahn and Friedman, 1999), resulting in the translocation of the enzyme from the cytosol to the plasma membrane. PKC phosphorylates MHC (Dulyaninova, et al., 2007) to causes the disassembly of MHC from actin filaments, forming myosin light chains (Yumura and Fukui, 1985). The myosin light chains then translocate to the posterior end of the cell where they reassemble into actin-MHC by ATPase (Yumura and Fukui, 1985). The reaction ceases as DAG is converted into PA by DGK. The abnormal localization of MHC in *dgkA*⁻ (Ax2) cells is, therefore, a result of enzyme loss as *D. discoideum* cells entering the developmental cycle are chemotactically competent through cAMP stimulation.

Cell growth was then investigated in both the absence and presence of VPA. Both WT (Ax2) and *dgkA*⁻ (Ax2) cells grew at a similar rate in the absence of VPA, consistent with that found in *dgkA*⁻ (JH10) cells (Abu-Elneel, Karchi and Ravid, 1996). In the presence of VPA, both cell lines had a dose-dependent reduction in cell number with increasing VPA concentration, suggesting DGKA is not the target of VPA during cell growth. This result is consistent with *DgkA* expression during the *D. discoideum* developmental cycle (Parikh, et al., 2010; Stajdohar, et al., 2015). DGKA was an enzyme of interest as DGK- β (Ishisaka, et al., 2013), - δ (Leach, et al., 2007) and - ϵ (Rodriguez de Turco, et al., 2001) have been linked to seizure activity in mice and DGK δ was found disrupted in a human epilepsy patient (Musto and Bazán, 2006). These studies have, therefore, shown a role of DGK isoforms in seizure generation.

VPA sensitivity was then investigated during the initial stages of the *D. discoideum* developmental cycle, when the *DgkA* gene is highly expressed (Parikh, et al., 2010; Stajdohar, et al., 2015). In the absence of VPA, WT, *dgkA*⁻ and *dgkA*^{-/+} cells had a similar behaviour in displacement, circularity, number of membrane protrusions

and motility. Acute VPA treatment of 0.3 mM upwards resulted in the inhibition of WT cell movement and rounding of the cells. In contrast, acute VPA treatment of 0.3 mM and 0.5 mM on *dgkA*⁻ cells resulted in similar values for displacement, membrane protrusions and motility compared with control conditions in the absence of VPA, where cells maintained their amoeboid shape. However, treatment of 0.7 mM VPA resulted in inhibition of cell displacement, membrane protrusions and circularity, which caused rounding of *dgkA*⁻ cells. WT VPA sensitivity was restored in *dgkA*^{-/+} cells. The partial resistance of *dgkA*⁻ cells to therapeutic VPA concentrations may be due to the drug targeting, or regulating, DGKA, causing enzyme inhibition. DGKA inhibition would result in the accumulation of DAG, which would upregulate the Kennedy pathway. Previous work using *D. discoideum* has shown components of the Kennedy pathway (PE and PC) are upregulated following approximately 30 minutes of VPA treatment (Elphick, et al., 2012). Both PE and PC are synthesised from DAG, as the mode of action of DGK is located at the branch point of the Kennedy pathway which utilises DAG for the synthesis of PE and PC (Kennedy and Weiss, 1956; Gibellini and Smith, 2010). Upregulation of the Kennedy pathway would enable the PI salvage pathway to bypass the formation of PA from DAG, allowing the PI salvage pathway to continue. Therefore, cells will continue movement as all PI salvage pathway molecules continue to be synthesized.

DGKA was then further investigated as a target for VPA during fruiting body formation. Ablation of *DgkA* resulted in the development of fruiting bodies containing a spore head, stalk and basal disc, however, these fruiting bodies were smaller in size compared with WT (Ax2). Small sized fruiting bodies were also identified in *dgkA*⁻ (JH10) cells, however, these fruiting bodies developed after 42-44 hours with upward extensions protruding from the spore head (Abu-Elneel, Karchi and Ravid, 1996). In contrast, *dgkA*⁻ (Ax2) fruiting bodies developed after 24 hours with no protrusions from the spore head. On reintroduction of *DgkA* in *dgkA*^{-/+} (Ax2) cells, fruiting body size was restored back to that of WT (Ax2). This result suggests fruiting body size is dependent on DGKA. In *D. discoideum* cells the height of a fruiting body is determined by the number of cells within the aggregation stream. A typical fruiting body will contain 0.2-1.0x10⁵ cells, whereas in

mutants which produce smaller fruiting bodies, such as the small aggregate formation protein mutant (*smf*⁻), only 5×10^3 cells are present (Brock and Gomer, 1999). Vesicle aggregates are produced when PLC activation causes DAG synthesis at the plasma membrane in the bacteria *Bacillus cereus* (Villar, Alonso and Goñi, 2000) and *Listeria monocytogenes* (Montes, et al., 2004). In a similar mechanism to *smf*⁻, *dgkA*⁻ cells therefore contain less cells in the aggregation stream which form the fruiting body compared with WT as a result of PLC activation from cAMP, thereby resulting in smaller fruiting bodies.

The effects of VPA were then investigated on *dgkA*⁻ cell development. In the presence of 0.3 mM and 0.5 mM VPA, WT cells developed into fingers or mounds, whereas *dgkA*⁻ cells continued to develop into mature fruiting bodies, resembling control conditions. In the presence of 1 mM VPA, *dgkA*⁻ development was inhibited at the mound stage at 24 hours. VPA sensitivity was restored in *dgkA*^{-/+} cells, suggesting DGKA is a target for, or regulated by, VPA at therapeutic concentrations during *D. discoideum* development. Resistance of *dgkA*⁻ cells to therapeutic VPA concentrations is of interest since epilepsy is associated with a reduction in dendritic spine formation, where DGK β is responsible for both the promotion and maturation of dendritic spines (Hozumi, et al., 2009). In a mouse model, VPA has been shown to revert this by promoting dendritic spine formation (Yang, et al., 2016), highlighting the neuroprotective effects of the drug during development.

A range of anti-seizure compounds and the BD treatment LiCl were then investigated on fruiting body development. At concentrations where WT cells developed into mounds after 24 hours, *dgkA*⁻ cells were resistant to VPD, PIA, DA, OA, 4-EOA and LiCl as they developed into mature fruiting bodies resembling control conditions. In the presence of the non- active compound 4-MHA, both WT and *dgkA*⁻ cells developed into mounds. Resistance to these compounds was dependent on DGKA, demonstrated by WT sensitivity being restored in *dgkA*^{-/+} cells. These results suggest that the structurally related VPA compounds and the main MCT diet constituents, control seizures through a similar mechanism, by targeting or regulating, DGKA. Of interest was *dgkA*⁻ cell resistance to the BD

treatment LiCl above the therapeutic concentration (0.6 mM-1 mM) (Singh, et al., 2013). This result shows there is a conserved mechanism of action between both epilepsy and BD treatments, through DGKA, in *D. discoideum*. Previous work has implicated the inhibition of PKC signalling, which is controlled by DAG and reversed by DGK, in BD patients following LiCl (Wang and Friedman, 1989; Bitran, et al., 1990) and VPA (Chen, et al., 1994) treatment. In conjunction with PKC inhibition, lithium treatment has been shown to result in the accumulation of DAG (Drummond and Raeburn, 1984; Bami, Leli and Hauser, 1993). Two DGK isoforms, DGK- β and - η have been linked with BD, where a single nucleotide polymorphism in DGK η had strong association with BD (Baum, et al., 2008). In addition, a significant increase in DGK η was later found in post mortem brains of BD patients (Squassina, et al., 2009; Moya, et al., 2010). A DGK β knockout mouse demonstrated lithium sensitive behaviours, such as reduced depression and anxiety, as well as hyperactivity which was lessened with lithium treatment (Kakefuda, et al., 2010). This result highlights a strong association of DGK isoforms in BD development and treatment.

Changes in DAG levels in the presence of all the compounds *dgkA*⁻ cells were resistant to were then quantified using a DAG specific ELISA assay. In the absence of treatment, DAG levels in *dgkA*⁻ cells was lower than that of WT and this was only partially rescued in *dgkA*^{-/+} cells. This reduction in DAG levels compared with WT is also seen in DGK η knockout mice under control conditions and when seizures are stimulated with electroconvulsive shock (Rodriguez de Turco, et al., 2001). Treatment of VPA and LiCl resulted in an accumulation of DAG in WT cells, which was contrasted with *dgkA*⁻ cells where there was little, or no, DAG detected. In *dgkA*^{-/+} cells, DAG levels were increased compared with control conditions following treatment of VPA and LiCl, however, DAG levels were not restored back to the WT concentration. Treatment of VPD, PIA, DA, OA and 4-EOA all resulted in a significant accumulation of DAG levels in WT cells compared with control, showing at the molecular level, both epilepsy and BD treatments work through a similar mechanism of action. VPA has previously been linked to reducing both inositol

phosphate and DAG signalling in *C. elegans* where it was thought VPA works through reducing inositol-1- phosphate and DAG synthesis (Tokuoka, Saiardi and Nurrish, 2008).

7.6 Summary

D. discoideum DGKA is not essential for cell survival and so a knockout approach was taken. To determine the resulting phenotype was due to ablation of the DGKA gene, a rescue cell line in which the gene was re-inserted into knockout cells was created, *dgkA*^{+/+}. Expression of GFP-DGKA in *dgkA*^{+/+} cells was confirmed by Western blotting and protein localization. Localization studies showed GFP-DGKA within the cytosol. Since *DgkA* had been ablated in *D. discoideum* JH10 cells where MHC localization was investigated, this was also examined here. In the vegetative phase, MHC was localised to the cytosol in WT (Ax2) and *dgkA*⁻ (Ax2) cells, however, in chemotactically competent cells stimulated with cAMP, MHC delocalized to the cell cortex, consistent with the previous findings. During cell growth, *dgkA*⁻ cells showed dose-dependent reduction in cell number, consistent with WT cells. However, during acute cell behaviour and development, when the *DgkA* gene is expressed, *dgkA*⁻ cells were resistant to VPA at 0.3 mM and 0.5 mM, spanning the therapeutic concentrations (0.3 mM- 0.6 mM) indicating a role for DGKA in the mechanism of action of VPA during development. The *dgkA*⁻ cells were also resistant to other anti-seizure compounds (VPD, PIA, DA, OA, 4-EOA) and the BD treatment LiCl during *D. discoideum* development at concentrations which blocked WT fruiting body formation. This result suggested a similar mechanism of action for treating both epilepsy and BD. At the molecular level, *dgkA*⁻ cells had a reduction in DAG levels compared with WT cells, suggesting DAG, the substrate of DGKA, is being upregulated via another pathway, potentially the Kennedy pathway. Treatment of all anti-seizure compounds tested and LiCl resulted in an accumulation of DAG levels in WT cells, however, little to no DAG was detected in the presence of VPA and LiCl in *dgkA*⁻ cells. On the reintroduction of *DgkA* into *dgkA*⁻ cells, drug sensitivity during acute cell behaviour and development to all treatments tested was restored back to WT, suggesting the resistant phenotype to the compounds

investigated is due to ablation of *DgkA*. These results, therefore, suggest DGKA is a target for, or is regulated by, VPA, VPD, PIA, DA, OA, 4-EOA and LiCl in *D. discoideum*. This in turn suggests that both epilepsy and BD treatments work through a similar mechanism of action.

Chapter 8

Conclusions

8. Conclusions

8.1 Background

A third of epilepsy and BD patients are resistant to medication that is currently available, when administered as monotherapy (a single drug) or as polytherapy (a combination of 2 or more compounds). This highlights a need for new drugs to be identified and made available to patients. One of the most effective and therefore highly prescribed AEDs is VPA (Haroon, et al., 2012). VPA, like many therapeutic treatments, has undesirable side effects, the most severe being hepatotoxicity (liver damage) (Kesterson, Granneman and Machinist, 1984) and teratogenicity (defects in developing embryos) (Hauck and Nau, 1989). Despite these side effects, VPA continues to be used to control seizures in epilepsy patients. VPA is also used to treat mania in BD patients (Pope, et al., 1991) and is effective in controlling migraines (Hering and Kuritzky, 1992; Yurekli, et al., 2008). Currently, studies are also investigating VPA as a potential treatment option for cancer, with research being conducted using murine prostate cancer cells (Witt, et al., 2013), transformed hematopoietic progenitor cells, carcinoma cells, a rat model and leukemic blast cells from patients of myeloid leukaemia (Göttlicher, et al., 2001; Tang, et al., 2004). Due to the numerous diseases VPA is used to treat, many studies have focused on elucidating the molecular target of the drug. To date, the mechanism of action of VPA involves enhancing brain γ -amino butyrate levels (Godin, et al., 1969) and reducing or inhibiting voltage gated potassium, sodium and calcium channels (VanDongen, VanErp and Voskuyl, 1986; Kelly, Gross and Macdonald, 1990); NMDA excitation (Slater, Stelzer and Galvan, 1985; Holmes, et al., 1990; Zeise, Kasparow and Zieglgänsberger, 1991); histone deacetylase (Göttlicher, et al., 2001); inositol phosphate and phosphoinositide levels (Williams, et al., 2002; Eickholt, et al., 2005; Chang, et al., 2012; Chang, Walker and Williams, 2014). In relation to phosphoinositide signalling, VPA causes a dose-dependent reduction of the molecule PIP_2 . This is achieved independently of PI3K activity, inositol recycling and *de novo* inositol biosynthesis (Chang, et al., 2012; Frej, et al.,

2016), leaving the PI salvage pathway. This project has, therefore, been aimed at determining whether the molecular target of VPA is a component of the PI salvage pathway or reduces PIP₂ levels through an interlinking pathway.

8.2 Proteins Dismissed as VPA Targets

In this thesis a total of 11 proteins in *D. discoideum* were investigated as potential targets of VPA (**Table 8.1**). These included all 5 PI3Ks, PTEN, PLC, LPIN2, CDSA, CDIPT and DGKA. Of these proteins, the 5 PI3Ks, PTEN, PLC, LPIN2 and CDSA were dismissed as VPA targets, as each of the knockout or overexpressing mutants demonstrated VPA sensitivity during acute cell behaviour, development and/or growth. In this work, VPA sensitivity of the 5 PI3K and PTEN null cells (*pi3k1-5*^{-/-}/*pten*⁻) has been identified, consistent with a previous study which showed a significant reduction in PIP and PIP₂ levels when treated with VPA (Chang, et al., 2012). Therefore, other VPA targets must be present in *D. discoideum*

Cell Line	Experiment			
	Growth	Acute Cell Behaviour	Development	ELISA
<i>pi3k1-5⁻/pten⁻</i>	-	Resistant to 0.5 mM VPA.	Sensitive to all compounds.	-
<i>plc⁻</i>	-	VPA sensitive.	Sensitive to all compounds.	-
<i>lpin2⁻</i>	-	VPA sensitive.	Sensitive to all compounds.	-
WT::RFP- <i>cdsA</i>	VPA sensitive.	-	Sensitive to all compounds.	-
WT::RFP- <i>cdipt</i>	Resistant to VPA up to 0.5 mM.	-	Sensitive to VPD, DA, OA, 4-EOA, 2-MHA and LiCl. Resistant to 0.3 mM and 0.5 mM VPA and 1.4 mM PIA.	-
<i>dgkA⁻</i>	VPA sensitive.	Resistant to VPA up to 0.5 mM.	Resistant to 0.3 mM and 0.5 mM VPA, VPD, PIA, DA, OA, 4-EOA and LiCl.	Low levels of detectable DAG which was further reduced or abolished with treatment of 0.3 mM and 0.5 mM VPA and 8 mM LiCl.
<i>dgkA^{-/+}</i>	-	VPA sensitive.	Sensitive to all compounds.	DAG levels partially restored. DAG levels increased with treatment of 0.3 mM and 0.5 mM VPA and 8 mM LiCl.

Table 8.1. Summary of results obtained within this thesis. Table summarizing the mutant strains investigated during this thesis and the results of each experiment conducted to determine sensitivity or resistance to each compound tested. Compounds tested were VPA (0.01 mM -2 mM), VPD (6.5 mM), PIA (1.4 mM), DA (1.65 mM), OA (0.22 mM), 4-EOA (0.5mM), 2-MHA (0.5mM) and LiCl (8 mM).

8.3 Proteins Identified as Novel VPA Targets

Two mutants within the PI salvage pathway were found to be resistant to VPA at therapeutic concentrations in this study. One of these mutants was overexpressed and the other ablated. The first strain resistant to VPA was CDIPT. CDIPT is the enzyme responsible for the formation of PI from CDP-DAG and *myo*-inositol. CDIPT was an enzyme of interest as the enzyme product PI has been associated with seizure generation and progression through calcium signalling (Yoshida, et al., 1987; Alswied and Parekh, 2015). CDIPT is vital in yeast (Nikawa, Kodaki and Yamashita, 1987), *T. brucei* (Martin and Smith, 2006) and *Drosophila* (Wang and Montell, 2006) and may, therefore, be an essential protein in *D. discoideum*. CDIPT was characterized in both the absence and presence of VPA and a range of anti-seizure. Unfortunately, RFP-CDIPT was mostly present within membrane bound vesicles in these cells, suggesting the majority of the overexpressed protein is inactive and so these cells maintain a tightly regulated pool of CDP-DAG (Lykidis, et al., 1997). Interestingly, the overexpressed and sequestered RFP-CDIPT may act to reduce the level of the endogenous protein within these membrane bound vesicles, thereby creating a CDIPT knockdown, which has been shown for drug-induced phospholipidosis (Yamamoto, et al., 1971; Seiler and Wassermann, 1975). Furthermore, overexpressed PI has previously been associated with inclusion body formation (Matsuzawa and Hostetler, 1980).

WT::RFP-*cdipt* cells were resistant to therapeutic VPA concentrations during cell growth and development, suggesting the mechanism of VPA involves altering CDIPT activity. WT::RFP-*cdipt* cells were also resistant to PIA (1.4 mM), suggesting that the mechanisms of action of both VPA and PIA is likely to be regulated by CDIPT. However, it remains to be determined whether this resistant phenotype is through the small

elevation of cytosolic RFP-CDIPT or through reduction of endogenous CDIPT levels in cells through sequestration.

A second strain showing resistance to VPA contained disruption of the *DgkA* gene. DGKA is the enzyme responsible for the phosphorylation of DAG into PA. This enzyme was of interest as DAG levels are increased during seizures (Yoshida, et al., 1987) and VPA could work through inhibiting this increase. Similarly to WT cells, *dgkA*⁻ cells had a dose-dependent reduction in cell growth when exposed to increasing VPA concentrations. Investigations continued as *D. discoideum* DGKA is highly expressed 8 and 24 hours into the developmental phase (Parikh, et al., 2010; Stajdohar, et al., 2015). Cells were stimulated to enter the developmental cycle where *dgkA*⁻ cells were resistant to therapeutic VPA concentrations (0.3 mM and 0.5 mM) during both acute cell behaviour and development, suggesting DGKA is a potential target, or is regulated by, VPA in *D. discoideum*. This was confirmed by the creation of *dgkA*^{-/+} cells, where drug sensitivity was restored when treated with 0.3 mM and 0.5 mM VPA during both acute cell behaviour and development. These results confirm that DGKA is either a target, or is regulated by, VPA in *D. discoideum*.

VPA targeting or regulating DGKA was further investigated by quantifying changes in molecular DAG levels in both the absence and presence of VPA in WT, *dgkA*⁻ and *dgkA*^{-/+} cells. In the absence of VPA, DAG levels in *dgkA*⁻ cells were lower than that of WT and only partially restored in *dgkA*^{-/+} cells. VPA treatment (0.3 mM and 0.5 mM) resulted in an increase in DAG levels in both WT and *dgkA*^{-/+} cells. This was contrasted in *dgkA*⁻ cells, where there was a reduction of DAG levels compared with control conditions. This reduction of DAG levels following VPA treatment has been shown previously in *C. elegans* (Tokuoka, Saiardi and Nurrish, 2008).

Other anti-seizure medications were also investigated on *dgkA*⁻ cell development. The *dgkA*⁻ cells were resistant to VPD, PIA, DA, OA and 4-

EOA and the BD treatment LiCl at concentrations which inhibited WT cell development. Sensitivity to these compounds was restored in *dgkA*^{-/+} cells, indicating DGKA is a target, or is regulated by, these compounds. To determine whether these compounds have a similar mode of action to VPA, DAG levels were quantified. The effects of LiCl (8 mM) on WT, *dgkA*⁻ and *dgkA*^{-/+} cells on DAG levels was similar to that of VPA, where WT and *dgkA*^{-/+} cells had a rise in DAG levels, contrasted with no detectable DAG in the *dgkA*⁻ cells. The rise in DAG levels in response to LiCl treatment is consistent with previous studies using pituitary tumour (Drummond and Raeburn, 1984) and mouse neuroblastoma-rat glioma (Brami, Leli and Hauser, 1991) cells and mouse (Sade, et al., 2016) and rat (Sherman, et al., 1981) animal models. As DAG levels were not detectable on therapeutic VPA concentrations, nor LiCl treatment in *dgkA*⁻ cells, only WT cells were treated with the remaining compounds. Like VPA and LiCl, all compounds tested (VPD, PIA, DA, OA and 4-EOA), resulted in a significant rise in DAG levels in WT cells. These results suggest that all of these compounds (LiCl, VPD, PIA, DA, OA and 4-EOA) have a similar mode of action in *D. discoideum*, by targeting or regulating DGKA. These compounds could, therefore, potentially be new AEDs which could replace VPA, as they have the same mechanism of action and have demonstrated anti-seizure effects (Williams, et al., 1999; Eickholt, et al., 2005; Williams, et al., 2002; Elphick, et al., 2012; Chang, et al., 2012; Chang, et al., 2013; Chang, Walker and Williams, 2014; Chang, et al., 2015; Chang, et al., 2016).

8.4 Predicted Mechanism of Action of VPA

Seizures are stimulated from an increase in calcium signalling, initiated from the release of IP₃ from PIP₂ hydrolysis (Paulus and Kennedy, 1960; Prottey and Hawthorne, 1967; Whatmore, et al., 1999). This results in a rise in DAG levels (Yoshida, et al., 1987) and reduction in PC (Corazzi, et al., 1986), correlated with no change in PE levels (Marku, et al., 1987). The excess DAG is then converted into triglycerides (Yoshida, et al., 1987) and

free fatty acids (Bazán, 1970; Bazán and Rakowski, 1970; Bazán, Morelli de Liberti and Rodriguez de Turco, 1982; Rodriguez de Turco, Morelli de Liberti and Bazán, 1983) which are utilized during mitochondrial β -oxidation (**Figure 8.1A**). However, during VPA treatment, the rise in DAG levels (Drummond and Raeburn, 1984; Bami, Leli and Hauser, 1993) is associated with a rise in pERK activity (Ludtmann, Boeckeler and Williams, 2011), PE, PC (Elphick, et al., 2012), CDP-DAG (Watson, Shipman and Godfrey, 1990; Stubbs Jr., et al., 1992; Stubbs Jr. and Agranoff, 1993; Ju and Greenberg, 2003) and plasma and hepatic triglyceride levels (Seçkin, Başaran-Küçükgergin and Uysal, 1999) whilst inhibiting β -oxidation (Coudé, et al., 1983; Kesterson, Granneman and Machinist, 1984; Granneman, et al., 1984) (**Figure 8.1B**).

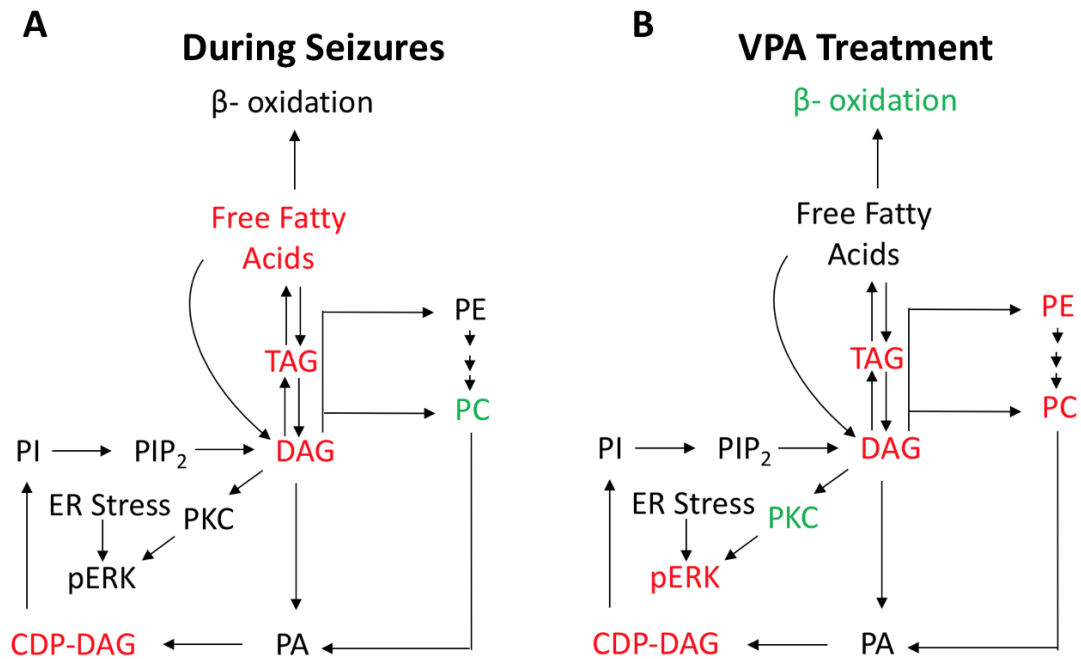


Figure 8.1. Schematic comparing changes in cellular components during seizures

and valproic acid treatment. Schematic comparing the changes in cellular components (A) during seizures and (B) valproic acid (VPA) treatment. The phosphatidylinositol salvage pathway components diacylglycerol levels (DAG), phosphatidic acid (PA), cytidine diphosphate- diacylglycerol (CDP-DAG), phosphatidylinositol (PI) and phosphatidylinositol-4,5-bisphosphate (PIP₂). Components of the Kennedy pathway, phosphatidylethanolamine (PE) and phosphatidylcholine (PC) and triacylglycerol (TAG) are converted into free fatty acids and used for β-oxidation and protein kinase C (PKC) are also shown. Phosphorylated extracellular signal-regulated kinase (pERK) is regulated by PKC or is activated as a result of ER stress. Components which are increased during seizures or VPA treatment are shown in red and those reduced are shown in green.

Taken with the results from this thesis, it can be hypothesised that the overexpression of CDIPT and inhibition or dysregulation of DGKA by VPA causes cellular changes to occur. Inhibition of DGKA would block the formation of PA through the PI salvage pathway. This effect is counteracted by the upregulation of the Kennedy pathway to ensure PA and therefore, PI, a regulator of the cell cycle (Deguchi, et al., 2002), are

synthesised (**Figure 8.2**). Increased calcium signalling and the accumulation of CDP-DAG would result in endoplasmic reticulum stress, which is known to activate pERK (Lumley, et al., 2017) independent of PKC (Wang and Friedman, 1989; Bitran, et al., 1990; Chen, et al., 1994). pERK reduces activity of the cell cycle (Brewer and Diehl, 2000) so to increases apoptosis and autophagy (Tallóczy, et al., 2002). This would be achieved by the binding of the Unc-51 autophagy activating kinase to CDIPT enriched subdomains of the endoplasmic reticulum to initiate PI synthesis from the excess CDP-DAG, via the overexpression of CDIPT. The excess PI could then be packaged into punctate autophagosomes (Nishimura, et al., 2017) as shown in WT::RFP-*cdipt* cells and in mammalian models of phospholipidosis (Yamamoto, et al., 1971; Seiler and Wassermann, 1975). Due to the packaging of PI into membrane bound vesicles for degradation, excess PI is limited, resulting in reduced synthesis of PIP₂ and thereby preventing hydrolysis into IP₃ and DAG. This in turn inhibits calcium release and seizure generation. DAG levels then fall as the molecule is synthesised at a reduced rate and that produced is utilized via the Kennedy pathway. This enables the cell cycle to continue to function, however, at a reduced rate. The role of pERK as a suppressor of cell proliferation whilst increasing apoptosis has been investigated in the development of cancer treatments. Targeting pERK for cancer treatment has been both successful, resulting in reduced tumour growth in HT29 colorectal carcinoma cells (Bi, et al., 2005) and mouse embryonic fibroblasts (Blais, et al., 2006) and unsuccessful, where tumour growth increased in human oesophageal and breast cell lines (Bobrovnikova-Marjon, et al., 2010). In cancer treatment, VPA may work in a similar way to the histone deacetylase inhibitor Vorinostat, which was approved for cutaneous T-cell lymphoma treatment in 2007 (Mann, et al., 2007), whose anti-tumour activity involves activating pERK (Kahali, et al., 2010).

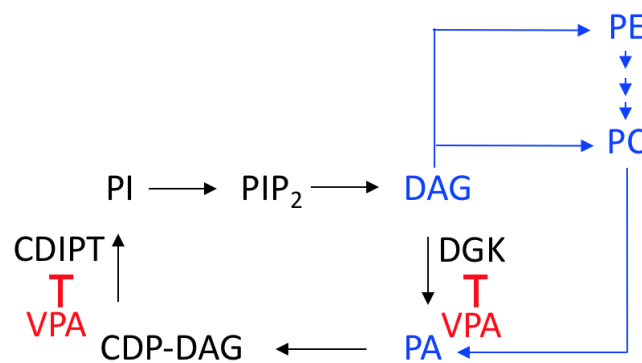


Figure 8.2. Schematic of proposed mechanism of action of VPA. Schematic of the proposed mechanisms of action of VPA (shown in blue) whereby VPA inhibits diacylglycerol kinase (DGK) activity (red “T”), which results in a rise (red arrow) of diacylglycerol levels (DAG). The accumulation of DAG results in the upregulation of the Kennedy pathway where DAG is converted into phosphatidylethanolamine (PE) and then phosphatidylcholine (PC), or directly into PC from DAG. PC is then converted into phosphatidic acid (PA), restarting the phosphatidylinositol salvage pathway via the synthesis of cytidine diphosphate- diacylglycerol (CDP-DAG), phosphatidylinositol (PI) via CDP-DAG-inositol 3 phosphatidyltransferase (CDIPT) and phosphatidylinositol-4,5-bisphosphate (PIP₂).

This hypothesis of the mode of action of VPA is supported by many studies which have linked several DGK isoforms, DGK- β (Ishisaka, et al., 2013), - δ (Leach, et al., 2007) and - ϵ (Rodriguez de Turco, et al., 2001; Musto and Bazán, 2006) with epilepsy. The results presented here also correlate with previous studies which associated epilepsy with a reduction in dendritic spine formation, a process regulated by DGK β (Hozumi, et al., 2009) and reversed with VPA treatment in a mouse model (Yang, et al., 2016). This links the mechanism of disease progression and the therapeutic treatment counteracting this effect, through DGK.

Another outcome from this study was that the mechanisms of action of the anti-seizure compounds VPD, PIA, DA, OA and 4-EOA and the BD treatment LiCl are also through targeting, or regulating, DGKA in *D. discoideum*. This is because other mutants of PI salvage pathway proteins were sensitive to

treatment. This was with the exception of WT::RFP-*cdipt* cells which were also resistant to 1.4 mM PIA. Of particular interest was *dgkA*⁻ cell resistance to LiCl treatment during the development assay and the changes in DAG levels mimicking that of VPA treatment in WT, *dgkA*⁻ and *dgkA*^{-/+} cells. These results suggest that both VPA and LiCl work through a similar target, DGKA, in *D. discoideum*. The similarity in the mechanism of action of both VPA and LiCl is supported in literature where DGK isoforms have been linked with BD (DGK- β and - η) (Baum, et al., 2008; Squassina, et al., 2009; Moya, et al., 2010; Kakefuda, et al., 2010) and epilepsy (DGK- β , - δ and - ϵ) (Rodriguez de Turco, et al., 2001; Musto and Bazán, 2006; Leach, et al., 2007; Ishisaka, et al., 2013). Both VPA and LiCl have also been found to inhibit PKC signalling. PKC is activated in BD patients by DAG from the hydrolysis of PIP₂, with calcium being released by IP₃ (Hahn and Friedman, 1999), which is believed to be responsible for the different mood states (Dubovsky, et al., 1989) of BD patients. In support of the results presented in this thesis, LiCl treatment causes a rise in DAG levels in pituitary tumour cells (Drummond and Raeburn, 1984), rat brain slices (Wang and Friedman, 1989), a human leukaemia cell line (Bitran, et al., 1990) and mouse neuroblastoma-rat glioma cells (Brami, Leli and Hauser, 1993). In 1984, Drummond and Raeburn proposed the mechanism for this increase in DAG was through LPIN2, with the excess DAG being redirected to PS or triacylglycerol biosynthesis. The data presented in this thesis builds upon this previous work as *lpin2*⁻ cells were sensitive to VPA and LiCl treatment, thereby dismissing LPIN2 as a target of VPA and LiCl in *D. discoideum*. In addition, PS is synthesised via the CDP-DAG pathway which is regulated by the CDP-DAG pool (Paulus and Kennedy, 1960; Kiyasu, et al., 1963; Kanfer and Kennedy, 1964). CDS, the enzyme responsible for the synthesis of CDP-DAG from PA, was also investigated as both VPA and LiCl treatment cause a rise in CDP-DAG levels in platelets (Watson, Shipman and Godfrey, 1990), human neutrophils (Stubbs, Jr., et al., 1992), human neuroblastoma (Stubbs, Jr. and Agranoff, 1993) and yeast (Ju and Greenberg, 2003) cells. It was suggested that the rise in CDP-DAG levels is a secondary effect

resulting from the increase in DAG (Stubbs, Jr., et al., 1992), however, the overexpressing WT::RFP-*cdsA* cells were sensitive to both VPA and LiCl treatment, suggesting this enzyme is not regulated by either drug. This overlap between the mechanisms of action of epilepsy and BD treatments is also supported by an African population study which showed relatives of epilepsy or BD patients have an approximate 13 % increased chance of developing the other disorder compared with individuals with no family history of either condition (Jidda, et al., 2010).

8.5 Implications of These Findings

The findings from this thesis have provided a step forward in elucidating the mechanism of action of VPA. By identifying DGKA and CDIPT as either novel targets, or enzymes regulated by VPA, new AEDs can be developed which inhibit DGK and/or overexpress CDIPT to ensure a similar potency to VPA. In addition to targeting a DGKA and CDIPT-related mechanism, new compounds can be designed which lack the teratogenic side effects of VPA by removing specific chemical structures (a free carboxyl group, α -hydrogen atom and branching on carbon 2) (Nau, Hauck and Ehlers, 1991). Examples of new potential antiepileptic treatments which could replace VPA include those investigated in this thesis which have the same mechanisms of action as VPA- PIA, DA, OA and 4-EOA. Development of new AEDs may help the third of epilepsy patients resistant to currently available medication.

These findings also highlight a common molecular mechanism between epilepsy and BD treatments. As both VPA and LiCl treatment causes a rise in DAG levels, which is abolished in *dgkA*⁻ cells, AEDs and BD treatments whose mechanisms of action involves regulating DGK, could be used to treat both disorders. This, therefore, increases the range of medications available to patients of both diseases, benefitting the third of epilepsy and BD patients resistant to currently available medication.

To continue with this project this work would need to be translated into a mammalian model. Translation of these findings would determine whether single or multiple DGK isoform are being regulated by VPA. Both humans, mice and rats contain 10 DGK isoforms, of which type 2 DGKs contain pleckstrin homology domains which bind PI lipids and would therefore be likely targets of VPA.

To overcome the unsuccessful attempts of creating *CdsA* and *Cdipt* ablated cell lines, a knockdown approach could be taken. A knockdown approach reduces the expression of essential genes and can be achieved by short hairpin RNA or by RNA interference (Friedrich, et al., 2015). RNA interference involves the transformation of small-double stranded interfering RNAs into cells which are complementary to the target messenger RNA. Gene silencing occurs as small-double stranded interfering RNAs are used by the RNA- induced silencing complex as a template to locate the target messenger RNA which is then cleaved by a ribonuclease.

8.6 Summary

This thesis has described the characterization of proteins in response to VPA within, and interlinking with, the PI salvage pathway, to help identify potential molecular targets of VPA in *D. discoideum*. From the results obtained, VPA has been shown to target DGKA and CDIPT, or regulate the signalling of these two proteins, as ablation of *DgkA* and overexpression of CDIPT results in reduced VPA sensitivity. In addition, a range of other anti-seizure compounds, VPD, PIA, DA, OA and 4-EOA, also appear to function through DGKA. Interestingly, the BD treatment LiCl, also functions through DGKA. The effect of VPA and other compounds (VPD, PIA, DA, OA, 4-EOA and LiCl) through DGKA-dependent signalling is also validated at the molecular level where treatment resulted in a rise in DAG levels, dependent on the presence of DGKA. These results suggest that both VPA

and LiCl function through DGKA-related signalling, within the PI salvage pathway, highlighting a conserved mechanism of action of both epilepsy and BD treatments.

References

- Aboukhatwa, M. A. and Undieh, A. S. (2010). Antidepressant stimulation of CDP-diacylglycerol synthesis does not require monoamine reuptake inhibition. *BMC Neuroscience*. **(11)**, 11-21.
- Abu-Elneel, K., Karchi, M. and Ravid, S. (1996). *Dictyostelium* Myosin II Is Regulated during Chemotaxis by a Novel Protein Kinase C. *The Journal of Biological Chemistry*. **(271)**, 977-984.
- Agranoff, B. W., Bradley, R. M. and Brady, R. O. (1958). The enzymatic synthesis of inositol phosphatide. *The Journal of Biological Chemistry*. **(233)**, 1077-1083.
- Ahmed, M. Y., Al-Khayat, A., Al-Murshedi, F., Al-Futaisi, A., Chioza, B. A., Fernandez-Murray, J. P., Self, J. E., Salter, C. G., Harlalka, G. V., Rawlins, L. E., Al-Zuhaibi, S., Al-Azri, F., Al-Rashdi, F., Cazenave-Gassiot, A., Wenk, M. R., Al-Salmi, F., Patton, M. A., Silver, D. L., Baple, E. L., McMaster, C. R. and Crosby, A. H. (2017). A mutation of EPT1 (SELENOI) underlies a new disorder of Kennedy pathway phospholipid biosynthesis. *Brain*. **(140)**, 547-554.
- Aitchison, A. J., Arsenault, D. J. and Ridgway, N. D. (2015). Nuclear-localized CTP:phosphocholine cytidyltransferase α regulates phosphatidylcholine synthesis required for lipid droplet biogenesis. *Molecular Biology of the Cell*. **(26)**, 2927-2938.
- Allison, J. H., Blisner, M. E., Holland, W. H., Hipps, P. P. and Sherman, W. R. (1976). Increased brain myo -inositol 1-phosphate in lithium-treated rats. *Biochemical and Biophysical Research Communications*. **(71)**, 664-670.
- Alswied, A. and Parekh, A. B. (2015). Ca^{2+} Influx through Store-operated Calcium Channels Replenishes the Functional Phosphatidylinositol 4,5-Bisphosphate Pool Used by Cysteinyl Leukotriene Type I Receptors. *The Journal of Biological Chemistry*. **(290)**, 29555-29566.
- Altamura, A. C., Basile, R., Mauri, M. and Cazzullo, C. L. (1986). Valpromide (Depamide) in the treatment of acute psychotic states. Open clinical study. *Acta Psychiatrica Belgica*. **(86)**, 297-304.
- Altschul, S. F., Gish, W., Miller, W., Meyers, E. W. and Lipman, D. J. (1990). Basic Local Alignment Search Tool. *Journal of Molecular Biology*. **(215)**, 403-410.
- Antonsson, B. (1997). Phosphatidylinositol synthase from mammalian tissues. *Biochimica et Biophysica Acta*. **(1328)**, 179-186.
- Arcaro, A. and Wymann, M. P. (1993). Wortmannin is a potent phosphatidylinositol 3-kinase inhibitor: the role of phosphatidylinositol 3,4,5-trisphosphate in neutrophil responses. *The Biochemical Journal*. **(296)**, 297-301.

- Arzimanoglou, A., Lagae, L., Cross, J., Beghi, E., Mifsud, J., Bennett, C., Schmidt, D., Wait, S. and Harvey, G. (2014). The administration of rescue medication to children with prolonged acute convulsive seizures in a non-hospital setting: an exploratory survey of healthcare professionals' perspectives. *European Journal of Pediatrics*. **(173)**, 773-779.
- Atkinson, K. D., Jensen, B., Kolat, A. I., Storm, E. M., Henry, S. A. and Fogel, S. (1980). Yeast mutants auxotrophic for choline or ethanolamine. *Journal of Bacteriology*. **(141)**, 558-564.
- Augustin, K., Khabbush, A., Williams, S., Eaton, S., Orford, M., Cross, J. H., Heales, S. J. R., Walker, M. C. and Williams, R. S. B. (2018). Mechanisms of action for the medium-chain triglyceride ketogenic diet in neurological and metabolic disorders. *Lancet Neurology*. **(17)**, 84-93.
- Axe, E. L., Walker, S. A., Manifava, M., Chandra, P., Roderick, H. L., Habermann, A., Griffiths, G. and Ktistakis, N. T. (2008). Autophagosome formation from membrane compartments enriched in phosphatidylinositol 3-phosphate and dynamically connected to the endoplasmic reticulum. *The Journal of Cell Biology*. **(182)**, 685-701.
- Backman, S.A., Stambolic, V., Suzuki, A., Haight, J., Elia, A., Pretorius, J., Tsao, M., Shannon, P., Bolon, B., Ivy, G. O. and Mak, T. W. (2001). Deletion of Pten in mouse brain causes seizures, ataxia and defects in soma size resembling Lhermitte-Duclos disease. *Nature Genetics*. **(29)**, 396-403.
- Banfić, H., Zizak, M., Divecha, N. and Irvine, R. F. (1993). Nuclear diacylglycerol is increased during cell proliferation in vivo. *The Biochemical Journal*. **(290)**, 633-636.
- Bankaitis, V. A. and Grabon, A. (2011). Phosphatidylinositol synthase and diacylglycerol platforms bust a move. *Developmental Cell*. **(21)**, 810-812.
- Basu, S., Fey, P., Pandit, Y., Dodson, R., Kibbe, W. A. and Chisholm, R. L. (2013). DictyBase 2013: integrating multiple Dictyostelid species. *Nucleic Acids Research*. **(41)**, D676-D683.
- Baum, A. E., Akula, N., Cabanero, M., Cardona, I., Corona, W., Klemens, B., Schulze, T. G., Cichon, S., Rietschel, M., Nöthen, M. M., Georgi, A., Schumacher, J., Schwarz, M., Jamra, R. A., Höfels, S., Propping, P., Satagopan, J., Detera-Wadleigh, S. D., Hardy, J. and McMahon, F. J. (2008). A genome-wide association study implicates diacylglycerol kinase eta (DGKH) and several other genes in the etiology of bipolar disorder. *Molecular Psychiatry*. **(13)**, 197-207.

- Bazán Jr., N. G. and Rakowski, H. (1970). Increased levels of brain free fatty acids after electroconvulsive shock. *Life Sciences*. **(9)**, 501-507.
- Bazán Jr., N. G., (1970). Effects of ischemia and electroconvulsive shock on free fatty acid pool in the brain. *Biochimica Et Biophysica Acta (BBA)-Lipids and Lipid Metabolism*. **(218)**, 1-10.
- Bazán, N. G., Morelli de Liberti, S. A. and Rodriguez de Turco, E. B. (1982). Arachidonic acid and arachidonoyl-diglycerols increase in rat cerebrum during bicuculline-induced status epilepticus. *Neurochemical Research*. **(7)**, 839-843.
- Becerra, J. L., Ojeda, J., Corredera, E. and Ruiz-Giménez, J. (2011). Review of Therapeutic Options for Adjuvant Treatment of Focal Seizures in Epilepsy. *CNS Drugs*. **(25)**, 3-16.
- Berg, A. T., Berkovic, S. F., Brodie, M. J., Buchhalter, J., Cross, J. H., van Emde Boas, W., Engel, J., French, J., Glauser, T. A., Mathern, G. W., Moshé, S. L., Nordli, D., Plouin, P. and Scheffer, I. E. (2010). Revised terminology and concepts for organization of seizures and epilepsies: report of the ILAE Commission on Classification and Terminology, 2005-2009. *Epilepsia*. **(51)**, 676-685.
- Berridge, M. J., (1983). Rapid accumulation of inositol trisphosphate reveals that agonists hydrolyse polyphosphoinositides instead of phosphatidylinositol. *The Biochemical Journal*. **(212)**, 849-858.
- Bi, M., Naczki, C., Koritzinsky, M., Fels, D., Blais, J., Hu, N., Harding, H., Novoa, I., Varia, M., Raleigh, J., Scheuner, D., Kaufman, R.J., Bell, J., Ron, D., Wouters, B. G. and Koumenis, C. (2005). ER stress-regulated translation increases tolerance to extreme hypoxia and promotes tumor growth. *The EMBO Journal*. **(24)**, 3470-3481.
- Bitran, J. A., Potter, W. Z., Manji, H. K. and Gusovsky, F. (1990). Chronic Li⁺ attenuates agonist- and phorbol ester-mediated Na⁺/H⁺ antiporter activity in HL-60 cells. *European Journal of Pharmacology*. **(188)**, 193-202.
- Blais, J. D., Addison, C. L., Edge, R., Falls, T., Zhao, H., Wary, H., Koumenis, C., Harding, H. P., Ron, D., Holcik, M. and Bell, J. C. (2006). Perk-Dependent Translational Regulation Promotes Tumor Cell Adaptation and Angiogenesis in Response to Hypoxic Stress. *Molecular and Cellular Biology*. **(26)**, 9517-9532.
- Bloomfield, G., Tanaka, Y., Skelton, J., Ivens, A. and Kay, R. R. (2008). Widespread duplications in the genomes of laboratory stocks of *Dictyostelium discoideum*. *Genome Biology*. **(9)**, R75.
- BNF. (2018). *Migraine Treatment Summary*. Viewed 13 June 2018. <<https://bnf.nice.org.uk/treatment-summary/migraine.html>>.

- Bobrovnikova-Marjon, E., Grigoriadou, C., Pytel, D., Zhang, F., Ye, J., Koumenis, C., Cavener, D. and Diehl, J. A. (2010). PERK promotes cancer cell proliferation and tumor growth by limiting oxidative DNA damage. *Oncogene*. **(29)**, 3881-3895.
- Bodjarian, N., Carpentier, P., Blanchet, G., Baubichon, D. and Lallement, G. (1993). Cholinergic activation of phosphoinositide metabolism during soman-induced seizures. *Neuroreport*. **(4)**, 1191-1193.
- Bouma, P. A., Peters, A. C., Arts, R. J., Stijnen, T. and Van Rossum, J. (1987). Discontinuation of antiepileptic therapy: a prospective study in children. *Journal of Neurology, Neurosurgery, and Psychiatry*. **(50)**, 1579-1583.
- Bourgoin, S. G., Harbour, D and Poubelle, P. E. (1996). Role of protein kinase C alpha, Arf, and cytoplasmic calcium transients in phospholipase D activation by sodium fluoride in osteoblast-like cells. *Journal of Bone and Mineral Research: The Official Journal of the American Society for Bone and Mineral Research*. **(11)**, 1655-1665.
- Brami B.A., Leli, U. and Hauser, G. (1991). Influence of lithium on second messenger accumulation in NG108-15 cells. *Biochemical and Biophysical Research Communications*. **(2)**, 606.
- Brami, B. A., Leli, U. and Hauser, G. (1993). Elevated phosphatidyl-CMP is not the source of diacylglycerol accumulation induced by lithium in NG108-15 cells. *Journal of Neurochemistry*. **(60)**, 1137-1142.
- Brewer, J. W. and Diehl, J. A. (2000). PERK Mediates Cell-Cycle Exit during the Mammalian Unfolded Protein Response. *Proceedings of the National Academy of Sciences of the United States of America*. **(97)**, 12625-12630.
- Brock, D. A. and Gomer, R. H. (1999). A cell-counting factor regulating structure size in *Dictyostelium*. *Genes and Development*. **(13)**, 1960-1969.
- Brodie, M. J. and Sills, G. J. (2011). Combining antiepileptic drugs—rational polytherapy? *Seizure*. **(20)**, 369-375.
- Bruni J., Wilder, B. J., Bauman, A. W. and Willmore, L. J. (1980). Clinical efficacy and long-term effects of valproic acid therapy on spike-and-wave discharges. *Neurology*. **(30)**, 42-46.
- Burgering ,B. M. T. and Coffey, P. J. (1995). Protein kinase B (c-Akt) in phosphatidylinositol-3-OH kinase signal transduction. *Nature*. **(376)**, 599-602.
- Calabrese, J. R. and Delucchi, G. A. (1990). Spectrum of efficacy of valproate in 55 patients with rapid-cycling bipolar disorder. *American Journal of Psychiatry*. **(147)**, 431-434.

- Carman, G. M. and Dougherty, M. (1980). Subcellular localization of Phosphatidylinositol synthase from germinating soybeans. *Journal of Food Biochemistry*. **(4)**, 153-158.
- Carman, J. S. and Wyatt, R. J. (1979). Calcium: bivalent cation in the bivalent psychoses. *Biological Psychiatry*. **(14)**, 295-336.
- Carmant, L., Liu, Z., Werner, S. J., Mikati, M. A. and Holmes, G. L. (1995). Effect of kainic acid-induced status epilepticus on inositol-trisphosphate and seizure-induced brain damage in mature and immature animals. *Developmental Brain Research*. **(89)**, 67-72.
- Carpio, L. C. and Dziak, R. (1998). Phosphatidic acid effects on cytosolic calcium and proliferation in osteoblastic cells. *Prostaglandins, Leukotrienes and Essential Fatty Acids*. **(59)**, 101-109.
- Carraz, G., Fau, R., Chateau, R. and Bonnin, J. (1964). Communication concerning 1st clinical tests of the anticonvulsive activity of N-Dipropylacetic acid (sodium salt). *Annales Médico-Psychologiques*. **(122)**, 577-585.
- Cerbón J., Falcon, A., Hernández-Luna, C. and Segura-Cobos, D. (2005). Inositol phosphoceramide synthase is a regulator of intracellular levels of diacylglycerol and ceramide during the G1 to S transition in *Saccharomyces cerevisiae*. *The Biochemical Journal*. **(388)**, 169-176.
- Chang, P., Augustin, K., Boddum, K., Williams, S., Sun, M., Terschak, J. A., Hardege, J. D., Chen, P. E., Walker, M. C. and Williams, R. S. B. (2016). Seizure control by decanoic acid through direct AMPA receptor inhibition. *Brain: A Journal of Neurology*. **(139)**, 431-443.
- Chang, P., Orabi, B., Deranieh, R. M., Dham, M., Hoeller, O., Shimshoni, J. A., Yagen, B., Bialer, M., Greenberg, M. L., Walker, M. C. and Williams, R. S. B. (2012). The antiepileptic drug valproic acid and other medium-chain fatty acids acutely reduce phosphoinositide levels independently of inositol in *Dictyostelium*. *Disease Models and Mechanisms*. **(5)**, 115-124.
- Chang, P., Terbach, N., Plant, N., Chen, P. E., Walker, M. C. and Williams, R. S. B. (2013). Seizure control by ketogenic diet-associated medium chain fatty acids. *Neuropharmacology*. **(69)**, 105-114.
- Chang, P., Walker, M. C. and Williams, R. S. B. (2014). Seizure-induced reduction in PIP3 levels contributes to seizure-activity and is rescued by valproic acid. *Neurobiology of Disease*. **(62)**, 296-306.

- Chang, P., Zuckermann, A. M. E., Williams, S., Close, A. J., Cano-Jaimez, M., McEvoy, J. P., Spencer, J., Walker, M. C. and Williams, R. S. B. (2015). Seizure control by derivatives of medium chain fatty acids associated with the ketogenic diet show novel branching-point structure for enhanced potency. *The Journal of Pharmacology and Experimental Therapeutics*. **(352)**, 43-52.
- Chang, R., Chou, M., Hung, L., Wang, M., Hsu, M. and Chiu, C. (2016). Study of Valproic Acid-Enhanced Hepatocyte Steatosis. *BioMed Research International*. **(2016)**, 9576503.
- Chen, G., Manji, H. K., Hawver, D. B., Wright, C. B. and Potter, W. Z. (1994). Chronic sodium valproate selectively decreases protein kinase C alpha and epsilon in vitro. *Journal of Neurochemistry*. **(63)**, 2361-2364.
- Cipriani, A., Saunders, K., Attenburrow, M. J., Stefaniak, J., Panchal, P., Stockton, S., Lane, T. A., Tunbridge, E. M., Geddes, J. R. and Harrison, P. J. (2016). A systematic review of calcium channel antagonists in bipolar disorder and some considerations for their future development. *Molecular Psychiatry*. **(21)**, 1324-1332.
- Cole, R. A. and Williams, K. L. (1994). The *Dictyostelium discoideum* mitochondrial genome: a primordial system using the universal code and encoding hydrophilic proteins atypical of metazoan mitochondrial DNA. *Journal of Molecular Evolution*. **(39)**, 579-588.
- Corazzi, L., Piccinin, G. L., Marku, N. and Arienti, G. (1986). Cerebellar metabolism of phosphatidylcholine and its hydrosoluble precursors during bicuculline-induced convulsive seizures. *Neurochemical Research*. **(11)**, 401-406.
- Coudé, F. X., Grimmer, G., Pelet, A. and Benoit, Y. (1983). Action of the antiepileptic drug, valproic acid, on fatty acid oxidation in isolated rat hepatocytes. *Biochemical and Biophysical Research Communications*. **(115)**, 730-736.
- Couto, C. A., Wang, H. Y., Green, J. C. A., Kiely, R., Siddaway, R., Borer, C., Pears, C. J. and Lakin, N. D. (2011). PARP regulates nonhomologous end joining through retention of Ku at double-strand breaks. *The Journal of Cell Biology*. **(194)**, 367-375.
- Cunliffe, V. T., Baines, R. A., Giachello, C. N. G., Lin, W. H., Morgan, A., Reuber, M., Russell, C., Walker, M. C. and Williams, R. S. B. (2014). Epilepsy research methods update: Understanding the causes of epileptic seizures and identifying new treatments using non-mammalian model organisms. *Seizure*. **(24)**, 44-51.
- D'Souza, K., Kim, Y. J., Balla, T. and Epand, R. M. (2014). Distinct properties of the two isoforms of CDP-diacylglycerol synthase. *Biochemistry*. **(53)**, 7358-7367.

- Dahlqvist, A., Stahl, U., Lenman, M., Banas, A., Lee, M., Sandager, L., Ronne, H. and Stymne, S. (2000). Phospholipid:diacylglycerol Acyltransferase: An Enzyme That Catalyzes the Acyl-CoA-Independent Formation of Triacylglycerol in Yeast and Plants. *Proceedings of the National Academy of Sciences of the United States of America*. **(97)**, 6487-6492.
- Davidson, A. J., King, J. S. and Insall, R. H. (2013). The use of streptavidin conjugates as immunoblot loading controls and mitochondrial markers for use with *Dictyostelium discoideum*. *Biotechniques*. **(55)**, 39-41.
- Davis, R., Peters, D. H. and McTavish, D. (1994). Valproic acid. A reappraisal of its pharmacological properties and clinical efficacy in epilepsy. *Drugs*. **(47)**, 332-372.
- De Abreu, L. N., Lafer, B., Baca-Garcia, E. and Oquendo, M. A. (2009). Suicidal ideation and suicide attempts in bipolar disorder type I: an update for the clinician. *Revista Brasileira De Psiquiatria*. **(31)**, 271-280.
- De Fusco, M., Marconi, R., Silvestri, L., Atorino, L., Rampoldi, L., Morgante, L., Ballabio, A., Aridon, P. and Casari, G. (2003). Haploinsufficiency of ATP1A2 encoding the Na⁺/K⁺ pump alpha2 subunit associated with familial hemiplegic migraine type 2. *Nature Genetics*. **(33)**, 192-196.
- De La Roche, M. A., Smith, J. L., Rico, M., Carrasco, S., Merida, I., Licate, L., Côté, G. P. and Egelhoff, T. T. (2002). *Dictyostelium discoideum* has a single diacylglycerol kinase gene with similarity to mammalian theta isoforms. *The Biochemical Journal*. **(368)**, 809-815.
- Deguchi, A., Segawa, K., Hosaka, K., Weinstein, I. B. and Umezawa, K. (2002). Overexpression of Phosphatidylinositol Synthase Enhances Growth and G1 Progression in NIH3T3 cells. *Japanese Journal of Cancer Research*. **(93)**, 157-166.
- Dichgans, M., Freilinger, T., Eckstein, G., Babini, E., Lorenz-Depiereux, B., Biskup, S., Ferrari, M. D., Herzog, J., van den Maagdenberg, A. M., Pusch, M. and Strom, T. M. (2005). Mutation in the neuronal voltage-gated sodium channel SCN1A in familial hemiplegic migraine. *The Lancet*. **(366)**, 371-377.
- Dilsaver, S. C. (2010). An estimate of the minimum economic burden of bipolar I and II disorders in the United States: 2009. *Journal of Affective Disorders*. **(129)**, 79-83.
- Drayer, A. L., Van der Kaay, J., Mayr, G. W. and van Haastert, P. J. M. (1994). Role of phospholipase C in Dictyostelium: Formation of inositol 1,4,5-trisphosphate and normal development in cells lacking phospholipase C activity. *The EMBO Journal*. **(13)**, 1601-1609.

- Drummond, A. H. and Raeburn, C. A. (1984). The interaction of lithium with thyrotropin-releasing hormone-stimulated lipid metabolism in GH3 pituitary tumour cells. Enhancement of stimulated 1,2-diacylglycerol formation. *The Biochemical Journal*. **(244)**, 129-136.
- Dubovsky, S. L., Christiano, J., Daniell, L. C., Franks, R. D., Murphy, J., Adler, L., Baker, N. and Harris, R. A. (1989). Increased platelet intracellular calcium concentration in patients with bipolar affective disorders. *Archives of General Psychiatry*. **(46)**, 632-638.
- Dulyaninova, N. G., House, R. P., Betapudi, V. and Bresnick, A. R. (2007). Myosin-IIA heavy-chain phosphorylation regulates the motility of MDA-MB-231 carcinoma cells. *Molecular Biology of the Cell*. **(18)**, 3144-3155.
- Dwyer, J. R., Donkor, J., Zhang, P., Csaki, L. S., Vergnes, L., Lee, J. M., Dewald, J., Brindley, D. N., Atti, E., Tetradis, S., Yoshinaga, Y., De Jong, P. J., Fong, L. G., Young, S. G. and Reue, K. (2012). Mouse lipin-1 and lipin-2 cooperate to maintain glycerolipid homeostasis in liver and aging cerebellum. *Proceedings of the National Academy of Sciences*. **(109)**, e2495.
- Ehninger, D., Han, S., Shilyansky, C., Zhou, Y., Li, W., Kwiatkowski, D. J., Ramesh V. and Silva, A. J., (2008). Reversal of learning deficits in a Tsc2 +/- mouse model of tuberous sclerosis. *Nature Medicine*. **(14)**, 843-848.
- Eichinger, L., Pachebat, J.A., Glöckner, G., Rajandream, M. A., Sucgang, R., Berriman, M., Song, J., Olsen, R., Szafranski, K., Xu, Q., Tunggal, B., Kummerfeld, S., Madera, M., Konfortov, B. A., Rivero, F., Bankier, A. T., Lehmann, R., Hamlin, N., Davies, R., Gaudet, P., Fey, P., Pilcher, K., Chen, G., Saunders, D., Sodergren, E., Davies, P., Kerhornou, A., Nie, X., Hall, N., Anjard, C., Hemphill, L., Bason, N., Farbrother, P., Desany, B., Just, E., Morio, T., Rost, R., Churcher, C., Cooper, J., Haydock, S., van Driessche, N., Cronin, A., Goodhead, I., Muzny, D., Mourier, T., Pain, A., Lu, M., Harper, D., Lindsay, R., Hauser, H., James, K., Quiles, M., Madan, Dabu, M., Saito, T., Buchriesser, C., Wardroper, A., DFelder, M., Thangavelu, M., Johnson, D., Knights, A., Loulseged, H., Mungall, K., Oliver, K., Price, C., Quail, M. A., Urushihara, H., Hernandez, J., Rabinowitsch, E., Steffen, D., Sanders, M., Ma, J., Kohara, Y., Sharp, S., Simmonds, M., Spiegler, S., Tivory, A., Sugano, S., White, B., Walker, S., Woodward, J., Winckler, T., Tanaka, Y., Shaulsky, G., Schleicher, M., Weinstock, G., Rosenthal, A., Cox, E. C., Chisholm, R. L., Gibbs, R., Loomis, W. F., Platzer, M., Kay, R. R., Williams, J., Dear, P. H., Noegel, A. A., Barrell, B. and Kuspa, A. (2005). The genome of the social amoeba *Dictyostelium discoideum*. *Nature*. **(435)**, 43-57.

- Eickholt, B. J., Towers, G. J., Ryves, W. J., Eikel, D., Adley, K., Ylinen, L. M. J., Chadborn, N. H., Harwood, A. J., Nau, H. and Williams, R. S. B. (2005). Effects of valproic acid derivatives on inositol trisphosphate depletion, teratogenicity, glycogen synthase kinase-3 β inhibition, and viral replication: a screening approach for new bipolar disorder drugs derived from the valproic acid core structure. *Molecular Pharmacology*. **(67)**, 1426-1433.
- Elphick, L. M., Pawolleck, N., Guschina, I. A., Chaieb, L., Eikel, D., Nau, H., Harwood, J. L., Plant, N. J. and Williams, R. S. B. (2012). Conserved valproic-acid-induced lipid droplet formation in *Dictyostelium* and human hepatocytes identifies structurally active compounds. *Disease Models and Mechanisms*. **(5)**, 231-240.
- Emrich, H. M., von Zerssen, D., Kissling, W., Möller, H. J. and Windorfer, A. (1980). Effect of sodium valproate on mania. The GABA-hypothesis of affective disorders. *Archiv Für Psychiatrie Und Nervenkrankheiten*. **(299)**, 1-16.
- Escalante, R. and Vicente, J. J. (2000). *Dictyostelium discoideum*: a model system for differentiation and patterning. *The International Journal of Developmental Biology*. **(44)**, 819-835.
- Faix, J., Kreppel, L., Shaulsky, G., Schleicher, M. and Kimmel, A. R. (2004). A rapid and efficient method to generate multiple gene disruptions in *Dictyostelium discoideum* using a single selectable marker and the Cre-loxP system. *Nucleic Acids Research*. **(32)**, e143.
- Falkenburger, B. H., Jensen, J. B., Dickson, E. J., Suh, B. C. and Hille, B. (2010). Phosphoinositides: lipid regulators of membrane proteins. *The Journal of Physiology*. **(588)**, 3179-3185.
- Fantl, W. J., Escobedo, J. A., Martin, G. A., Turck, C. W., del Rosario, M., McCormick, F. and Williams, L. T. (1992). Distinct phosphotyrosines on a growth factor receptor bind to specific molecules that mediate different signaling pathways. *Cell*. **(69)**, 413-423.
- Farese, R. V., DiMarco, P. E., Barnes, D. E., Sabir, M. A., Larson, R. E., Davis, J. S. and Morrison, A. D. (1986). Rapid glucose-dependent increases in phosphatidic acid and phosphoinositides in rat pancreatic islets. *Endocrinology*. **(118)**, 1498-1503.
- Favel, P., Cartier, J., Gratadou, J. P. and Gratadou, G. (1973). Depamide in the treatment of epilepsy. A clinical trial. *Epilepsia*. **(14)**, 329-334.
- Ferrari, C. M., de Sousa, R. M., Castro, L. H.M, (2013). Factors associated with treatment non-adherence in patients with epilepsy in Brazil. *Seizure*. **(22)**, 384-389.

- Fey, P., Dodson, R. J., Basu, S. and Chisholm, R. L. (2013). One stop shop for everything *Dictyostelium*: dictyBase and the Dicty Stock Center in 2012. *Methods in Molecular Biology*. **(983)**, 59-92.
- Fischl, A. S., Homann, M. J., Poole, M. A. and Carman, G. M. (1986). Phosphatidylinositol synthase from *Saccharomyces cerevisiae*. Reconstitution, characterization, and regulation of activity. *The Journal of Biological Chemistry*. **(261)**, 3178-3183.
- Flint, A. P., Leat, W. M., Sheldrick, E. L. and Stewart, H. J. (1986). Stimulation of phosphoinositide hydrolysis by oxytocin and the mechanism by which oxytocin controls prostaglandin synthesis in the ovine endometrium. *The Biochemical Journal*. **(237)**, 797-805.
- Forsgren, L., Beghi, E., Öun, A. and Sillanpää, M. (2005). The epidemiology of epilepsy in Europe – a systematic review. *European Journal of Neurology*. **(12)**, 245-253.
- Franke, T. F., Yang, S., Chan, T. O., Datta, K., Kazlauskas, A., Morrison, D. K., Kaplan, D. R. and Tsichlis, P. N. (1995). The protein kinase encoded by the Akt proto-oncogene is a target of the PDGF-activated phosphatidylinositol 3-kinase. *Cell*. **(81)**, 727-736.
- Freeman, T. W., Clothier, J. L., Pazzaglia, P., Lesem, M. D. and Swann, A. C. (1992). A double-blind comparison of valproate and lithium in the treatment of acute mania. *American Journal of Psychiatry*. **(149)**, 108-111.
- Frej, A. D., Clark, J., Le Roy, C. I., Lilla, S., Thomason, P. A., Otto, G. P., Churchill, G., Insall, R. H., Claus, S. P., Hawkins, P., Stephens, L. and Williams, R. S. B. (2016). The inositol-3-phosphate synthase biosynthetic enzyme has distinct catalytic and metabolic roles. *Molecular and Cellular Biology*. **(36)**, 1464-1479.
- Friedrich, M., Meier, D., Schuster, I. and Nellen, W. (2015) A simple retroelement based knock-down system in *Dictyostelium*: further insights into RNA interference mechanisms. *PLoS One*. **(10)**, e0131271.
- Fry, M. and Green, D. E. (1981). Cardiolipin requirement for electron transfer in complex I and III of the mitochondrial respiratory chain. *The Journal of Biological Chemistry*. **(256)**, 1874-1880.
- Fukami, K. and Takenawa, T. (1992). Phosphatidic acid that accumulates in platelet-derived growth factor-stimulated Balb/c 3T3 cells is a potential mitogenic signal. *The Journal of Biological Chemistry*. **(267)**, 10988-10993.
- Fukui, Y., (1990). Actomyosin organization in mitotic *Dictyostelium* amoebae. *Annals of the New York Academy of Sciences*. **(582)**, 156-165.

- Ganong, B. R. and Raetz, C. R. (1982). Massive accumulation of phosphatidic acid in conditionally lethal CDP-diglyceride synthetase mutants and cytidine auxotrophs of *Escherichia coli*. *The Journal of Biological Chemistry*. **(257)**, 389-394.
- Ge, L., Melville, D., Zhang, M. and Schekman, R. (2013). The ER-Golgi intermediate compartment is a key membrane source for the LC3 lipidation step of autophagosome biogenesis. *eLife*. **(2)**, e00947.
- Geddes, J. R. and Miklowitz, D. J. (2013). Treatment of bipolar disorder. *The Lancet*. **(381)**, 1672-1682.
- Gibellini, F. and Smith, T. K. (2010). The Kennedy pathway--De novo synthesis of phosphatidylethanolamine and phosphatidylcholine. *IUBMB Life*. **(62)**, 414-428.
- Godin, Y., Heiner, L., Mark, J. and Mandel, P. (1969). Effects of DI-n-propylacetate, and anticonvulsive compound, on GABA metabolism. *Journal of Neurochemistry*. **(16)**, 869-873.
- Göttlicher, M., Minucci, S., Zhu, P., Krämer, O. H., Schimpf, A., Giavara, S., Sleeman, J. P., Lo Coco, F., Nervi, C., Pelicci, P. G. and Heinzl, T. (2001). Valproic acid defines a novel class of HDAC inhibitors inducing differentiation of transformed cells. *The EMBO Journal*. **(20)**, 6969-6978.
- Granneman, G. R., Wang, S. I., Kesterson, J. W. and Machinist, J. M. (1984). The hepatotoxicity of valproic acid and its metabolites in rats. II. Intermediary and valproic acid metabolism. *Hepatology*. **(4)**, 1153-1158.
- Gustavsson, A., Svensson, M., Jacobi, F., Allgulander, C., Alonso, J., Beghi, E., Dodel, R., Ekman, M., Faravelli, C., Fratiglioni, L., Gannon, B., Jones, D H., Jennum, P., Jordanova, A., Jönsson, L., Karampampa, K., Knapp, M., Kobelt, G., Kurth, T., Lieb, R., Linde, M., Ljungcrantz, C., Maercker, A., Melin, B., Moscarelli, M., Musayev, A., Norwood, F., Preisig, M., Pugliatti, M., Rehm, J., Salvador-Carulla, L., Schlehofer, B., Simon, R., Steinhausen, H. C., Stovner, L. J., Vallat, J. M., van den Bergh, P., van Os, J., Vos, P., Xu, W., Wittchen, H. U., Jönsson, B., and Olesen, J. (2011). Cost of disorders of the brain in Europe 2010. *European Neuropsychopharmacology*. **(21)**, 718-779.
- Hahn, C. G. and Friedman, E. (1999). Abnormalities in protein kinase C signaling and the pathophysiology of bipolar disorder. *Bipolar Disorders*. **(1)**, 81-86.
- Haidukewych, D., Forsythe, W. I. and Sills, M. (1982). Monitoring octanoic and decanoic acids in plasma from children with intractable epilepsy treated with medium-chain triglyceride diet. *Clinical Chemistry*. **(28)**, 642-645.
- Hamasaki, M., Furuta, N., Matsuda, A., Nezu, A., Yamamoto, A., Fujita, N., Oomori, H., Noda, T., Haraguchi, T., Hiraoka, Y., Amano, A. and Yoshimori, T. (2013).

- Autophagosomes form at ER-mitochondria contact sites. *Nature*. **(495)**, 389-393.
- Han, G. S., O'Hara, L., Carman, G. M. and Siniossoglou, S. (2008). An Unconventional Diacylglycerol Kinase That Regulates Phospholipid Synthesis and Nuclear Membrane Growth. *The Journal of Biological Chemistry*. **(283)**, 20433-20442.
- Hara, H., Yonezawa, K., Sakaue, H., Ando, A., Kotani, K., Kitamura, T., Kitamura, Y., Ueda, H., Stephens, L., Jackson, T. R., Waterfield, M. D. and Kasuga, M. (1994). 1-Phosphatidylinositol 3-Kinase Activity is Required for Insulin-Stimulated Glucose Transport But not for RAS Activation in CHO Cells. *Proceedings of the National Academy of Sciences of the United States of America*. **(91)**, 7415-7419.
- Haroon, A., Tripathi, M., Khanam, R. and Vohora, D. (2012). Antiepileptic drugs prescription utilization behavior and direct costs of treatment in a national hospital of India. *Annals of Indian Academy of Neurology*. **(15)**, 289-293.
- Hauck, R. S. and Nau, H. (1989). Asymmetric synthesis and enantioselective teratogenicity of 2- n-propyl-4-pentenoic acid (4-en-VPA), an active metabolite of the anticonvulsant drug, valproic acid. *Toxicology Letters*. **(49)**, 41-48.
- Headache Classification Committee of the International Headache Society, (IHS), (2013). The International Classification of Headache Disorders, 3rd edition (beta version). *Cephalalgia*. **(33)**, 629-808.
- Heid, P.J., Wessels, D., Daniels, K .J., Gibson, D .P., Zhang, H., Voss, E. and Soll, D. R. (2004). The role of myosin heavy chain phosphorylation in Dictyostelium motility, chemotaxis and F-actin localization. *Journal of Cell Science*. **(117)**, 4819-4835.
- Henneberry, A. L. and McMaster, C. R. (1999). Cloning and expression of a human choline/ethanolaminephosphotransferase: synthesis of phosphatidylcholine and phosphatidylethanolamine. *The Biochemical Journal*. **(339)**, 291-298.
- Henry, S. A., Kohlwein, S. D. and Carman, G. M. (2012). Metabolism and regulation of glycerolipids in the yeast *Saccharomyces cerevisiae*. *Genetics*. **(190)**, 317-349.
- Hering, R. and Kuritzky, A. (1992). Sodium Valproate in The Prophylactic Treatment of Migraine: A Double-Blind Study Versus Placebo. *Cephalalgia*. **(12)**, 81-84.
- Hoeller, O. and Kay, R. R. (2007). Chemotaxis in the Absence of PIP3 Gradients. *Current Biology*. **(17)**, 813-817.
- Hogan, A., Shepherd, L., Chabot, J., Quenneville, S., Prescott, S. M., Topham, M. K. and Gee, S. H. (2001). Interaction of gamma 1-syntrophin with diacylglycerol kinase-zeta. Regulation of nuclear localization by PDZ interactions. *The Journal of Biological Chemistry*. **(276)**, 26526-26533.

- Holmes, K. H., Bilkey, D. K., Laverty, R. and Goddard, G. V. (1990). The N-methyl-D-aspartate antagonists aminophosphonovalerate and carboxypiperazinephosphonate retard the development and expression of kindled seizures. *Brain Research*. **(506)**, 227-235.
- Houssa, B., de Widt, J., Kranenburg, O., Moolenaar, W. H. and van Blitterswijk, W. J. (1999). Diacylglycerol kinase theta binds to and is negatively regulated by active RhoA. *The Journal of Biological Chemistry*. **(274)**, 6820-6822.
- Hozumi, Y., Watanabe, M., Otani, K. and Goto, K. (2009). Diacylglycerol kinase beta promotes dendritic outgrowth and spine maturation in developing hippocampal neurons. *BMC Neuroscience*. **(10)**, 99.
- Huffman, T. A., Mothe-Satney, I. and Lawrence, J. C. (2002). Insulin-stimulated phosphorylation of lipin mediated by the mammalian target of rapamycin. *Proceedings of the National Academy of Sciences of the United States of America*. **(99)**, 1047-1052.
- Illingworth, J. L., Watson, P. and Ring, H. (2014). Why do seizures occur when they do? Situations perceived to be associated with increased or decreased seizure likelihood in people with epilepsy and intellectual disability. *Epilepsy and Behavior*. **(39)**, 78-84.
- Ishisaka, M., Tsuruma, K., Shimazawa, M., Shirai, Y., Saito, N. and Hara, H. (2013). Increased Seizure Susceptibility in a Mouse with Diacylglycerol Kinase β Deficiency. *Neuroscience and Medicine*. **(4)**, 117-122.
- Jarman, K. E., Moretti, P. A. B., Zebol, J. R. and Pitson, S. M. (2010). Translocation of Sphingosine Kinase 1 to the Plasma Membrane Is Mediated by Calcium- and Integrin-binding Protein 1. *The Journal of Biological Chemistry*. **(285)**, 483-492.
- Jaworski, J., Spangler, S., Seeburg, D. P., Hoogenraad, C. C. and Sheng, M. (2005). Control of Dendritic Arborization by the Phosphoinositide-3'-Kinase-Akt-Mammalian Target of Rapamycin Pathway. *Journal of Neuroscience*. **(25)**, 11300-11312.
- Jean, S. and Kiger, A. A. (2014). Classes of phosphoinositide 3-kinases at a glance. *Journal of Cell Science*. **(127)**, 923-928.
- Jidda, M. S., Rabbebe, I. B., Wakil, M. A., Mohammed, A. O., Abdulmalik, J. O. and Bello, S.O. (2010). An investigation into the genetic relationship between bipolar affective disorder and (idiopathic) epilepsy in a sub-saharan African population. *Journal of Affective Disorders*. **(122)**, S70.

- Ju, S. and Greenberg, M. L. (2003). Valproate disrupts regulation of inositol responsive genes and alters regulation of phospholipid biosynthesis. *Molecular Microbiology*. **(49)**, 1595-1604.
- Kahali, S., Sarcar, B., Fang, B., Williams, E. S., Koomen, J. M., Tofilon, P. J. and Chinnaiyan, P. (2010). Activation of the Unfolded Protein Response Contributes toward the Antitumor Activity of Vorinostat. *Neoplasia*. **(12)**, 80-86.
- Takefuda, K., Oyagi, A., Ishisaka, M., Tsuruma, K., Shimazawa, M., Yokota, K., Shirai, Y., Horie, K., Saito, N., Takeda, J. and Hara, H. (2010). Diacylglycerol Kinase β Knockout Mice Exhibit Lithium-Sensitive Behavioral Abnormalities. *PLoS One*. **(5)**, e13447.
- Kamer, K. J., Grabarek, Z. and Mootha, V. K. (2017). High-affinity cooperative Ca^{2+} binding by MICU1–MICU2 serves as an on–off switch for the uniporter. *EMBO Reports*. **(18)**, 1397-1411.
- Kanfer, J. and Kennedy, E. P. (1964). Metabolism and function of bacterial lipids. II. Biosynthesis of phospholipids in *Escherichia coli*. *The Journal of Biological Chemistry*. **(239)**, 1720-1726.
- Kanner, A. M., (2003). The Pharmacology of Parenteral Valproate. *Epilepsy Currents*. **(3)**, 109-111.
- Kaszkis, M., Richards, J. and Kinzel, V. (1992). Proposed Role of Phosphatidic Acid in the Extracellular Control of the Transition from G2 Phase to Mitosis Exerted by Epidermal Growth Factor in A431 Cells. *Cancer Research*. **(52)**, 5627-5634.
- Katz, J. and Wood, H. G. (1960). The use of glucose-C14 for the evaluation of the pathways of glucose metabolism. *The Journal of Biological Chemistry*. **(235)**, 2165-2177.
- Kawase, T. and Suzuki, A. (1990). Initial responses of a clonal osteoblast-like cell line, MOB 3–4, to phosphatidic acid *in vitro*. *Bone and Mineral*. **(10)**, 61-70.
- Keizer-Gunnink, I., Kortholt, A. and van Haastert, P. J. M. (2007). Chemoattractants and chemorepellents act by inducing opposite polarity in phospholipase C and PI3-kinase signaling. *Journal of Cell Biology*. **(177)**, 579-585.
- Kelly, K. M. and Chung, S. S. (2011). Surgical treatment for refractory epilepsy: review of patient evaluation and surgical options. *Epilepsy Research and Treatment*. **(2011)**, 303624.
- Kelly, K. M., Gross, R. A. and Macdonald, R. L. (1990). Valproic acid selectively reduces the low-threshold (T) calcium current in rat nodose neurons. *Neuroscience Letters*. **(116)**, 233-238.

- Kennedy, E. P. and Weiss, S. B. (1956). The function of cytidine coenzymes in the biosynthesis of phospholipides. *The Journal of Biological Chemistry*. **(222)**, 193-214.
- Kesterson, J. W., Granneman, G. R. and Machinist, J. M. (1984). The hepatotoxicity of valproic acid and its metabolites in rats. I. Toxicologic, biochemical and histopathologic studies. *Hepatology*. **(4)**, 1143-1152.
- Kim, D., Jun, K. S., Lee, S. B., Kang, N. G., Min, D. S., Kim, Y. H., Ryu, S. H., Suh, P. G. and Shin, H. S. (1997). Phospholipase C isozymes selectively couple to specific neurotransmitter receptors. *Nature*. **(389)**, 290-293.
- Kim, H., Jo, S., Park, K. W., Han, S. H. and Lee, S. A. (2016). A Case of Phenytoin-induced Rhabdomyolysis in Status Epilepticus. *Journal of Epilepsy Research*. **(6)**, 36-38.
- Kishimoto, A., Takai, Y., Mori, T., Kikkawa, U. and Nishizuka, Y. (1980). Activation of calcium and phospholipid-dependent protein kinase by diacylglycerol, its possible relation to phosphatidylinositol turnover. *The Journal of Biological Chemistry*. **(255)**, 2273-2276.
- Kiyasu, J. Y., Pieringer, R. A., Paulus, H. and Kennedy, E. P. (1963). The biosynthesis of phosphatidylglycerol. *The Journal of Biological Chemistry*. **(238)**, 2293-2298.
- Kortholt, A., Kataria, R., Keizer-Gunnink, I., van Egmond, W. N., Khanna, A. and van Haastert, P. J. M. (2011). *Dictyostelium* chemotaxis: essential Ras activation and accessory signalling pathways for amplification. *EMBO Reports*. **(12)**, 1273-1279.
- Kuchler, K., Daum, G. and Paltauf, F. (1986). Subcellular and submitochondrial localization of phospholipid-synthesizing enzymes in *Saccharomyces cerevisiae*. *Journal of Bacteriology*. **(165)**, 901-910.
- Kumar, S., Stecher, G. and Tamura, K. (2016). MEGA7: Molecular Evolutionary Genetics Analysis Version 7.0 for Bigger Datasets. *Molecular Biology and Evolution*. **(33)**, 1870-1874.
- Kumar, V., Zhang, M., Swank, M. W., Kunz, J. and Wu, G. Y. (2005). Regulation of Dendritic Morphogenesis by Ras-PI3K-Akt-mTOR and Ras-MAPK Signaling Pathways. *Journal of Neuroscience*. **(25)**, 11288-11299.
- Kume, A., Kawase, K., Komenoi, S., Usuki, T., Takeshita, E., Sakai, H. and Sakane, F. (2016). The Pleckstrin Homology Domain of Diacylglycerol Kinase η Strongly and Selectively Binds to Phosphatidylinositol 4,5-Bisphosphate. *The Journal of Biological Chemistry*. **(291)**, 8150-8161.
- Kurian, M. A., Meyer, E., Vassallo, G., Morgan, N. V., Prakash, N., Pasha, S., Hai, N. A., Shuib, S., Rahman, F., Wassmer, E., Cross, J. H., O'Callaghan, F. J., Osborne,

- J. P., Scheffer, I. E., Gissen, P. and Maher, E. R. (2010). Phospholipase C beta 1 deficiency is associated with early-onset epileptic encephalopathy. *Brain : A Journal of Neurology*. **(133)**, 2964-2970.
- Kuspa, A. and Loomis, W. F. (1996). Ordered Yeast Artificial Chromosome Clones Representing the Dictyostelium discoideum Genome. *Proceedings of the National Academy of Sciences of the United States of America*. **(93)**, 5562-5566.
- Kwon, O. and Park, S. (2014). Depression and Anxiety in People with Epilepsy. *Journal of Clinical Neurology*. **(10)**, 175-188.
- Lampen, A., Siehler, S., Ellerbeck, U., Göttlicher, M. and Nau, H. (1999). New Molecular Bioassays for the Estimation of the Teratogenic Potency of Valproic Acid Derivatives in Vitro: Activation of the Peroxisomal Proliferator-Activated Receptor (PPAR δ). *Toxicology and Applied Pharmacology*. **(160)**, 238-249.
- Leach, N. T., Sun, Y., Michaud, S., Zheng, Y., Ligon, K. L., Ligon, A. H., Sander, T., Korf, B. R., Lu, W., Harris, D. J., Gusella, J. F., Maas, R. L., Quade, B. J., Cole, A. J., Kelz, M. B. and Morton, C. C. (2007). Disruption of Diacylglycerol Kinase Delta (DGKD) Associated with Seizures in Humans and Mice. *The American Journal of Human Genetics*. **(80)**, 792-799.
- Lecocq, J. and Ballou, C. E. (1964). On the structure of cardiolipin. *Biochemistry*. **(3)**, 976-980.
- Lee, D. C., Gladwell, D., Hatswell, A. J., Porter, J., Brereton, N., Tate, E. and Saunders, A. L. (2014). A comparison of the cost-effectiveness of treatment of prolonged acute convulsive epileptic seizures in children across Europe. *Health Economics Review*. **(4)**, 1-15.
- Lee, D., Kim, E. and Tanaka-Yamamoto, K. (2016). Diacylglycerol Kinases in the Coordination of Synaptic Plasticity. *Frontiers in Cell and Developmental Biology*. **(4)**, 92.
- Lilley, A.C., Major, L., Young, S., Stark, M. J. R. and Smith, T. K. (2014). The essential roles of cytidine diphosphate-diacylglycerol synthase in bloodstream form *Trypanosoma brucei*. *Molecular Microbiology*. **(92)**, 453-470.
- Lipton, R. B., Stewart, W. F., Diamond, S., Diamond, M. L. and Reed, M. (2001). Prevalence and Burden of Migraine in the United States: Data From the American Migraine Study II. *Headache: The Journal of Head and Face Pain*. **(41)**, 646-657.
- Liu, Y., Wang, W., Shui, G. and Huang, X. (2014). CDP-diacylglycerol synthetase coordinates cell growth and fat storage through phosphatidylinositol metabolism and the insulin pathway. *PLoS Genetics*. **(10)**, e1004172.

- Löfke, C., Ischebeck, T., König, S., Freitag, S. and Heilmann, I. (2008). Alternative metabolic fates of phosphatidylinositol produced by phosphatidylinositol synthase isoforms in *Arabidopsis thaliana*. *The Biochemical Journal*. **(413)**, 115-124.
- Ludtmann, M. H. R., Boeckeler, K. and Williams, R. S. B. (2011). Molecular pharmacology in a simple model system: Implicating MAP kinase and phosphoinositide signalling in bipolar disorder. *Seminars in Cell and Developmental Biology*. **(22)**, 105-113.
- Lumley, E. C., Osborn, A. R., Scott, J. E., Scholl, A. G., Mercado, V., McMahan, Y. T., Coffman, Z. G. and Brewster, J. L. (2017). Moderate endoplasmic reticulum stress activates a PERK and p38-dependent apoptosis. *Cell Stress and Chaperones*. **(22)**, 43-54.
- Lung, M., Shulga, Y. V., Ivanova, P. T., Myers, D. S., Milne, S. B., Brown, H. A., Topham, M. K. and Epand, R. M. (2009). Diacylglycerol kinase epsilon is selective for both acyl chains of phosphatidic acid or diacylglycerol. *The Journal of Biological Chemistry*. **(284)**, 31062-31073.
- Lykidis, A., Jackson, P. D., Rock, C. O. and Jackowski, S. (1997). The Role of CDP-Diacylglycerol Synthetase and Phosphatidylinositol Synthase Activity Levels in the Regulation of Cellular Phosphatidylinositol Content. *The Journal of Biological Chemistry*. **(272)**, 33402-33409.
- Ma, W. N., Park, S. Y. and Han, J. S. (2010). Role of phospholipase D1 in glucose-induced insulin secretion in pancreatic beta cells. *Experimental and Molecular Medicine*. **(42)**, 456-464.
- Mahmood, F., Mozere, M., Zdebik, A. A., Stanescu, H. C., Tobin, J., Beales, P. L., Kleta, R., Bockenhauer, D. and Russell, C. (2013). Generation and validation of a zebrafish model of EAST (epilepsy, ataxia, sensorineural deafness and tubulopathy) syndrome. *Disease Models and Mechanisms*. **(6)**, 652-660.
- Mann, B. S., Johnson, J. R., Cohen, M. H., Justice, R. and Pazdur, R. (2007). FDA approval summary: vorinostat for treatment of advanced primary cutaneous T-cell lymphoma. *The Oncologist*. **(12)**, 1247-1252.
- Marku, N., Corazzi, L., Piccinin, G. L. and Arienti, G. (1987). Cerebellar metabolism of phosphatidylethanolamine and its water-soluble precursors during bicuculline-induced convulsive seizures. *Neurochemical Research*. **(12)**, 341-344.
- Martin, K. L. and Smith, T. K. (2006). Phosphatidylinositol synthesis is essential in bloodstream form *Trypanosoma brucei*. *The Biochemical Journal*. **(396)**, 287-295.
- Mato, J. M. and Marin-Cao, D. (1979). Protein and Phospholipid Methylation during Chemotaxis in Dictyostelium discoideum and Its Relationship to Calcium

- Movements. *Proceedings of the National Academy of Sciences of the United States of America*. **(76)**, 6106-6109.
- Mato, J. M., Krens, F. A., van Haastert, P. J. M. and Konijn, T. M. (1977). 3':5'-Cyclic AMP-Dependent 3':5'-Cyclic GMP Accumulation in *Dictyostelium discoideum*. *Proceedings of the National Academy of Sciences of the United States of America*. **(74)**, 2348-2351.
- Matsuzawa, Y. and Hostetler, K. Y. (1980). Studies on drug-induced lipidoses: subcellular localization of phospholipid and cholesterol in the liver of rats treated with chloroquine or 4,4'-bis (diethylaminoethoxy)alpha, beta-diethyldiphenylethane. *Journal of Lipid Research*. **(21)**, 202-214.
- McGuffin, P., Rijsdijk, F., Andrew, M., Sham, P., Katz, R. and Cardno, A. (2003). The Heritability of Bipolar Affective Disorder and the Genetic Relationship to Unipolar Depression. *Archives of General Psychiatry*. **(60)**, 497-502.
- Meijer, I. A., Sasarman, F., Maftai, C., Rossignol, E., Vanasse, M., Major, P., Mitchell, G. A. and Brunel-Guitton, C. (2015). LPIN1 deficiency with severe recurrent rhabdomyolysis and persistent elevation of creatine kinase levels due to chromosome 2 maternal isodisomy. *Molecular Genetics and Metabolism Reports*. **(5)**, 85-88.
- Meikle, L., Pollizzi, K., Egnor, A., Kramvis, I., Lane, H., Sahin, M. and Kwiatkowski, D. J. (2008). Response of a neuronal model of tuberous sclerosis to mammalian target of rapamycin (mTOR) inhibitors: effects on mTORC1 and Akt signaling lead to improved survival and function. *Journal of Neuroscience*. **(28)**, 5422-5432.
- Merikangas, K. R., Jin, R., He, J. P., Kessler, R. C., Lee, S., Sampson, N. A., Viana, M. C., Andrade, L. H., Hu, C., Karam, E. G., Ladea, M., Medina-Mora, M. E., Ono, Y., Posada-Villa, J., Sagar, R., Wells, J. E. and Zarkov, Z. (2011). Prevalence and correlates of bipolar spectrum disorder in the world mental health survey initiative. *Archives of General Psychiatry*. **(68)**, 241-251.
- Meunier, H., Carraz, G., Neunier, Y., Eymard, P. and Aimard, M. (1963). Pharmacodynamic properties of N-dipropylacetic acid. *Thérapie*. **(18)**, 435-438.
- Michael, J. R. and Mitch, W. E. (1976). Reversible renal failure and myositis caused by phenytoin hypersensitivity. *JAMA*. **(236)**, 2773-2775.
- Michot, C., Hubert, L., Brivet, M., de Meirleir, L., Valayannopoulos, V., Müller-Felber, W., Venkateswaran, R., Ogier, H., Desguerre, I., Altuzarra, C., Thompson, E., Smitka, M., Huebner, A., Husson, M., Horvath, R., Chinnery, P.,

- Vaz, F. M., Munnich, A., Elpeleg, O., Delahodde, A., de Keyzer, Y. and de Lonlay, P. (2010). LPIN1 gene mutations: a major cause of severe rhabdomyolysis in early childhood. *Human Mutation*. **(31)**, E1564-E1573.
- Michot, C., Hubert, L., Romero, N., Gouda, A., Mamoune, A., Mathew, S., Kirk, E., Viollet, L., Rahman, S., Bekri, S., Peters, H., McGill, J., Glamuzina, E., Farrar, M., von der Hagen, M., Alexander, I. E., Kirmse, B., Barth, M., Laforet, P., Benlian, P., Munnich, A., JeanPierre, M., Elpeleg, O., Pines, O., Delahodde, A., de Keyzer, Y. and de Lonlay, P. (2012). Study of LPIN1, LPIN2 and LPIN3 in rhabdomyolysis and exercise-induced myalgia. *Journal of Inherited Metabolic Disease*. **(35)**, 1119-1128.
- Milne, S. B., Ivanova, P. T., Armstrong, M. D., Myers, D. S., Lubarda, J., Shulga, Y. V., Topham, M. K., Brown, H. A. and Epand, R. M. (2008). Dramatic differences in the roles in lipid metabolism of two isoforms of diacylglycerol kinase. *Biochemistry*. **(47)**, 9372-9379.
- Montes, L. R., Goñi, F. M., Johnston, N. C., Goldfine, H. and Alonso, A. (2004). Membrane fusion induced by the catalytic activity of a phospholipase C/sphingomyelinase from *Listeria monocytogenes*. *Biochemistry*. **(43)**, 3688-3695.
- Morand, J. N. and Kent, C. (1989). Localization of the membrane-associated CTP:phosphocholine cytidyltransferase in Chinese hamster ovary cells with an altered membrane composition. *The Journal of Biological Chemistry*. **(264)**, 13785-13792.
- Morriss, R. (2015). Mandatory implementation of NICE Guidelines for the care of bipolar disorder and other conditions in England and Wales. *BMC Medicine*. **(13)**, 246.
- Moya, P. R., Murphy, D. L., McMahon, F. J. and Wendland, J. R. (2010). Increased gene expression of diacylglycerol kinase ϵ in bipolar disorder. *The International Journal of Neuropsychopharmacology*. **(13)**, 1127-1128.
- Musto, A. and Bazán, N. G. (2006). Diacylglycerol Kinase Epsilon Modulates Rapid Kindling Epileptogenesis. *Epilepsia*. **(47)**, 267-276.
- Mutani, R., Doriguzzi, T., Fariello, R. and Furlan, P. M. (1968). Anti-epileptic action of the sodium salt of N-dipropylacetic acid. Experimental study in the cat. *Rivista Di Patologia Nervosa E Mentale*. **(89)**, 24-33.
- National Institute of Health. (2017). *Genetic and Genomic Resources for Model Organisms*. Viewed 25 June 2018.
<<https://www.nigms.nih.gov/Research/models/>>.
- Nau, H., Hauck, R. S. and Ehlers, K. (1991). Valproic acid-induced neural tube defects in mouse and human: aspects of chirality, alternative drug

- development, pharmacokinetics and possible mechanisms. *Pharmacology and Toxicology*. **(69)**, 310-321.
- Newell, P. C., Telser, A and Sussman, M. (1969). Alternative developmental pathways determined by environmental conditions in the cellular slime mold *Dictyostelium discoideum*. *Journal of Bacteriology*. **(100)**, 763-768.
- Nickels Jr., J. T., Buxeda, R. J. and Carman, G. M. (1994). Regulation of phosphatidylinositol 4-kinase from the yeast *Saccharomyces cerevisiae* by CDP-diacylglycerol. *The Journal of Biological Chemistry*. **(269)**, 11018-11024.
- Niespodziany, I., Klitgaard, H. and Margineanu, D. G. (2001). Levetiracetam inhibits the high-voltage-activated Ca(2+) current in pyramidal neurones of rat hippocampal slices. *Neuroscience Letters*. **(306)**, 5-8.
- Nigou, J. and Besra, G. S. (2002). Cytidine diphosphate-diacylglycerol synthesis in *Mycobacterium smegmatis*. *The Biochemical Journal*. **(367)**, 157-162.
- Nikawa, J., Kodaki, T. and Yamashita, S. (1987). Primary structure and disruption of the phosphatidylinositol synthase gene of *Saccharomyces cerevisiae*. *The Journal of Biological Chemistry*. **(262)**, 4876-4881.
- Nishimura, T., Tamura, N., Kono, N., Shimanaka, Y., Arai, H., Yamamoto, H. and Mizushima, N. (2017). Autophagosome formation is initiated at phosphatidylinositol synthase-enriched ER subdomains. *The EMBO Journal*. **(36)**, 1719-1735.
- Nobori, K., Okimasu, E., Sato, E. F. and Utsumi, K. (1987). Activation of protein kinase C with cardiolipin-containing liposomes in relation to membrane-protein interaction. *Cell Structure and Function*. **(12)**, 375-385.
- Nogly, P., Gushchin, I., Remeeva, A., Esteves, A. M., Borges, N., Ma, P., Ishchenko, A., Grudinin, S., Round, E., Moraes, I., Borshchevskiy, V., Santos, H., Gordeliy, V. and Archer, M. (2014). X-ray structure of a CDP-alcohol phosphatidyltransferase membrane enzyme and insights into its catalytic mechanism. *Nature Communications*. **(5)**, 4169.
- Nurnberger Jr., J. I., Koller, D. L., Jung, J., Edenberg, H. J., Foroud, T., Guella, I., Vawter, M. P. and Kelsoe, J. R. (2014). Identification of pathways for bipolar disorder: a meta-analysis. *JAMA Psychiatry*. **(71)**, 657-664.
- Nuwayhid, S. J., Vega, M., Walden, P. D. and Monaco, M. E. (2006). Regulation of de novo phosphatidylinositol synthesis. *Journal of Lipid Research*. **(47)**, 1449-1456.
- Okada, T., Kawano, Y., Sakakibara, T., Hazeki, O. and Ui, M. (1994). Essential role of phosphatidylinositol 3-kinase in insulin-induced glucose transport and

- antilipolysis in rat adipocytes. Studies with a selective inhibitor wortmannin. *The Journal of Biological Chemistry*. **(269)**, 3568-3573.
- Olmez, A., Arslan, U., Turanli, G. and Aysun, S., (2008). Risk of recurrence after drug withdrawal in childhood epilepsy. *Seizure*. **(18)**, 251-256.
- Ophoff, R. A., Terwindt, G. M., Vergouwe, M. N., van Eijk, R., Oefner, P. J., Hoffman, S. M., Lamerdin, J. E., Mohnenweiser, H. W., Bulman, D. E., Ferrari, M., Haan, J., Lindhout, D., van Ommen, G. J., Hofker, M. H., Ferrari, M. D. and Frants, R. R. (1996). Familial hemiplegic migraine and episodic ataxia type-2 are caused by mutations in the Ca²⁺ channel gene CACNL1A4. *Cell*. **(87)**, 543-552.
- Pacifici, G. M., Tomson, T., Bertilsson, L. and Rane, A. (1985). Valpromide/carbamazepine and risk of teratogenicity. *The Lancet*. **(1)**, 397-398.
- Paradies, G., Petrosillo, G., Pistolese, M., Di Venosa, N., Federici, A. and Ruggiero, F. M. (2004). Decrease in mitochondrial complex I activity in ischemic/reperfused rat heart: involvement of reactive oxygen species and cardiolipin. *Circulation Research*. **(94)**, 53-59.
- Parent, C. A. and Devreotes, P. N. (1996). Molecular genetics of signal transduction in *Dictyostelium*. *Annual Review of Biochemistry*. **(65)**, 411-440.
- Parikh, A., Miranda, E. R., Katoh-Kurasawa, M., Fuller, D., Rot, G., Zagar, L., Curk, T., Sugang, R., Chen, R., Zupan, B., Loomis, W. F., Kuspa, A. and Shaulsky, G. (2010). Conserved developmental transcriptomes in evolutionarily divergent species. *Genome Biology*. **(11)**, R35.
- Paulus, H. and Kennedy, E. P. (1960). The enzymatic synthesis of inositol monophosphate. *The Journal of Biological Chemistry*. **(235)**, 1303-1311.
- Perlis, R. H., Ostacher, M. J., Patel, J. K., Marangell, L. B., Zhang, H., Wisniewski, S. R., Ketter, T. A., Miklowitz, D. J., Otto, M. W., Gyulai, L., Reilly-Harrington, N. A., Nierenberg, A. A., Sachs, G. S. and Thase, M. E. (2006). Predictors of recurrence in bipolar disorder: primary outcomes from the systematic treatment enhancement program for bipolar disorder (STEP-BD). *American Journal of Psychiatry*. **(163)**, 217-224.
- Phiel, C. J., Zhang, F., Huang, E. Y., Guenther, M., G., Lazar, M. A. and Klein, P. S. (2001). Histone deacetylase is a direct target of valproic acid, a potent anticonvulsant, mood stabilizer, and teratogen. *The Journal of Biological Chemistry*. **(276)**, 36734-36741.
- Pini, S., de Queiroz, V., Pagnin, D., Pezawas, L., Angst, J., Cassano, G. B. and Wittchen, H. U. (2005). Prevalence and burden of bipolar disorders in European countries. *European Neuropsychopharmacology*. **(15)**, 425-434.

- Pope Jr., H. G., McElroy, S. L., Keck, Jr., P. E. and Hudson, J. I. (1991). Valproate in the treatment of acute mania. A placebo-controlled study. *Archives of General Psychiatry*. **(48)**, 62-68.
- Prottey, C. and Hawthorne, J. N. (1967). The biosynthesis of phosphatidic acid and phosphatidylinositol in mammalian pancreas. *The Biochemical Journal*. **(105)**, 379-392.
- Pryse-Phillips W. E., Dodick, D. W., Edmeads, J. G., Gawel, M. J., Nelson, R. F., Purdy, R. A., Robinson, G., Stirling, D. and Worthington, I. (1997). Guidelines for the diagnosis and management of migraine in clinical practice. *Canadian Medical Association Journal*. **(156)**, 1273-1287.
- Qi, Y., Kapterian, T. S., Du, X., Ma, Q., Fei, W., Zhang, Y., Huang, X., Dawes, I. W. and Yang, H. (2016). CDP-diacylglycerol synthases regulate the growth of lipid droplets and adipocyte development. *Journal of Lipid Research*. **(57)**, 767-780.
- Raetz, C. R. H. and Kennedy, E. P. (1973). Function of Cytidine Diphosphate-Diglyceride and Deoxycytidine Diphosphate-Diglyceride in the Biogenesis of Membrane Lipids in *Escherichia coli*. *The Journal of Biological Chemistry*. **(3)**, 1098-1105.
- Rakhimova, A., Ura, S., Hsu, D. W., Wang, H. Y., Pears, C. J. and Lakin, N. D. (2017). Site-specific ADP-ribosylation of histone H2B in response to DNA double strand breaks. *Scientific Reports*. **(7)**, 43750.
- Ramgopal, S., Thome-Souza, S., Jackson, M., Kadish, N. E., Sánchez Fernández, I., Klehm, J., Bosl, W., Reinsberger, C., Schachter, S. and Loddenkemper, T. (2014). Seizure detection, seizure prediction, and closed-loop warning systems in epilepsy. *Epilepsy and Behavior*. **(37)**, 291-307.
- Raper, K. B., (1935). *Dictyostelium discoideum*, a new species of slime mold from decaying forest leaves. *Journal of Agricultural Research*. **(60)**, 135-147.
- Ridsdale, R., Tseu, I., Wang, J. and Post, M. (2001). CTP:phosphocholine cytidyltransferase alpha is a cytosolic protein in pulmonary epithelial cells and tissues. *The Journal of Biological Chemistry*. **(276)**, 49148-49155.
- Rodriguez de Turco, E. B., Tang, W., Topham, M. K., Sakane, F., Marcheselli, V. L., Chen, C., Taketomi, A., Prescott, S. M. and Bazán, N. G. (2001). Diacylglycerol Kinase ϵ Regulates Seizure Susceptibility and Long-Term Potentiation Through Arachidonoyl-Inositol Lipid Signaling. *Proceedings of the National Academy of Sciences of the United States of America*. **(98)**, 4740-4745.

- Rodriguez de Turco, E. B., Morelli de Liberti, S. and Bazán, N. G. (1983). Stimulation of free fatty acid and diacylglycerol accumulation in cerebrum and cerebellum during bicuculline-induced status epilepticus. Effect of pretreatment with alpha-methyl-p-tyrosine and p-chlorophenylamine. *Journal of Neurochemistry*. **(40)**, 252-259.
- Sabry, J. H., Moores, S. L., Ryan, S., Zang, J. H. and Spudich, J. A. (1997). Myosin heavy chain phosphorylation sites regulate myosin localization during cytokinesis in live cells. *Molecular Biology of the Cell*. **(8)**, 2605-2615.
- Sade, Y., Toker, L., Kara, N. Z., Einat, H., Rapoport, S., Moechars, D., Berry, G. T., Bersudsky, Y. and Agam, G. (2016). IP3 accumulation and/or inositol depletion: two downstream lithium's effects that may mediate its behavioral and cellular changes. *Translational Psychiatry*. **(6)**, e968.
- Sakane, F., Yamada, K., Imai, S and Kanoh, H. (1991). Porcine 80-kDa diacylglycerol kinase is a calcium-binding and calcium/phospholipid-dependent enzyme and undergoes calcium-dependent translocation. *The Journal of Biological Chemistry*. **(266)**, 7096-7100.
- Sanjuan, M. A., Pradet-Balade, B., Jones, D. R., Martinez-A, C., Stone, J. C., Garcia-Sanz, J. A. and Merida, I. (2003). T cell activation *in vivo* targets diacylglycerol kinase alpha to the membrane: a novel mechanism for Ras attenuation. *Journal of Immunology*. **(170)**, 2877-2883.
- Santos, T., Carrasco, S., Jones, D. R., Mérida, I. and Eguinoa, A. (2002). Dynamics of diacylglycerol kinase zeta translocation in living T-cells. Study of the structural domain requirements for translocation and activity. *The Journal of Biological Chemistry*. **(277)**, 30300-30309.
- Sato, N., Hagio, M., Wada, H. and Tsuzuki, M. (2000). Requirement of phosphatidylglycerol for photosynthetic function in thylakoid membranes. *Proceedings of the National Academy of Sciences of the United States of America*. **(97)**, 10655-10660.
- Saul, D., Fabian, L., Forer, A. and Brill, J. A. (2004). Continuous phosphatidylinositol metabolism is required for cleavage of crane fly spermatocytes. *Journal of Cell Science*. **(117)**, 3887-3896.
- Schmitz, E. B., Robertson, M. M. and Trimble, M. R. (1999). Depression and schizophrenia in epilepsy: social and biological risk factors. *Epilepsy Research*. **(35)**, 59-68.
- Seçkin, S., Başaran-Küçükgergin, C. and Uysal, M. (1999). Effect of acute and chronic administration of sodium valproate on lipid peroxidation and antioxidant system in rat liver. *Pharmacology and Toxicology*. **(85)**, 294-298.

- Seiler, K. U. and Wassermann, O. (1975). Drug-induced phospholipidosis. II. Alterations in the phospholipid pattern of organs from mice, rats and guinea-pigs after chronic treatment with chlorphentermine. *Naunyn-Schmiedeberg's Archives of Pharmacology*. **(288)**, 261-268.
- Shen, H. and Dowhan, W. (1996). Reduction of CDP-diacylglycerol synthase activity results in the excretion of inositol by *Saccharomyces cerevisiae*. *The Journal of Biological Chemistry*. **(271)**, 29043-29048.
- Shen, H., Heacock, P. N., Clancey, C. J. and Dowhan, W. (1996). The CDS1 gene encoding CDP-diacylglycerol synthase in *Saccharomyces cerevisiae* is essential for cell growth. *The Journal of Biological Chemistry*. **(271)**, 789-795.
- Sherman, W. R., Leavitt, A. L., Honchar, M.P., Hallcher, L. M. and Phillips, B. E. (1981). Evidence that lithium alters phosphoinositide metabolism: chronic administration elevates primarily D-myo-inositol-1-phosphate in cerebral cortex of the rat. *Journal of Neurochemistry*. **(36)**, 1947-1951.
- Shinoda, S., Schindler, C. K., Meller, R., So, N. K., Araki, T., Yamamoto, A., Lan, J. Q., Taki, W., Simon, R. P. and Henshall, D. C. (2004). Bim regulation may determine hippocampal vulnerability after injurious seizures and in temporal lobe epilepsy. *Journal of Clinical Investigation*. **(113)**, 1059-1068.
- Shorvon, S. D., (2011). The etiologic classification of epilepsy. *Epilepsia*. **(52)**, 1052-1057.
- Sillanpää, M. and Shinnar, S. (2010). Long-term mortality in childhood-onset epilepsy. *The New England Journal of Medicine*. **(363)**, 2522-2529.
- Singh, N., Halliday, A. C., Thomas, J. M., Kuznetsova, O. V., Baldwin, R., Woon, E. C. Y., Aley, P. K., Antoniadou, I., Sharp, T., Vasudevan, S. R. and Churchill, G. C. (2013). A safe lithium mimetic for bipolar disorder. *Nature Communications*. **(4)**, 1332-1146.
- Slater, N. T., Stelzer, A. and Galvan, M. (1985). Kindling-like stimulus patterns induce epileptiform discharges in the guinea pig in vitro hippocampus. *Neuroscience Letters*. **(60)**, 25-31.
- Smith, E. and Williams, K. L. (1981). The age-dependent loss of cells from the rear of a *Dictyostelium discoideum* slug is not tip controlled. *Journal of Embryology and Experimental Morphology*. **(61)**, 61-67.
- Squassina, A., Manchia, M., Congiu, D., Severino, G., Chillotti, C., Arda, R., Piccardi, M. and Zompo, M. D. (2009). The diacylglycerol kinase eta gene and bipolar disorder: a replication study in a Sardinian sample. *Molecular Psychiatry*. **(14)**, 350-351.

- Stajdohar, M., Jeran, L., Kokosar, J., Blenkus, D., Janez, T., Kuspa, A., Shaulsky, G. and Zupan, B. (2015). *dictyExpress: visual analytics of NGS gene expression in Dictyostelium*. Viewed 25 July 2017. <<http://www.dictyexpress.org>>.
- Steinlein, O. K. (2014). Calcium signaling and epilepsy. *Cell and Tissue Research*. **(357)**, 385-393.
- Streb, H., Irvine, R. F., Berridge, M. J. and Schulz, I. (1983). Release of Ca²⁺ from a nonmitochondrial intracellular store in pancreatic acinar cells by inositol-1,4,5-trisphosphate. *Nature*. **(306)**, 67-69.
- Stubbs Jr., E. B. and Agranoff, B. W. (1993). Lithium enhances muscarinic receptor-stimulated CDP-diacylglycerol formation in inositol-depleted SK-N-SH neuroblastoma cells. *Journal of Neurochemistry*. **(60)**, 1292-1299.
- Stubbs Jr., E. B., Walker, B. A., Owens, C.A., Ward, P. A. and Agranoff, B. W. (1992). Formyl peptide stimulates and ATP gamma S potentiates [3H]cytidine 5'-diphosphate diglyceride accumulation in human neutrophils. *The Journal of Immunology*. **(148)**, 2242-2247.
- Szyperski, T., Fernandez, C., Mumenthaler, C. and Wuthrich, K. (1998). Structure comparison of human glioma pathogenesis-related protein GliPR and the plant pathogenesis-related protein P14a indicates a functional link between the human immune system and a plant defense system. *Proceedings of the National Academy of Sciences of the United States of America*. **(96)**, 2262-2266.
- Takei, N., Inamura, N., Kawamura, M., Namba, H., Hara, K., Yonezawa, K. and Nawa, H. (2004). Brain-derived neurotrophic factor induces mammalian target of rapamycin-dependent local activation of translation machinery and protein synthesis in neuronal dendrites. *Journal of Neuroscience*. **(24)**, 9760-9769.
- Tallóczy, Z., Jiang, W., Virgin IV, H. W., Leib, D. A., Scheuner, D., Kaufman, R. J., Eskelinen, E. L. and Levine, B. (2002). Regulation of starvation- and virus-induced autophagy by the eIF2 α kinase signaling pathway. *Proceedings of the National Academy of Sciences of the United States of America*. **(99)**, 190-195.
- Tan, W. W., Kong, S. T., Chan, D. W. S. and Ho, P. C. (2012). A retrospective study on the usage of antiepileptic drugs in Asian children from 2000 to 2009 in the largest pediatric hospital in Singapore. *Pharmacoepidemiology and Drug Safety*. **(21)**, 1074-1080.
- Tang, R., Faussat, A. M., Majdak, P., Perrot, J. Y., Chaoui, D., Legrand, O. and Marie, J. P. (2004). Valproic acid inhibits proliferation and induces apoptosis in acute myeloid leukemia cells expressing P-gp and MRP1. *Leukemia*. **(18)**, 1246-1251.

- Tang, S. J., Reis, G., Kang, H., Gingras, A. C., Sonenberg, N and Schuman, E. M. (2002). A rapamycin-sensitive signaling pathway contributes to long-term synaptic plasticity in the hippocampus. *Proceedings of the National Academy of Sciences of the United States of America*. **(99)**, 467-472.
- Tang, W., Bunting, M., Zimmerman, G. A., McIntyre, T. M. and Prescott, S. M. (1996). Molecular cloning of a novel human diacylglycerol kinase highly selective for arachidonate-containing substrates. *The Journal of Biological Chemistry*. **(271)**, 10237-10241.
- Taylor, M. M., MacDonald, K., Morris, A. J. and McMaster, C. R. (2005). Enhanced apoptosis through farnesol inhibition of phospholipase D signal transduction. *FEBS Journal*. **(272)**, 5056-5063.
- Terbach, N., Shah, R., Kelemen, R., Klein, P. S., Gordienko, D., Brown, N. A., Wilkinson, C. J. and Williams, R. S. B. (2011). Identifying an uptake mechanism for the antiepileptic and bipolar disorder treatment valproic acid using the simple biomedical model Dictyostelium. *Journal of Cell Science*. **(124)**, 2267-2276.
- Thompson, W. and MacDonald, G. (1975). Isolation and characterization of cytidine diphosphate diglyceride from beef liver. *The Journal of Biological Chemistry*. **(250)**, 6779-6785.
- Thompson, W. and MacDonald, G. (1976). Cytidine diphosphate diglyceride of bovine brain. Positional distribution of fatty acids and analysis of major molecular species. *European journal of biochemistry*. **(65)**, 107-111.
- Tokuoka, S. M., Saiardi, A. and Nurrish, S. J. (2008). The mood stabilizer valproate inhibits both inositol- and diacylglycerol-signaling pathways in *Caenorhabditis elegans*. *Molecular Biology of the Cell*. **(19)**, 2241-2250.
- Tong, V., Teng, X. W., Chang, T. K. H. and Abbott, F. S. (2005). Valproic acid I: time course of lipid peroxidation biomarkers, liver toxicity, and valproic acid metabolite levels in rats. *Toxicological Sciences: An Official Journal of the Society of Toxicology*. **(86)**, 427-435.
- Tu-Sekine, B. and Raben, D. M. (2011). Regulation and roles of neuronal diacylglycerol kinases: a lipid perspective. *Critical Reviews in Biochemistry and Molecular Biology*. **(46)**, 353-364.
- Tulloch, I. F., Walter, D. S., Hown, G. M. and Howe, S. J. (1982). The relationship between plasma concentration of valproic acid and its anticonvulsant and behavioural effects in the rat. *Neuropharmacology*. **(21)**, 555-562.
- Tyeryar, K. R., Vongtau, H. O. U. and Undieh, A. S. (2008). Diverse antidepressants increase CDP-diacylglycerol production and phosphatidylinositol resynthesis in depression-relevant regions of the rat brain. *BMC Neuroscience*. **(9)**, 12.

- van Baal, J., de Widt, J., Divecha, N. and van Blitterswijk, W. J. (2005). Translocation of diacylglycerol kinase theta from cytosol to plasma membrane in response to activation of G protein-coupled receptors and protein kinase C. *The Journal of Biological Chemistry*. **(280)**, 9870-9878.
- van Vliet, E. A., Forte, G., Holtman, L., den Burger, J. C. G., Sinjewel, A., de Vries, H. E., Aronica, E. and Gorter, J. A. (2012). Inhibition of mammalian target of rapamycin reduces epileptogenesis and blood-brain barrier leakage but not microglia activation. *Epilepsia*. **(53)**, 1254-1263.
- VanDongen A. M. J., VanErp, M. G. and Voskuyl, R. A. (1986). Valproate reduces excitability by blockage of sodium and potassium conductance. *Epilepsia*. **(27)**, 177-182.
- Vázquez-Calvo, Á, Martín-Acebes, M. A., Sáiz, J. C., Ngo, N., Sobrino, F. and de la Torre, J. C. (2013). Inhibition of multiplication of the prototypic arenavirus LCMV by valproic acid. *Antiviral Research*. **(99)**, 172-179.
- Villar, A. V., Alonso, A. and Goñi, F. M. (2000). Leaky vesicle fusion induced by phosphatidylinositol-specific phospholipase C: observation of mixing of vesicular inner monolayers. *Biochemistry*. **(39)**, 14012-14018.
- Walker, A. J., Draeger, A., Houssa, B., van Blitterswijk, W. J., Ohanian, V. and Ohanian, J. (2001). Diacylglycerol kinase theta is translocated and phosphoinositide 3-kinase-dependently activated by noradrenaline but not angiotensin II in intact small arteries. *The Biochemical Journal*. **(353)**, 129-137.
- Walker, C. P., Duddy, M. J. and Sagar, G. (1993). Case report: Rhabdomyolysis following grand mal seizures presenting as a delayed and increasingly dense nephrogram. *Clinical Radiology*. **(47)**, 139-140.
- Wang, H. Y. and Friedman, E. (1989). Lithium inhibition of protein kinase C activation-induced serotonin release. *Psychopharmacology*. **(99)**, 213-218.
- Wang, T. and Montell, C. (2006). A phosphoinositide synthase required for a sustained light response. *Journal of Neuroscience*. **(26)**, 12816-12825.
- Watson, S. P., Shipman, L. and Godfrey, P. P. (1990). Lithium potentiates agonist formation of [3H]CDP-diacylglycerol in human platelets. *European Journal of Pharmacology*. **(188)**, 273-276.
- Wennstroem, S., Siegbahn, A., Yokote, K., Arvidsson, A. K., Heldin, C. H., Mori, S. and Claesson-Welsh, L. (1994). Membrane ruffling and chemotaxis transduced by the PDGF beta -receptor require the binding site for phosphatidylinositol 3' kinase. *Oncogene*. **(9)**, 651-660.

- Werling, U., Siehler, S., Litfin, M., Nau, H. and Göttlicher, M. (2001). Induction of differentiation in F9 cells and activation of peroxisome proliferator-activated receptor delta by valproic acid and its teratogenic derivatives. *Molecular Pharmacology*. **(59)**, 1269-1276.
- Wessels, D., Schroeder, N. A., Voss, E., Hall, A. L., Condeelis, J. and Soll, D. R. (1989). cAMP-Mediated Inhibition of Intracellular Particle Movement and Actin Reorganization in *Dictyostelium*. *The Journal of Cell Biology*. **(109)**, 2841-2851.
- Whatmore, J., Wiedemann, C., Somerharju, P., Swigart, P. and Cockcroft, S. (1999). Resynthesis of phosphatidylinositol in permeabilized neutrophils following phospholipase C β activation: transport of the intermediate, phosphatidic acid, from the plasma membrane to the endoplasmic reticulum for phosphatidylinositol resynthesis is not dependent on soluble lipid carriers or vesicular transport. *Biochemical Journal*. **(341)**, 435-444.
- Wilden, J. A. and Cohen-Gadol, A. A. (2012). Evaluation of first nonfebrile seizures. *American Family Physician*. **(86)**, 334-340.
- Wilkins, M. R. and Williams, K. L. (1995). The extracellular matrix of the *Dictyostelium discoideum* slug. *Experientia*. **(51)**, 1189-1196.
- Williams, R. S. B. (2005). Pharmacogenetics in model systems: Defining a common mechanism of action for mood stabilisers. *Progress in Neuropsychopharmacology and Biological Psychiatry*. **(29)**, 1029-1037.
- Williams, R. S. B., Boeckeler, K., Gräf, R., Müller-Taubenberger, A., Li, Z., Isberg, R. R., Wessels, D., Soll, D. R., Alexander, H. and Alexander, S. (2006). Towards a molecular understanding of human diseases using *Dictyostelium discoideum*. *Trends in Molecular Medicine*. **(12)**, 415-424.
- Williams, R. S. B., Cheng, L., Mudge, A. W. and Harwood, A. J. (2002). A common mechanism of action for three mood-stabilizing drugs. *Nature*. **(417)**, 292-295.
- Williams, R. S. B., Eames, M., Ryves, W. J., Viggars, J. and Harwood, A. J. (1999). Loss of a prolyl oligopeptidase confers resistance to lithium by elevation of inositol (1,4,5) trisphosphate. *The EMBO Journal*. **(18)**, 2734-2745.
- Williamson, F. A. and Morré, D. J. (1976). Distribution of phosphatidylinositol biosynthetic activities among cell fractions from rat liver. *Biochemical and Biophysical Research Communications*. **(68)**, 1201-1205.
- Wilmshurst, J. M., Berg, A. T., Lagae, L., Newton, C. R. and Cross, J. H. (2014). The challenges and innovations for therapy in children with epilepsy. *Nature Reviews. Neurology*. **(10)**, 249-260.

- Witt, D., Burfeind, P., von Hardenberg, S., Opitz, L., Salinas-Riester, G., Bremmer, F., Schweyer, S., Thelen, P., Neesen, J. and Kaulfuss, S. (2013). Valproic acid inhibits the proliferation of cancer cells by re-expressing cyclin D2. *Carcinogenesis*. **(34)**, 1115-1124.
- World Health Organization. (2001). *World Health Report 2001: Mental Health, New Understanding, New Hope*. World Health Organization. Albany.
- World Health Organisation. (2017). *The Selection and Use of Essential Medicines WHO Technical Report Series 1006*. World Health Organisation.
- World Health Organisation. (2018). *Epilepsy*. Viewed 13 June 2018, <<http://www.who.int/news-room/fact-sheets/detail/epilepsy>>.
- Wu, L., Niemeyer, B., Colley N., Socolich, M. and Zuker, C.S. (1995). Regulation of PLC-mediated signalling in vivo by CDP-diacylglycerol synthase. *Nature*. **(373)**, 216-222.
- Xu, X., Müller-Taubenberger, A., Adley, K. E., Pawolleck, N., Lee, V. W. Y., Wiedemann, C., Sihra, T. S., Maniak, M., Jin, T. and Williams, R. B. S. (2007). Attenuation of phospholipid signaling provides a novel mechanism for the action of valproic acid. *Eukaryotic Cell*. **(6)**, 899-906.
- Xu, Y., Condell, M., Plesken, H., Edelman-Novemsky, I., Ma, J., Ren, M. and Schlame, M. (2006). A *Drosophila* model of Barth Syndrome. *Proceedings of the National Academy of Sciences of the United States of America*. **(103)**, 11584-11588.
- Yamada, K., Sakane, F., Matsushima, N. and Kanoh, H. (1997). EF-hand motifs of alpha, beta and gamma isoforms of diacylglycerol kinase bind calcium with different affinities and conformational changes. *The Biochemical Journal*. **(321)**, 59-64.
- Yamamoto, A., Adachi, S., Kitani, T., Shinji, T. and Seki, K. (1971). Drug-induced lipidosis in human cases and in animal experiments. Accumulation of an acidic glycerophospholipid. *Journal of Biochemistry*. **(69)**, 613-615.
- Yang, E. J., Ahn, S., Lee, K., Mahmood, U. and Kim, H. S. (2016). Early behavioral abnormalities and perinatal alterations of PTEN/AKT pathway in valproic acid autism model mice. *PLoS One*. **(11)**, e0153298.
- Yoshida, S., Ikeda, M., Busto, R., Santiso, M., Martinez, E. and Ginsberg, M. D. (1987). Cerebral phosphoinositide, triacylglycerol and energy metabolism during sustained seizures induced by bicuculline. *Brain Research*. **(412)**, 114-124.
- Yumura, S. and Fukui, Y. (1985). Reversible cyclic AMP-dependent change in distribution of myosin thick filaments in *Dictyostelium*. *Nature*. **(314)**, 194-196.

- Yurekli, V. A., Akhan, G., Kutluhan, S., Uzar, E., Koyuncuoglu, H. R. and Gultekin, F. (2008). The effect of sodium valproate on chronic daily headache and its subgroups. *The Journal of Headache and Pain*. **(9)**, 37-41.
- Zarate Jr., C. A., Tohen, M., Narendran, R., Tomassini, E. C., McDonald, J., Sederer, S. and Madrid, A. R. (1999). The adverse effect profile and efficacy of divalproex sodium compared with valproic acid: a pharmacoepidemiology study. *The Journal of Clinical Psychiatry*. **(60)**, 232-236.
- Zeise, M. L., Kasparow, S. and Zieglgänsberger, W. (1991). Valproate suppresses N-methyl- d-aspartate-evoked, transient depolarizations in the rat neocortex *in vitro*. *Brain Research*. **(544)**, 345-348.
- Zeng, L. H., Xu, L., Gutmann, D. H. and Wong, M. (2008). Rapamycin prevents epilepsy in a mouse model of tuberous sclerosis complex. *Annals of Neurology*. **(63)**, 444-453.

Supplementary Material

<i>Primer Name</i>	<i>Primer Sequence (5'-3')</i>	<i>Use</i>
Blasticidin cassette pLPBLP Forward	AAAAGATAAAGCTGACCCGAAAG	PCR Screening
Blasticidin cassette pLPBLP Reverse	TCAAATAATAATTAACCAACCCAAG	PCR Screening
<i>CdsA</i> Knockout 5' pLPBLP Forward	AATGGATCCGATTTCGTCAAAAGATG	Cloning
<i>CdsA</i> Knockout 5' pLPBLP Reverse	ATACTGCAGCAGGATAATAGTTTGC	Cloning
<i>CdsA</i> Knockout 3' pLPBLP Forward	TATAAGCTTGAATCATTACATTGTACTAG	Cloning
<i>CdsA</i> Knockout 3' pLPBLP Reverse	TTAGGTACCCAGTAATAGTACCAAGTG	Cloning
<i>CdsA</i> Knockout 5' Fragment Genomic Control Forward	ATGAGGACAGATAACATTAG	PCR Screening
<i>CdsA</i> Knockout 5' Fragment Genomic Control Reverse	GTGATTAAGATTGGTTTAGC	PCR Screening
<i>CdsA</i> Knockout 5' Fragment Vector Control Forward	GATTCGTCAAAAGATGAAGAAACCAAGTACA	PCR Screening
<i>CdsA</i> Knockout 3' Fragment Genomic Control Forward	CTAGAGATCCAGTATTCTTG	PCR Screening
<i>CdsA</i> Knockout 3' Fragment Genomic Control Reverse	GTAAACTCTATGGATTGTTTC	PCR Screening
<i>CdsA</i> Knockout 3' Fragment Vector Control Reverse	GTAAACTCTATGGATTGTTTC	PCR Screening
<i>CdsA</i> Overexpressing Primer Forward	TGGGATCCATGAGGACAGATAAC	Cloning
<i>CdsA</i> Overexpressing Primer Reverse	GCGGAATTCCTATGCAGTAATAG	Cloning
<i>Cdipt</i> Knockout 1 5' pLPBLP Forward	GCGGGATCCGTATTACGAAATTATTA	Cloning
<i>Cdipt</i> Knockout 1 5' pLPBLP Reverse	ATACTGCAGTGGCACATAAACGTGC	Cloning
<i>Cdipt</i> Knockout 1 3' pLPBLP Forward	ATACCATGGGAAGGTTTCTTCCTT	Cloning
<i>Cdipt</i> Knockout 1 3' pLPBLP Reverse	GCGGGTACCACTAGTGCATTA	Cloning
<i>Cdipt</i> Knockout 1 5' Fragment Genomic Control Forward	CATACATACACCTACACCAATATATA	PCR Screening
<i>Cdipt</i> Knockout 1 5' Fragment Genomic Control Reverse	GGCACATAAACGTGCAA	PCR Screening
<i>Cdipt</i> Knockout 1 5' Fragment Vector Control Forward	CAAAAGTTTACACCTATGTACCAA	PCR Screening
<i>Cdipt</i> Knockout 1 3' Fragment Genomic Control Forward	GAAGGTTTCTTCCTTTTCTC	PCR Screening
<i>Cdipt</i> Knockout 1 3' Fragment Genomic Control Reverse	CCAGTGCACCCAATAAAATCTC	PCR Screening

Supplementary Material

<i>Cdipt</i> Knockout 1 3' Fragment Vector Control Reverse	GATGACAACGCCTTTGAATAT	PCR Screening
<i>Cdipt</i> Knockout 2 5' pLPBLP Forward	TATGGATCCGTTTACACCTATGTACC	Cloning
<i>Cdipt</i> Knockout 2 5' pLPBLP Reverse	TTACTGCAGCATCTATCTGTAATCATATC	Cloning
<i>Cdipt</i> Knockout 2 3' pLPBLP Forward	ATAAAGCTTCAATTGCATTAATGGTAG	Cloning
<i>Cdipt</i> Knockout 2 3' pLPBLP Reverse	TATGGTACCATCATCAACAGCTTGG	Cloning
<i>Cdipt</i> Knockout 2 5' Fragment Genomic Control Forward	GTAGTATTACGAAATTATTATAATGG	PCR Screening
<i>Cdipt</i> Knockout 2 5' Fragment Genomic Control Reverse	GCTCCAAATTGTGAACC	PCR Screening
<i>Cdipt</i> Knockout 2 5' Fragment Vector Control Forward	GGATATTTTCAGAGTTATTTTTGC	PCR Screening
<i>Cdipt</i> Knockout 2 3' Fragment Genomic Control Forward	GGTAGTATTATCACATTTCTATAAAG	PCR Screening
<i>Cdipt</i> Knockout 2 3' Fragment Genomic Control Reverse	CGTTTCTTTAGATGACCAAC	PCR Screening
<i>Cdipt</i> Knockout 2 3' Fragment Vector Control Reverse	GACTGACGATATCTAAGGTA	PCR Screening
<i>Cdipt</i> Overexpressing Primer Forward	GCCGGATCCATGGCATTTCAAAAG	Cloning
<i>Cdipt</i> Overexpressing Primer Reverse	GCCGAATTCCTATTTTTTTAATTTTGTGG	Cloning
<i>DgkA</i> Knockout 5' pLPBLP Forward	ATAGGATCCGGGGTATTTGCACACAAG	Cloning
<i>DgkA</i> Knockout 5' pLPBLP Reverse	ATACTGCAGCCTTCAACCCAATGATG	Cloning
<i>DgkA</i> Knockout 3' pLPBLP Forward	GTACCATGGGTGGACTTATGGGGTG	Cloning
<i>DgkA</i> Knockout 3' pLPBLP Reverse	ATAAAGCTTGAGGTTGTGATTGAGGT	Cloning
<i>DgkA</i> Knockout 5' Fragment Genomic Control Forward	CTTTCTAACACACTCAATAAAATTC	PCR Screening
<i>DgkA</i> Knockout 5' Fragment Genomic Control Reverse	GCAATATATCTACATTCACTACAC	PCR Screening
<i>DgkA</i> Knockout 5' Fragment Vector Control Forward	GGGGTATTTGCACACAAGGATTTCAATG	PCR Screening
<i>DgkA</i> Knockout 3' Fragment Genomic Control Forward	GTGGACTTATGGGGTGC	PCR Screening
<i>DgkA</i> Knockout 3' Fragment Genomic Control Reverse	CGGTTCTGGTGATTGGGGTG	PCR Screening
<i>DgkA</i> Knockout 3' Fragment Vector Control Reverse	GAGGTTGTGATTGAGGTGG	PCR Screening
<i>DgkA</i> RT-PCR Forward	TGTATACATTGTATGGAACC	RT-PCR

<i>DgkA</i> RT-PCR Reverse	GGTATAGTTGATGGAACC	RT-PCR
Ig7 Forward	ACCTACAAGTCGATCAGAGAC	RT-PCR Control
Ig7 Reverse	CACCTCAGTCCTCTCGTAC	RT-PCR Control

Table S1. List of primer oligonucleotide sequences used for PCR amplification of DNA fragments for cloning and PCR screening protocols. The left column gives the names of the primer oligonucleotide sequences. The middle column states the DNA sequences which were used for the corresponding primers and the right column describes the procedure (cloning or PCR screening) which the corresponding oligonucleotide was used for.

Organism	Protein Name	Accession Number	Protein Length (aa)	Identity (%)	E-value
<i>Dictyostelium discoideum</i> (social amoeba)	PikA	P54673	1571	100	0
<i>Homo sapiens</i> (human)	Pik3ca	P42336	1068	37	1e ⁻¹⁶¹
	Pik3cb	P42338	1070	35	3e ⁻¹⁷³
	Pik3cg	P48736	1102	34	1e ⁻¹⁵¹
	Pik3cd	O00329	1044	35	2e ⁻¹⁵¹
	Pik3r1	P27986	724	No significant identity	
	Pik3r2	O00459	728		
	Pik3r3	Q92569	461		
	Pik3r4	Q99570	1358		
	Pik3r5	Q8WYR1	880		
	Pik3r6	Q5UE93	754		
	Pik3c2a	O00443	1686	38	5e ⁻¹³⁵
	Pik3c2b	O00750	1634	40	2e ⁻¹³¹
	Pik3c2g	O75747	1445	38	8e ⁻¹⁰⁸
	Pik3c3	Q8NEB9	887	32	6e ⁻⁵⁶
<i>Dictyostelium discoideum</i> (social amoeba)	PikB	P54673	1571	100	0
<i>Homo sapiens</i> (human)	Pik3ca	P42336	1068	37	6e ⁻¹⁴⁷
	Pik3cb	P42338	1070	38	3e ⁻¹⁴⁷
	Pik3cg	P48736	1102	43	5e ⁻¹³⁸
	Pik3cd	O00329	1044	38	6e ⁻¹⁴⁶
	Pik3r1	P27986	724	No significant identity	
	Pik3r2	O00459	728		
	Pik3r3	Q92569	461		
	Pik3r4	Q99570	1358		
	Pik3r5	Q8WYR1	880		
	Pik3r6	Q5UE93	754		
	Pik3c2a	O00443	1686	34	7e ⁻¹²¹
	Pik3c2b	O00750	1634	35	2e ⁻¹²³
	Pik3c2g	O75747	1445	37	4e ⁻¹⁰³
	Pik3c3	Q8NEB9	887	30	2e ⁻⁵¹
<i>Dictyostelium discoideum</i> (social amoeba)	PikC	P54673	1571	100	0
<i>Homo sapiens</i> (human)	Pik3ca	P42336	1068	35	7e ⁻¹²⁹
	Pik3cb	P42338	1070	37	1e ⁻¹²⁹
	Pik3cg	P48736	1102	36	8e ⁻¹³¹
	Pik3cd	O00329	1044	33	2e ⁻¹²⁸
	Pik3r1	P27986	724	No significant identity	
	Pik3r2	O00459	728		
	Pik3r3	Q92569	461		

	Pik3r4	Q99570	1358		
	Pik3r5	Q8WYR1	880		
	Pik3r6	Q5UE93	754		
	Pik3c2a	O00443	1686	34	6e ⁻¹²⁹
	Pik3c2b	O00750	1634	36	5e ⁻¹³⁵
	Pik3c2g	O75747	1445	36	3e ⁻¹⁰⁵
	Pik3c3	Q8NEB9	887	31	1e ⁻⁵²
<i>Dictyostelium discoideum</i> (social amoeba)	PikF	P54673	1571	100	0
<i>Homo sapiens</i> (human)	Pik3ca	P42336	1068	36	1e ⁻¹³⁹
	Pik3cb	P42338	1070	39	2e ⁻¹⁴⁹
	Pik3cg	P48736	1102	36	1e ⁻¹³¹
	Pik3cd	O00329	1044	37	1e ⁻¹⁴²
	Pik3r1	P27986	724	No significant identity	
	Pik3r2	O00459	728		
	Pik3r3	Q92569	461		
	Pik3r4	Q99570	1358		
	Pik3r5	Q8WYR1	880		
	Pik3r6	Q5UE93	754		
	Pik3c2a	O00443	1686	40	4e ⁻¹²⁷
	Pik3c2b	O00750	1634	40	1e ⁻¹³⁶
	Pik3c2g	O75747	1445	35	3e ⁻¹⁰⁴
	Pik3c3	Q8NEB9	887	31	4e ⁻⁵⁰
<i>Dictyostelium discoideum</i> (social amoeba)	PikG	P54673	1571	100	0
<i>Homo sapiens</i> (human)	Pik3ca	P42336	1068	40	1e ⁻⁷³
	Pik3cb	P42338	1070	44	3e ⁻⁷⁵
	Pik3cg	P48736	1102	40	2e ⁻⁸⁶
	Pik3cd	O00329	1044	41	1e ⁻⁷⁸
	Pik3r1	P27986	724	No significant identity	
	Pik3r2	O00459	728		
	Pik3r3	Q92569	461		
	Pik3r4	Q99570	1358		
	Pik3r5	Q8WYR1	880		
	Pik3r6	Q5UE93	754		
	Pik3c2a	O00443	1686	42	7e ⁻⁹¹
	Pik3c2b	O00750	1634	42	6e ⁻⁹¹
	Pik3c2g	O75747	1445	48	2e ⁻⁸⁸
	Pik3c3	Q8NEB9	887	33	3e ⁻⁴⁶
<i>Dictyostelium discoideum</i> (social amoeba)	PTEN	Q8T9S7	533	100	0
<i>Homo sapiens</i> (human)	PTEN	P60484	403	51	9e ⁻⁸¹

Table S2. *D. discoideum* and *H. sapiens* PI3K and PTEN protein homology search results identifying related proteins. The accession numbers of related proteins are given and the

name of the organism to which they relate. Protein length in number of amino acids are stated in addition to the percentage of identity relating to the *D. discoideum* protein. Statistical significance of a given pairwise alignment relating to the scoring system and size of the database used for comparison is shown by the E-value, with lower E-values indicating greater significance in homology. Results obtained using the NCBI protein-protein BLAST database.

Organism	Protein Name	Accession Number	Protein Length (aa)	Identity (%)	E-value
<i>Dictyostelium discoideum</i> (social amoeba)	PLC	Q02158	801	100	0
<i>Homo sapiens</i> (human)	PLC β 1	Q9NQ66	1216	34	2e ⁻⁷⁶
	PLC β 2	Q00722	1185	31	1e ⁻⁶⁶
	PLC β 3	Q01970	1234	31	6e ⁻⁷³
	PLC β 4	Q15147	1175	29	2e ⁻⁷²
	PLC γ 1	P19174	1290	29	3e ⁻⁴⁸
	PLC γ 2	P16885	1265	30	2e ⁻⁴⁷
	PLC δ 1	P51178	756	30	3e ⁻⁵³
	PLC δ 3	Q8N3E9	789	29	2e ⁻¹⁰⁵
	PLC δ 4	Q9BRC7	762	32	3e ⁻⁶²
	PLC ϵ 1	Q9P212	2302	45	3e ⁻⁴³
	PLC ζ 1	Q86YW0	608	29	2e ⁻⁸²

Table S3. *D. discoideum* and *H. sapiens* PLC protein homology search results identifying related proteins. The accession numbers of related proteins are given and the name of the organism to which they relate. Protein length in number of amino acids are stated in addition to the percentage of identity relating to the *D. discoideum* protein. Statistical significance of a given pairwise alignment relating to the scoring system and size of the database used for comparison is shown by the E-value, with lower E-values indicating greater significance in homology. Results obtained using the NCBI protein-protein BLAST database.

Organism	Protein Name	Accession Number	Protein Length (aa)	Identity (%)	E-value
<i>Dictyostelium discoideum</i> (social amoeba)	LPIN2	XP_645519	1325	100	0
<i>Homo sapiens</i> (human)	LPIN1	Q14693	890	31	6e ⁻⁷⁵
	LPIN2	Q92539	896	33	4e ⁻⁸⁶
	LPIN3	Q9BQK8	851	30	2e ⁻⁷⁷

Table S4. *D. discoideum* and *H. sapiens* LPIN2 protein homology search results identifying related proteins. The accession numbers of related proteins are given and the name of the organism to which they relate. Protein length in number of amino acids are stated in addition to the percentage of identity relating to the *D. discoideum* protein. Statistical significance of a given pairwise alignment relating to the scoring system and size of the database used for comparison is shown by the E-value, with lower E-values indicating greater significance in homology. Results obtained using the NCBI protein-protein BLAST database.

Homo sapiens (human)	CDS1	1	-----MLEL	RRHGSCPGPREAVSP	20
Homo sapiens (human)	CDS2	1	-----MTEL	RQVAHEPVAP	15
Dictyostelium discoideum (social amoeba)	CDSA	1	---MRTD---	NIRNRKEQLKQEKDFD	22
Mus musculus (mouse)	CDS1	1	-----MLEL	RRHGGCPGPGGAGAPP	20
Mus musculus (mouse)	CDS2	1	-----MTEL	RQVVRE-DAP	14
Danio rerio (zebrafish)	CDS1	1	-----MTEL	RRRG	9
Danio rerio (zebrafish)	CDS2	1	-----MAEL	RQRGATDKELK	15
Drosophila melanogaster (fruit fly)	CDSA	1	-----MAEV	RRRKGEDPLEDTAIS	20
Xenopus tropicalis (frog)	CDS1	0	-----		0
Xenopus tropicalis (frog)	CDS2	1	-----MTEL	RQVVGREQPQEGEDKL	20
Caenorhabditis elegans (worm)	CDS	1	---MSDQPPAENADV	RQRAPESFVTERLRA	28
Arabidopsis thaliana (plant)	CDS1	0	-----		0
Arabidopsis thaliana (plant)	CDS2	0	-----		0
Arabidopsis thaliana (plant)	CDS3	1	MAMEKDLSPNSPRI	RKLRTDTSYPTTPTSRM	30
Saccharomyces cerevisiae (budding yeast)	CDS1	1	---MSDNPE---	MKPHGT	12
Rhizophagus irregularis (fungi)	CDS	1	-----MTKKR		5
Escherichia coli (bacteria)	CDSA	0	-----		0
Homo sapiens (human)	CDS1		HREGAAGGDHETEST	-----SDKETDID	44
Homo sapiens (human)	CDS2		-----	P-----EDKESSES	23
Dictyostelium discoideum (social amoeba)	CDSA		S-----SKDEETS	-----TSDEESS	38
Mus musculus (mouse)	CDS1		PREGEAAGGDHETEST	-----SDKETDID	44
Mus musculus (mouse)	CDS2		-----	P-----EDKESSES	22
Danio rerio (zebrafish)	CDS1		-----GDQDS AENI	-----SDKEADGD	26
Danio rerio (zebrafish)	CDS2		-----HQHS	-----EDKGS ET	26
Drosophila melanogaster (fruit fly)	CDSA		GSDAAN	-----K-----RNSAADSS	35
Xenopus tropicalis (frog)	CDS1		-----		0
Xenopus tropicalis (frog)	CDS2		PYDPQD-QDQDQDQDQ	-----EQGEAES	42
Caenorhabditis elegans (worm)	CDS		PARDDAR	-----P-----TSDES DME	44
Arabidopsis thaliana (plant)	CDS1		-----	MEEENVTSSTPTPV	14
Arabidopsis thaliana (plant)	CDS2		-----	MQKEIAGDAPSAPT	14
Arabidopsis thaliana (plant)	CDS3		NT--NNQRDNHYPNIPNSPRDNYNTPSPT		58
Saccharomyces cerevisiae (budding yeast)	CDS1		-----SKEIVE SV	-----T DATSKAI	28
Rhizophagus irregularis (fungi)	CDS		-----KGGKTHENSH	-----EQSGE	20
Escherichia coli (bacteria)	CDSA		-----		0
Homo sapiens (human)	CDS1		--D-----RY	-----GDLDSRTD	55
Homo sapiens (human)	CDS2		---EAKVDG	---ETA-----SDSESRAE	40
Dictyostelium discoideum (social amoeba)	CDSA		GGNRKSKIAGKENH	QNKNIINQKTNNNNNNN	68
Mus musculus (mouse)	CDS1		--D-----RY	-----GDLDARGD	55
Mus musculus (mouse)	CDS2		---EAKLDG	---ETA-----SDSESRAE	39
Danio rerio (zebrafish)	CDS1		--DLAFPD	---EGD-----GEMVGD SK	44
Danio rerio (zebrafish)	CDS2		---EGK-ER	---DGA-----SDSE	38
Drosophila melanogaster (fruit fly)	CDSA		--DHVDSEE	---EKI-----PEEKFVD	52
Xenopus tropicalis (frog)	CDS1		-----		0
Xenopus tropicalis (frog)	CDS2		--EVKTDG	---ETA-----SDSES KTD	59
Caenorhabditis elegans (worm)	CDS		--GILQDESD	---AGS-----KNKEEKL	64
Arabidopsis thaliana (plant)	CDS1		--HRLR	---HRR-----RSNEVMD	29
Arabidopsis thaliana (plant)	CDS2		--TRVR	---HRK-----RNSDV GAG	29
Arabidopsis thaliana (plant)	CDS3		--ARIR	---HRR-----RSSEN LAE	73
Saccharomyces cerevisiae (budding yeast)	CDS1		--DKLQ	-----	33
Rhizophagus irregularis (fungi)	CDS		---ELP	-----TKVN	27
Escherichia coli (bacteria)	CDSA		-----		0
Homo sapiens (human)	CDS1		SDIPEIPPS	SDRTPEILK KALSGLS SRWKN	85
Homo sapiens (human)	CDS2		SA--PLPVSADDTPEVLNRRALS NLS SRWKN		68
Dictyostelium discoideum (social amoeba)	CDSA		NIK EKDIIDSSVNADNLKATDPPSAKYK		98
Mus musculus (mouse)	CDS1		SDVPEVPPS	SDRTPEILK KALSGLS SRWKN	85
Mus musculus (mouse)	CDS2		TA--PLPTSVD DTPPEVLNRRALS NLS SRWKN		67
Danio rerio (zebrafish)	CDS1		AETPDAPPSTDNTPQCLN KALEGLS SRWKN		74
Danio rerio (zebrafish)	CDS2		-TKPEVPVSADDTPEVLN KALSGLS SRWKN		67
Drosophila melanogaster (fruit fly)	CDSA		ELAKNL PQGTDKTP EILDSAL KLDLP DRWKN		82
Xenopus tropicalis (frog)	CDS1		-----		0
Xenopus tropicalis (frog)	CDS2		TGGTQQGTPTDDTPEVLNRRALANLS SRWKN		89
Caenorhabditis elegans (worm)	CDS		RLTQAIPQDKGSLGVFADSMLEALPPWRN		94
Arabidopsis thaliana (plant)	CDS1		-----GD---KVN	---ASPLL VDRN KYKS	48
Arabidopsis thaliana (plant)	CDS2		-----AG---KPN	---GNHLLVND SKKYKS	48
Arabidopsis thaliana (plant)	CDS3		-----VN---RSN	VSRVSNLLLGDKN KYRS	95
Saccharomyces cerevisiae (budding yeast)	CDS1		EL--HKDASE	SVTPVTKESTATKESRKYN	61
Rhizophagus irregularis (fungi)	CDS		-----GLVKSEETQP	---IDPSQQMSOKWKN	50
Escherichia coli (bacteria)	CDSA		-----		0
Homo sapiens (human)	CDS1		WWLRGILTLTMTISLFFLII	-----Y	105
Homo sapiens (human)	CDS2		WWVRGILTLAMIAFFFI	II-----Y	88
Dictyostelium discoideum (social amoeba)	CDSA		LAIRSVMGAFMIGFFITVL	-----S	118
Mus musculus (mouse)	CDS1		WWLRGILTLTMTISLFFLII	-----Y	105
Mus musculus (mouse)	CDS2		WWVRGILTLAMIAFFFI	II-----Y	87
Danio rerio (zebrafish)	CDS1		WWLRGILSLTMIIGFFLII	-----Y	94
Danio rerio (zebrafish)	CDS2		WWVRGILTLAMISFFFI	II-----Y	87
Drosophila melanogaster (fruit fly)	CDSA		WVLRGIFTWIMICGEALII	-----Y	102
Xenopus tropicalis (frog)	CDS1		-----		0
Xenopus tropicalis (frog)	CDS2		WWVRGILTLAMISFFFI	II-----Y	109
Caenorhabditis elegans (worm)	CDS		WVVRGLFSIIMISTFTFIV	-----T	114
Arabidopsis thaliana (plant)	CDS1		FMVRTYSTLWMIIGFVLV	-----Y	68
Arabidopsis thaliana (plant)	CDS2		FLTRAYSTFWMIIGFALIV	-----Y	68
Arabidopsis thaliana (plant)	CDS3		MWIRTCSSLWMLGGVVFI	II-----Y	115
Saccharomyces cerevisiae (budding yeast)	CDS1		FFIRTVWTFVMSGFFITL	-----A	81
Rhizophagus irregularis (fungi)	CDS		MTVRITIWTFVMIIGFFLIL	-----G	70
Escherichia coli (bacteria)	CDSA		-----MLKYRLISA	FVLIPVVI AALFLLP	25

Supplementary Material

	Homo sapiens (human)	CDS1	MGSF	MLMLLLV	LGIVQVCF	FHEIITIGYRVYH	135																							
	Homo sapiens (human)	CDS2	LGP	MVLMII	VMCVQIKCF	FHEIITIGYRVYH	118																							
Dictyostelium discoideum (social amoeba)	CDSA	TDH	FIV	ALFVIALQ	LVFKEMIA	RYIEAK	148																							
	Mus musculus (mouse)	CDS1	MGSF	MLMLLLV	LGIVQVCF	FHEIITIGYRVYH	135																							
	Mus musculus (mouse)	CDS2	LGP	MVLMMMI	VMCVQIKCF	FHEIITIGYRVYH	117																							
	Danio rerio (zebrafish)	CDS1	LGP	IMLIIV	VMGVQIKCF	FHEIITIGYRVYH	124																							
	Danio rerio (zebrafish)	CDS2	LGP	MVLMMMI	VLVCVQIKCF	QBIITIGYSVYH	117																							
Drosophila melanogaster (fruit fly)	CDSA	GGP	LALM	MITTLLV	QVCKFQ	BIISIGYQVYR	132																							
	Xenopus tropicalis (frog)	CDS1					0																							
	Xenopus tropicalis (frog)	CDS2	LGP	IVLMMI	VMCVQIKCF	FHEIIMTIGYRVYH	139																							
	Caenorhabditis elegans (worm)	CDS	RGAT	WLMFLV	FLIQPKCF	QBIISIGLAVYR	144																							
	Arabidopsis thaliana (plant)	CDS1	MGH	LYITAM	VVVIQIFMA	KELFNLLRKAPE	98																							
	Arabidopsis thaliana (plant)	CDS2	LGH	LYITAM	VVVIQIFMA	RELFFNLLRKTHE	98																							
	Arabidopsis thaliana (plant)	CDS3	MGL	LYIWAM	VVVIQIFMA	KELFNLLRRAHE	145																							
Saccharomyces cerevisiae (budding yeast)	CDS1	SGH	AWCIVL	ILGCIQ	IAITFKECIA	VTASASGR	118																							
Rhizophagus irregularis (fungi)	CDS	LGH	IWIV	IFLVVVI	QTLVYKEV	IAIAHVPSSK	100																							
Escherichia coli (bacteria)	CDSA	VGF	AI	TVTLVV	CML-----	-----AAWE	42																							
	Homo sapiens (human)	CDS1	SYDL	PWF	R---	TL	SWYFLLCVNYFFYGETV	162																						
	Homo sapiens (human)	CDS2	SYDL	PWF	R---	TL	SWYFLLCVNYFFYGETV	145																						
Dictyostelium discoideum (social amoeba)	CDSA	EKK	IP	PHF	R---	TL	NWFFLTSFFFFYAKPI	175																						
	Mus musculus (mouse)	CDS1	SYDL	PWF	R---	TL	SWYFLLCVNYFFYGETV	145																						
	Mus musculus (mouse)	CDS2	SYDL	PWF	R---	TL	SWYFLLCVNYFFYGETV	144																						
	Danio rerio (zebrafish)	CDS1	SYDL	PWF	R---	TL	SWYFLLCVNYFFYGETV	151																						
	Danio rerio (zebrafish)	CDS2	SYDL	PWF	R---	TL	SWYFLLCVNYFFYGETV	144																						
Drosophila melanogaster (fruit fly)	CDSA	IHL	G	PWF	R---	SL	SWYFLLTSNYPFYGENL	159																						
	Xenopus tropicalis (frog)	CDS1				---	NVRH-----LC	FRYFLLCVNYFFYGETL	23																					
	Xenopus tropicalis (frog)	CDS2	SYDL	PWF	R---	TL	SWYFLLCVNYFFYGETV	166																						
	Caenorhabditis elegans (worm)	CDS	LYDF	PWF	R---	AL	SWYFLLTSNYPFFGESL	171																						
	Arabidopsis thaliana (plant)	CDS1	DKCL	PYIK	---	QL	NWHFFFTAMLFVYGRIL	125																						
	Arabidopsis thaliana (plant)	CDS2	DKQL	PGR	---	LL	NWHFFFTAMLFVYGRIL	125																						
	Arabidopsis thaliana (plant)	CDS3	ERR	LPG	FW---	LL	NWHFFFTAMLFVYGRIL	172																						
Saccharomyces cerevisiae (budding yeast)	CDS1	ENK	N	PLTK	---	TL	NWYFLFTIYYDLGKSL	138																						
Rhizophagus irregularis (fungi)	CDS	EKL	P	WF	K---	TL	NWYFLISTYYFLYGESL	127																						
Escherichia coli (bacteria)	CDSA	WGQ	L	SG	F	ET	TRSQRVWLA	VL	CGLL	LALML	--	70																		
	Homo sapiens (human)	CDS1	ADY	FAT	FVQREE	QL----	Q	FLIRYHRFISF	181																					
	Homo sapiens (human)	CDS2	TDY	FFTLVQ	REEPL	-----	RL	ISKYHRFISF	179																					
Dictyostelium discoideum (social amoeba)	CDSA	LIT	L	A	N	Y-----	Y	P	D	FQ	H	FVRYHLWHSF	199																	
	Mus musculus (mouse)	CDS1	ADY	FAT	FVQREE	QL----	Q	FLIRYHRFISF	180																					
	Mus musculus (mouse)	CDS2	TDY	FFTLVQ	REEPL	-----	RL	ISKYHRFISF	178																					
	Danio rerio (zebrafish)	CDS1	ADY	F	GALVQ	REEPL	----	RL	F	V	RYHRFISF	177																		
	Danio rerio (zebrafish)	CDS2	TDY	FFTLVQ	REEPL	-----	RL	ISKYHRFISF	170																					
Drosophila melanogaster (fruit fly)	CDSA	VDY	F	GVVINR	VEYL	----	K	F	L	V	T	YHRFLSF	185																	
	Xenopus tropicalis (frog)	CDS1	ADY	FAT	LVQREEM	L----	Q	FLIRYHRFISF	49																					
	Xenopus tropicalis (frog)	CDS2	TDY	FFTLVQ	REEPL	-----	RL	ISKYHRFISF	192																					
	Caenorhabditis elegans (worm)	CDS	IDY	WGIVL	KKDNFL	----	H	F	L	V	A	YHRLVSF	197																	
	Arabidopsis thaliana (plant)	CDS1	SQRL	AN	TMTADQ	FFYRLV	SGLIK	YHMAICY	155																					
	Arabidopsis thaliana (plant)	CDS2	SQRL	VNTV	TPDKVLYR	LVSTLIK	YHMAICY	155																						
	Arabidopsis thaliana (plant)	CDS3	QQQL	VNTV	SSDRFI	YKLVSG	LK	YQMVICY	202																					
Saccharomyces cerevisiae (budding yeast)	CDS1	KFF	FQAT	FYEY	EPVL	----	N	F	I	P	T	NHKKFICY	164																	
Rhizophagus irregularis (fungi)	CDS	IY	FKA	FVMD	DAFL	----	L	F	A	T	H	R	FISF	153																
Escherichia coli (bacteria)	CDSA													93																
	Homo sapiens (human)	CDS1	ALY	L	A	G	F	C	M	F	V	L	S	-----	L	V	K	K	H	Y	R	L	Q	F						
	Homo sapiens (human)	CDS2	TLY	L	I	G	F	C	M	F	V	L	S	-----	L	V	K	K	H	Y	R	L	Q	F						
Dictyostelium discoideum (social amoeba)	CDSA	SLY	C	I	G	F	V	L	F	I	L	T	-----	L	R	K	G	V	Y	R	Y	Q	L	F						
	Mus musculus (mouse)	CDS1	ALY	L	A	G	F	C	M	F	V	L	S	-----	L	V	K	K	H	Y	R	L	Q	F						
	Mus musculus (mouse)	CDS2	ALY	L	T	G	F	C	M	F	V	L	S	-----	L	V	K	K	H	Y	R	L	Q	F						
	Danio rerio (zebrafish)	CDS1	ALY	L	A	G	F	C	M	F	V	L	S	-----	L	V	K	K	H	Y	R	L	Q	F						
	Danio rerio (zebrafish)	CDS2	ALY	L	T	G	F	C	M	F	V	L	S	-----	L	V	K	K	H	Y	R	L	Q	F						
Drosophila melanogaster (fruit fly)	CDSA	ALY	I	G	F	V	W	F	V	L	S	-----	L	V	K	K	Y	I	K	Q	F									
	Xenopus tropicalis (frog)	CDS1	AFY	L	I	G	F	C	M	F	V	L	S	-----	L	V	K	K	H	Y	R	L	Q	F						
	Xenopus tropicalis (frog)	CDS2	ALY	L	T	G	F	C	M	F	V	L	S	-----	L	V	K	K	H	Y	R	L	Q	F						
	Caenorhabditis elegans (worm)	CDS	ALY	C	I	G	F	V	S	F	V	L	S	-----	L	R	K	G	Y	M	R	Q	F							
	Arabidopsis thaliana (plant)	CDS1	LLY	I	I	G	F	M	W	F	I	L	T	-----	L	K	K	M	Y	K	Y	Q	F							
	Arabidopsis thaliana (plant)	CDS2	SLY	I	S	G	F	V	W	F	I	L	T	-----	L	K	K	M	Y	K	Y	Q	F							
	Arabidopsis thaliana (plant)	CDS3	FLY	I	A	G	L	I	W	F	I	L	T	-----	L	K	N	K	M	Y	K	Y	Q	F						
Saccharomyces cerevisiae (budding yeast)	CDS1	CLY	L	M	G	F	V	L	F	V	C	S	-----	L	R	K	G	F	L	K	F	Q	F							
Rhizophagus irregularis (fungi)	CDS	VLY	C	I	G	F	V	F	F	V	A	N	-----	L	K	K	H	Y	K	F	Q	F								
Escherichia coli (bacteria)	CDSA	GW	W	I	V	A	L	L	L	V	L	F	P	G	S	A	I	W	R	N	S	K	T	L	R	L	I	F		
	Homo sapiens (human)	CDS1	YMF	A	W	T	H	V	T	L	L	I	T	V	T	O	S	H	L	V	I	Q	N	L	F	E	G	M	I	W
	Homo sapiens (human)	CDS2	YMF	G	W	T	H	V	T	L	L	I	V	V	T	O	S	H	L	V	I	H	N	L	F	E	G	M	I	W
Dictyostelium discoideum (social amoeba)	CDSA	SQ	L	T	W	T	L	M	I	L	M	M	V	V	Q	S	N	F	L	I	S	I	Y	Q	G	L	I			
	Mus musculus (mouse)	CDS1	YMF	A	W	T	H	V	T	L	L	I	T	V	T	O	S	H	L	V	I	Q	N	L	F	E	G	M	I	W
	Mus musculus (mouse)	CDS2	YMF	G	W	T	H	V	T	L	L	I	V	V	T	O	S	H	L	V	I	H	N	L	F	E	G	M	I	W
	Danio rerio (zebrafish)	CDS1	YMF	A	W	T	H	V	T	L	L	I	V	V	T	O	S	H	L	V	I	H	N	L	F	E	G	M	I	W
	Danio rerio (zebrafish)	CDS2	YMF	G	W	T	H	V	T	L	L	I	V	V	T	O	S	H	L	I	H	N	L	F	E	G	M	I	W	
Drosophila melanogaster (fruit fly)	CDSA	S	F	A	W	T	H	V	S	L	L	I	V	V	T	O	S	Y	L	I	I	Q	N	I	F	E	G	L	I	W
	Xenopus tropicalis (frog)	CDS1	YMF	G	W	T	H	V	T	L	L	I	T	V	T	O	S	H	L	V	I	H	N	L	F	E	G	M	I	W
	Xenopus tropicalis (frog)	CDS2	YMF	G	W	T	H	V	T	L	L	I	V	V	T	O	S	H	L	V	I	H	N	L	F	E	G	M	I	W
	Caenorhabditis elegans (worm)	CDS	S	F	A	W	T	H	L	T	L	L	I	V	S	O	S	F	I	L	I	Q	N	I	F	O	G	L	I	W
	Arabidopsis thaliana (plant)	CDS1	G	O	Y	A	W	T	H	M	I	L	I	V	V	T	O	S	S	F	T	V	A	N	I	F	E	G	I	W
	Arabidopsis thaliana (plant)	CDS2	G	O	Y	A	W	T	H	M	I	L	I	V	V	T	O	S	S	F	T	V	A	N	I	F	E	G	I	W
	Arabidopsis thaliana (plant)	CDS3	G	O	Y	A	W	T	H	M	I	L	I	V	V	T	O	S	S	F	T	V	A	N	I	F	E	G	I	W
Saccharomyces cerevisiae (budding yeast)	CDS1	G	S	L	C	V	T	H	M	V	L	L	V	V	F	Q	A	H	L	I	T	K	N	V	L	N	G	L	F	W
Rhizophagus irregularis (fungi)	CDS	T	Q	F	A	W	T	H	M	T	L	I	V	V	C	O	S	H	I	I	N	I	N	F	E	G	L	I	W	
Escherichia coli (bacteria)	CDSA	G	V	L	I	V	F	F	F	G	M	L	A	R	A	W	H	Y	D	E	N	N	H	S	G	A	I			

Homo sapiens (human)	CDS1	FLVFISSVICNDITAYLFGFFFG	GR----	TP	267
Homo sapiens (human)	CDS2	FIVFISCVICNDIMAYMFGFFFG	GR----	TP	250
Dictyostelium discoideum (social amoeba)	CDSA	FILPVSIIVCNDIFAYNGFFLGK	KFINRP		282
Mus musculus (mouse)	CDS1	FLVFISSVICNDITAYLFGFFFG	GR----	TP	267
Mus musculus (mouse)	CDS2	FIVFISCVICNDIMAYMFGFFFG	GR----	TP	249
Danio rerio (zebrafish)	CDS1	FIVFISIVICNDIMAYLFGFFFG	GR----	TP	256
Danio rerio (zebrafish)	CDS2	FIVFISCVICNDIMAYMFGFFFG	GR----	TP	249
Drosophila melanogaster (fruit fly)	CDSA	FIVPVSMIVCNDVMAYVFGFFFG	GR----	TP	264
Xenopus tropicalis (frog)	CDS1	FIVFISIVICNDIMAYIFGFFFG	GR----	TP	128
Xenopus tropicalis (frog)	CDS2	FIVFISCVICNDIMAYMFGFFFG	GR----	TP	271
Caenorhabditis elegans (worm)	CDS	FLAPVAMTICCDIMSVMFGFFFG	GK----	TP	276
Arabidopsis thaliana (plant)	CDS1	FLLPASLIIINDIFAYIFGFFFG	GR----	TP	234
Arabidopsis thaliana (plant)	CDS2	FLLPASLIVINDIFAYICGFFFG	GR----	TP	234
Arabidopsis thaliana (plant)	CDS3	FLLPAALIAMNDVAAYFGFYFGK	----	TP	281
Saccharomyces cerevisiae (budding yeast)	CDS1	FLLFCGLVIVNDIFAYLCGITFGK	----	TK	243
Rhizophagus irregularis (fungi)	CDS	FVLPVSLVICNDIFAYICGFFFG	GR----	TP	232
Escherichia coli (bacteria)	CDSA	LLYVMILVWGAPSGAYMFGKLF	GKH----	KL	180
Homo sapiens (human)	CDS1	LIKLSPKKTWEGFIGGFFSTVVF	FGFIAAYV		297
Homo sapiens (human)	CDS2	LIKLSPKKTWEGFIGGFFATVVF	FGLLSYV		280
Dictyostelium discoideum (social amoeba)	CDSA	LMKISPNKTWEGFIGATGWTL	FAYYFCGF		312
Mus musculus (mouse)	CDS1	LIKLSPKKTWEGFIGGFFSTVVF	FGFIAAYV		297
Mus musculus (mouse)	CDS2	LIKLSPKKTWEGFIGGFFATVVF	FGLLSYV		279
Danio rerio (zebrafish)	CDS1	LIKLSPKKTWEGFIGGFFATVVF	LSFFFAYL		286
Danio rerio (zebrafish)	CDS2	LIKLSPKKTWEGFIGGFFSTVVF	FGLLSYV		279
Drosophila melanogaster (fruit fly)	CDSA	LIKLSPKKTWEGFIGGFFATVVF	FGLFSYV		294
Xenopus tropicalis (frog)	CDS1	LIKLSPKKTWEGFIGGFMTVVF	FGFLFAYI		158
Xenopus tropicalis (frog)	CDS2	LIKLSPKKTWEGFIGGFFSTVVF	FGLLSYV		301
Caenorhabditis elegans (worm)	CDS	LIKLSPKKTWEGFIGGAFSTVVF	FGLLSLA		306
Arabidopsis thaliana (plant)	CDS1	LIKLSPKKTWEGFIGASVTIIS	SAFVLANI		264
Arabidopsis thaliana (plant)	CDS2	LIKLSPKKTWEGFIGASITTVIS	AFLLANI		264
Arabidopsis thaliana (plant)	CDS3	LIKLSPKKTWEGFIGASVATIIS	AFIFANV		311
Saccharomyces cerevisiae (budding yeast)	CDS1	LIEISPKKTLEGFLGAWFF	TALASILTRI		273
Rhizophagus irregularis (fungi)	CDS	LIKLSPKKTWEGFVGALICTIIF	GGFWSSL		262
Escherichia coli (bacteria)	CDSA	APKVSFGKTWQGFICGLATAA	VISWGYG--		208
Homo sapiens (human)	CDS1	LSKYQYFVCPVEYRSVDVNSF	-VTECEPSEL		326
Homo sapiens (human)	CDS2	MSGYRCFVCPVEYNNDTNSF	-TVDCPEPSDL		309
Dictyostelium discoideum (social amoeba)	CDSA	LLKYDWIVCPKGN---TGFM	SLHCTRDPV		339
Mus musculus (mouse)	CDS1	LSKYQYFVCPVEYRSVDVNSF	-VTECEPSEL		326
Mus musculus (mouse)	CDS2	MSGYRCFVCPVEYNNDTNSF	-TVDCPEPSDL		308
Danio rerio (zebrafish)	CDS1	LSQYQYFVCPVEYDSETNRF	-AVECEPSNL		315
Danio rerio (zebrafish)	CDS2	MAGYSYFVCPVEFNNDNSNRF	-TVDCQPSSEL		308
Drosophila melanogaster (fruit fly)	CDSA	LCNYQYFICPIQYSEEQGRM	-TMSQVPSYL		323
Xenopus tropicalis (frog)	CDS1	LAQFYQYFVCPVEYSSENSF	-STKCEPSEI		187
Xenopus tropicalis (frog)	CDS2	MAGYSYFVCPVEFNNETNRF	-TVDCPEPSEL		330
Caenorhabditis elegans (worm)	CDS	LYNRPFVCPVQHYQTD---	SSNCTIPLA		332
Arabidopsis thaliana (plant)	CDS1	LGRFPWLTCPRQDLSTG---	WLQCDADFL		290
Arabidopsis thaliana (plant)	CDS2	MGRFLWLTCPRDLSTG---	WLCDPGL		290
Arabidopsis thaliana (plant)	CDS3	LGGFQWLTCPRKDLSTG---	WLHCDPGL		337
Saccharomyces cerevisiae (budding yeast)	CDS1	LSPTYTYLTCPEVDLH--N	FFSNLTCLNPV		302
Rhizophagus irregularis (fungi)	CDS	LRRWDMYICPAQDLTTTAFY	GRLTCEPNPV		292
Escherichia coli (bacteria)	CDSA	-----	-----		208
Homo sapiens (human)	CDS1	FQLQTYSLPPFLKA----	VLRQERVSLY		350
Homo sapiens (human)	CDS2	FRLQEYNIPGVTSQ----	VI--GWKTVRMY		333
Dictyostelium discoideum (social amoeba)	CDSA	FLEKEFIFPPEITITIAFKYL	GITLLPFTYI		369
Mus musculus (mouse)	CDS1	FQLQNYSLPPFLQA----	VLSRETVSLY		350
Mus musculus (mouse)	CDS2	FRLQEYNIPGVTSQ----	AI--GWKTVRMY		332
Danio rerio (zebrafish)	CDS1	FMIQEYTLPAVVQN----	AL--RWKTVNLY		339
Danio rerio (zebrafish)	CDS2	FQLQDYSLPVLSQ----	IT--GWTVKLY		332
Drosophila melanogaster (fruit fly)	CDSA	FTPQEYSCLKLFG-----	IGKTLNLY		343
Xenopus tropicalis (frog)	CDS1	FRLHYVVPAYLQP----	L--GRRTVSMY		211
Xenopus tropicalis (frog)	CDS2	FQLQEYHIPAMFHS----	VI--SWKTVVMY		354
Caenorhabditis elegans (worm)	CDS	FQLQDYVPVRPFSEVYKILR	--KEPIIQLC		360
Arabidopsis thaliana (plant)	CDS1	FKPEPFALPAWTEPWF-----	PWKEMTIL		314
Arabidopsis thaliana (plant)	CDS2	FKQETHALPGWISDWL-----	PWKEISIL		314
Arabidopsis thaliana (plant)	CDS3	FRPEYYPFPSWITPFS-----	PWKISTL		361
Saccharomyces cerevisiae (budding yeast)	CDS1	FLPQVYRLPPIFFDKV-----	QINSITVK		326
Rhizophagus irregularis (fungi)	CDS	FIPQRYDLNPWLTL	SLFRRLTFKDIRSVWIA		322
Escherichia coli (bacteria)	CDSA	-----	MWANLDVA		216
Homo sapiens (human)	CDS1	PFQIHSIALSTFASLIGPFGG	FFASGFKRA		380
Homo sapiens (human)	CDS2	PFQIHSIALSTFASLIGPFGG	FFASGFKRA		363
Dictyostelium discoideum (social amoeba)	CDSA	PIQFHALVLALFGLIAPFGG	FFASGFKRA		399
Mus musculus (mouse)	CDS1	PFQIHSIALSTFASLIGPFGG	FFASGFKRA		380
Mus musculus (mouse)	CDS2	PFQIHSIALSTFASLIGPFGG	FFASGFKRA		362
Danio rerio (zebrafish)	CDS1	PFQIHSIALSSFASLIGPFGG	FFASGFKRA		369
Danio rerio (zebrafish)	CDS2	PFQIHSIALSSFASIMGPF	GGFFASGFKRA		362
Drosophila melanogaster (fruit fly)	CDSA	PFIWHSISLSLFSSTIGPFGG	FFASGFKRA		373
Xenopus tropicalis (frog)	CDS1	PFQIHSIALSSFASLIGPFGG	FFASGFKRA		241
Xenopus tropicalis (frog)	CDS2	PFQIHSIALSTFASLIGPFGG	FFASGFKRA		384
Caenorhabditis elegans (worm)	CDS	PFVFHSIALSLFASILGPFGG	FFASGFKRA		390
Arabidopsis thaliana (plant)	CDS1	PVQWHALCLGLFASITAPFGG	FFASGFKRA		344
Arabidopsis thaliana (plant)	CDS2	PVQWHALCLGLFASITAPFGG	FFASGFKRA		344
Arabidopsis thaliana (plant)	CDS3	PVQWHAFLGLFASIMAPFGG	FFASGFKRA		391
Saccharomyces cerevisiae (budding yeast)	CDS1	PIYFHALNLATFASLFA	PFGGFFASGLKRT		356
Rhizophagus irregularis (fungi)	CDS	PLQWHVLVMAFASLIAPFGG	FFASGFKRA		352
Escherichia coli (bacteria)	CDSA	PVTL--LICSIVAALASVGL	DLTEMFKRE		244

Homo sapiens (human)	CDS1	FKIKDFANTI	PGHGGIM	DRFDCQYLM	-ATF	409
Homo sapiens (human)	CDS2	FKIKDFANTI	PGHGGIM	DRFDCQYLM	-ATF	392
Dictyostelium discoideum (social amoeba)	CDSA	YKVKDFDTIF	PGHGGVTDRT	DCQFIM	-GLF	428
Mus musculus (mouse)	CDS1	FKIKDFANTI	PGHGGIM	DRFDCQYLM	-ATF	409
Mus musculus (mouse)	CDS2	FKIKDFANTI	PGHGGIM	DRFDCQYLM	-ATF	391
Danio rerio (zebrafish)	CDS1	FKIKDFADTI	PGHGGIM	DRFDCQYLM	-ATF	398
Danio rerio (zebrafish)	CDS2	FKIKDFANTI	PGHGGIM	DRFDCQYLM	-ATF	391
Drosophila melanogaster (fruit fly)	CDSA	FKIKDFGDMI	PGHGGIM	DRFDCQFLM	-ATF	402
Xenopus tropicalis (frog)	CDS1	FKIKDFADTI	PGHGGIM	DRFDCQYLM	-ATF	270
Xenopus tropicalis (frog)	CDS2	FKIKDFANTI	PGHGGIM	DRFDCQYLM	-ATF	413
Caenorhabditis elegans (worm)	CDS	FKIKDFGDVI	PGHGGIM	DRFDCQLLM	-GTF	419
Arabidopsis thaliana (plant)	CDS1	FKIKDFGDSI	PGHGGIT	DRMDCQMVM	-AVF	373
Arabidopsis thaliana (plant)	CDS2	FKIKDFGDSI	PGHGGIT	DRMDCQMVM	-AVF	373
Arabidopsis thaliana (plant)	CDS3	FKIKDFGDSI	PGHGGIT	DRMDCQMVM	-AVF	420
Saccharomyces cerevisiae (budding yeast)	CDS1	FKVKDFGHSI	PGHGGIT	DRVDCQFIM	-GSF	385
Rhizophagus irregularis (fungi)	CDS	FNIKDFGHSI	PGHGGIT	DRMDCQFLM	-GCF	381
Escherichia coli (bacteria)	CDSA	AGIKDSGHLI	PGHGGIL	DRIDSLTAAV	PFV	274
Homo sapiens (human)	CDS1	VHVIITS	FIRGNPS	---KVLQ	QLLVLPQE	436
Homo sapiens (human)	CDS2	VNVYIAS	FIRGNPS	---KLIQ	QFLTLRPD	419
Dictyostelium discoideum (social amoeba)	CDSA	IHVYNTFI	KLTLE	TDPT-FIWQ	NIMMLSME	457
Mus musculus (mouse)	CDS1	VHVIITS	FIRGNPS	---KVLQ	QLLVLPQE	436
Mus musculus (mouse)	CDS2	VNVYIAS	FIRGNPS	---KLIQ	QFLTLRPD	418
Danio rerio (zebrafish)	CDS1	VHVIITS	FIRGNPS	---KVLQ	QLLVLPQE	425
Danio rerio (zebrafish)	CDS2	VNVYIAS	FIRGNPS	---KVIQ	QLLALRPD	418
Drosophila melanogaster (fruit fly)	CDSA	VNVYISS	FIRTPSPA	---KLIT	QIYNLKP	429
Xenopus tropicalis (frog)	CDS1	VHVIIAS	FIRGNPS	---KVLQ	QLLVLPQE	297
Xenopus tropicalis (frog)	CDS2	VNVYIAS	FIRGNPS	---KLIQ	QFLTLRPD	440
Caenorhabditis elegans (worm)	CDS	VMVYIHS	FIRVPDAS	---KLLK	QIMTLEPQ	446
Arabidopsis thaliana (plant)	CDS1	AYIYLQSF	IVSQSVSDKIL	DI	ILTNLTFF	403
Arabidopsis thaliana (plant)	CDS2	AYIYHQS	FVPEVLSVDK	LLDQ	ITSLTLE	403
Arabidopsis thaliana (plant)	CDS3	AYIYIQSF	IVNRDYSVEMIL	DQ	ISRSILGE	450
Saccharomyces cerevisiae (budding yeast)	CDS1	ANLYYETFI	SEHRI	TVDTVLSTIL	MNLNDK	415
Rhizophagus irregularis (fungi)	CDS	SHMYYS	QSFIMSSSLTV	GAVLQTI	IVNSILKPQ	411
Escherichia coli (bacteria)	CDSA	ACLLLLV	ERTL	-----	-----	285
Homo sapiens (human)	CDS1	QQLNIYKTL	KTHLIEK	-GILQ	PTLKV---	461
Homo sapiens (human)	CDS2	QQLHIFNTL	RSHLIDK	-GMLT	STTEDE---	445
Dictyostelium discoideum (social amoeba)	CDSA	EKMVIYEKL	KQSI	EFTTG	TITA-----	479
Mus musculus (mouse)	CDS1	QQLNIYRTL	KIHLTEK	-GILQ	PTLKV---	461
Mus musculus (mouse)	CDS2	QQLHIFNTL	KSHLTDK	-GILT	SALEDE---	444
Danio rerio (zebrafish)	CDS1	QQLGIFNTL	RNQLREK	-GLLP	PAVEEAQ---	452
Danio rerio (zebrafish)	CDS2	QQLHIFNSL	KAHLTEK	-GLLP	PALEEEA---	444
Drosophila melanogaster (fruit fly)	CDSA	QQYQIYQSL	KDNLDGM	-LT---	-----	447
Xenopus tropicalis (frog)	CDS1	QQLNIYKAL	RAHLIEK	-GMTD	ALHNQ---	323
Xenopus tropicalis (frog)	CDS2	QQIHIFNTL	KSHLTEN	-GILAN	DNGV----	465
Caenorhabditis elegans (worm)	CDS	DQLNIFNL	QSELSKT	-GLT	-----	465
Arabidopsis thaliana (plant)	CDS1	EQQALFVKL	GMLKDK	-LS---	-----	421
Arabidopsis thaliana (plant)	CDS2	EQQALLVKL	GMLQEK	-VIGS	-----	423
Arabidopsis thaliana (plant)	CDS3	EQKMLYEKL	GDILQHK	-LQGR	-----	471
Saccharomyces cerevisiae (budding yeast)	CDS1	QIIELDIDL	IRFLSKK	-GISA	KNFEKLAD	444
Rhizophagus irregularis (fungi)	CDS	DQIELFNRL	KQYLLSQ	-GLLE	ERGATN---	437
Escherichia coli (bacteria)	CDSA	-----	-----	-----	-----	285
Homo sapiens (human)	CDS1	-----	-----	-----	-----	461
Homo sapiens (human)	CDS2	-----	-----	-----	-----	445
Dictyostelium discoideum (social amoeba)	CDSA	-----	-----	-----	-----	479
Mus musculus (mouse)	CDS1	-----	-----	-----	-----	461
Mus musculus (mouse)	CDS2	-----	-----	-----	-----	444
Danio rerio (zebrafish)	CDS1	-----	-----	-----	-----	452
Danio rerio (zebrafish)	CDS2	-----	-----	-----	-----	444
Drosophila melanogaster (fruit fly)	CDSA	-----	-----	-----	-----	447
Xenopus tropicalis (frog)	CDS1	-----	-----	-----	-----	323
Xenopus tropicalis (frog)	CDS2	-----	-----	-----	-----	465
Caenorhabditis elegans (worm)	CDS	-----	-----	-----	-----	465
Arabidopsis thaliana (plant)	CDS1	-----	-----	-----	-----	421
Arabidopsis thaliana (plant)	CDS2	-----	-----	-----	-----	423
Arabidopsis thaliana (plant)	CDS3	-----	-----	-----	-----	471
Saccharomyces cerevisiae (budding yeast)	CDS1	IFNVTKKSL	TNHS	-----	-----	457
Rhizophagus irregularis (fungi)	CDS	-----	-----	-----	-----	437
Escherichia coli (bacteria)	CDSA	-----	-----	-----	-----	285

Figure S1. CDS full sequence alignment. Full sequence alignment of CDS proteins found in a range of organisms. The names of the species used for comparison in the alignment are shown to the left with the amino acid start position shown to the left of the sequence and the end amino acid residue number of each line shown to the right of the alignment. Identical amino acids to the *D. discoideum* protein are highlighted in blue. The multiple sequence alignment was produced using Clustal Omega and Multiple Align Show (bioinformatics.org).

Homo sapiens (human)	CDIPT1	-----M	PDE	---NIFL	8
Dictyostelium discoideum (social amoeba)	CDIPT1	-----M	AFS	---KYYT	8
Mus musculus (mouse)	CDIPT1	-----M	PEE	---NIFL	8
Danio rerio (zebrafish)	CDIPT1	-----M	TEE	---NIFL	8
Drosophila willistoni (fruit fly)	CDIPT1	-----M	AEHD	---NFI	11
Xenopus tropicalis (frog)	CDIPT1	-----M	QE	---NIFL	8
Pristionchus pacificus (parasitic nematode)	CDIPT1	-----M	VSALSS	---PWWL	13
Arabidopsis thaliana (plant)	CDIPT1	-----M	AKKERPREKL	---SVYL	16
Saccharomyces cerevisiae (budding yeast)	CDIPT1	-----M	SSNSTPEKVTAE	---HWLW	17
Escherichia coli (bacteria)	CDIPT1	MSKL	PFLSRAAFARITTP	IARGLLRVGLTP	30
Homo sapiens (human)	CDIPT	FVPNLIGYARIVFAIIS	FYFMPCCPLTASS		38
Dictyostelium discoideum (social amoeba)	CDIPT	FVPNLIGYARIVFAIIS	FYFMPCCPFTASS		38
Mus musculus (mouse)	CDIPT	FVPNLIGYARIVFAIIS	FYFMPCCPFTASS		38
Danio rerio (zebrafish)	CDIPT	FVPNLIGYARIVLALVS	FFLMPCCPGPAVF		38
Drosophila willistoni (fruit fly)	CDIPT	FVPNLIGYARIVLALIA	AFWFMSTNYVIAGW		41
Xenopus tropicalis (frog)	CDIPT	FVPNLIGYARIVFAFVA	FYFMPSTSPVLAST		38
Pristionchus pacificus (parasitic nematode)	CDIPT	FVPNLIGYARIVLALISM	WMVFPSPAVTAMF		43
Arabidopsis thaliana (plant)	CDIPT	YIPNIVGYMRVLLNCV	AFVCFCSNKPFLFSV		46
Saccharomyces cerevisiae (budding yeast)	CDIPT	YIPNIGYVRVITAAIS	FFVMKNHPTATWTW		47
Escherichia coli (bacteria)	CDIPT	DVVTLLGTTASVAGAL	TLFFPMGKLFAGACV		60
Homo sapiens (human)	CDIPT	FYLLSGLLDAFDGHAAR	ALNQGTRFGAMLD		68
Dictyostelium discoideum (social amoeba)	CDIPT	FYALSALLDMADGHAAR	LLNQCSQFGLLD		68
Mus musculus (mouse)	CDIPT	FYLLSGLLDAFDGHAAR	ALNQGTRFGAMLD		68
Danio rerio (zebrafish)	CDIPT	CYLLSALLDAFDGHAAR	ALNQGTRFGAMLD		68
Drosophila willistoni (fruit fly)	CDIPT	CYIISALLDAVDGHAAR	AFNQSTRFGAMLD		71
Xenopus tropicalis (frog)	CDIPT	FYLLSGLLDAFDGHAAR	LLNQGTRFGAMLD		68
Pristionchus pacificus (parasitic nematode)	CDIPT	CYALSALLDAFDGWAAR	TYNQSRFGAMLD		73
Arabidopsis thaliana (plant)	CDIPT	LYFFSFCCDAVDGWVARR	FNQVSTFGAVLD		76
Saccharomyces cerevisiae (budding yeast)	CDIPT	LYSTSCLLDALDGTMARK	YQVSSLGAVLD		77
Escherichia coli (bacteria)	CDIPT	-VWFFVLLFMDLDGAMAR	EGRGGTRFGAVLD		89
Homo sapiens (human)	CDIPT	MLTDRCSTMCLLVN	LALLY---	PGATLFF	94
Dictyostelium discoideum (social amoeba)	CDIPT	MITDRCSTIALM	VVLSHFY---	KDYENFY	94
Mus musculus (mouse)	CDIPT	MLTDRCATMCLLVN	LALLY---	PRATLFF	94
Danio rerio (zebrafish)	CDIPT	MLTDRCATMCLLVN	LALLY---	PSYTFLE	94
Drosophila willistoni (fruit fly)	CDIPT	QLTDRCGTGLLVTL	LSYFY---	PNYMPWF	97
Xenopus tropicalis (frog)	CDIPT	MLTDRCATMCLLVN	LSLLY---	PSYTLLE	94
Pristionchus pacificus (parasitic nematode)	CDIPT	QLTDRCALLSLVMT	LCVLY---	PRWQFL	99
Arabidopsis thaliana (plant)	CDIPT	MVTDREVSTACLVL	LSQIY---	RPSLVF-	101
Saccharomyces cerevisiae (budding yeast)	CDIPT	MVTDREVSTAGLW	CFLCVQY---	PQCVCF-	103
Escherichia coli (bacteria)	CDIPT	ATCDRI	SDGAVFCGLLWW	IAFHMRRDRLVI	119
Homo sapiens (human)	CDIPT	QISMSLDVASHWLHL	HSSVVRGSESHK	MID	124
Dictyostelium discoideum (social amoeba)	CDIPT	IALLITLDIVSHFAR	LCATLQSGSKSHKAVK		124
Mus musculus (mouse)	CDIPT	QLSMSLDVASHWLHL	HSSVVRGSESHK	MID	124
Danio rerio (zebrafish)	CDIPT	QLSMCLDVASHWLHL	HSSMMKCATSHK	AI	124
Drosophila willistoni (fruit fly)	CDIPT	QLSIAIDVACHWLY	MQTSVVVGR	TSHKV--	125
Xenopus tropicalis (frog)	CDIPT	QLSMSLDIASHWLHL	HSSILKGSSESHK	TIN	124
Pristionchus pacificus (parasitic nematode)	CDIPT	QLSAVLDIASHWLHL	HATDL	SGKTHKQ--	127
Arabidopsis thaliana (plant)	CDIPT	LSLLALDIASHWLQ	MYSTPLAGKS	SHKDVK	131
Saccharomyces cerevisiae (budding yeast)	CDIPT	QLMLGLDITSHYMHMY	ASISAGKTSHKS	VG	133
Escherichia coli (bacteria)	CDIPT	ATLILCLVT-SQV---	ISYIKARAEASGLR		144
Homo sapiens (human)	CDIPT	LSGNPVLRIYYT	SRPALFTLCAGNELFYCL		154
Dictyostelium discoideum (social amoeba)	CDIPT	ENHIKIMKIYYGNKY	FLAFMCFGNEGFFLF		154
Mus musculus (mouse)	CDIPT	LSGNPVLRIYYT	SRPALFTLCAGNELFYCL		154
Danio rerio (zebrafish)	CDIPT	LSGNPILRLYYT	SRPVLFFMCMGNELEFCL		154
Drosophila willistoni (fruit fly)	CDIPT	-NDNFVMR	IYYQ-KDVLTFMCCAGNELFYVC		153
Xenopus tropicalis (frog)	CDIPT	LAGNPVLRLYYT	SRPVLFFMCCAGNELFYCM		154
Pristionchus pacificus (parasitic nematode)	CDIPT	-SSNPVLHLYYT	SRPVLGFMCCAGNEAFYFL		156
Arabidopsis thaliana (plant)	CDIPT	DSTS	WLFRLYYGNRIEMCVCCVSC	EVLYII	161
Saccharomyces cerevisiae (budding yeast)	CDIPT	EGESRLHLHY	YTRRDVLFITICAFNELFYAG		163
Escherichia coli (bacteria)	CDIPT	GDGGFT	ER--PERLIIVLTGAGVSD	E---	168
Homo sapiens (human)	CDIPT	LYLFHF	SEGPL-----VGSVGLFRMGL		176
Dictyostelium discoideum (social amoeba)	CDIPT	SYLYHFYATSSV	F-----YILW		171
Mus musculus (mouse)	CDIPT	LYLFNE	SEGPL-----VGSVGLFRMGL		176
Danio rerio (zebrafish)	CDIPT	LYIMFYIEEPQ	VW---LQ-----WLL		172
Drosophila willistoni (fruit fly)	CDIPT	LYLLHFTYGPLIL	-----GASLFFKLLA		175
Xenopus tropicalis (frog)	CDIPT	LYLLHFTYEGPSV	I---LGPVGAIGLFRILIV		181
Pristionchus pacificus (parasitic nematode)	CDIPT	LYITHFYFPGPS	LL-----GISLMAFLT		178
Arabidopsis thaliana (plant)	CDIPT	LLLIAKQSEN	LLNVVVATLTQTSPLSFLL		191
Saccharomyces cerevisiae (budding yeast)	CDIPT	QLMLGLDITSHYMHMY	ASISAGKTSHKS	VG	193
Escherichia coli (bacteria)	CDIPT	---	PVPPPAL-----SVGMWLL		184
Homo sapiens (human)	CDIPT	WVTA	PIALLKSLISVIHLIT	AARNMAALDA	206
Dictyostelium discoideum (social amoeba)	CDIPT	GFFFPICAAKQI	INAIQFFQAVDDIVSLDD		201
Mus musculus (mouse)	CDIPT	WVTA	PIALLKSVISVIHLIT	AARNMAALDA	206
Danio rerio (zebrafish)	CDIPT	GVC	GVVCLKSGISFLHLIT	ASRNMAAIDV	202
Drosophila willistoni (fruit fly)	CDIPT	FLSG	FFAVLKALISVMHAYVAGD	DLAAVDV	205
Xenopus tropicalis (frog)	CDIPT	WLCC	PTSLIKSLISLIHLVT	ASSNIALSLD	211
Pristionchus pacificus (parasitic nematode)	CDIPT	FLAF	PIAAVKSAISVIHLGTAAAD	VVEIDE	208
Arabidopsis thaliana (plant)	CDIPT	ALT	LFGWSMKQITINVIQMTAA	DVCVLYDI	221
Saccharomyces cerevisiae (budding yeast)	CDIPT	EGESRLHLHY	YTRRDVLFITICAFNELFYAG		223
Escherichia coli (bacteria)	CDIPT	AVASV	ITCVQRLHTVWTS	SPGAIIRMAIPGK	214

Homo sapiens (human)	CDIPT	ADRAKKK-----	213
Dictyostelium discoideum (social amoeba)	CDIPT	QQKLKK-----	207
Mus musculus (mouse)	CDIPT	ADRAKKK-----	213
Danio rerio (zebrafish)	CDIPT	ADREKERSKAQ-----	213
Drosophila willistoni (fruit fly)	CDIPT	RERQEKRNKKPSSEPSGKKIE	226
Xenopus tropicalis (frog)	CDIPT	AERSKKK-----	218
Pristionchus pacificus (parasitic nematode)	CDIPT	RSRNQRKQ-----	216
Arabidopsis thaliana (plant)	CDIPT	EKQQKP-----	227
Saccharomyces cerevisiae (budding yeast)	CDIPT	KNANEKNTY-----	233
Escherichia coli (bacteria)	CDIPT	GDR-----	217

Figure S2. CDIPT full sequence alignment. Full sequence alignment of CDIPT proteins found in a range of organisms. The names of the species used for comparison in the alignment are shown to the left with the amino acid start position shown to the left of the sequence and the end amino acid residue number of each line shown to the right of the alignment. Identical amino acids to the *D. discoideum* protein are highlighted in blue. The multiple sequence alignment was produced using Clustal Omega and Multiple Align Show (bioinformatics.org).